

**Molecular Mechanisms of C9ORF72-linked  
Frontotemporal Dementia and  
Amyotrophic Lateral Sclerosis**

Frédérique Wivinneke Riemsdagh

The work described in this thesis was performed at the department of Clinical Genetics in the Erasmus Medical Center, Rotterdam, The Netherlands.

The studies presented in this thesis were financially supported by:  
European Joint Programme - Neurodegenerative Disease Research  
The Netherlands Organization for Health Research and Development  
(PreFrontALS: 733051042 to R. Willemsen and J.C. van Swieten)  
Alzheimer Nederland Grand Cycle 2012 (WE03.2012-XX to R.Willemsen) and  
Grant Cycle 2018 (WE.03-2018-08 to R. Willemsen and F.W. Riemsлагh).

The production costs of this thesis were supported by the Erasmus University Rotterdam.

**ISBN:** 978-94-6323-674-4

**Author:** Frédérique Riemsлагh

**Cover design & Layout:** Frédérique Riemsлагh

**Printed by:** Gildeprint, Enschede

Copyright © Frédérique Riemsлагh, 2019. All rights reserved. No part of this thesis may be reproduced, stored in a retrieval system, or transmitted in any form by any means, without prior written permission from the author.

# **Molecular Mechanisms of C9ORF72-linked Frontotemporal Dementia and Amyotrophic Lateral Sclerosis**

Moleculaire mechanismen van C9ORF72  
geassocieerde frontotemporale dementie en  
amyotrofische laterale sclerose

## **Proefschrift**

ter verkrijging van de graad van doctor aan de  
Erasmus Universiteit Rotterdam  
op gezag van de  
rector magnificus

Prof.dr. R.C.M.E. Engels

en volgens besluit van het College voor Promoties.  
De openbare verdediging zal plaatsvinden op

woensdag 26 juni 2019 om 13:30 uur

door

**Frédérique Wivinneke Riemsлагh**

geboren te Amsterdam

**Promotiecommissie:**

**Promotoren:** Prof.dr. R. Willemsen  
Prof.dr. J.C. van Swieten

**Overige leden:** Prof.dr. J.M. Kros  
Prof.dr. P. Heutink  
Dr. D.G. Wansink

**Copromotor:** Dr. R.K. Hukema

# Contents

<b>Chapter 1</b>	7
Introduction	
<b>Chapter 2</b>	47
Reduction of oxidative stress and inhibition of the integrated stress response rescues poly-GR and poly-PR mediated toxicity in zebrafish embryos	
<b>Chapter 3</b>	71
Inducible expression of human <i>C9ORF72</i> 36x G <sub>4</sub> C <sub>2</sub> hexanucleotide repeats is sufficient to cause RAN translation and rapid muscular atrophy in mice	
<b>Chapter 4</b>	99
HR23B pathology preferentially co-localizes with p62, pTDP-43 and poly-GA in <i>C9ORF72</i> -linked frontotemporal dementia and amyotrophic lateral sclerosis	
<b>Chapter 5</b>	131
Poly-GR is not detected in CSF and PBMCs of <i>C9ORF72</i> -linked frontotemporal dementia and amyotrophic lateral sclerosis cases and carriers	
<b>Chapter 6</b>	147
General discussion	
<b>Appendix</b>	169
References	
List of abbreviations	
Summary & Samenvatting	
CV, List of publications & PhD Portfolio	
Dankwoord	



# Chapter 1

## Introduction



### **Abstract**

**Frontotemporal dementia (FTD) and amyotrophic lateral sclerosis (ALS) are two devastating neurological disorders that share clinical, genetic and pathological overlap. The discovery of a hexanucleotide G<sub>4</sub>C<sub>2</sub> repeat expansion in the chromosome 9 open reading frame 72 (C9ORF72) gene as a major cause of FTD and ALS confirmed the genetic link between these two neurodegenerative diseases, collectively referred to as C9FTD/ALS. Many different hypotheses about the possible pathogenic mechanisms of this repeat have been proposed, including haploinsufficiency leading to partial loss of function of the endogenous C9ORF72 protein product, RNA toxicity caused by RNA molecules or RNA foci that bind and sequester RNA-binding proteins or production of toxic dipeptide repeat proteins (DPR) by repeat-associated non-AUG initiated (RAN) translation of the repeat. In this introduction, we review both clinical and functional studies that support one or more of these possibilities. Identification of the pathological pathways underlying neurodegeneration could guide future research and lead to new treatments and is therefore of great importance for the FTD/ALS field.**



## 1. Clinical and genetic factors in the FTD/ALS spectrum

### 1.1 General clinical introduction

In 1892 the neuropsychiatrist Arnold Pick (1851-1924) described several cases of patients with FTD-like clinical features[1]. This was the basis of Pick's Disease (PiD) but also of the entire spectrum of FTD[1]. FTD is a form of neurodegenerative presenile dementia with predominant frontal and anterior temporal lobe involvement[1]. The clinical picture consists of two different types of manifestations: behavioral-variant FTD (bvFTD) or predominant language impairment variant, also called primary progressive aphasia (PPA)[2]. bvFTD is characterized by progressive behavioral and personality changes and executive dysfunction[2]. PPA can be further divided into fluent speech with impaired word finding and comprehension, so-called semantic variant PPA (svPPA)[3]. PPA can also manifest in two forms of non-fluent speech: with agrammatism and sometimes apraxia of speech (nonfluent variant nfvPPA) or with word-finding problems and repetition (logopenic variant lvPPA)[3]. In all FTD forms, perception and memory are relatively preserved[4]. FTD is the second most common cause of dementia after Alzheimer's disease (AD) for people younger than 65 years of age[5]. The prevalence of FTD is estimated at 15-22 in 100.000 people and the incidence at 2.7-4.1 in 100.000 people[6]. The survival time after symptoms start is very variable between patients and ranges from 3 to 14 years[6].

ALS was first described by Jean-Martin Charcot in 1869 and is the most common form of motor neuron disease (MND) in which patients display signs of both upper and lower motor neuron (UMN and LMN) degeneration[7]. Other forms of motor neuron disease include primary lateral sclerosis (PLS), progressive muscular atrophy (PMA) or progressive bulbar palsy (PBP)[7]. Symptoms include muscular spasticity, weakening, hyperreflexia, muscular atrophy, fasciculations, speech and swallowing difficulties[8]. Patients with ALS can also develop psychological and cognitive difficulties, including depression, impaired executive functions, and problems with social behavior[8]. The prevalence of ALS is 5 per 100.000 people and it has an incidence of 1.7 per 100.000 people[8]. The average life expectancy is two to five years and death is usually caused by respiratory failure[8, 9]. Two FDA approved drugs are available for ALS patients: Riluzole and Edaravone. Riluzole prolongs survival with a few months by decreasing glutamate levels and delaying motor neuron damage[10]. However, Riluzole does not reverse neuronal damage nor halt the disease progress[10]. For Edaravone, the exact mechanism is unknown but it has antioxidant properties that could protect against oxidative stress in motor neurons in ALS[11].

FTD and ALS may seem very distinct diseases at first sight, but they are part of a disease spectrum. About 15% of FTD patients develop MND and about 50% of MND patients show some signs of cognitive impairment[12]. The neuropsychological deficits in ALS can be extremely heterogeneous and impact patient survival[13]. The cognitive profile of FTD and ALS shows similarities, including deficits in social cognition, verbal memory, fluency and executive functions[14]. When specified for *C9ORF72* repeat expansion carriers, 30% of FTD patients develop ALS symptoms and 27% of ALS patients show symptoms of FTD[15].

### 1.2 Genetic factors in the FTD and ALS spectrum

Family history is observed in up to 50% of FTD patients and in about 10% of ALS patients, implying a role for genetic factors in the development of both diseases[16]. There are some 'pure' FTD and 'pure' ALS genes, including microtubule-associated protein tau (*MAPT*) and progranulin (*GRN*) for FTD and superoxide dismutase 1 (*SOD1*) for ALS[17]. Next to these 'pure' genes, the list of 'shared' genes between FTD and ALS has become quite extensive in the past 10 years (reviewed in [16, 18]). Trans-activation response element DNA-binding protein 43 encoding gene (*TARDBP*) and fused in sarcoma (*FUS*) are thought to be major ALS genes but are occasionally found in FTD patients as well[17, 19]. The other way around, the charged multivesicular body protein 2B gene (*CHMP2B*) is seen as FTD gene but there are some rare occurrences in ALS patients[20]. Mutations in *C9ORF72*, valosin-containing protein (*VCP*), P62/sequestosome-1 (*SQSTM1*), ubiquilin 2 (*UBQLN2*), Optineurin (*OPTN*), Coiled-coil-helix-coiled-coil-helix domain containing 10 (*CHCHD10*), TANK-binding kinase 1 (*TBK1*) and heterogeneous nuclear ribonucleoprotein A1 (*HNRNPA1*) and A2/B1 (*HNRNPA2/B1*) are found in both disorders[16-20]. Variants in transmembrane protein 106 B (*TMEM106B*) can modify the disease penetrance of FTD in *GRN* carriers and protects *C9ORF72* repeat carriers from developing FTD, but not from developing MND[21].

Linkage to a locus on chromosome 9 in the 9p21.2–p13.3 region for FTD and ALS was already found in 2006[20]. In 2011, the hexanucleotide G<sub>4</sub>C<sub>2</sub> repeat expansion in the *C9ORF72* gene was discovered as cause of FTD and ALS[22, 23]. The *C9ORF72* mutation accounts for 26% of FTD, 34% of ALS and 88% of familial FTD-ALS patients worldwide[15, 24]. In sporadic ALS, it accounts for about 6-9% and in sporadic FTD it is found in 5-10% of all cases[25, 26]. The *C9ORF72* repeat expansion is thus the most common genetic cause of FTD and ALS[15, 25, 27]. The highest mutation frequencies were observed in Cauca-

sian populations of Europe and North America with a peak in Finland, Sweden and Denmark[28]. The existence of a common northern European founder has been suggested[25, 29, 30], but haplotype analysis on Swedish *C9ORF72* expansion mutation carriers indicates that the *C9ORF72* expansion mutation arose on at least two risk haplotypes[31] and screening of Ashkenazi and North Africa Jews indicates the existence of two founder populations with the same risk haplotypes[32].

### 1.3 Clinical phenotype of C9FTD/ALS

Patients harboring the *C9ORF72* repeat expansion can develop FTD, ALS or both and are therefore associated with wide clinical diversity[24, 33-36]. *C9ORF72* repeat expansion mutations leading to motor neuron disease symptoms is almost always classified as ALS (C9ALS) and only rarely with PLS, PMA or PBP[33, 37]. Around 70% of C9ALS cases display a spinal onset[23, 37]. *C9ORF72* caused FTD (C9FTD) was in almost all of the cases enriched in the behavioral variant with most common symptoms being disinhibition, forgetfulness, anxiety and compulsive or stereotyped behavior[33, 34]. PPA is a fairly rare phenotype of *C9ORF72* expansions[34]. Although FTD patients sometimes show Parkinsonism, the prevalence of the *C9ORF72* repeat expansion in patients with Parkinson's disease (PD) is lower than 1%[33, 34]. Also AD patients only rarely harbor a repeat expansion[33]. The mean age of onset of C9FTD/ALS is 57 years[35, 36]. Survival is longer in *C9ORF72* patients diagnosed with FTD compared to ALS diagnosis and overall disease duration ranges from 1 to 22 years[24, 35, 36]. At the start of ALS symptoms, survival is dramatically reduced to an average of 1.8 years[15, 36]. Neuronal loss and gliosis in the frontal and temporal cortical regions of the brain are the major pathological changes in FTD patients[34, 38]. For ALS patients, motor neuron loss in the brainstem and spinal cord are observed in post-mortem brain sections[34, 37]. In addition to predominant atrophy in frontal and temporal areas, C9FTD patients show more thalamic, posterior insula and cerebellar atrophy than non-*C9ORF72* FTD patients in imaging studies[34].

### 1.4 Effect of the *C9ORF72* repeat size on clinical phenotype

The exact number of repeats that causes C9FTD/ALS has not been determined, but repeat sizes of 30 – 4400 have been reported so far[39]. Healthy individuals often carry alleles with 2, 8 or 24 repeats[39], but some controls have been identified with longer repeats[40], which might be explained by reduced penetrance that is reported for C9FTD/ALS[41]. Repeat sizes vary a lot between fam-

ily members, even between monozygotic twins and different tissues of the same person[42-46]. Patients often have longer repeats in brain tissue than in DNA isolated from blood samples[42-46] and the repeat expansions in the cerebellum seem to be smaller and more stable[43]. There have been some reports of ALS and FTD cases with 20-30 repeats in blood[47, 48], but their repeat size could be longer in brain due to somatic mosaicism[42-46]. Associations between repeat size and FTD or ALS clinical diagnosis have not resulted in a clear picture[42-46], only intermediate allele sizes appear to specifically associate more frequently with neuropsychiatric phenotypes[49]. The age of onset is highly variable, ranging from 27 to 83 years and is considered fully penetrant around the age of 80[25, 41]. Genetic anticipation could play a role, based on the instability of expanded repeats that have the tendency to further increase in size with each generation and may lead to a younger age of onset. But so far, multiple studies indicate that the repeat size can both extend or shorten over generations[42, 44, 50]. Correlations between repeat size and age of onset, disease progression or survival have been reported[42-46]. However, repeat sizes measured in blood are very variable and correlations could rely on the confounding factor age at collection[42]. Thus, the exact repeat size that triggers disease onset and the influence of repeat size on many clinical characteristics is unknown and seems to be personal and highly variable.

## **2. Pathological features of C9FTD/ALS**

Post-mortem brain and spinal cord tissue of patients with C9FTD/ALS harbors some characteristic pathological features such as RNA foci and protein aggregates containing: dipeptide repeats (DPRs), autophagy protein p62/sequestosome 1 (p62) and phosphorylated 43kDa TAR DNA-binding protein (pTDP-43). In this section, we describe their amount, cellular localization pattern and spreading throughout the central nervous system (CNS). We shortly introduce the mechanism of RAN translation and more specific the production of DPRs. Information about possible correlation with clinical features, neurodegeneration or co-localization between pathological features are discussed in chapter 6 (general discussion).

### 2.1 RNA foci

The presence of RNA foci in postmortem brain tissue from C9FTD/ALS patients was first described by DeJesus-Hernandez at the discovery of the *C9ORF72* G<sub>4</sub>C<sub>2</sub> repeat expansion[22]. This initial report has been confirmed and quantified

by multiple studies since then[51]. The precise content of RNA foci is unclear. They might contain only  $G_4C_2$  repeat RNA, the spliced intron 1 or the complete *C9ORF72* (pre-)mRNA. Increased levels of sense and antisense *C9ORF72* mRNA containing intron 1 were found in frontal cortex of C9FTD cases[52, 53]. Downstream introns seem to be correctly spliced out[54]. Intron 1 retention of polyadenylated *C9ORF72* mRNA in the cytoplasm and nucleus has also been identified in frontal cortex of C9FTD/ALS cases[54]. However, it remains unclear if these intron 1-containing mRNA molecules can form RNA foci. In the rest of this thesis and in most studies, probes were used to visualize sense  $G_4C_2$  or antisense  $C_4G_2$  repeats.

Both sense and antisense foci are observed throughout the CNS (figure 1): in frontal cortex (average 25% of cells containing sense foci, 15% antisense) [22, 55-58], hippocampus dentate gyrus (average 30% sense, 17% antisense) [56, 59, 60] and cornu ammonis (average 60% sense, 43% antisense, only 1 study[60]), spinal cord (average 44% sense, 72% antisense)[22, 51, 60, 61] and cerebellum granular layer (average 35% sense, 4% antisense)[56, 58, 60, 61] and Purkinje cells (average 63% sense, 80% antisense)[58, 60]. Foci were also observed in the cingulate cortex, striatum, inferior temporal gyrus, entorhinal cortex, pre- and post-central gyrus, medial pulvinar thalamus and calcarine cortex[59]. Sense foci seem to be more common than antisense foci in most brain areas, only Purkinje cells and spinal cord motor neurons contain more antisense foci[51]. Foci are sometimes also found in astrocytes, oligodendrocytes, microg-

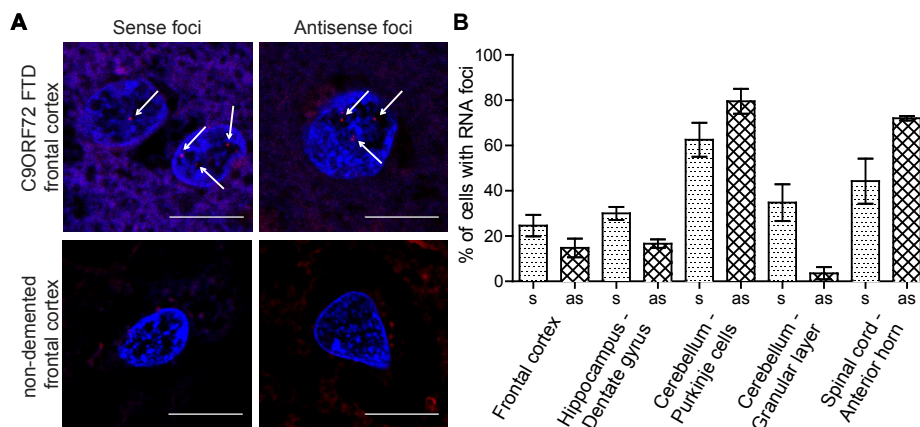


**Figure 1: Distribution of RNA foci over several brain areas.** A) Both sense and antisense RNA foci (red dots) are present in nuclei (blue) of C9FTD post-mortem frontal cortex but not in non-demented controls. Scale bars are 10 $\mu$ m. B) Quantification of the number of cells harboring sense and antisense RNA foci in several brain areas. Error bars are standard error of the mean (SEM). Values are based on data from publications [22, 51, 55-61].

lia and peripheral blood leukocytes[55, 56]. Motor and cortical neurons generated from induced pluripotent stem cells (iPSCs) also contain foci[62]. Fibroblasts from symptomatic and asymptomatic *C9ORF72* repeat carriers contain foci as well[61, 63]. In general, foci are predominantly localized in the nucleus and only sparsely in the cytoplasm[56, 58]. The number of foci per nucleus is usually low (1-3) but occasionally higher, especially for antisense foci[56, 58]. Sense and antisense foci can sometimes be found together in the same nucleus, but not necessary in the same spot. Around 14% of all nuclei in the frontal cortex, 7% of nuclei in the hippocampus and 3% of nuclei in the cerebellum contained both sense and antisense foci[56]. Co-localization of sense and antisense foci occurred for less than 15% nuclei in frontal cortex, hippocampus and cerebellum[56] and for 18% in spinal cord[51]. Any correlations between clinical features and the number of foci or their abundance in certain brain areas have not yet been determined. Correlation studies with other pathological features are also not yet performed.

## 2.2 RAN translation and DPR proteins

Repeat-associated non-AUG (RAN) translation was first described by Zu et al. in 2011 for spinocerebellar ataxia type 8 (SCA8) and myotonic dystrophy type 1 (DM1)[64]. By now, RAN proteins have also been reported in fragile X-associated tremor/ataxia syndrome (FXTAS), Huntington's disease (HD), DM type 2 (DM2) and SCA type 31 and 37 (SCA31/37)[65]. In 2013, it was shown that RAN translation also occurs in cases with the *C9ORF72* repeat expansion[57, 66, 67]. RAN translation occurs in all reading frames of sense and antisense transcripts resulting in 6 different DPRs: poly-glycine-alanine (GA), poly-glycine-proline (GP) and poly-glycine-arginine (GR) from the sense strand and poly-proline-alanine (PA), poly-proline-arginine (PR) and poly-proline-glycine (PG) from the antisense strand. Note that poly-GP and -PG contain similar repeated amino acids but can have a different N- and C-terminus. All RAN products were shown to be present in post-mortem brain tissue of C9FTD/ALS cases (figure 2)[52, 55, 57, 66, 67]. C-terminal specific antibodies were produced for almost all DPR, except for the antisense poly-PG DPR that harbors a stop codon immediately after the repeat[52, 55]. Expression of FMRpolyG (one of the RAN product of FXTAS) with its C-terminus in primary mouse cortical neurons and *Drosophila* models was more toxic than expression of FMRpolyG without C-terminus[68]. The possible toxicity of N- or C-termini of RAN products in C9FTD/ALS is yet unknown but might also influence DPR toxicity.

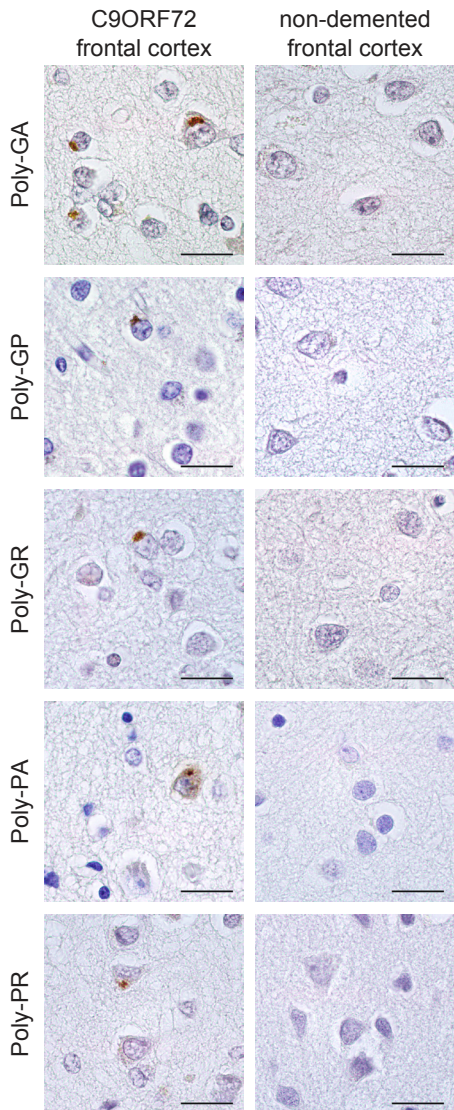


**Figure 2: DPR pathology in C9FTD cases.**

Frontal cortex post-mortem brain sections from C9FTD patients shows perinuclear DPRs stained with DAB (brown). Non-demented control frontal cortex did not contain any DPRs. Slides were counterstained with mayers heamatoxylin to visualize cell nuclei (blue). All scale bars are 20 $\mu$ m.

Ash et al. were the first to quantify the presence of DPR inclusions in 24 brain regions of 30 cases of C9FTD/ALS and found widespread neuronal cytoplasmic and small round intranuclear inclusions[67]. Since then, the presence of DPRs has been confirmed many times[51, 69]. For a detailed overview of the pathology, see the recent review of Vatsavayai who made a list of all 17 studies that have investigated DPR pathology so far[51]. In general, DPRs are most abundant in cortices, hippocampus (especially cornu ammonis), amygdala, thalamus and cerebellum granular layer. DPRs are less often observed in basal ganglia, brain stem nuclei and spinal cord[51]. To date, no DPRs have been found in as-

trocytes, microglia and oligodendrocytes[51], but they are present in ependymal and subependymal cells of the lateral ventricle[70]. Sense products are more frequent than antisense products and the order of abundance is poly-GA, -GP and -GR, -PA and -PR[51]. Several studies quantified absolute numbers of DPRs in several brain areas, but use different methods which makes it hard to combine results[69-73]. Furthermore, reported numbers of poly-GA aggregates vary from averages of 7 to 82 per mm<sup>2</sup> in the frontal cortex[69, 73]. Poly-GP and -GR vary from 11-23 and 4-14 aggregates per mm<sup>2</sup> in the frontal cortex[69, 73]. Absolute numbers of DPRs in spinal cord anterior horn are consistently low[69, 71]. Most DPRs are round or star-like neuronal cytoplasmic (NCI) inclusions, but can also be found as neuronal intranuclear inclusions (NII), dystrophic neurites (DNs) and diffuse cytoplasmic staining[51].

Different DPRs can be produced in the same cell and have been found to co-localize in hippocampal and cerebellar neurons[52]. Poly-GR neuronal cytoplasmic inclusions in these areas co-localized with poly-PR or poly-PA for about 5-18%[52]. Poly-GA has been reported to sequester poly-GR into aggregates[74]. The different DPRs all have different biophysical properties, which can influence their localization and aggregation pattern. Poly-GA is very hydrophobic, insoluble and aggregation prone and can form filamentous structures[75]. In contrast poly-GP is very soluble[76]. Poly-GR and -PR are positively charged, which could influence their interactions with other proteins[77]. The possible toxicity of DPRs is discussed in part 5 of the introduction.

The mechanism of RAN translation and factors needed to evoke this newly identified translation mechanism are largely unknown. Known factors influencing RAN translation are the upstream human flanking region that may contain some AUG-like start codons, repeat length and expression levels, but these factors can be different per reading frame[55, 57, 66, 78]. Poly-GA expression has been detected in constructs with repeat sizes of 38 or higher, suggesting that the translation mechanism has a certain repeat length threshold[66, 79]. Poly-GP products were only detected at very long repeat sizes (~145 repeats)[66]. Furthermore, frame shifting can produce combined DPRs in one product[80]. Several reports show that RAN translation is cap- and eIF4A-dependent[81, 82] but cap-independent translation initiation can also cause DPR expression[83]. More insight into the mechanism of RAN translation may provide suggestions for new therapeutic strategies, as new drugs that target this process could lower the expression levels of DPRs and thereby limit the impact of DPRs.



### 2.3 pTDP-43 and p62 pathology

TDP-43 is an RNA-binding protein involved in many cellular functions including splicing regulation and translational repression[93, 94]. Patients carrying the *C9ORF72* repeat expansion display pTDP-43 inclusions, which can be neuronal cytoplasmic and/or intranuclear[51, 84]. pTDP-43 is predominantly found in areas that are known to display substantial neurodegeneration[85-87]. In C9FTD patients, pTDP-43 aggregates are present in the frontal and temporal regions of the cerebral cortex and also in subcortical structures, including striatum, hippocampus, basal ganglia, and substantia nigra[84, 90]. pTDP-43 pathology in C9FTD is usually categorized as type B, with moderate amount of NCI and a few DNIs in all layers[51, 84, 90]. However, pTDP-43 inclusion load is variable and sometimes even undetectable[27, 91]. C9ALS patients present with NCI pTDP-43 in the spinal cord and extensive microglial pathology in the medulla and motor cortex[51, 92]. Almost all neurons with cytoplasmic pTDP-43 aggregates show nuclear clearing of TDP-43[88, 89]. Knock-out of mouse homologue TAR DNA binding protein (*TARDBP*) causes embryonic lethality and partial knock-down of TDP-43 causes motor neuron loss and a motor phenotype in mice[93, 94], indicating the importance of TDP-43.

In addition to pTDP-43-positive neuronal and glial inclusions, C9FTD/ALS patients exhibit ubiquitin- and p62-positive, pTDP-43-negative neuronal and cytoplasmic inclusions[51]. Binding of ubiquitin to a substrate protein can cause degradation via the proteasome, but can also affect cellular location, activity and protein interactions. P62, also called sequestosome 1, has multiple functions involved in the degradation of proteins. Once the polyubiquitin chain of a substrate protein binds to p62, it is transported to the proteasome for degradation. P62 is also involved the autophagic/lysosomal pathway by binding aggregated proteins prior to their inclusion in autophagosomes[95]. P62 pathology in C9FTD/ALS has a wider distribution than pTDP-43 pathology, extending to the pyramidal cell layer of the hippocampus, cortex, thalamus, basal ganglia, and cerebellum, where they far exceeded the number of pTDP-43 inclusions[36, 37]. After the identification of DPRs in aggregates in the brain of C9FTD/ALS patients, it became evident that DPRs were present in p62-positive/p-TDP-43-negative inclusions[51]. Double immunolabeling revealed co-localization of p62 and poly-GA in 75% of the inclusions and about 10% of all p62 inclusions were also positive for poly-AP and -PR staining[52].

The role of pTDP-43 and ubiquitin inclusions in the pathogenesis of the *C9ORF72* repeat expansion is not clear; they are believed to be harmful but

could also be a protective cell mechanism that has been proposed to cope with protein toxicity[96]. The co-localization with RNA foci and the relationship between DPRs and pTDP-43 is unknown and needs further investigation. Knowledge about the order of pathological events might give new insight in the pathogenesis of C9FTD/ALS.

### Pathological mechanisms of C9FTD/ALS

Three possible pathological mechanisms have been proposed to explain the pathogenic effect of *C9ORF72* repeat expansions; first, haploinsufficiency may lead to a partial loss of function of the endogenous *C9ORF72* protein product (part 3 of the general introduction). Secondly, RNA toxicity can be caused by the sequestration of RNA-binding proteins (RBPs) (part 4). Finally, production of t DPRs by RAN translation of the  $G_4C_2$  repeat can be toxic(part 5). In these parts of the introduction, we will focus on functional studies that could tell us more about the pathological mechanisms implicated in C9FTD/ALS.

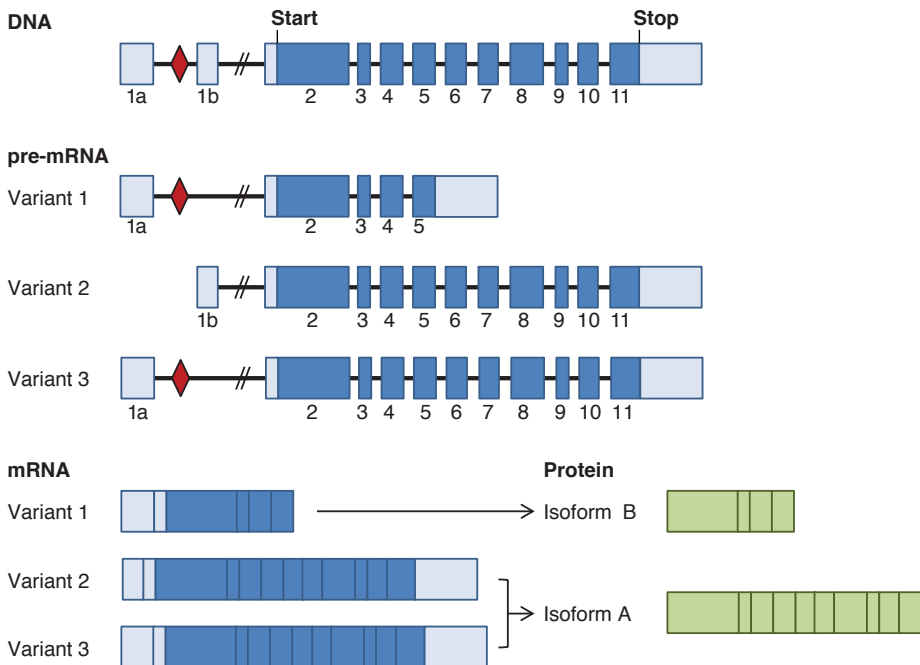


**Figure 3: The *C9ORF72* gene with the  $G_4C_2$  repeat expansion, its RNA transcripts and protein isoforms.** The  $G_4C_2$  repeat expansion is shown as red diamond and is located between two non-coding exons of the *C9ORF72* gene (exon 1a and exon 1b, light blue). RNA variant 1 is predicted to result in a short *C9ORF72* protein of 222 amino acids (exons 2–5, isoform B), whereas RNA variants 2 and 3 encode a long *C9ORF72* protein of 481 amino acids (exons 2–11, isoform A). Image adjusted with permission from Gendron et al., 2017[98] Copyright @ Cold Spring Harbor Press.

### 3. Loss of function

#### 3.1 Expression pattern of the *C9ORF72* gene

The *C9ORF72* gene is located on chromosome 9p21 and consists of 11 exons. Pre-mRNA transcript variants 2 and 3 encode C9ORF72-long protein (isoform A, 481 amino acids, exons 2-11), and transcript variant 1 encodes C9ORF72-short protein (isoform B, 222 amino acids, exons 2-5). The hexanucleotide expansion is located between exon 1a and 1b. This is part of the promoter region of transcript variant 2 or in the first intron of transcripts 1 and 3 (figure 3). All three transcript variants of the *C9ORF72* mRNA are present in a large variety of tissues; kidney, lung, liver, heart, testis, lymphoblasts, brain; cerebellum, frontal cortex, hippocampus[22], temporal cortex, hypothalamus, medulla, occipital cortex, putamen, spinal cord, thalamus, white matter and substantia nigra[23]. Expression of *C9ORF72* is also high in CD14+ myeloid cells, involved in immunity[97]. Especially variant 2 is highly expressed in the CNS[97].

Xi et al. detected two cytosine-phosphate-guanine (CpG) islands immediately flanking the hexanucleotide repeat of *C9ORF72*, but only the region 5' of the repeat revealed evidence of hypermethylation[99]. This 5' CpG island was significantly more methylated in C9ALS expansion carriers versus non-*C9ORF72* ALS cases and healthy controls[77]. Another study found that hypermethylation extended into the repeat expansion and is associated with reduced expression of *C9ORF72* mRNA[100]. Demethylation by 5-aza-2-deoxycytidine (5-AZA) or bromodomain-inhibitor treatment of patient derived fibroblasts increased *C9ORF72* mRNA expression[101, 102]. Histone methylation can also reduce gene expression and can be influenced by age[101] and oxidative stress[103]. Histones that are trimethylated at lysine residues strongly bind to *C9ORF72* expanded repeats in frontal cortex and cerebellum tissue, but not to control length repeats[101]. Hypermethylation has been associated with reduced RNA foci, DPR levels and reduced neuronal and gray matter loss in patients with C9FTD/ALS[104, 105]. But the effect of hypermethylation is still under debate, as it has been linked to later age-of-onset and a longer survival of C9FTD/ALS patients in some studies[44, 106] but reduced disease duration before death in another study[99].

The reduction of *C9ORF72* mRNA transcripts has been validated by multiple studies and occurs in blood lymphocytes, iPSC derived neurons, frontal cortex, motor cortex, cerebellum and spinal cord of *C9ORF72* carriers[77]. The reduction in mRNA levels is on average 50% compared with controls[27, 107]. Sense and antisense pre-mRNA transcripts upstream of the repeat and transcripts that contain intron 1 are elevated[53, 77, 98], and seem to terminate in the

repeat[55]. Higher levels of transcript 1 in the frontal cortex and cerebellum are associated with increased survival[53], which might implicate a role for the short isoform of the C9ORF72 protein in neuronal survival.

Next to mRNA levels, C9ORF72 protein levels also seem to be reduced in the cerebellum of C9ORF72 repeat carriers[108]. However, no associations between cerebellar protein levels and clinical phenotypes were observed[108]. Some studies found almost 50% reduction in the frontal cortex, occipital cortex but not in the motor cortex nor cerebellum[72, 109]. The long isoform (C9-L) seems to be the predominant expressed isoform, but expression levels are very low[108]. An antibody against C9-L shows a diffuse cytoplasmic staining in neurons and labeled large speckles in cerebellar Purkinje cells[110]. In human iPSC derived motor neurons, C9-L localized to lysosomes and pre-synapses[108]. The short isoform (C9-S) is more difficult to detect but a localization along the nuclear membrane has been reported[110]. Aberrant localization of C9-S to the plasma membrane was observed in diseased motor neurons of post-mortem spinal cord sections of C9ALS patients[110]. The different localization of the two C9ORF72 protein isoforms could implicate that they have different cellular functions.

### 3.2 Cellular function of the C9ORF72 protein

The C9ORF72 gene is highly conserved between vertebrate species[111]. The hexanucleotide expansion itself is only conserved within primates but the genomic site is also conserved between mouse and human (58.3%)[111]. This could indicate an important regulatory function of this genomic area[111]. The C9ORF72 protein is a homologue of 'differentially expressed in normal and neoplastic cells' (DENN) proteins, which are Rab-GDP/GTP exchange factors (GEFs)[112]. GEFs interact with the GDP-bound, inactive form of Rabs and exchange GDP for GTP to activate the Rab. Rabs are small GTPases, important in signal transduction, endo- and exocytosis and intracellular (vesicle) trafficking. Membrane trafficking can be fine-tuned by the modulation of Rab activity[113]. Some DENN domains interact with one Rab while mediating GEF activity of a second Rab, so DENN domains may be the link between different Rab cell signaling pathways[114]. Importantly, several DENN domain proteins have been linked to neurodegeneration[115, 116].

Knock-down of C9ORF72 protein in HeLa, HEK295 and SY5Y cells and primary murine neurons inhibits autophagy and causes p62 and pTDP-43 aggregation[117, 118]. Overexpression of C9ORF72 protein in the same cell lines increases the amount of autophagosomes[117]. Especially the long isoform of

C9ORF72 protein seems to be implicated in autophagy[118]. C9ORF72 protein binds SMCR8 and WDR41 and together with these proteins exchanges GDP for GTP of several Rabs (Rab1a, 3, 5, 7, 8a, 11 and 39b have all been implicated) [108, 117-121]. In this way, C9ORF72 protein regulates Rab-dependent trafficking of the ULK1 autophagy initiation complex to the phagophore [117, 118, 120]. SMCR8 is phosphorylated by TBK1, which might enhance C9ORF72 GEF activity and autophagy[118]. Loss-of-function mutations in TBK1 are also associated with FTD and ALS[122]. Impaired autophagy and enhanced sensitivity to autophagy inhibitors is also observed in iPSC derived neurons from C9FTD/ALS patients[117, 123, 124], which was rescued by increasing autophagy with an SRC-ABL pathway inhibitor[125].

Next to its function in autophagy, C9ORF72 protein also plays a role in endosomal and lysosomal trafficking. Reduced endocytosis and reduced trafficking of endosomal vesicles was observed after knock-down of C9ORF72 protein in neuronal cell cultures[121] and in patient fibroblasts and iPSC derived neurons[124]. C9ORF72 protein interacts with endosomes and was required for normal intracellular vesicle trafficking in iPSC derived motor neurons of C9ALS patients[126]. These motor neurons also showed reduced number of lysosomes compared with motor neurons of controls[126]. Furthermore, motor neurons also show accumulation of glutamate receptors and enhanced sensitivity to excitotoxicity[126, 127].

### 3.3 Animal models of C9ORF72 loss-of-function

To study loss of C9ORF72 *in vivo*, Therrien et al. created a null mutation in the *C. elegans* C9ORF72 orthologue F18A1.6, also called alfa-1[128]. Alfa-1 null mutants are morphologically normal but develop age-dependent paralysis, similar to ALS models expressing TDP-43 and FUS proteins in *C. elegans* motor neurons[129]. The motor phenotype is probably caused by the loss of GABAergic motor neurons, which coordinate body movement in worms[128]. Alfa-1 mutants were highly sensitive to osmotic stress, which led to increased motor neuron degeneration[128].

Knockdown of the zebrafish orthologue of C9ORF72 (zC9ORF72) by two specific antisense morpholino oligonucleotides causes locomotion deficits and results in major morphological abnormalities[130]. Similar to previous genetic models of ALS in zebrafish (TDP-43, FUS and SOD1)[131, 132], knockdown of zC9ORF72 resulted in shortened and disturbed arborization of motor neuron axons[130]. Touch-evoked escape response and spontaneous swimming was also

deficient in a large percentage of the morpholino-injected zebrafish (morphants) [130]. All phenotypes were rescued by the introduction of human *C9ORF72* mRNA long transcript, illustrating specificity of the knockdown[130].

Next to the research in worms and fish, 10 *C9ORF72* knock-out mouse models have been published to date. For a list and overview of these studies, please see the recent review of Balendra & Isaacs[77]. In all studies, heterozygous mice are completely normal, only homozygous knock-out mice have a reduced live span[77]. Homozygous knock-out mice show immune system dysregulation, enlarged spleen and lymph nodes, increased levels of cytokines and changes in the number of myeloid and lymphoid cells[77]. Transcriptomics confirmed changes in immune pathways, also observed in the CNS of C9FTD/ALS patients[133]. Interestingly, C9FTD/ALS patients show an increased prevalence of autoimmune disease[134, 135]. None of the mouse models show neuronal loss and FTD or ALS phenotypes[77], only some mild late-onset motor and cognitive defects have been found in two models[136, 137]. This suggests that haploinsufficiency is not sufficient to cause C9FTD/ALS symptoms. The function of the *C9ORF72* protein in both autophagy and endosome and lysosome function and trafficking might influence disease progression. Future research will be needed to elucidate interactions between loss- and gain-of-function mechanisms in C9FTD/ALS.

#### **4. RNA gain of function**

The possibility of a RNA toxic gain of function mechanism was already proposed at the discovery of the *C9ORF72* repeat expansion by DeJesus-Hernandez et al.[22] and Renton et al.[23] in 2011. The mechanism of RNA gain-of-function is well known from other repeat disorders[62]. In myotonic dystrophy 1 the expanded CUG repeat sequesters muscleblind-like 1 (MBNL1), causing abnormal splicing of key transcripts in muscle and brain. The resulting toxicity can be suppressed by boosting MBNL protein expression[138]. The  $G_4C_2$  expansion in the *C9ORF72* gene might work in a similar manner. It can form multiple secondary structures that can bind and sequester several proteins, summarized below.

##### 4.1 Secondary structures of the $G_4C_2$ repeat

The sense strand of the  $G_4C_2$  repeat is capable of forming G-quadruplexes (a stack of G-quartets on a square configuration) both on DNA and RNA level[78, 139-141]. A graphic interpretation of the secondary structures are shown in figure 4. G-quadruplexes have been known to occur in telomeric regions, but have now

also been shown to occur in promotor and intronic regions of more than hundred genes[142]. G-quadruplexes can influence multiple biological processes including transcription, alternative splicing, translation regulation, genetic instability, telomere regulation and RNA transport and degradation[140, 143]. Interestingly, G-quadruplexes located in the 3' UTR of mRNAs can alter the localization of mRNAs to dendrites via interaction with the FMRP protein[144]. However, the presence of G-quadruplexes *in vivo* is not confirmed yet due to the lack of visualization techniques[142]. Transcribed  $G_4C_2$  repeat RNA can bind to  $C_4G_2$  repeat DNA or vice versa and form R-loops, a three-strand structure formed by a DNA:RNA hybrid plus a displaced DNA strand[139, 145]. Formation of R-loops can cause transcription disruption and genome instability[62, 139, 145]. The C-rich antisense sequence might also be able to form I-motifs, a four-stranded secondary structure, on DNA and RNA level[146, 147].  $G_4C_2$  repeat-containing RNA may even form more structures, like hairpins[78, 139], stem-loops and RNA duplexes[62, 77].

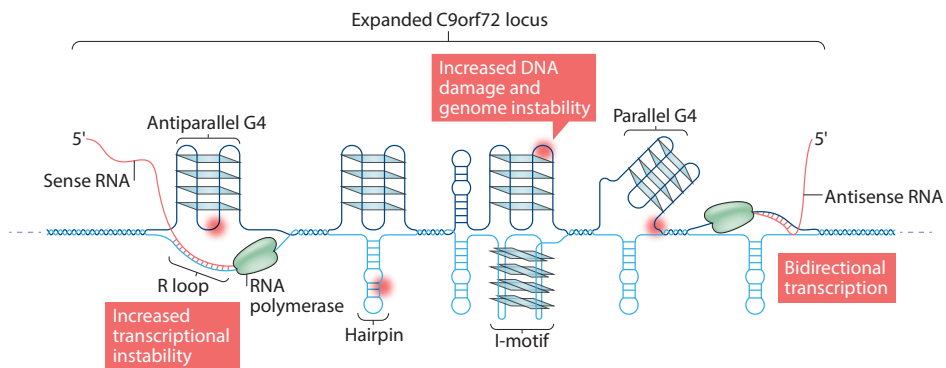


**Figure 4: Schematic representation of secondary structures formed by the  $G_4C_2$  repeat expansion on DNA and RNA level.** Hairpins and G-quadruplexes (a stack of G-quartets on a square configuration) can be present on both DNA and RNA level. Transcribed repeat RNA can bind to repeat DNA and form R-loops, a three-strand structure formed by a DNA:RNA hybrid plus a displaced DNA strand. The C-rich antisense sequence might also be able to form I-motifs, a four-stranded secondary structure, on DNA and RNA level. Secondary structures can lead to genomic and transcriptional instability and cause DNA damage. Image adjusted with permission from Haeusler et al., 2017.[62] Copyright @ Nature reviews neuroscience.

#### 4.2 Sequestration of proteins by RNA foci

Repeat-containing RNA or secondary RNA structures can be bound by several RNA-binding proteins. The secondary structure of the *C9ORF72* repeat can influence the binding affinity to several proteins, for example nucleolin and Ran-GAP preferentially bind G-quadruplexes but hnRNP-H binds both hairpins and G-quadruplexes[62]. Several studies using pull-down or proteomic arrays have delivered large lists of  $G_4C_2$  repeat RNA-binding proteins, which sometimes show overlap[62]. Binding of important cellular proteins to *C9ORF72* repeat RNA or their sequestration in RNA foci can cause depletion of these proteins and subsequent dysfunction of cellular processes. We summarized proteins that specifically have been shown to co-localize with RNA foci in table 1. Some proteins have been validated to co-localize with RNA foci in C9FTD/ALS patient iPSC derived neurons or in post-mortem brain sections of C9FTD/ALS patients. We will shortly introduce these proteins.

ADARB2 was found to interact with 5'Cy5-labeled 6.5x  $G_4C_2$  repeat RNA hybridized to a protein array and co-localizes with sense foci in C9ALS iPSC derived neurons[107]. Knockdown of ADARB2 leads to a 50% reduction of sense RNA foci in iPSC derived neurons, which might indicate that ADARB2 enables the formation or stabilization of RNA foci[107]. C9ALS iPSC derived neurons show enhanced sensitivity to glutamate, and knock-down of ADARB2 in control iPSC derived neurons causes the same phenotype[107]. This suggests that the sequestration of ADARB2 in RNA foci of C9ALS patients could lead to enhanced vulnerability to glutamate of C9ALS iPSC derived neurons[107]. ADARB2 is part of the RNA editing family which performs post-transcriptional deamination of adenosine to inosine (A-I) of mRNAs and one of the targets of ADAR proteins is the Q/R site of the GluR2 AMPA receptor[156].

ALYREF was found to bind 5x  $G_4C_2$  biotinylated RNA in a pull-down experiment using whole cell and nuclear extract of SH-SY5Y cells and extract of dissected human cerebellum[61]. Cooper-Knock found 26% co-localization of sense RNA foci with ALYREF in cerebellar granule cells and 29% co-localization in motor neurons of C9ALS cases[61]. In another study they showed 7.8% co-localization with *antisense* foci in cerebellar Purkinje neurons of C9ALS patients[60]. ALYREF is a nuclear protein that functions as a molecular chaperone and is involved in the nuclear export of spliced RNAs[157].

By far the biggest group of RNA-binding proteins known to bind  $G_4C_2$  repeat RNA is the heterogeneous nuclear ribonucleoprotein group (hnRNP). Examples are hnRNP-A1[150, 151], -A2/B1[123, 150], -A3[150], -H[152, 158], -F[139],



Protein	Identified by	Detection method	Co-localization with RNA foci	Confirmed by others	Function (source: Uniprot)
ADARB2	Donnelly et al., 2013[107]	6.5x G <sub>4</sub> C <sub>2</sub> repeat RNA proteome array to yeast-expressed human proteome.	ADARB2 co-localization with G <sub>4</sub> C <sub>2</sub> RNA foci in the nucleus of C9 iPSNs and C9ALS motor cortex[107].	Not mentioned as hit in any other screen - to our knowledge.	Post-transcriptional modification: A-I editing of mRNAs.
ALYREF	Cooper-Knock et al. 2014[61]	Pull-down with 5x G <sub>4</sub> C <sub>2</sub> RNA and whole cell and nuclear extract of SH-SY5Y cells and dissected human cerebellum extract.	In cerebellar granule cells 26% co-localization of RNA foci with ALYREF. In motor neurons 29% co-localization[61]. In cerebellar Purkinje neurons 7.8% co-localization with <i>antisense</i> foci[60].	Cooper-Knock et al., 2015 confirmed co-localization with <i>antisense</i> foci[60]. Hautbergue et al., 2017 confirmed binding with G <sub>4</sub> C <sub>2</sub> RNA[148].	Nuclear protein that functions as a molecular chaperone and is involved in the nuclear export of spliced RNAs.
eIF2 $\alpha$ and $\beta$	Rossi et al., 2015[149]	Pull-down with 31x G <sub>4</sub> C <sub>2</sub> repeats with extract from mouse brain and spinal cord.	Overexpression of 31x G <sub>4</sub> C <sub>2</sub> in NSC34 and HeLa cells caused sequestration of eIF2 $\alpha$ in sense RNA foci[149].	Not mentioned as hit in any other screen - to our knowledge.	Phosphorylation of eIF2 $\alpha$ causes translation inhibition.
FUS	Mori et al., 2013[150]	23x G <sub>4</sub> C <sub>2</sub> repeat RNA pull down with HEK293 nuclear cell extract.	Overexpression of 31x G <sub>4</sub> C <sub>2</sub> in NSC34 and HeLa cells caused co-localization of FUS with sense RNA foci[149]. No co-localization in the cerebellar granule layer[61]. Not found in iPSNs of C9ALS patients in 3 studies [107, 123, 151].	Rossi et al., 2015[149]. Cooper-Knock et al. 2014[61] found interaction but no co-localization with RNA foci.	RNA-binding protein, part of the hnRNP complex. Involved in transcription, splicing and mRNA transport.

hn-RNP-A1	Mori et al., 2013[150]	23x G <sub>4</sub> C <sub>2</sub> repeat RNA pull down with HEK293 nuclear cell extract.	In cerebellar granule cells 27% co-localization of RNA foci with hnRNP-A1[61]. In cerebellar Purkinje neurons 21% co-localization with <i>antisense</i> foci[60]. Co-localized with RNA foci in iPSC derived motor neurons in one study[151], but not in another study[107].	Sareen et al., 2013[151]. Cooper-Knock et al. 2014[61] and 2015[60].	The hnRNP family is involved in pre-mRNA splicing and the export of mRNA to the cytoplasm. HnRNP-A1 is one of the most abundant proteins of hnRNP complexes. hnRNP A2/B1 contains two RNA recognition motifs that provide sequence-specific recognition of RNA substrates. HnRNP-A1 and -A2/B1 are known binding partners of TDP-43. hnRNP-A3 plays a role in cytoplasmic trafficking of RNA. hnRNP-H is involved in exon skipping.
hn-RNP-A2/B1	Mori et al., 2013[150]	23x G <sub>4</sub> C <sub>2</sub> repeat RNA pull down with HEK293 nuclear cell extract.	Not found in iPSCs of C9ALS patients in two studies[123, 151].	Rossi et al., 2015[149] confirmed binding to 31x G <sub>4</sub> C <sub>2</sub> repeat RNA.	
hn-RNP-A3	Mori et al., 2013[150]	23x G <sub>4</sub> C <sub>2</sub> repeat RNA pull down with HEK293 nuclear cell extract.	hnRNP-A3 positive neuronal cytoplasmic and intranuclear inclusions in the hippocampus DG and granular layer of the cerebellum[150]. hnRNP-A3 did not co-localize with RNA foci in iPSC derived motor neurons[151].	Not mentioned as hit in any other screen - to our knowledge.	
hn-RNP-H	Lee et al., 2013[152]	Found in pull down with 72x G <sub>4</sub> C <sub>2</sub> and nuclear lysate from SH-SY5Y cells and in second independent pull down with 48x G <sub>4</sub> C <sub>2</sub> repeats and rat brains.	hnRNP-H co-localized with 70% of G <sub>4</sub> C <sub>2</sub> RNA foci in the cerebellum of C9FTD/ALS patients[152] and [61]. In motor neurons 19% co-localization[61]. In cerebellar Purkinje neurons 3.4% co-localization with <i>antisense</i> foci[60]. Not found in iPSCs of C9ALS patients[123].	Haeusler et al., 2014[139], Mori et al., 2013[150], Xu et al., 2013[153] and Rossi et al., 2015[149]. Cooper-Knock et al. 2014[61]. 2015[60].	

ILF2 and ILF3	Mori et al., 2013[150]	23x G <sub>4</sub> C <sub>2</sub> repeat RNA pull down with HEK293 nuclear cell extract.	Overexpression of 31x G <sub>4</sub> C <sub>2</sub> in NSC34 and HeLa cells caused sequestration of ILF3 with sense RNA foci[149].	Xu et al., 2013[153]. Cooper-Knock et al. 2014[61] found interaction but did not mention co-localization with RNA foci.	RNA-binding protein that plays an essential role in the biogenesis of circular RNAs. Participates in the innate antiviral response.
Nucleolin (NCL)	Haeusler et al., 2014[139]	4x G <sub>4</sub> C <sub>2</sub> repeat RNA in hairpin or G-quadruplex conformation pull down with HEK293T cells. NCL preferably binds G-quadruplexes.	Nucleoli fractured in the nucleus of C9ALS iPSCs[139]. Nucleolin co-localizes with RNA foci in the motor cortex of C9ALS patients[139]. In cerebellar Purkinje neurons <u>no</u> co-localization of nucleolin with <i>antisense</i> foci[60].	Cooper-Knock et al. 2014[61] found interaction but no co-localization with RNA foci[60].	The major nucleolar protein, associated with intranuclear and pre-ribosomal particles. It induces chromatin de-condensation by binding to histone H1.
Pur-alpha	Xu et al., 2013[153]	10x G <sub>4</sub> C <sub>2</sub> repeat RNA pull down with mouse spinal cord lysates.	Pur-alpha inclusions in C9FTD cerebellum[153]. Co-localization of pur-alpha and RNA foci in iPSC derived motor neurons[151] and a zebrafish model for C9orf72[154]. Not found in iPSCs of C9ALS patients of another study[107].	Sareen et al., 2013[151] Cooper-Knock et al., 2014[61] and Rossi et al., 2015[149].	DNA and RNA binding protein, functions in initiation of DNA replication, DNA repair, control of transcription and mRNA translation.

RanGAP	Donnelly et al., 2013[107]	6.5x G <sub>4</sub> C <sub>2</sub> repeat RNA proteome array to yeast-expressed human proteome.	RanGAP co-localized with G <sub>4</sub> C <sub>2</sub> RNA foci in C9ALS iPSNs and mis-localized in C9ALS motor cortex[155].	Zhang et al., 2015 [155] showed that Ran-GAP preferentially binds the sense RNA G-quadruplex.	RanGAP functions in the cytoplasm to stimulate Ran, to change GTP to GDP, required for nuclear transport.
SC35	Lee et al., 2013[152]	Not found in pull down with 72x G <sub>4</sub> C <sub>2</sub> and nuclear lysate from SH-SY5Y cells.	SC35 co-localized with G <sub>4</sub> C <sub>2</sub> RNA foci in SH-SY5Y cells transfected with 48x G <sub>4</sub> C <sub>2</sub> repeat[152], but rarely (<5%) co-localized with G <sub>4</sub> C <sub>2</sub> RNA foci in cerebellum of C9FTD/ALS patients[152].	Not mentioned as hit in any other screen - to our knowledge.	Serine-arginine-rich splicing factor 35 (SC35) is probably involved in intron recognition and spliceosome assembly.
SRSF2 = SF2	Coo-per-Knock et al. 2014[61]	SRSF2 found in pull-down with 5x G <sub>4</sub> C <sub>2</sub> RNA and whole cell and nuclear extract of SH-SY5Y cells and dissected human cerebellum whole extract.	In cerebellar granule cells 33% co-localization of RNA foci with SRSF2[61]. In motor neurons 30% co-localization[61]. In cerebellar Purkinje neurons 34% co-localization with <i>antisense</i> foci[60]. SF2 co-localized with G <sub>4</sub> C <sub>2</sub> RNA foci in SH-SY5Y cells transfected with 48x G <sub>4</sub> C <sub>2</sub> repeat[152], but rarely (<5%) co-localized with G <sub>4</sub> C <sub>2</sub> RNA foci in cerebellum of C9FTD/ALS patients[152].	Hautbergue et al., 2017 showed binding of SRSF with G <sub>4</sub> C <sub>2</sub> RNA[148]. Interaction of SF2 with G <sub>4</sub> C <sub>2</sub> RNA confirmed by Reddy et al., 2013[143].	Serine-arginine-rich splicing factor 2 (SRSF2), alternative name pre-mRNA-splicing factor SF2, plays a role in preventing exon skipping, ensuring splicing accuracy and regulating alternative splicing.

**Table 1: List of proteins that interact with G<sub>4</sub>C<sub>2</sub> repeat RNA and co-localized with RNA foci. Multiple studies have found large lists of proteins that are capable to interact with G<sub>4</sub>C<sub>2</sub> repeat RNA. We focused on proteins that have been shown to localize to RNA foci**

-K[139], -L[150] and -U[139]. Sequestration of these proteins can lead to splicing alterations of many genes[62]. hnRNP-A1 and -A3 are known to shuttle between nucleus and cytoplasm and function in pre-mRNA splicing, nuclear import and cytoplasmic trafficking of mRNA, mRNA stability and turnover and translation[150]. Cooper-knock found 27% co-localization of sense RNA foci with hnRNP-A1 in cerebellar granule cells[61] and 21% with *antisense* foci in cerebellar Purkinje neurons in post-mortem brain tissue of C9ALS patients[60]. C9FTD/ALS cases show a reduction in nuclear staining of hnRNP-A3 and the appearance of dot-like nuclear and cytoplasmic inclusions in neurons[150]. About 20 percent of p62-positive inclusions co-localized with hnRNP-A3 staining in hippocampus dentate gyrus (DG) of both C9FTD and C9FTD/ALS[150]. Lee et al. (2013) found hnRNP-H in pull-down experiments with biotinylated 48x G<sub>4</sub>C<sub>2</sub> repeat RNA[152]. hnRNP-H co-localized with about 70% of sense RNA foci in C9ALS/FTD patient cerebellum[152]. hnRNP-H is a splicing factor that is necessary to include exon 7 into the mature TARBP2 RNA, it strongly binds to G-rich intronic sequences to enhance exon skipping and it can also bind G-rich RNA quadruplexes[152]. Saareen et al. (2013) found that RNA foci frequently co-localized with hnRNP-A1 and Pur-alpha in C9ALS iPSC derived neurons, but could not confirm involvement of hnRNP-A3 and -A2/B1[151]. The hnRNP protein family contains an RNA recognition motif also present in pTDP-43 and FUS[62]. HnRNP-A1 and -A2/B1 are known binding partners of TDP-43[159] and were recently linked to ALS[160]. In conclusion, the involvement of the hnRNP protein family seems obvious, but the contribution of each individual protein it is not clear yet.

Pur-alpha is another G<sub>4</sub>C<sub>2</sub> RNA binding protein that was found to co-localize with RNA foci in C9ALS iPSC-derived motor neurons[151] and in a zebrafish model for C9ORF72 repeat toxicity[154]. Pur-alpha was also found in intranuclear inclusions in the molecular layer of the cerebellum of C9FTD cases, although these were sometimes also observed in non-demented controls[153]. Pur-alpha is a DNA- and RNA-binding protein implicated in the initiation of DNA replication, DNA repair, control of transcription, mRNA translation and cell cycle regulation[161]. Moreover, it is critical for postnatal brain development and is involved in the transport of specific mRNAs to the synapse[161].

Nucleolin was found to bind the G<sub>4</sub>C<sub>2</sub> G-quadruplex structure and co-localized with foci in motor cortex of C9FTD/ALS patients[139]. C9ALS iPSC derived neurons[139] and C9-BAC primary mouse neurons showed dispersion of nucleolin from the nucleolus[162]. Lymphoblastoid cell lines, fibroblasts and iPSC derived neurons from C9ALS patients showed a disturbed nucleolus and more

processing-bodies, indicative of nucleolar stress[139]. Some studies have shown that RNA foci sometimes surround the nucleolus and form a so called 'peri-nucleolar' studding pattern[51, 59, 163, 164]. Especially antisense foci were found to surround the nucleolus, and did so more often in disease relevant brain areas[164]. Neurons with sense foci positioned around their nucleoli exhibited larger nucleoli than cells without peri-nucleolar localization of sense foci[163]. However, another study investigated hippocampus cornu ammonis (CA) and frontal cortex of C9FTD cases and healthy controls and did not find any difference in the size of the nucleoli[70]. Thus, peri-nucleolar studding remains an enigmatic phenomena that awaits further study.

$G_4C_2$  repeat RNA associates with paraspeckle proteins and RNA like SFPQ and hLinc-p21[165]. Paraspeckles are ribonuclear bodies with unknown function, but they could affect post-transcriptional processes and cause nuclear retention of RNA's[165]. An increase in paraspeckle bodies has been reported in the early phase of motor neuron degeneration in ALS[166]. Ran-GAP is also capable of binding  $G_4C_2$  RNA[107] and is found to co-localize with  $G_4C_2$  RNA foci in C9ALS iPSC derived neurons and mis-localizes in C9ALS motor cortex[155]. Expression of Ran-GAP rescued repeat toxicity in *Drosophila* eyes and motor neurons[155]. This indicates the involvement of nucleocytoplasmic transport in C9FTD/ALS pathogenesis[155].

Finally, serine-arginine-rich splicing factor 2 (SRSF2, alternative name SF2) and serine-arginine-rich splicing factor 35 (SC35) are both found to co-localize with  $G_4C_2$  RNA foci in SH-SY5Y cells transfected with 48x  $G_4C_2$  repeat[152], but rarely (<5%) co-localized with  $G_4C_2$  RNA foci in cerebellum of C9FTD/ALS patients[152]. In another study, SRSF2 showed a higher percentage (33%) of co-localization with RNA foci in cerebellar granule cells and in motor neurons (30%) of C9ALS patients[61]. SRSF2 also co-localizes with *antisense* foci, for 34% in Purkinje neurons of C9ALS cases[60]. SRSF2 and SC35 ensure the accuracy of splicing and regulating alternative splicing, which again indicates that important splicing factors can be sequestered by RNA foci.

All of the above and in table 1 mentioned proteins that are known to bind RNA foci have a function in RNA processing. This can be at the initiation of transcription (eIF2 $\alpha$  and  $\beta$ ), chromatin remodeling (nucleolin) and transcription control (pur-alpha, FUS). Next are factors involved in splicing of mRNAs (FUS, hnRNP-A1, -A3, ILF2/3, SC35, SRSF2, SF2), exon skipping (hnRNP-H, SRSF2, SF2) or other modifications (ADARB2). Also mRNA transport (FUS, hnRNP-A1, -A3) and export out of the nucleus (ALYREF, Ran-GAP) can be affected by pro-

teins that are sequestered in RNA foci. Finally, proteins that function in cytoplasmic trafficking of mRNAs (hnRNP-A1, -A3), mRNA stability (hnRNP-A1, -A3) and translation (hnRNP-A1, -A3, pur-alpha) can also be sequestered by RNA foci. Analyses of transcriptome changes in iPSC derived neurons[107, 151] and different brain areas of C9FTD/ALS cases[107, 158, 167] revealed aberrant gene expression and splicing. Together, this could implicate that RNA toxicity of the G<sub>4</sub>C<sub>2</sub> repeat expansion mainly works via the sequestration of factors involved in RNA processing.

## 5. DPR toxicity

The impact of DPRs on cellular functioning has been studied extensively. In this part of the introduction, we first describe studies that examine DPR toxicity and later focus on downstream mechanism underlying their toxicity. To complete the picture of gain-of-function mechanisms, we will also summarize all gain-of-function mouse models.

### 5.1 Direct toxicity of different DPRs

To study the toxicity of DPRs without the relative contribution of RNA gain-of-function mechanisms, Mizielinska was the first to change the G<sub>4</sub>C<sub>2</sub> repeat sequence into alternative codons that contain A or T nucleotides but encode the same dipeptides[168]. Multiple cell and animal models have now indicated the detrimental effect of expression of the arginine-containing DPRs, poly-GR and poly-PR[77, 168] and the slightly less toxic poly-GA[75, 77]. Synthetic poly-GA, -GR and -PR are toxic to primary neurons and cultured human astrocytes[169, 170]. Transfection of constructs encoding DPRs into different cell lines indicates that of all DPRs, especially poly-GR and poly-PR are toxic[171-174]. Not all of these studies found an effect of poly-GA, but some others focused only on poly-GA and confirmed its toxicity *in vitro*[75, 175]. When expressed in *Drosophila* models, poly-GR and -PR caused reduced survival, a locomotor phenotype and severe eye degeneration[74, 168, 171, 176-178]. Poly-GA only caused a mild reduction in survival in one of these studies[168], and poly-PA and poly-GP did not show toxic effects in *Drosophila*[168, 171, 177]. In zebrafish, expression of poly-GR caused developmental abnormalities and reduced locomotor activity and survival[179]. Also expression of poly-GA evoked toxic effects in zebrafish[180].

Even though these studies clearly show a toxic effect of DPRs, caution is required with interpretation, as they often use overexpression systems which might not reflect the endogenous mechanisms that occur in C9FTD/ALS patients.

## 5.2 Downstream mechanisms

DPRs can bind many proteins and molecules in the cell and thus affecting multiple molecular pathways. To date, an overwhelming amount of different downstream mechanisms implicated in the pathogenesis of DPRs have been reported. We will summarize these processes and will mainly focus on the effect of poly-GR, –GA and -PR, since they are considered to be the most toxic dipeptides (as discussed above).

Poly-GR and poly-PR are capable of binding to proteins that contain low-complexity domains (LCDs)[176, 181]. Many RNA-binding proteins, such as TDP-43 and FUS, contain LCDs[182]. LCD proteins can form droplets by liquid-liquid phase separation. In this way, LCD proteins can form membrane-less organelles, such as nucleoli, the nuclear pore complex and stress granules. DPRs can disturb this process and have been shown to alter the dynamics of stress granules[173, 176, 183]. Nucleolar stress can also lead to splicing and mRNA translation defects[173, 176]. Nucleocytoplasmic transport (NCT) defects are often found in *Drosophila* models of C9ORF72[155, 177, 178]. Knock-down of several LCD proteins rescues the eye phenotype in *Drosophila* that express poly-GR[176].

Interactome studies indicate that poly-GR and poly-PR can bind many RNA-binding proteins, nucleolar proteins, hnRNPs and spliceosome components and thereby disrupt splicing[173, 174, 184]. Especially the U2 small nuclear ribonucleoprotein (snRNP) is found in many interactome studies[176, 181, 184] and is mis-localized in the cytoplasm of C9FTD and C9ALS iPSC derived motor neurons[184]. Splicing alterations are found in postmortem brain tissue of C9ALS patients[158] and 50% of these are U2 snRNP-dependent[184]. Poly-GR and –PR accumulated in the nucleolus in cultured cells, primary neurons, astrocyte cultures, C9FTD/ALS iPSC derived neurons and *Drosophila*, leading to altered nucleolar morphology[70, 163, 169, 171, 173, 185]. Nucleolar changes have also been observed in C9FTD/ALS patients[163], that is, overall *smaller* neuronal nucleoli were observed but nucleoli were *larger* in neurons that contained poly-GR aggregates[163].

The aberrant formation of RNA-binding protein complexes and altered splicing processes due to expression of poly-GR and –PR may affect ribosomal RNA maturation and ribosome biogenesis[169]. Poly-GR and -PR can also directly bind to mRNAs, ribosomal proteins and translation initiation factors and as a consequence block translation[174]. Translation inhibition and accumulation of poly-A mRNA have been shown in both NSC34 and HeLa cell lines[149, 174,



176]. Poly-GR co-localized with hnRNP-A1, an RNA-binding protein, in post-mortem brain sections of C9ALS patients[174] and altered the biophysical properties of hnRNP-A1 *in vitro*[176]. Furthermore, overexpression of poly-GR and poly-PR caused stress granule formation in HeLa cells[149, 176, 183] and primary neurons[171]. Stress granules are cytoplasmic aggregates of RNAs and proteins with stalled translation pre-initiation complexes and are a marker of translation arrest.

Next to affecting RNA metabolism, poly-GR and –PR also affect nucleocytoplasmic transport. This can occur in multiple ways. First, splicing of Ran-GAP was found to be altered[169]. Second, importins, NUPs and the lamin B receptor can bind to poly-GR and –PR which might reduce their functionality[176, 186, 187]. Poly-PR can even directly bind to the nuclear pore and reduce trafficking through the pore[187]. Third, NCT factors can localize to stress granules, which can disrupt nucleocytoplasmic transport[188]. Inhibition of stress granule assembly rescued NCT defects and neurodegeneration in C9ALS iPSC derived neurons and a *Drosophila* model[188]. iPSC derived neurons of C9ALS patients show reduced nucleocytoplasmic Ran gradient and the nuclear import of proteins and export of RNAs was reduced[155, 177]. Ran-GAP, Nup107 and Nup205 were also found as perinuclear aggregates and showed nuclear retention in the motor cortex of C9ALS patients[155]. Finally, several screens have identified NCT as modifier of poly-GR and poly-PR toxicity in yeast[189] and *Drosophila*[178].

To date, mitochondrial and DNA damage are only linked to poly-GR. Poly-GR can directly bind to mitochondrial proteins[186]. DNA damage and oxidative stress were higher in iPSC derived motor neurons from C9FTD and C9ALS patients compared with controls[186]. Expression of poly-GR in control derived iPSC motor neurons was sufficient to cause DNA damage, which was rescued by reduction of oxidative stress using antioxidant treatment[186]. An increase in DNA damage has also been reported in spinal cord neurons of C9ALS patients[145, 190].

Poly-GA toxicity probably acts via the ubiquitin-proteasome system (UPS). Poly-GA interacts with proteasomal subunits, ubiquitin related proteins ubiquitin 1 and 2 and Unc119[175]. Unc119 is a transport factor linked to neuromuscular and axonal function[175]. Unc119 overexpression partially rescues poly-GA toxicity in primary neurons and co-localizes with 9.5% of poly-GA inclusions in the frontal cortex, but only with 1.6% of poly-GA inclusions in the cerebellum of C9FTD/ALS patients[175]. Expression of poly-GA in HEK293T and neuro2a cells[172] and primary mouse cortical neurons caused increased p62

expression and accumulation of ubiquitinated proteins[75]. In these cell models, proteasome activity was decreased and ER stress induced[75]. Neuro2a cells expressing poly-GA were more sensitive to UPS inhibition[172]. Interestingly, ER stress inhibitors provided protection against poly-GA toxicity[75]. The other way around, iPSC derived neurons of C9ALS patients were more sensitive to ER stress inducers[139].

Thus, DPRs probably affect multiple cellular pathways simultaneously. Poly-GR and -PR bind many proteins involved in splicing and the translational machinery. Furthermore, they seem to impact nucleocytoplasmic transport by direct binding to importins, nups and the nuclear pore itself. Next to these direct effects, DPRs also influence the formation of membrane-less organelles, which further impairs the function of the nucleolus, the nuclear pore and stress granules. The role of poly-GR in mitochondrial and DNA damage is recently being recognized and not completely understood yet. Finally, poly-GA mainly impacts the UPS, which further enhances the involvement of aberrant cellular stress response. Further research is needed to complete the picture of downstream mechanisms involved in the pathogenesis of C9FTD/ALS and to identify possible targets for drug development.

### 5.3 Mouse models of C9ORF72 gain-of-function

In 2015, Chew et al. published the first gain-of-function mouse model[191] (mouse models are summarized in table 2). This model was generated by AAV-virus driven expression of 66x pure G<sub>4</sub>C<sub>2</sub> repeats injected in the ventricle of wildtype C57BL/6J mice. After 6 months, about 50% of neurons contained sense RNA foci and sense DPRs were present in cortex and hippocampus. Both foci and DPRs were less frequent in cerebellum and spinal cord. Mice developed a behavioral and motor phenotype in the open field test and on the rotarod. When sacrificed at 6 months, brain weight was reduced and neurodegeneration was observed in the whole cortex and in Purkinje cells specifically. pTPD-43 pathology was also sparsely observed. This mouse model was the first to recapitulate the symptoms seen in C9FTD/ALS patients and has proven that expression of 66 pure G<sub>4</sub>C<sub>2</sub> repeats is enough to evoke this phenotype, thereby supporting a gain-of-function mechanism.

Next, four BAC mouse models have been published in which both expression levels and expression pattern of the C9ORF72 repeat expansions reflect the human situation[136, 162, 192, 193]. All of the BAC mouse models contain sense and antisense RNA foci and sense DPRs, however antisense DPRs

have not been observed. Interestingly, two out of four mouse models did not show any behavioral and motor phenotype, nor showed any neurodegeneration or pTDP-43 neuropathology[162, 192]. The third mouse model only showed some memory and anxiety deficits and some mild neurodegeneration in the hippocampus, which only became apparent after 12 months[136]. Expression levels might be too low to cause a phenotype. The last BAC mouse model did show a very strong C9FTD/ALS phenotype, complete with locomotor abnormalities, grip strength loss, paralysis and decreased survival. Neuronal loss is observed in cortical areas and in the spinal cord, including the presence of reduced ChAT neurons. In addition, neuromuscular junctions were disrupted[193]. This model differs from the first three by the genetic background and some different flanking regions[193]. It will be interesting to compare expression levels between the BAC mice or to back-cross these models into the same genetic background.

Finally, the effect of long pure and interrupted (TCGAG sequence without stop codons)  $G_4C_2$  repeats were investigated *in vivo*[194, 195]. AAV-virus mediated expression of both short (10x) and long (102x) interrupted  $G_4C_2$  C9ORF72 repeat expansions cause the formation of abundant RNA foci in mice[194]. But only the mice expressing the long (interrupted) repeat expansion developed DPR and p62 pathology, Purkinje cell apoptosis, neuromuscular junction abnormalities and gait and cognitive defects[194]. AAV-149x pure repeat mice developed sense and antisense RNA foci, sense and antisense DPRs, p62 and pTDP-43 pathology[195]. This is the first mouse model that clearly shows nucleocytoplasmic inclusions of DPRs and pTDP-43[195]. Also these mice show neurodegeneration and behavior abnormalities (see table 2). This indicates that repeat length also plays an important role in the development of a phenotype and pathological features such as antisense DPRs and clear pTDP-43 pathology. Still, one must be cautious with comparing mouse models, as it remains difficult to compare expression levels between mice and between pure and interrupted repeats.

All of these mouse models show the impact of  $G_4C_2$  repeat expression *in vivo* and support a toxic gain-of-function mechanism underlying the pathogenesis of C9FTD/ALS. Administration of an AON that targets the repeat sequence has proven to prevent the formation of RNA foci, DPRs and the development of a phenotype in one of the BAC models of C9FTD/ALS[136], which further highlights expression of the  $G_4C_2$  repeat as toxic gain-of-function mechanism. Mouse models that express the  $G_4C_2$  repeat interrupted with stop codons or DPRs only (made by alternative codons) might further disentangle the contribution of RNA and DPR protein gain-of-function.

<b>Study</b>	<b>Chew et al., 2015</b>	<b>Peters et al., 2015</b>	<b>O'Rourke et al., 2015</b>	<b>Jiang et al., 2016</b>	<b>Liu et al., 2016</b>	<b>Heranz-Martin et al., 2017</b>	<b>Chew et al., 2019</b>
<b>Generation of mouse model and number of mouse lines</b>	AAV2/9 – 66xG <sub>4</sub> C <sub>2</sub> and AAV2/9 – 2xG <sub>4</sub> C <sub>2</sub> with 119 bp up- and 100 bp down-stream human flanking regions. ICV injections at P0.	BAC mice with exon 1-6 including 500 repeats and 141 kb of upstream region.	BAC mice with exon 1-11, 110 kb up- and 20 kb down-stream. 1 line with 15 repeats and 2 lines with 100-1000 repeats (F112 and F113).	BAC mice with exon 1-5 and 140 kb upstream. One mouse line with 110 repeats and three mouse lines with 450 repeats (A, B and C).	BAC mice with exon 1-11, 52 kb up- and 19 kb down-stream. 4 mouse lines: 29/36 repeats, 37 repeats, 32/500 and 500 repeats.	AAV9-102xG <sub>4</sub> C <sub>2</sub> interrupted and AAV9-10x G <sub>4</sub> C <sub>2</sub> pure. ICV injections (cisterna magna) at P1.	AAV2/9 – 149xG <sub>4</sub> C <sub>2</sub> with 119 bp upstream and 100 bp downstream human flanking regions. ICV injections at P0.
<b>Mouse strain</b>	C57BL/6J	SJL/BL6	C57BL/6J	C57BL6/C3H	FVB/NJ	C57BL/6J	C57BL/6J
<b>RNA foci sense and antisense</b>	40-54% of neurons with nuclear sense foci in cortex, CA1-3 and purkinje cells of 66x G <sub>4</sub> C <sub>2</sub> repeat mice.	Intranuclear sense foci from 3 months on and increased by 10 and 24 months. Antisense foci after 10 to 24 months but less frequent.	Lines F112 and F113 showed 40-80% of cells with sense and antisense RNA foci in the CNS at 3 months. No foci in 15 repeat mouse.	Sense and antisense foci from 2 months on in all 450x G <sub>4</sub> C <sub>2</sub> mouse lines, stable over time. More foci in lines with higher expression.	Sense and antisense foci from 2 months on in 500/32 and 500 mouse lines, not in 36/29 and 37 lines. No difference over time.	Sense foci in brain stem, purkinje cells, CA1, and cortex. Less in spinal cord. No difference between AAV-10 and AAV-102 mice.	26-58% of neurons in cortex, hippocampus, cerebellum with sense foci, increase over time. 4-24% of cells with antisense foci, constant over time.

<b>DPR pathology</b>	Only in 66 repeat mice: mostly nuclear and some cytoplasmic GA, GP and GR inclusions in cortex and hippocampus. Less frequent in cerebellum and spinal cord. More GA and GP than GR.	GP detected by immun assay in 4 months old mice in cerebellum, spinal cord, sciatic nerve and liver. GP levels in assay decreased but perinuclear aggregates in brain increased over time.	GP inclusions rare at 6 months but frequent at 20 months. GP also detected by immun assay at 6 months in cerebellum, cortex and hippocampus. Low levels in spinal cord.	Perinuclear GA, GP and GR from 3 months in retrosplenial cortex, hippocampus and DG and frontal cortex. Less in cerebellum and spinal cord. No PR and PA detected. DPRs increased over time and with expression.	GA throughout the brains of 500/32, 500 and 36/29 lines. GP in cortex and thalamus of 500/32 and 500 lines. More GA over time and with onset of phenotype. P62 pathology also observed.	Only in AAV-102 mice: nuclear and cytoplasmic GA in cerebellum and brain stem. Unable to detect GP and GR probably due to antibody cross-reactivity. P62 pathology present.	All 5 DPRs (also antisense) cytoplasmic aggregates in brain and spinal cord that increase from 3 to 12 months. GP also observed as diffuse nuclear.
<b>Expression levels</b>	Average of about 17,000 GP ng/mg protein in whole brain lysates (immun assay).	Similar to C9ORF72 RNA levels in human frontal cortex. GP levels lower than in C9ALS patients.	All three lines had similar C9orf72 RNA and protein levels. Line 112 had the highest GP levels, but similar to C9FTD patient cortical tissue.	Line 450A similar to human C9 and mouse C9 RNA levels. Line 450B and 110x had higher and similar expression. Line 450C is the highest.	Similar human C9 RNA levels as endogenous C9 mouse RNA. Line 500/32 and 36/29 are expressed 2x higher.	No comparison between AAV-10 and AAV-102 mice reported.	No comparison between AAV-2, AAV-66 and AAV-149 reported.

<b>Neurodegeneration</b>	Reduced brain weight. 17% neuron loss in whole cortex and 23% in motor cortex. 11% less purkinje cells. No cell loss in hippocampus.	No neuronal loss.	No effect on body weight. No neuronal loss.	Mild (10%) neuronal loss in CA1 and DG at 12 months in high expression lines 450B and C. No loss in 110x G <sub>4</sub> C <sub>2</sub> repeat line.	Extensive neuron loss in cortex, cerebellum and hippo of symptomatic 500/32, 500 and 36/29 mice.	Only in AAV-102 mice: more PARP and cleaved-caspase-3 in cerebellum. No neurodegeneration, only some neuronal loss in CA1.	Loss of NeuN positive cells in the cortex at 6 months.
<b>Spinal cord pathology</b>	No cell loss in spinal cord. Some DPR pathology observed.	Extensive characterization but no pathology or neuronal loss observed.	Not observed.	No loss of ChAT neurons.	Atrophy and vacuoles in (motor)-neurons of symptomatic 500/32, 500 and 36/29 mice.	No spinal cord neuron loss reported. Only few sense RNA foci found.	No neuron loss in the spinal cord reported. Low amount of RNA foci and DPRs.
<b>NMJ pathology</b>	Not reported.	No denervation of NMJ seen in 2 year old mice.	No differences observed.	NMJ innervation normal and functional.	Denervation of nerve terminals of the NMJ in TA en diaphragm in symptomatic 500/32, 500 and 36/29 repeat mice.	Abnormal NMJ: neurofilament nerve terminal blebbing and reduced AChRs density.	Not reported.

<b>(p)TDP-43 pathology</b>	Only in 66 repeat mice: 7-8% of cells with nuclear and some cytoplasmic pTDP-43 inclusions in cortex and hippocampus.	Not observed.	Not observed.	Not observed.	No mis-localization or aggregation of pTDP-43. Higher levels of sarkosyl-soluble and insoluble fraction in line 450C at 22 months.	Nuclear and cytoplasmic aggregates in degenerating neurons of the brain of symptomatic 500/32, 500 and 36/29 mice.	Some (p) TDP-43 cytoplasmic aggregates found but no differences between AAV-10 and AAV-102 mice.	Clear pTDP-43 cytoplasmic inclusions that increase over time from 3 to 12 months.
<b>Microgliosis and/or astrogliosis</b>	Astrogliosis.	Not observed.	Not observed.	Not observed.	Not observed.	Astrogliosis and microgliosis.	No astrogliosis.	Astrogliosis starting at 3 months.
<b>Cognitive phenotype</b>	AAV-66 mice spent less time in open field but more distance and at a higher speed than AAV-2 mice. Reduced social interaction of AAV-66 mice compared to AAV-2 mice.	No changes in social behavior.	No effect on sociability, (social) novelty and memory Y-maze test.	Memory affected (Barnes and radial arm maze) and more anxiety (marble burying and elevated plus maze) in lines 450B/C. No effect on social & fear conditioning.	Slow progressive symptomatic mice of 500/32, 500 and 36/29 repeat lines show anxiety in open field.	AAV-102 mice less interested in novel object compared to AAV-10 mice.	Significant decrease in time spent freezing in contextual fear conditioning test.	

<b>Motor phenotype</b>	AAV-66 mice fell faster from the rotarod than AAV-2 mice.	No effect on rotarod or grip strength.	No effect on grip strength, rotarod or open field.	No motor deficits at 18 months (rotarod, grip strength).	Slow progressive mice show activity changes, claspings and seizures. Grip strength also affected.	Gait abnormalities in AAV-102 mice. No phenotype in open field and rotarod.	Hyperactivity in open field test and increased falls from the hanging wire test.
<b>Disease onset</b>	All behavior and pathological tests at 6 months. No report of earlier or later time points.	N.A.	N.A.	Cognitive phenotype started at 12 months and persisted until 18 months.	At 16 weeks first gait abnormalities, from 20 weeks onset of acute phenotype in 500/32 and 500 repeat mice. 36/29 have later onset.	All pathological tests at 12 months. Behavior at 6 months was normal but progressed into a motor phenotype at 12 months.	At 3 months first pathological effects observed (RNA foci, DPRs, astrogliosis). Behavior phenotypes and neuronal loss started at 6 months.
<b>Survival</b>	11% decrease in body weight of female mice at 6 months.	No effect; mice lived for 2 years.	Not reported.	No weight loss.	30-35% of female 500 and 500/32 mice show quick weight loss and decreased survival.	Not reported.	Not reported.



<b>Additional discoveries</b>	1 <sup>st</sup> publication of C9ORF72 gain-of-function mouse model.	miRNA targeting exon 3 of human C9ORF72 gene reduced the level of all C9ORF72 transcripts and GP levels in C9BAC mouse primary neuronal cultures.	ASO targeting exon 2 of human C9ORF72 gene suppressed RNA foci and GP levels in mouse primary neuronal culture.	Single IVC injection of AON in 3 months old mice decreased human C9 levels, sense foci and GP and GA levels. No effect on antisense RNA foci. Injection at 9 months resulted in behavior at 12-15 months.	First mouse model with clear NMJ abnormalities and affected gait.	AAV-102 repeats is enough to evoke RAN translation and a phenotype, while the same level of RNA foci without DPRs in AAV-10 mice is not enough to cause a phenotype.	First mouse model with antisense DPRs. Stress-granule components were found to aggregate with GR and pTDP-43. Nucleo-cytoplasmic transport defects were also observed.
-------------------------------	----------------------------------------------------------------------	---------------------------------------------------------------------------------------------------------------------------------------------------	-----------------------------------------------------------------------------------------------------------------	-----------------------------------------------------------------------------------------------------------------------------------------------------------------------------------------------------------	-------------------------------------------------------------------	----------------------------------------------------------------------------------------------------------------------------------------------------------------------	------------------------------------------------------------------------------------------------------------------------------------------------------------------------

**Table 2: Gain-of-function mouse models of C9ORF72.** In this table, we compare pathological and behavioral phenotypes of gain-of-function mouse models of the C9ORF72 repeat expansion. Three mouse models were generated with virus-mediated expression of 66 or 149 pure repeats or 102 interrupted repeats. Four mouse models were created by insertion of a human BAC containing - parts or the whole - C9ORF72 gene and the G<sub>4</sub>C<sub>2</sub> repeat expansion. AChRs = acetylcholine receptors, NMJ = neuromuscular junction, IVC=intracerebroventricular.

## 6. Remaining open questions in the research field of C9FTD/ALS

Despite the enormous amount and pace of published research articles on C9FTD/ALS, there are still some remaining open questions. In the following section, we identify important questions (summarized in box 1), set the aim for this thesis and explain how our research may address some of the knowledge gaps.

The most outstanding open question in the field is the determination of the contribution of the different proposed molecular mechanisms underlying neurodegeneration observed in C9FTD/ALS. The toxicity of DPRs has been studied extensively and expression of DPRs seems to be sufficient to cause cell death. On the other hand, RNA foci have been proven to sequester important proteins involved in splicing and depletion of these proteins could contribute to cellular toxicity. Loss-of-function does not cause FTD and/or ALS symptoms in mouse models of *C9ORF72*, but the function of the *C9ORF72* protein in autophagy and endosomal and lysosomal function could still contribute to *C9ORF72* pathogenesis. In order to be able to answer how these mechanisms all contribute to the pathogenesis of C9FTD/ALS, we need to understand the mode of action of the different components.

In the second chapter of this thesis, we study the effects of expression of either poly-GR and poly-PR in zebrafish embryos. Understanding the molecular pathways which are affected by these toxic peptides is important for elucidating the pathogenesis of C9FTD/ALS and might give new starting points for future drug development. In the third chapter of this thesis, we study the effect of expression of all sense DPRs in a murine model. DPRs were present as soluble peptides, which allows us to investigate another open question in the neurodegenerative field; is the soluble or aggregated state of certain proteins the most toxic form or could they also be protective? DPRs could also influence the aggregation of each other [74, 196], but the way that they affect availability for other binding partners and downstream mechanisms is still unclear.

So far, there has been an overwhelming number of studies investigating downstream molecular pathways involved in the pathogenesis of C9FTD/ALS. The main problem with these studies is that the identified pathways are probably all dysfunctional, but it is hard to distinguish primary from secondary effects. We try to address this problem by using a pharmacological approach in chapter 2. Drugs or compounds that show a full rescue of poly-GR and poly-PR toxicity indicate a primary or prominently affected pathway. Importantly, potential aberrant pathways are validated from *in vitro* and/or *in vivo* studies using post-mortem brain sections of C9FTD/ALS patients as described in chapter 4. The validation

**Box 1: Open questions in the research field of C9FTD/ALS.**

**1. What is the toxic culprit?** Many studies highlight the toxicity of (arginine-containing) DPRs in models for C9FTD/ALS. On the other hand, evidence of sequestration of several proteins into RNA foci and consequent cellular depletion has been put forward as pathological mechanism. In addition, the function of the C9ORF72 protein in autophagy could modify pathogenesis and should also be taken into account. The relative contribution of all of these mechanisms and their interactions to neurodegeneration is unknown.

**2. What molecular pathways are primary affected?** Both DPRs and  $G_4C_2$  RNA seem to influence the function of several cellular processes. It is important to distinguish primary from secondary effects in order to design drugs or compounds that prevent the major effects of DPRs or  $G_4C_2$  repeat RNA molecules. Drugs that prevent binding of DPRs or  $G_4C_2$  repeat RNA to important cellular proteins might reduce toxicity and prevent subsequent neurodegeneration.

**3. Is the aggregation of DPRs needed for their toxicity?** DPRs seem to differ in their mode of action depending on their conformational state and could possibly also influence each other on solubility, aggregation, interaction partners and downstream effects. It is unclear if aggregation of DPRs is causative or protective for neuronal death.

**4. How does RAN translation work?** As RAN translation is a relatively new concept, many questions are still unanswered. Minimal repeat size, necessary sequences and expression levels needed for the initiation of RAN translation are unknown. Mechanisms like frame shifting could produce chimeric DPRs, but we are still to discover what the contribution of all of these processes is to the final pool of DPRs in a cell.

**5. What is the possible time-window for treatment?** Administration of an AON has proven to prevent the formation of RNA foci, DPRs and the development of a phenotype in a BAC mouse model of C9FTD/ALS[136]. Is it also possible to block or reverse disease progression in the symptomatic phase? It is important to identify possible time-windows for treatment.

**6. Can we develop specific biomarkers for the C9FTD/ALS field?** Pathological hallmarks of C9FTD/ALS, including RNA foci and DPRs, might provide information on disease onset and progression. Their levels in blood, CSF and brain might be linked to certain clinical characteristics. As they are the targets of many new drugs, they could also be used as pharmacodynamics markers of target engagement in clinical trials.

of pathology in human neurons can be used as selection criteria to filter out any side effects or artifacts from overexpression models. We perform an extensive characterization of one of these identified new protein pathologies (HR23B) in chapter 4. We include HR23B co-localization patterns with DPRs, which can provide more information on the order of events and the differential effect of DPRs in the pathogenesis in the human brain.

Another main theme is RAN translation. This newly identified translation mechanism is subject of many studies investigating minimal requirements for RAN translation. The necessary flanking regions and repeat length can be different per reading frame and might also depend on expression levels. Each reading frame can contain different AUG-like start codons or Kozak sequences that enable translation. Frame shifting could also happen and might produce chimeric DPRs. The contribution of each of these mechanisms to the final proportion of DPRs in the cell is still a major gap of knowledge. We overexpress 36x G<sub>4</sub>C<sub>2</sub> repeats in a mouse model (chapter 3) to investigate if this repeat number is enough to evoke RAN translation and production of DPRs *in vivo*. Compounds that are capable of binding the G<sub>4</sub>C<sub>2</sub> RNA sequence or upstream start-like sites might block RAN translation and prevent the formation of toxic DPRs. Possibilities for drugs development are therefore increasing with every step made in understanding the mechanisms of RAN translation.

The last important step to make is the transition from many pre-clinical drug development studies to human clinical trials. In order to facilitate this process, it is important to investigate the time-window of treatment in an appropriate model. So far, some drugs have proven to prevent the formation of RNA foci or DPRs, but their effects in the symptomatic phase of the disease are unknown. We can use our mouse Tet-on model to turn expression of the C9ORF72 repeat on and off at several time-points and investigate the contribution of timing of expression to evoke the development and regression of disease symptoms. Another important tool for the successful assessment of clinical trials is the identification of reliable biomarkers that provide information on disease onset and progression. DPRs could be perfectly suited for this goal, as they are very specific for C9FTD/ALS and can be directly targeted by drugs. Poly-GP levels are found to be stable over time in CSF of C9ORF72 repeat carriers, but do not correlate with disease status, progression or other clinical characteristics[197]. In this thesis, we investigate the possibility of using poly-GR as fluid biomarker in chapter 5. The development of biomarkers is essential to gain information about disease onset and progression and to select and monitor patients in clinical trials.

**Aim of this thesis**

In summary, the aim of this thesis is to study the molecular mechanisms underlying the pathogenesis of C9FTD/ALS. In addition, these results will be essential for the development of new therapeutic strategies and to facilitate clinical research.





## Chapter 2

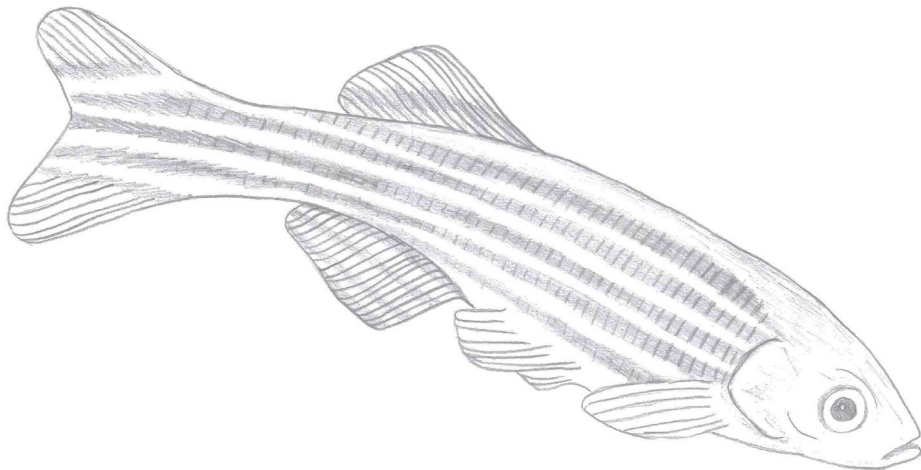
### **Reduction of oxidative stress and inhibition of the integrated stress response rescues poly-GR and poly-PR mediated toxicity in zebrafish embryos**

F.W. Riemslag<sup>1\*</sup>, R.F.M. Verhagen<sup>1</sup>, D. Smits<sup>1</sup>, W. Quint<sup>1</sup>, H. van der Linde<sup>1</sup>,  
A.M. Isaacs<sup>2</sup>, T. van Ham<sup>1</sup>, R. Willemsen<sup>1</sup>

<sup>1</sup>Department of Clinical Genetics, Erasmus University Medical Center Rotterdam, Rotterdam, The Netherlands.

<sup>2</sup>Department of Neurodegenerative Disease, UCL Institute of Neurology, London, UK.

\*Corresponding author: [f.w.riemslag@erasmusmc.nl](mailto:f.w.riemslag@erasmusmc.nl)



### Abstract

The G<sub>4</sub>C<sub>2</sub> hexanucleotide repeat expansion in the *C9ORF72* gene is the most common known pathogenic mutation linked to both frontotemporal dementia (FTD) and amyotrophic lateral sclerosis (ALS). This repeat can be translated into dipeptide repeat proteins (DPRs) via repeat-associated non-AUG (RAN) translation. DPRs are found throughout the brain of *C9ORF72*-linked FTD and ALS (C9FTD/ALS) patients. Especially the arginine-containing DPRs, poly-glycine-arginine (GR) and poly-proline-arginine (PR), are reported to be toxic in cell and animal models. In addition, poly-GR distribution correlates with neurodegeneration in postmortem C9FTD/ALS brains. Here, we report zebrafish models for poly-GR and -PR toxicity, using the Sec-A5 YFP fluorescent transgenic line that allows for easy detection and quantification of apoptosis *in vivo*. Microinjection of poly-GR or -PR encoding RNA into the yolk-sac of fertilized one-cell stage embryos was sufficient to evoke abundant apoptosis in the brain and abnormal motor neuron morphology in the tail of embryos at 1-4 days post fertilization (dpf). Poly-GR expression evoked elevated MitoSOX and γH2AX levels, indicative of oxidative stress and DNA damage. Both poly-GR and -PR expression caused inhibition of protein translation in cell culture. Inhibition of cellular stress pathways using either Trolox (reactive oxygen species inhibitor) or ISRIB (integrated stress response inhibitor) showed a full rescue of poly-GR and -PR toxicity, respectively. Our study indicates that poly-GR and -PR exert their toxicity via activation of cellular stress pathways. These zebrafish models can further elucidate molecular mechanisms underlying neurodegeneration in C9FTD/ALS and allow for (unbiased) drug screens.

### Keywords

*C9ORF72*, ALS, FTD, poly-GR, poly-PR, neurodegeneration, ISR



## Introduction

FTD and ALS are two neurological disorders that are characterized by degeneration of cortical neurons in the frontal and temporal cortices and motor neurons in the motor cortex and spinal cord[12]. The G<sub>4</sub>C<sub>2</sub> hexanucleotide repeat expansion in the *C9ORF72* gene is a shared genetic factor that has been linked to both FTD and ALS[22, 23]. Patients carrying this mutation can develop symptoms of both disorders[12]. How the G<sub>4</sub>C<sub>2</sub> repeat expansion causes neurodegeneration is currently unknown. Possible hypotheses include both loss- and gain-of-function mechanisms or a combination of both. Methylation of the repeat and surrounding CpG islands can silence the *C9ORF72* gene leading to haploinsufficiency[77]. Sense and antisense RNA containing the repeat accumulate in RNA foci and sequester multiple RNA binding proteins[77]. Furthermore, DPRs are produced by unconventional RAN translation of the repeat sequences in both sense and anti-sense direction, creating different DPRs: poly-glycine-alanine (GA), -glycine-proline (GP), -glycine-arginine (GR), -proline-arginine (PR), -proline-alanine (PA) and -proline-glycine (PG) [55, 57, 66, 67]. These DPRs are found throughout postmortem brain tissue of patients[198] but only poly-GR pathology correlates with neurodegeneration[72, 73].

The arginine-containing DPRs, poly-GR and -PR, have been reported to be very toxic in both cell and animal models[168, 171, 173, 174, 176, 179, 199]. Poly-GR and -PR interact with ribosomal proteins, heterochromatin, nucleolar proteins, RNA-binding proteins and proteins containing low-complexity domains (LCDs)[173, 174, 176, 181, 199, 200]. LCD proteins can form membrane-less organelles such as nucleoli, the nuclear pore and stress granules. Poly-GR and -PR have been shown to alter the dynamics and assembly of these organelles, leading to reduced mRNA translation, ribosomal stress, endoplasmic reticulum (ER) stress and aberrant nucleocytoplasmic transport (NCT)[176, 177, 183, 188, 199]. Poly-PR also disrupts the liquid phase of HP1 $\alpha$ , binds heterochromatin and causes abnormal histone H3 methylation, leading to repetitive element expression and accumulation of double-stranded RNA in a mouse model[200]. Overexpression of poly-PR in primary murine cortical neurons leads to an increase in stress granule formation[171]. In addition, overexpression of either poly-GR and -PR resulted in reduced translation in NSC34 and HeLa cells[149, 174], and in a mouse model for poly-GR[199]. Poly-GR and -PR can accumulate in the nucleus and co-localize with nucleoli in NSC24 and HEK293 cells[173], and nucleolar volume changes have been observed in C9FTD patient brain tissue[163]. Disrupted nucleolar function can lead to impaired ribosomal RNA maturation as observed

in HEK293T cells and *C9ORF72* iPSC-derived motor neurons[169, 184]. Furthermore, poly-GR can interact with mitochondrial ribosomal proteins and consequently impair mitochondrial function in C9FTD/ALS iPSC-derived neurons[186, 201]. Finally, poly-GR increases the amount of oxidative stress which can cause DNA damage in motor neurons differentiated from iPSCs[186]. Importantly, since all these processes can influence each other and lead to general cellular dysfunctioning, the primary start of the toxicity cascade is still unknown and warrants further investigation[169, 188].

To study poly-GR and -PR toxicity in a vertebrate *in vivo* system, we used zebrafish (*Danio rerio*). Zebrafish have been extensively used in (neuro) toxicity studies for multiple reasons (reviewed in[202, 203]). First, their genome can be easily manipulated using CRISPR-CAS9 technique or by injection of RNA encoding a protein of interest. Second, they are transparent and develop rapid as external embryos, allowing for easy detection of body and organ abnormalities. Fluorescent transgenic reporter zebrafish lines that label structures or cell types are readily available worldwide. In order to visualize apoptosis, we make use of the fluorescent Sec-A5 model that labels apoptotic clusters with YFP[204]. Third, basic (neuro)biological processes are conserved between vertebrates, making identification of aberrant cellular and molecular pathways in the pathogenesis of human disorders feasible[202, 205]. Fourth, zebrafish produce many offspring which are easily injected, allowing for medium-throughput experiments. Finally, they are perfectly suited for drug screens because they readily take up small molecules from the water[203].

Here, we inject RNA transcribed *in vitro* from DNA constructs encoding ATG-mediated codon-optimized 100xGR or 100xPR. High concentrations led to deceased and malformed fish, while low concentrations of only 10pg RNA encoding poly-GR and 5pg RNA encoding poly-PR were sufficient to evoke apoptosis in the brain and caused aberrant motor neuron morphology at 1-4 dpf. These models allow to screen for drugs that modify poly-GR and -PR toxicity, and we identified Trolox and ISRIB that show a full rescue for poly-GR and -PR, respectively. Trolox is an antioxidant that reduces reactive oxygen species (ROS), which are free radicals that can evoke oxidative stress and cause mitochondrial and DNA damage and are linked to many neurodegenerative diseases[206]. ISRIB is a known inhibitor of the cellular integrated stress response (ISR). The ISR can be activated by amino acid deprivation, viral infection, iron deficiency, and misfolding of proteins within the ER. The accumulation of misfolded proteins in the ER causes ER stress and activation of the ISR and the unfolded protein response (UPR)

[207]. Oxidative stress can worsen ER stress by reducing the efficiency of protein folding pathways and thereby increasing the amount of misfolded proteins[208]. The other way around, ER stress can cause ROS production[209]. In this study, we investigate the involvement of these cellular stress pathways in the pathogenesis of *C9ORF72*-linked ALS and FTD.

## Methods

### Constructs

DNA plasmids containing the pcDNA3.1+Peredox-mCherry-NLS (addgene cat. Nr 32384), pcDNA3.1+100xGlycine-Arginine and pcDNA3.1+100xProline-Arginine (Isaacs lab) were transformed into Top10 competent cells followed by DNA isolation with NucleoBond®Xtra maxi kit (BioKé). DNA constructs were linearized by digestion with *Apal* (NEB) and/or *NheI* (NEB), purified by phenol-chloroform extraction and quantified on Nanodrop (ThermoFisher). To obtain control constructs for injection of RNA, we performed site directed mutagenesis to mutate the ATG initiation codon using the QuickChange Lightning Site-Directed mutagenesis Kit (ThermoFisher, Waltham, Massachusetts, USA). The following primers were used to obtain the mutated start codons: for PR: forward 5'-CGAG-GACGAGGCACGGTGGGATCCGAG-3'. reverse 5'-CTCGGATCCCACCGTG-CCTCGTCCTCG-3' for GR: forward: 5'-CTCGTCCACG TCCCTAGGTGGGATCG – 3' reverse: 5'-GCTCGGATCCCACCTAGGGACGTGGAC– 3'. To denature the DNA template and anneal the mutagenic primers containing the desired mutation we used a thermal cycling protocol (1x(2min at 95°C), 18x (20sec at 95°C, 10 sec at 60°C, 3 min at 68°C), 1x (5min at 68°C)). After mutant strand synthesis the template DNA was digested by adding 1µl of the Dpn1 enzyme, mixtures were incubated for 5 minutes at 37°C. Mutated DNA constructs were transformed and isolated as described above.

### RNA synthesis

For the production of RNA the mMessage mMachine T7 transcription kit (Invitrogen) was used. 400 ug of linear template DNA was mixed with 2uL reaction buffer, 10uL NTP/CAP, 0.1uL RNase out and nuclease free water. The mixture was incubated at 37°C for 2 hours. After incubation 1uL TURBO DNase was added to remove template DNA at 37°C for 15 minutes. 30uL lithium chloride and 30 uL nuclease free water was added for precipitation and mixtures were placed at -20°C for at least 30 minutes. RNA was subsequently centrifuged at 4°C , washed with 70% ethanol, re-centrifuged, dried to air and dissolved in DEPC water and quan-

tified using Nanodrop (ThermoFisher). Samples were stored at  $-80^{\circ}\text{C}$  in aliquots.

### **Injections and fish maintenance**

For all experiments one cell stage zebrafish embryos of the AB wildtype or Sec-A5 YFP zebrafish reporter line[204] were injected in the yolk sac within 30 minutes after egg fertilization. Injection mixtures contained a standard amount of 400pg/nl mCherry-mRNA and 10% phenol red. The RNA encoding poly-GR and -PR constructs was added to these mixtures with a final concentration of 1 to 100 pg/nl. All zebrafish embryos were injected with 2 nl of injection mix. After injection, embryos were kept in a  $28^{\circ}\text{C}$  incubator for 1 till 4 days in E3-water and on the first day with additional methylene blue as antifungal aid. Propylthiouracil (PTU) (1:40) was added to E3-water to prevent pigmentation and keep the fish optically transparent. At 24 hours post fertilization (hpf) the embryos underwent visual inspection for dysmorphic features. Morphologically abnormal embryos and unfertilized eggs were excluded from all further experiments. Embryos were selected at 1 dpf time point based on their mCherry signal intensity in order to select only correctly injected embryos. The non-mCherry fluorescent embryos and mosaic embryos were disposed.

### **Apoptotic cluster count**

The apoptotic cluster quantification study was performed in the Sec-A5 YFP zebrafish reporter line[204] at 1 – 4 dpf with 3 separate injection rounds for each time point and minimal 10 fish per group per time point were imaged. Prior to imaging embryos were dechorionated, anesthetized with 10% tricaine in E3-water and embedded in 1.8% low melting point agarose in E3-water. The Leica SP5 AOBs confocal microscope and a HCX L 20.0x1.00 water dipping objective were used for the apoptotic cluster count. A z-stack step size of 4.2 micron was used ranging from the first till the last YFP+ cell on the Z-axis. Automatic quantification of apoptotic cells was done using Fiji software with the 3D object counter application with automated threshold and a minimum of 3 voxels. 1-way ANOVA with Barlett's test for equal variances showed a significant difference in the variance per group, so we performed a Kruskal-Wallis test that does not assume equal variances and post Dunn's multiple comparison test to compare groups.

### **TUNEL assay**

Wildtype AB strain fish injected with 5pg RNA encoding poly-PR, 10 pg RNA encoding poly-GR or 400pg RNA encoding mCherry were used for TUNEL assay

analysis. Fish were fixed at 2 dpf for 4h in 4% paraformaldehyde (PFA) in 0.1M PBS followed by washing in 0.1MPBS. Subsequently, fish were washed and kept in 100% MeOH at -20°C until further processing. Rehydration was obtained by incubating fish in decreasing concentrations of MeOH: 75% - 50% - 25% MeOH followed by PBS. After washing in PBS-T (0.2% Triton X-100; Sigma in 0.1M PBS) fish were treated with 10µg/ml Proteinase K in PBS-T for 15 minutes and refixed with 4% PFA for 20 min. After washing fish three times in PBS-T for 10 min, fish were incubated for 30 minutes with 100 µl TdT buffer (Click-iT Plus TUNEL Assay 647 dye; Invitrogen). Following initial incubation, fish were incubated overnight with 100µl TdT reaction mix (94µl TdT buffer; 2µl EdUTP; 4µl TdT enzyme). After incubation fish were washed with 3% bovine serum albumin (BSA; Sigma) in PBS-T three times followed by incubation with 100µl Click-iT reaction mix for 3h and washed three times with 3% BSA in PBS-T. Fish were mounted in 1.8% low melting point agarose (Invitrogen) in E3-water. Imaging was performed using a SP5 Intravital microscope equipped with HCX-APO L 20x/100W objective (Leica) for 10 fish per group.

### **Synaptic Vesicle 2 whole mount staining**

At 48h post injection with 5pg RNA encoding poly-PR, 10pg RNA encoding poly-GR or 400pg RNA encoding mCherry, Sec-A5 YFP zebrafish were fixed overnight in 4% PFA in 0.1M PBS. Fish were permeabilized with acetone for 1h at -20°C and blocked with 1% BSA / 1% DMSO / PBS-T (0.2% Triton X-100; Sigma in 0.1M PBS) for 1 h at room temperature. Subsequently, fish were immunostained overnight at 4°C with the anti-mouse SV2 antibody (1:200, AB231587, Developmental Studies Hybridoma Bank, University of Iowa). After incubation fish were washed 10 times in 0.5% Triton X-100 (Sigma) in PBS and incubated overnight with the secondary antibody Anti-mouse-Cy5 (1:200, Sigma Aldrich). The following day the fish were washed 6 times in 0.5% Triton X-100 and mounted with 1.8% low melting point agarose (ThermoFisher) in E3-water. Imaging was done with Leica SP5 AOBs confocal microscope and a HCX L 20.0x1.00 water dipping objective for 10 fish per group.

### **Fluorescent immunohistochemistry**

For immunohistochemical analysis fish from the AB wildtype strain were injected with 5pg RNA encoding poly-PR, 10pg RNA encoding poly-GR or 400pg RNA encoding mCherry only. Fish were fixed at 1-4 dpf (n = 30 per group) overnight in 4% PFA and subsequently embedded in paraffin. Tissues were cut into 6µm thick

sections using a rotary microtome. Sections were deparaffinized using xylene and rehydrated in an alcohol series (100%-96%-90%-80%-70%-50%). Antigen retrieval was done in 0.01M sodium citrate, pH6.0 using pressure cooker treatment. Endogenous peroxidase activity was blocked with 3% H<sub>2</sub>O<sub>2</sub> and 1,25% sodium azide in 0.1M PBS. Immunostaining was performed overnight at 4°C in PBS block buffer (0.1M PBS / 0.5% protifar / 0.15% glycine) and with primary antibodies (anti-PR 1:500 LifeTein, anti-GR 1:5000 LifeTein, γH2AX 1:750 GeneTEX) at 4°C. After incubation with the primary antibody, sections were washed with PBS block buffer and incubated with secondary anti-mouse/rabbit Cy2/3 linked antibodies (Jackson). To remove background staining, a 10 min incubation with Sudan Black (Sigma, 0.1 gr in 100ml 70% ethanol, filtered) was performed. To visualize nuclei, slides were incubated for 10 min with Hoechst 33342 (Invitrogen). Slides were mounted with ProLongGold (Invitrogen) and kept at 4°C until imaging at a Zeiss LSM700 Confocal microscope.

### **Enzyme Linked Immuno Sorbent Assay (ELISA)**

Poly-GR sandwich ELISA was performed at 1 – 4 dpf with 3 separate experiments for each time point and 30 SecA5 fish per group per time point. Prior to lysing, fish were dechorionated and euthanized. Mechanical lysis of fish was performed in RIPA buffer containing 0.05% protease inhibitors (Roche) and 0.3% 1M DTT (Invitrogen). After 30 min incubation, mechanical lysis was repeated and samples were centrifuged at 13.000xg for 15 min at 4°C, followed by 3x 1 min sonication. After sonication, samples were centrifuged at 13.000xg for 20 min at 4°C. Whole protein content was determined using BCA assay (Thermo Fisher Scientific). MaxiSorp 96 well F-bottom plates (Thermo Fisher) were coated for 2h with 5.0 µg/ml monoclonal GR antibody (LifeTein Services) followed by overnight blocking with 1% BSA in PBS-Tween (0.05% Tween-20 in 0.1M PBS) at 4°C. After washing, samples were added at 300µg total protein in one well and 2-fold diluted in PBS in a second well. Standard curve made with 15x GR synthetic peptide was added in duplo. All samples were incubated for 1h on the plate. After washing, all wells were incubated for 1h with biotinylated monoclonal anti-GR antibody (LifeTein Services) at a final concentration of 0.25 µg/ml in PBS-Tween/1% BSA. After washing, samples were incubated for 20 min with Streptavidin-HRP conjugate (R&D Sciences) diluted 1:200 in PBS-Tween/1% BSA. Following extensive washing, samples were incubated with substrate reaction mix (R&D Sciences) for 15 min and stopped using 2N H<sub>2</sub>SO<sub>4</sub>. Read-out was performed at 450nm and 570nm (Varioscan). We performed a two-way ANOVA with post Bonferroni test

for differences between groups over time.

### Rescue experiments

ISRIB (Sigma) was dissolved in 100% DMSO and diluted in E3-water to a final concentration of 2 $\mu$ M. Trolox (Sigma) was dissolved in 100% DMSO and diluted in E3-water to a final concentration of 50 $\mu$ M. Dissolved ISRIB, Trolox, or similar volumes of DMSO as a control, were added to the E3 water directly after micro-injections and refreshed every day. The amount of apoptotic clusters was determined at 1-4 dpf as described above. We used 30 Sec-A5 YFP zebrafish per group per time point. 1-way ANOVA with Barlett's test for equal variances showed a significant difference in the variance per group, so we performed a Kruskal-Wallis test that does not assume equal variances and post Dunn's multiple comparison test to compare groups.

### MitoSOX Assay

Wildtype AB strain fish injected with 10pg RNA encoding poly-GR or 400pg RNA encoding mCherry only were used for MitoSOX (Invitrogen) assay analysis. Fish were collected at 2 dpf, dechorionated and washed once with pre-warmed HBSS (HBSS Calcium Magnesium; Gibco) at 28°C. All fish were stained with 5 $\mu$ M MitoSOX reagent diluted in HBSS at 28°C for 20 min. Following incubation, all fish were washed 3 times with HBSS (28°C) and anesthetized with 1x Tricaine for 5 min. Fish were mounted in 1.8% low melting point agarose (Invitrogen). Imaging was performed using a SP5 Intravital microscope equipped with HCX-APO L 20x/100W objective (Leica) for 8 fish per group. F-test for equal variances  $p=0.91$  so variances are not significantly different so we performed a students't-test.

### ATF4b qPCR

Expression of the ATF4b gene in zebrafish larvae was determined using SYBR Green fluorescence (iQ Taq Universal SYBR Supermix; BioRad). Wildtype AB strain fish injected with 5pg RNA encoding poly-PR or 400pg RNA encoding mCherry only were used, with  $n = 30$  fish per group. All samples were run in triplicate. Primers for ATF4b gene: FW primer: 5'- GGA GCT CAT TGC TTC TCT GG- 3'; RV primer: 5'- GAC AGA GGC TGA TGG AGA GG - 3' and  $\beta$ -actin gene: FW primer: 5'- GCT GTT TTC CCC TCC ATT GTT - 3'; RV primer: 5'- TCC CAT GCC AAC CAT CAC T - 3'. Analysis was performed using the  $2^{-\Delta\Delta Ct}$  method with data normalized to  $\beta$ -actin. F-test for equal variances  $p=0.29$  so variances are not significantly different so we performed a students't-test.

### **Puromycin experiment**

COS7 cells were cultured in Dulbecco's modified Eagle's medium (DMEM, Gibco) supplemented with 10% fetal calf serum (FCS), 1% Penicillin/Streptomycin (P/S) and 1% non-essential amino acids (NEAA, Sigma-Aldrich) at 37°C in a 5% CO<sub>2</sub> humidified incubator. COS7 cells were plated at 150.000 cells/well in a 6-wells plate and transfected with 3 ul GeneJuice (Novagen) for 1ug DNA. The same DNA constructs were used for COS7 transfection as we used for RNA generation and injection of zebrafish embryos. The next day, cells were washed with 0.1M PBS and incubated with puromycin (1ug/ml) dissolved in supplemented DMEM medium for 1 hour. Afterwards, cells were washed with 0.1M PBS and fixed with 4% paraformaldehyde (PFA) for 20 min and permeabilized with 0.5% Triton X-100 in 0.1M PBS. Immunostaining was performed overnight at 4°C in 0.1M PBS with 1.5% BSA and anti-puromycin antibody 1:10.000 (MABE343 Merck). The next day, cells were washed with 1.5% BSA in 0.1M PBS and incubated with secondary antibody anti-mouse Cy3 (Jackson) 1:200 at room temperature for 1 hour. After washing with PBS, cells were shortly incubated with Hoechst 33342 (Invitrogen) and mounted with ProLong Gold (Invitrogen).

### **Results**

#### **Injection of poly-GR or -PR encoding RNA evokes apoptosis and aberrant motor neuron axon morphology in 1-4 dpf zebrafish embryos.**

We started with assessing the toxicity of poly-GR and -PR at the systemic level using a dosage-dependent approach. RNA was transcribed *in vitro* from ATG-100xGR or ATG-100xPR constructs, using alternative codons without the G<sub>4</sub>C<sub>2</sub> repeat sequence. Concentration series ranging from 1-200pg RNA were injected into the yolk-sac of fertilized oocytes at the one cell stage. Both Poly-GR and -PR encoding RNA showed a dose-dependent toxicity (supplementary figure 1), with high concentrations leading to deceased and undeveloped embryos and lower concentrations leading to malformations including heart edema and tail twists. For further experiments we chose a concentration that resulted in a robust and reproducible phenotype, without causing severe malformations. Amounts of 10pg poly-GR and 5pg poly-PR encoding RNA were used for all further experiments. These amounts still resulted in about 30% malformations, but all malformed fish were discarded and not used for further analyses. Lower concentrations did not show a clear and reproducible phenotype on apoptotic cluster count (data not shown). To determine the effect of poly-GR and -PR at the cellular level, we used the Sec-A5 reporter zebrafish line that fluorescently labels apoptotic clusters *in*



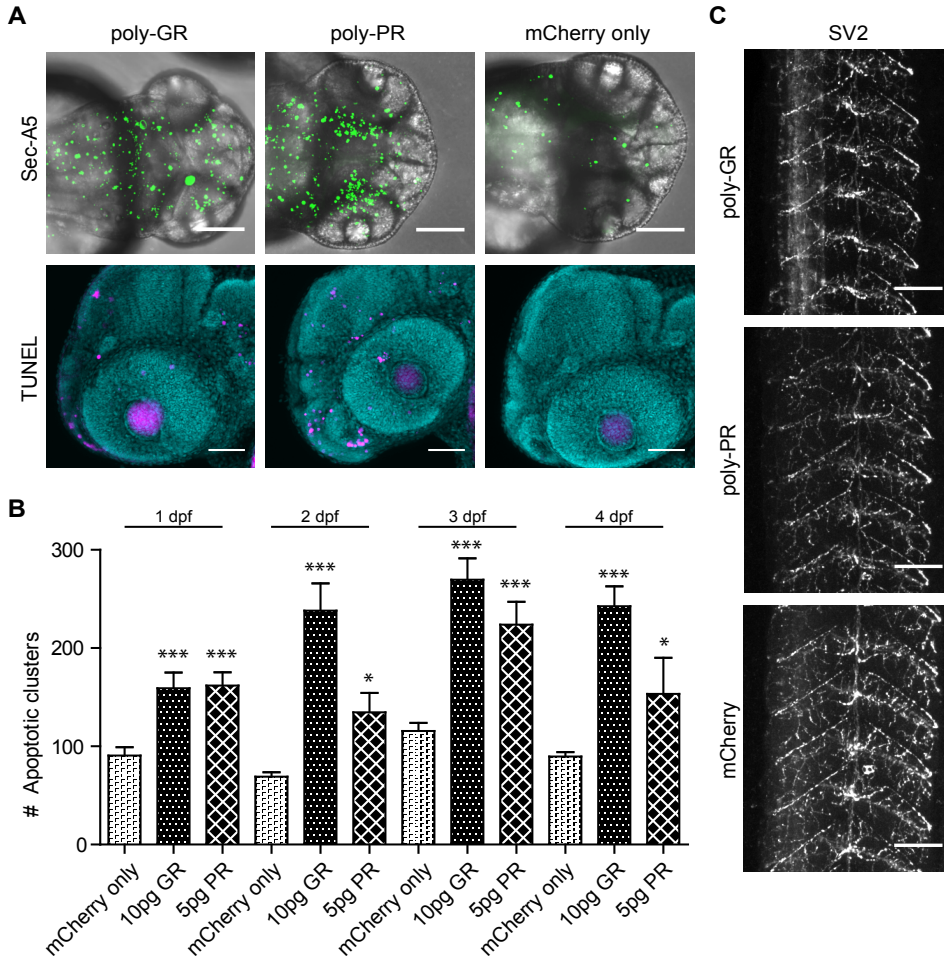


**Figure 1: Injection of poly-GR or -PR encoding RNA evokes apoptosis and aberrant motor neuron axon morphology in 1-4 dpf zebrafish embryos.** A) Upper panel shows max projection of z-stack images of the Sec-A5 YFP (green) fluorescent reporter line embryos 48 hours after injection with 10pg RNA encoding poly-GR, 5pg RNA encoding poly-PR or 400pg RNA encoding mCherry only. Scale bar is 100  $\mu$ m. Lower panel shows max projection of z-stack images of TUNEL assay in wildtype AB embryos 48 hours after injection with 10pg RNA encoding poly-GR, 5pg RNA encoding poly-PR or 400pg RNA encoding mCherry only. TUNEL positive signal is magenta, cell nuclei are stained with DAPI in blue. Scale bar is 50  $\mu$ m.  $n = 10$  per group. B) Quantification of z-stack images of the Sec-A5 YFP fluorescent reporter line embryos after injection with 10pg RNA encoding poly-GR, 5pg RNA encoding poly-PR or 400pg RNA encoding mCherry only at 1-4 dpf.  $N = 30$  fish/group/day. Kruskal-Wallis test ( $p = <0.0001$ ). Post Dunn's multiple comparison test \* =  $p < 0.05$ , \*\* =  $p < 0.001$  and \*\*\* =  $p < 0.0001$  differences of poly-GR and -PR RNA injected fish compared to mCherry only at 1-4 dpf. C) Synaptic vesicle (SV2) staining visualizes aberrant axonal protrusions in the tail of 2 dpf old embryos of the Sec-A5 YFP fluorescent reporter line after injection with 10pg RNA encoding poly-GR, 5pg RNA encoding poly-PR compared to 400pg mCherry only.  $n = 10$  per group. Scale bar is 50  $\mu$ m.

2

*vivo*[204]. As injections by themselves already cause a slight increase of cell death (data not shown), we used RNA from a mCherry-only construct as control. This marker was also used to select for correctly injected fish. Co-injection of mCherry RNA together with low concentrations of either poly-GR or -PR encoding RNA evoked massive apoptosis in zebrafish embryos at all stages (1-4 dpf) (figure 1A upper panel). Apoptosis was confirmed by TUNEL staining (figure 1A lower panel). To quantify the amount of apoptotic clusters, we made z-stack images of whole zebrafish heads *in vivo*. The YFP clusters in z-stack images were automatically quantified using FIJI software for 3D cluster counting. Both 10pg of poly-GR encoding RNA and 5pg of poly-PR encoding RNA was sufficient to cause a significant increase in the amount of apoptotic clusters in the brain of zebrafish embryos at 1-4 dpf compared to mCherry control injected fish (figure 1B, Kruskal-Wallis test with post Dunn's multiple comparison test  $p = < 0.0001$ ) without other gross morphological abnormalities. To further characterize our zebrafish model, we stained embryos for SV2, a marker for neuronal axons that labels presynaptic vesicles. This revealed that both poly-GR and -PR RNA injected fish display aberrant morphology with less axonal protrusions of the motor neuron axonal structure in the tail (figure 1C).

To study the specificity of our observed protein-toxicity, we used site-directed mutagenesis to mutagenize the ATG-start codon to a GTG-codon or a TAG-stop codon. This mutation disables translation of the RNA molecules into DPRs and can be considered as a control for RNA toxicity per se. Injection of high concentrations (50-200 pg) of RNA of TAG-100xGR or GTG-100xPR constructs caused an increase in deceased and malformed embryos (supplementary figure 1). Apparently, high concentration of non-coding RNA can have a small toxic effect on its own, even though this RNA does not contain a  $G_4C_2$  repeat sequence. Low concentrations (2-10 pg) of TAG/GTG-mediated poly-GR and -PR RNA were only slightly toxic compared to mCherry only (supplementary figure 1), while low concentrations of ATG-mediated poly-GR and -PR RNA evoked abundant apoptosis (figure 1). This shows the specificity of the detrimental effect of expressing poly-GR and -PR peptides. For further studies we used mCherry-only construct as a valid control.

Next, poly-GR and -PR peptides were visualized using immunofluorescent (IF) staining of whole body zebrafish at 1-4dpf. Poly-GR and -PR peptides were detected both diffusely and as nuclear and perinuclear puncta in embryos injected with a high concentration (20pg poly-PR and 40pg poly-GR), while embryos injected with low concentration (5pg poly-PR and 10pg poly-GR) only

showed some (peri)nuclear puncta dispersed throughout the body (figure 2A). Presence of poly-GR and -PR at these low concentrations was very difficult to detect with whole mount or IF staining on sections. We therefore performed a newly developed Enzyme-Linked Immuno Sorbent Assay (ELISA) to confirm the presence of poly-GR peptide in 1-4 dpf zebrafish embryos (figure 2B). Zebrafish embryos injected with 10pg of RNA encoding poly-GR showed a signal of 10-20

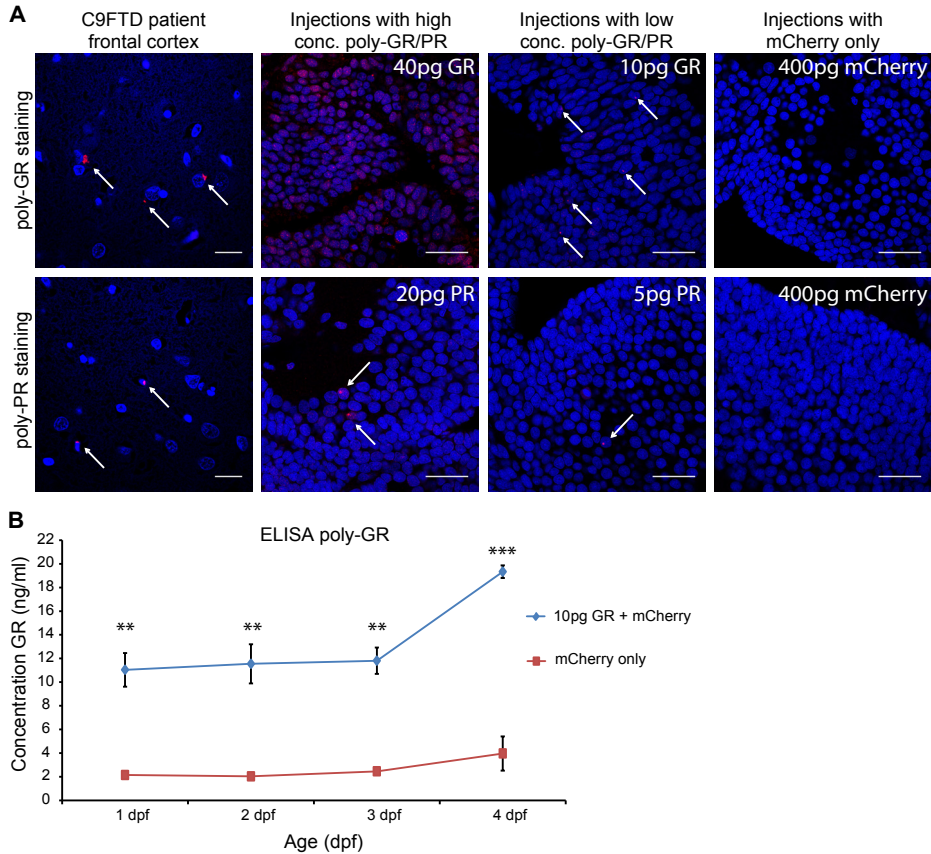


**Figure 2: Poly-GR and poly-PR peptides are detected as (peri)nuclear puncta in zebrafish embryos at 1-4dpf.** A) Immunofluorescence staining for poly-GR and poly-PR (red) in 2 dpf wt AB embryos after injection with high concentrations of RNA encoding poly-GR and -PR (40pg RNA poly-GR / 20pg RNA poly-PR) or low concentrations (10pg RNA poly-GR / 5pg RNA poly-PR) or 400pg RNA mCherry only. N = 30 per group. C9FTD patient frontal cortex sections were used as positive control. Poly-GR and -PR peptides are detected as nuclear or perinuclear (red) puncta in poly-GR and -PR RNA injected fish and in C9FTD patient frontal cortex. Nuclei were stained with Hoechst (blue). Scale bars are 20  $\mu$ m. B) ELISA for the detection of poly-GR shows a signal of 10-20pg peptide in 1-4 dpf wt AB embryos injected with 10pg RNA encoding poly-GR. Two-way ANOVA  $p = 0.0003$  with post Bonferroni test indicating that all time points were significantly different from mCherry-only injected fish. N = 90 fish per group per time point divided over 3 independent experiments (30 fish per group x 3 experiments per time point).

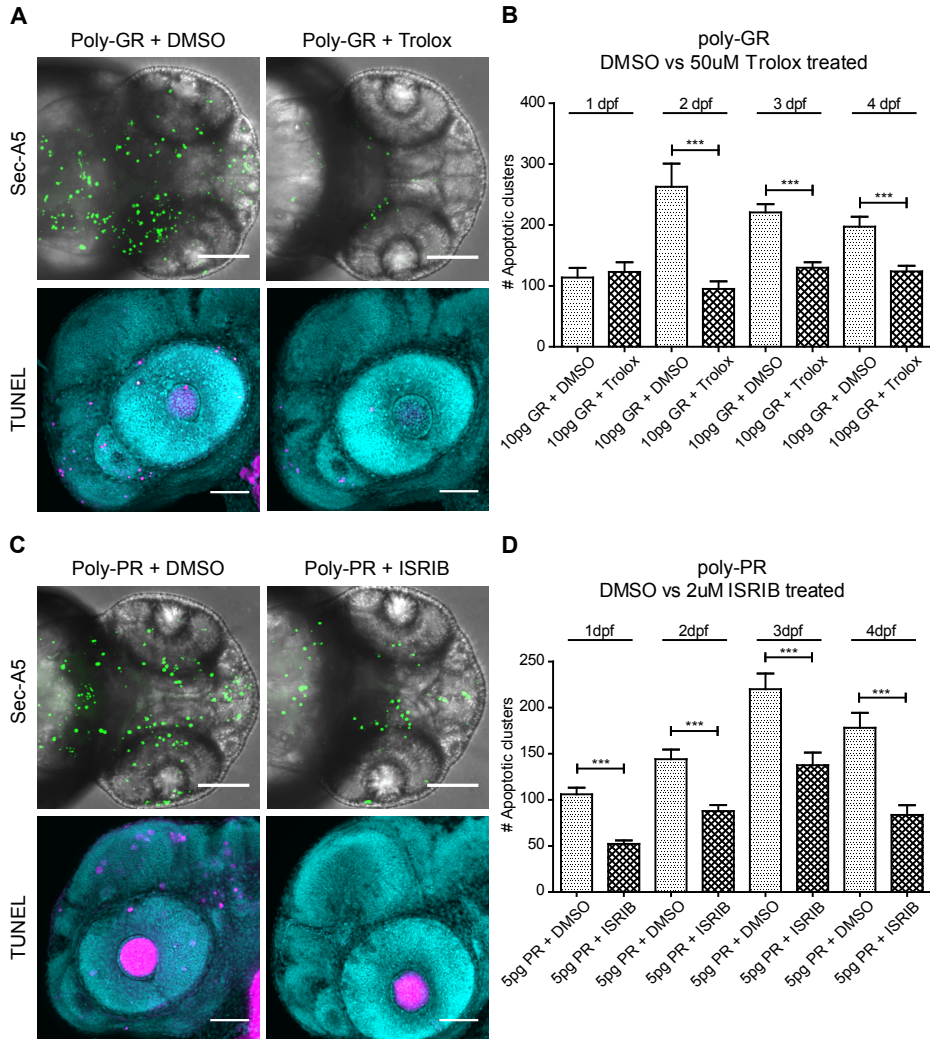
pg/ml peptide in our ELISA that was significantly different from mCherry-only injected fish (2-way-ANOVA  $p = 0.0003$ ). Unfortunately, we were unable to set-up a sensitive ELISA for the detection of the poly-PR peptide. In summary, ATG-mediated poly-GR and -PR encoding RNA is translated and detectable as (peri) nuclear puncta throughout the zebrafish body. Expression of poly-GR and -PR peptides causes abundant apoptosis in the developing zebrafish.

### **Inhibition of cellular stress responses, using Trolox and ISRIB, rescues poly-GR and -PR mediated toxicity.**

Poly-GR and -PR DPRs have been shown to disturb many cellular processes and pathways, but their main target is still unknown. To discriminate between primary and secondary effects, we used a pharmacological approach. Trolox, an antioxidant that reduces ROS, partially rescued toxicity in an iPSC-induced motor neuron model of C9FTD/ALS[186]. Also in our *in vivo* study, Trolox significantly reduced poly-GR-mediated apoptosis in 1-4 dpf embryos of the Sec-A5 zebrafish line (figure 3A and B) (Kruskal-Wallis test that does not assume equal variances  $p = <0.0001$ . Post Dunn's multiple comparison test showed \*\*\* =  $p < 0.0001$  difference between DMSO vs Trolox treated fish at 2-4 dpf). TUNEL staining confirmed the reduction of apoptotic cells in zebrafish embryo's treated with Trolox (figure 3A lower panel).

ISRIB, a small molecule that inhibits the cellular response to ER stress, was shown to prevent PR-mediated toxicity in cell culture[188, 210]. ISRIB significantly rescued poly-PR-mediated apoptosis at 1-4 dpf *in vivo* (figure 3C and D) (Kruskal-Wallis test that does not assume equal variances  $p = <0.0001$ . Post Dunn's multiple comparison test showed \*\*\* =  $p < 0.0001$  difference between DMSO vs ISRIB treated fish at 1-4 dpf). The observed rescue of Sec-A5 apoptotic clusters was confirmed by TUNEL staining in zebrafish embryo's treated with ISRIB (figure 3C lower panel). Unexpectedly, we observed a full rescue for both Trolox and ISRIB; apoptotic clusters were reduced to baseline level of mCherry-only injections. This underscores the significance and central role of the cellular stress response in the toxicity caused by these two DPRs.

Next, we wanted to further investigate the activation of these pathways. As Trolox is known to inhibit the formation of ROS, we used a whole-mount protocol to quantify the ROS in alive zebrafish by MitoSOX staining. Indeed, 10pg RNA encoding poly-GR injected fish showed an increase in MitoSOX staining compared to mCherry-only injected fish (figure 4A and B) (Students' t-test  $p=0.0002$ . F-test for equal variances  $p=0.914$  so variances are not significantly different).



2

**Figure 3: Trolax and ISRIB reduce the number of apoptotic clusters in SecA5 zebrafish embryos injected with 10pg RNA encoding poly-GR or 5pg RNA encoding poly-PR.** A) Upper panel: max projection of z-stack images of the Sec-A5 fluorescent reporter line embryos 48 hours after injection with 10pg RNA encoding poly-GR and treated with 50uM Trolox or DMSO. A) Lower panel: max projection of TUNEL staining of the same treatment groups in wt AB fish at 2dpf. Scale bars are 100  $\mu$ m. B) Quantification of Sec-A5 z-stack images. N = 30 fish per group per day. Kruskal-Wallis test  $p = <0.0001$ . Post Dunn's multiple comparison test \*\*\* =  $p < 0.0001$ . C) Upper panel: max projection of z-stack images of the Sec-A5 fluorescent reporter line embryos 48 hours after injection with 5pg RNA encoding poly-PR and treated with 2uM ISRIB or DMSO. C) Lower panel: max projection of TUNEL staining of the same treatment groups in wt AB fish at 2 dpf. Scale bar are 100  $\mu$ m. D) Quantification of Sec-A5 z-stack images. N = 30 fish per group per day for 1 and 2 dpf, n = 20 fish per group for 3 dpf and n= 10 fish per group for 4 dpf. Kruskal-Wallis test  $p = <0.0001$ . Post Dunn's multiple comparison test \*\*\* =  $p < 0.0001$ .

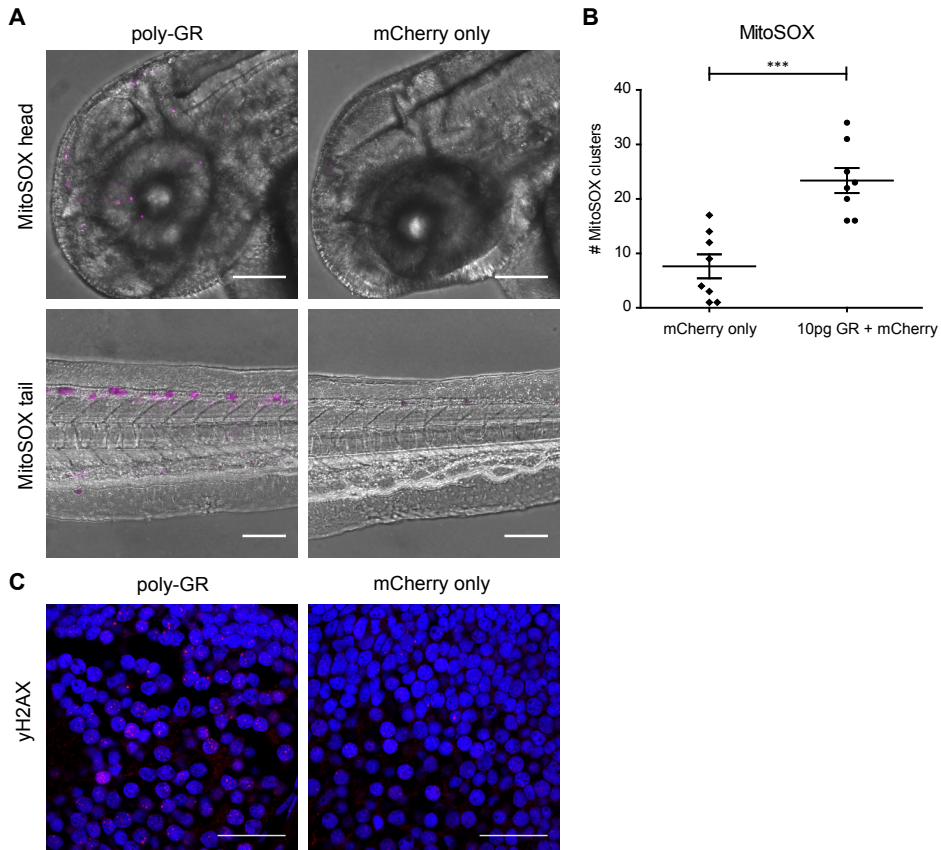


**Figure 4: Poly-GR increases oxidative stress and DNA damage in vivo.** A) MitoSOX red staining in 2 dpf wildtype AB embryos after injection with 10pg RNA encoding poly-GR or mCherry-only RNA. MitoSOX signal in magenta is seen as clusters in the brain and in spinal cord in the tail. Scale bars are 100  $\mu\text{m}$ . B) MitoSOX signal is significantly higher in 10pg RNA encoding poly-GR compared to mCherry-only RNA injected zebrafish embryos at 2 dpf.  $N = 8$  fish per group. Students'  $t$ -test  $p=0.0002$ .  $F$ -test for equal variances  $p=0.914$  so variances are not significantly different. C)  $\gamma\text{H2AX}$  immunostaining (red) in brain sections of 2 dpf embryos of the Sec-A5 fluorescent reporter line was detected after injection with 10pg RNA encoding poly-GR but not in mCherry-only RNA fish. Nuclei were stained with Hoechst (blue). Scale bars are 20  $\mu\text{m}$ .

As ROS can also evoke DNA damage, we stained for  $\gamma\text{H2AX}$ , a marker for DNA double strand breaks. 10pg RNA encoding poly-GR injected embryos showed  $\gamma\text{H2AX}$  nuclear puncta, while mCherry-only RNA injected embryos did not (figure 4C). This indicates that poly-GR evokes ROS and DNA damage *in vivo*.

For poly-PR, we assessed the induction of the integrated stress response. Activation of the ISR results in down regulation of general protein synthesis and the induction of transcription factors ATF4 and CHOP, that normally

promote cellular recovery. Under prolonged or severe stress, activation of ATF4 and CHOP can lead to apoptosis[211] (figure 5A). However, ATF4-b RNA levels were not significantly different between 5pg RNA encoding poly-PR injected vs mCherry-only RNA injected fish (figure 5B) (Students't-test  $p = 0.693$ . F-test for equal variances  $p = 0.29$ ). As the activation of the ISR may also result in inhibition of translation (figure 5A), we assessed the effect of poly-GR and -PR peptides on the incorporation of puromycin in newly synthesized peptides. For this purpose we used COS7 cells co-transfected with DNA encoding GFP and either poly-GR or poly-PR peptides. In these co-transfection studies we could not detect positive puromycin staining (figure 5C). In contrast, untransfected cells or cells transfected with GFP-only stained positive for puromycin, illustrating normal protein synthesis (figure 5C). These results suggest that overexpression of poly-GR and -PR peptides causes inhibition of protein translation.

## Discussion

In this study, we use a zebrafish model to readily visualize and quantify apoptosis in brain tissue evoked by injection of RNA encoding poly-GR and -PR DPRs. Poly-GR and -PR peptides were detectable as small (peri)nuclear puncta throughout the body and by an ELISA for poly-GR. Poly-GR evoked formation of reactive oxygen species and DNA damage, and both poly-GR and -PR inhibited translation in an overexpression COS7 cell model. We were able to fully rescue poly-GR by Trolox and poly-PR toxicity by ISRIB, inhibitors of oxidative stress and the integrated stress response, respectively. Our study indicates the importance of these cellular stress pathways in the pathogenesis of C9FTD/ALS.

Our model only focusses on single DPR-induced toxicity and does not take effects of  $G_4C_2$  repeat RNA-toxicity, haploinsufficiency of the normal C9ORF72 protein or simultaneous expression of different DPRs into account. Our constructs are ATG-mediated and use alternative codons to encode DPRs to circumvent  $G_4C_2$ -RNA toxicity. As an extra control for specificity, we used side-directed mutagenesis to change the start site of our constructs to TAG/GAG-codons to prevent translation and study non-coding RNA toxicity. Injection of extremely high RNA concentrations of TAG/GAG-constructs was toxic in embryos, showing that high expression of RNA molecules has a toxic effect. However, low concentrations of non-coding RNAs did not show an additional toxic effect compared with our control construct, mCherry-only. Swinnen et al. showed toxicity of RNA molecules containing 35-90x  $G_4C_2$  in a zebrafish model for C9ALS/FTD [154]. DPRs were undetectable in these fish, but interrupting the RNA constructs

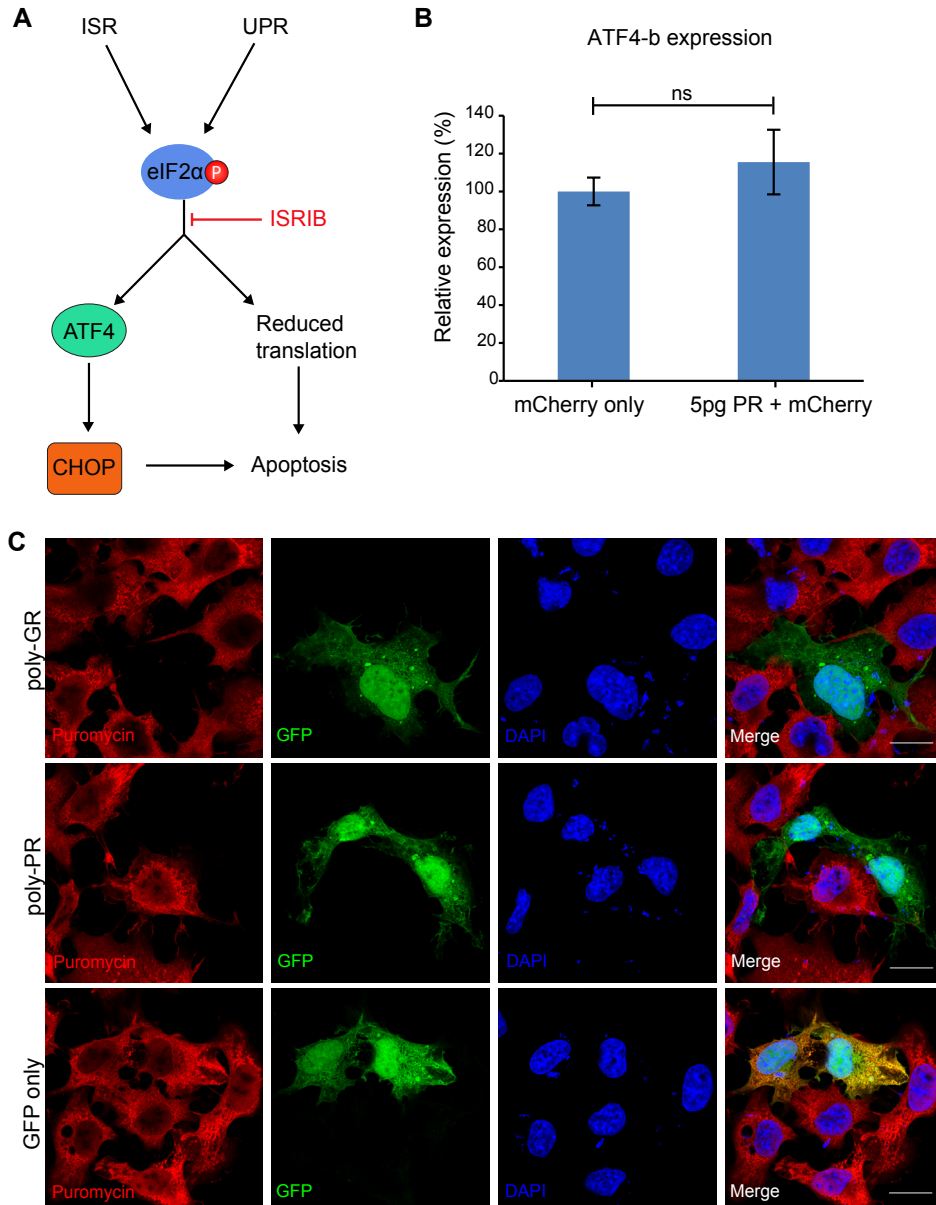


**Figure 5: Both poly-GR and -PR reduce translation in cell culture.** A) Activation of the integrated stress response (ISR) or the unfolded protein response (UPR) causes phosphorylation of eIF2 $\alpha$ . ISRIB inhibits downstream signaling of phosphorylated eIF2 $\alpha$ , which normally activates activating transcription factor 4 (ATF4) and subsequent transcription of pro-apoptotic C/EBP homologous protein (CHOP). Phosphorylation of eIF2 $\alpha$  can also inhibit protein translation. Chronic activation of this pathway ultimately leads to apoptosis. B) Q-PCR assessing the levels of ATF4-b mRNA in 2 dpf old wt AB zebrafish embryos injected with 5pg RNA encoding poly-PR or mCherry-only RNA.  $n = 30$  per group. Student's  $t$ -test  $p = 0.693$ .  $F$ -test for equal variances  $p = 0.29$ .



**Figure 5 continued:** C) Co-transfection of COS7 cells with DNA constructs encoding 100x poly-GR or 100x poly-GR peptides and GFP-only. One day after transfection, cells were treated with 1 $\mu$ g/ml puromycin for 1 hour, fixed and stained for puromycin to visualize translation (red). Poly-GR and -PR DNA transfected cells (in green) do not show any puromycin staining, while GFP-only DNA transfected cells (in green) show normal puromycin staining. Nuclei were stained with DAPI (blue). Scale bars are 20  $\mu$ m.

with stop codons reduced toxicity[154], indicating a combined effect of RNA and DPR toxicity. In *Drosophila* models, even high-level expression of RNA molecules containing 160x and 288x G<sub>4</sub>C<sub>2</sub> repeats with RNA foci but no DPRs caused little or no toxicity, supporting the importance of DPRs in C9ORF72 pathology[168, 212]. The TAG/GAG-constructs used in our study do not provide any information about RNA toxicity of the pure G<sub>4</sub>C<sub>2</sub> repeat structure. Thus, our models only provide information about poly-GR and -PR peptide toxicity, which was clearly higher than the sole effect of injections of the TAG/GAG-constructs.

Poly-GR and poly-PR peptides were mainly detected as nuclear puncta in the brain of RNA-injected zebrafish embryos. Immunofluorescence staining was not sensitive enough to robustly detect these DPRs and poly-GR expression was therefore confirmed by ELISA. Injection with very low amount of RNA may create a mosaic effect, which may explain why only some cells show nuclear poly-GR and -PR puncta throughout the zebrafish body. In addition, GR and PR aggregation can be influenced by co-expression of poly-GA[74], that is not expressed in our model. For poly-GA, toxicity was directly linked to its cytoplasmic aggregation in a mouse model and neuronal cell culture[213]. For poly-GR, cytoplasmic aggregation does not seem to be necessary to exert its toxic effect in our model and in a recently published mouse model[199]. Aggregation processes and consequences of the presence of solid aggregates may vary between individual DPRs.

Apoptosis is a normal event in the development of embryos from all species, and it plays a major role in proper (embryonic) development and organization of all tissues including the nervous system. However, in the adult brain apoptosis is linked to neurodegeneration[214]. Signs of apoptosis have been shown in spinal cord motor neurons of ALS patients[215, 216] and in neurons and astrocytes in brain tissue from FTD patients[217]. We observed increased apoptosis in zebrafish brain tissue upon expression of poly-GR and -PR peptides. The involvement of these DPRs in neuronal cell death may also be underlying the neurodegeneration observed in C9FTD/ALS patients. Next to apoptosis in brain tissue, overexpression of poly-GR and -PR in zebrafish models has been report-

ed to cause motor axon outgrowth defects such as shorter axons and aberrant branching[154, 179]. Our study confirms these findings and also shows similarities to motor axonal phenotypes in zebrafish models for other genetic causes for FTD and ALS[218, 219]. Interestingly, overexpression of poly-GA did evoke toxicity but no defects in motor neurons or motility in zebrafish[154, 180], indicating that this phenotype can not be generalized to all DPRs.

Our results show that inhibition of oxidative stress rescues poly-GR toxicity while inhibition of the ISR is sufficient to prevent apoptosis caused by poly-PR. Previous studies indicate that poly-GR and -PR share similar cellular targets, including mitochondrial and ribosomal proteins[174, 186, 201, 220]. It might therefore be interesting to test Trolox and ISRIB on both DPRs. ER stress and oxidative stress have been linked to each other in the pathophysiology of several diseases[208]. ROS and oxidative stress can cause a redox imbalance and reduce the efficiency of protein folding pathways[208]. Accumulation of misfolded proteins in the ER activates the ISR and the UPR[207]. Furthermore, activation of the ISR causes a (temporarily) stop on translation, and both poly-GR and -PR inhibit translation in our cell culture experiment, which has been described before[174, 199, 220]. Recent reports on mouse models for poly-GR and -PR show a downregulation of genes involved in ribosome biogenesis[200] and reduced translation[199]. Enhanced phosphorylation of eIF2 $\alpha$ , increased levels of ER foldase PDIA1 and upregulation of CHOP have been found in post mortem brain sections of ALS patients[221-224], indicating activation of the ISR. Furthermore, the ER membrane protein complex and ER-resident proteins such as TMX2 and CANX can modify poly-PR toxicity[210]. Dysregulation of the ER can also lead to disruptions in the membrane of mitochondria, since the two organelles are interconnected[225]. In *C9ORF72* iPSC-derived motor neurons that express both poly-GR and -PR, decreased cell survival is correlated with dysfunction in Ca<sup>2+</sup> homeostasis, increased ER stress, and reduced mitochondrial membrane potential[201]. The effect of poly-GR and -PR on mitochondrial function can also be direct via their binding to mitochondrial ribosomal proteins[186, 201]. Thus, poly-GR and -PR DPRs can evoke oxidative stress and activate the ISR via multiple ways.

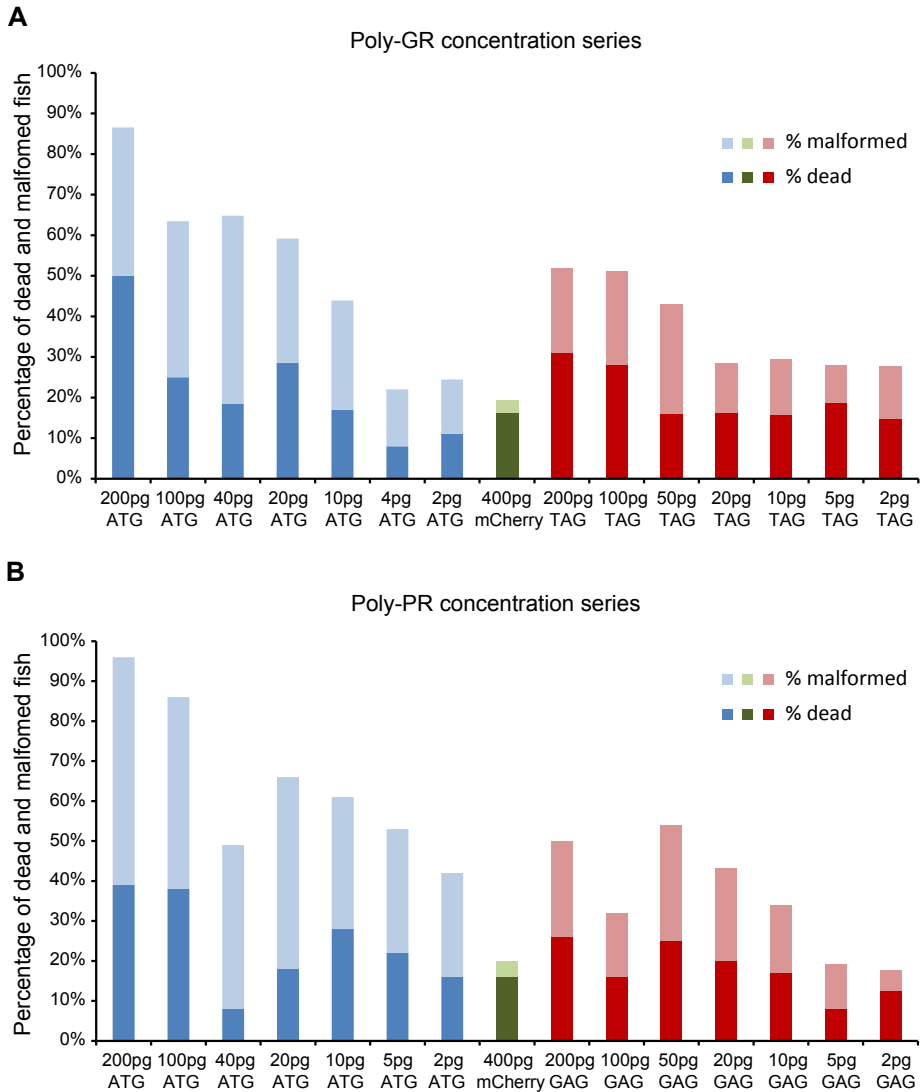
Another point of interest is the effect of ISRIB on RAN translation. Activation of the ISR and phosphorylation of eIF2 $\alpha$ , either by DPRs or through neuronal excitation and stress, can enhance RAN translation[82, 83, 226]. Upregulation of RAN translation results in the formation of more DPRs, which in turn activate the ISR. Inhibition of this positive feed-forward loop by ISRIB might decrease neuro-

toxicity by reduction of stress granule formation and restoring translation levels while at the same time prevent the formation of new toxic proteins. ISRIB might therefore have a double impact on cell viability.

The ability of poly-GR and -PR to induce massive apoptosis in the absence of the other DPRs,  $G_4C_2$  repeat RNA toxicity and haploinsufficiency illustrates the importance of these two DPRs in neuronal loss. Our toxicity model for poly-GR and -PR DPRs in zebrafish is perfectly suited for drug screens. To date, the effect of ISRIB and Trolox on the toxicity of DPRs has only been investigated in cell culture [186, 188, 210], and we are the first – to our knowledge – to confirm these rescue properties *in vivo*. Our study indicates a central role of oxidative stress and the integrated stress response in the pathogenesis of C9FTD/ALS. Additional drug screens can help to further identify and elucidate aberrant pathways involved in the neurodegeneration of C9FTD/ALS.

### **Acknowledgments**

Authors would like to thank animal caretakers of the zebrafish unit for their professional work and help with breedings and egg collection. This study was supported by the European Joint Programme - Neurodegenerative Disease Research and the Netherlands Organization for Health Research and Development (PreFrontALS: 733051042 to RW) and by Alzheimer Nederland Grant Cycle 2018 (WE.03-2018-08 to RW and FWR).



**Supplementary figure 1: Concentration series of poly-GR and –PR ATG-mediated and TAG/GAG-mediated constructs.** RNA of ATG and TAG/GAG constructs was injected in the yolk sac of fertilized oocytes in concentrations ranging from 1-200pg/nl. The amount of dead and malformed fish were assessed 24 hours after injection. Malformed embryos were defined as: severely undeveloped, having no head, a smaller head or only 1 eye. Fish with heart edema and/or tail twists were also scored as malformed. The average amount in mCherry injected fish is about 20% dead and only a few (1-5%) malformed fish. All malformed fish were taken out of any further analysis. N = 50 fish per construct per concentration.





## Chapter 3

### Inducible expression of human *C9ORF72* 36x G<sub>4</sub>C<sub>2</sub> hexanucleotide repeats is sufficient to cause RAN translation and rapid muscular atrophy in mice

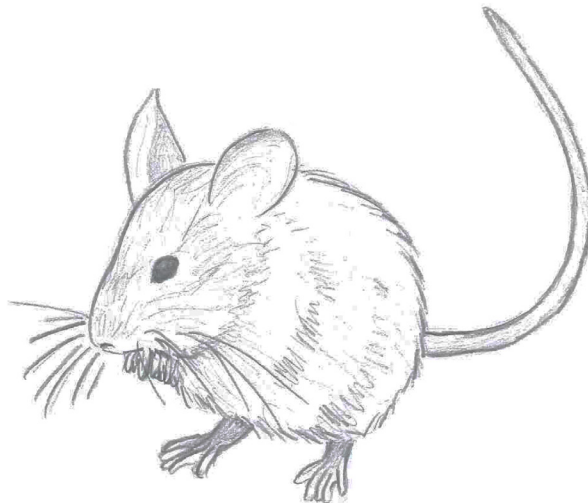
F.W. Riemsdagh<sup>1\*</sup>, E.C. van der Toorn<sup>1</sup>, R.F.M. Verhagen<sup>1</sup>, A. Maas<sup>2</sup>, L. Bosman<sup>3</sup>, R.K. Hukema<sup>1</sup> and R. Willemsen<sup>1</sup>

<sup>1</sup>Department of Clinical Genetics, Erasmus University Medical Center Rotterdam, Rotterdam, The Netherlands.

<sup>2</sup>Department of Cell Biology, Erasmus University Medical Center Rotterdam, Rotterdam, The Netherlands.

<sup>3</sup>Department of Neuroscience, Erasmus University Medical Center Rotterdam, Rotterdam, The Netherlands.

\*Corresponding author: [f.w.riemslagh@erasmusmc.nl](mailto:f.w.riemslagh@erasmusmc.nl)



### **Abstract**

The hexanucleotide G<sub>4</sub>C<sub>2</sub> repeat expansion in the first intron of the *C9ORF72* gene explains the majority of frontotemporal dementia (FTD) and amyotrophic lateral sclerosis (ALS) cases. Numerous studies have indicated the toxicity of dipeptide repeats (DPRs) which are produced via repeat-associated non-AUG (RAN) translation from the repeat expansion and accumulate in the brain of C9FTD/ALS patients. Mouse models expressing the human *C9ORF72* repeat and/or DPRs show variable pathological, functional and behavioral characteristics of FTD and ALS. Here, we report a new Tet-on inducible mouse model that expresses 36x pure G<sub>4</sub>C<sub>2</sub> repeats with ~100bp upstream and downstream human flanking regions. Brain specific expression causes the formation of sporadic sense DPRs aggregates within 6 months but no apparent neurodegeneration. Ubiquitous expression evokes abundant sense DPRs in multiple organs, leading to weight loss, neuromuscular junction disruption, myopathy and a locomotor phenotype within the time frame of four weeks. We did not observe any RNA foci nor pTDP-43 pathology. Two weeks of expression followed by two weeks of wash-out (no expression) reduced but did not completely clear DPRs. This short time period was not enough to reverse the myopathy phenotype. Thus, expression of 36x G<sub>4</sub>C<sub>2</sub> repeats, including 100bp human flanking regions, is sufficient for RAN translation of sense DPRs. In addition, expression of sense DPRs is sufficient to evoke a functional locomotor phenotype. Further research on this inducible mouse model is necessary to establish reversibility possibilities and time-windows to prevent cellular toxicity.

### **Keywords**

*C9ORF72*, ALS, FTD, mouse model, inducible, DPRs, RAN translation



## Introduction

FTD is a neurological disease characterized by neuronal loss in the frontal and temporal lobes leading to behavior and personality changes and language deficits[1, 2]. The prevalence of FTD is approximately 15-20 cases per 100.000 people and the age of onset is usually between 45 to 65 years[1]. FTD is part of a disease spectrum that also comprises ALS[13, 227]. ALS is a rapid progressive motor neuron disorder which affects the upper motor neurons in the motor cortex and the lower motor neurons in the anterior horn of the spinal cord[8, 9]. ALS patients develop muscle weakness, spasticity, atrophy and eventually paralysis[8, 9]. The prevalence of ALS is about 5 in 100.000 people and the age of onset is between 50 and 60 years of age[8, 9]. The hexanucleotide G<sub>4</sub>C<sub>2</sub> repeat expansion in the *C9ORF72* gene explains almost 90% of the families presenting with both FTD and ALS symptoms[22, 23] (referred to as C9FTD/ALS). Patients can be mosaic for repeat size and often have longer repeats in brain tissue than in DNA isolated from blood samples[42, 43, 46]. So far, repeat sizes of 30 – 4400 have been reported[39]. Associations between repeat size and FTD or ALS clinical diagnosis have not resulted in a clear picture [42-44]. Thus, the exact repeat size that triggers disease onset is not known.

Three mechanisms for the *C9ORF72* repeat expansion have been proposed to cause C9FTD/ALS[77]: 1) Hypermethylation of the repeat and surrounding CpG islands can lead to reduced levels of the normal *C9ORF72* protein[101, 109]. *C9orf72* knock-out mice have shown its essential function in immunity, but do not present with FTD or ALS symptoms[77]. However, haploinsufficiency can still modify the effects of gain-of-function mechanisms via the function of *C9ORF72* protein in autophagy and lysosomal biogenesis[118, 126]. 2) Repeat containing RNA from both sense and antisense direction can form secondary structures[78, 146] and RNA foci[56, 57]. Repeat-containing RNA or RNA foci can sequester RNA-binding proteins and prevent their normal functioning in the cell[62]. 3) The G<sub>4</sub>C<sub>2</sub> repeat can also be translated into dipeptide repeats (DPRs) via repeat-associated non-ATG (RAN) translation [57, 66, 67]. RAN translation occurs in all reading frames of sense and antisense transcripts and results in the formation of poly-glycine-alanine (GA), poly-glycine-proline (GP), poly-glycine-arginine (GR), poly-proline-alanine (PA) and poly-proline-arginine (PR). DPRs have been found throughout the brains of C9FTD/ALS patients[69] and especially poly-GR has been associated with neurodegeneration[72, 73]. Multiple cell and animal models have indicated the detrimental effect of expression of both arginine-containing DPRs poly-GR and poly-PR and the slightly less toxic

poly-GA[74, 77, 168, 169, 171-174, 178, 179, 189]. DPRs have been studied extensively (reviewed in [77]), but possible reversibility and the exact number of repeats needed for RAN translation *in vivo* are still not determined[65, 79].

So far, several mouse models of *C9ORF72* have been published, including 11 loss-of-function models and 10 gain-of-function models (reviewed in [77, 228]), and 4 DPR-only mouse models investigating the role of poly-GA[213, 229], poly-GR[199] and poly-PR[200]. All mouse models support a gain-of-function hypothesis in C9FTD/ALS, although not all BAC mouse models show neurodegeneration or a motor phenotype associated with ALS[77,228]. Here, we describe the generation and characterization of a mouse model that expresses human *C9ORF72* 36x pure G<sub>4</sub>C<sub>2</sub> repeats with 100bp upstream and downstream human flanking regions under the expression of an inducible Tet-on promotor. This system allows for temporal and spatial expression of the repeat expansion. We study both brain specific expression using a Ca<sup>2+</sup>/calmodulin-dependent protein kinase II linked reverse tetracycline-controlled trans-activator (Camk2-alpha-rtTA) driver and ubiquitous expression using a heterogeneous nuclear ribonucleoprotein 2B1 (hnRNP-rtTA) driver. Expression of 36x pure G<sub>4</sub>C<sub>2</sub> repeats was sufficient to produce low levels of sense DPRs and a locomotor phenotype upon four weeks after induction of expression.

## Material and Methods

### Cloning

DNA obtained from a C9FTD patient was assessed for the *C9ORF72* repeat expansion by Asuragen kit according to manufacturer's protocol and contained at least 54 repeats. DNA was amplified in three consecutive rounds of PCR with primers flanking the *C9ORF72* repeat expansion (forward primer 5'-CCACG-GAGGGATGTTCTTTA-3' and reverse primer 5'-GAAACCAGACCCAAACACAGA-3') and a PCR mix containing 50% betaine. The PCR program started with 10 min at 98 °C, followed by 35 cycles of 35 sec at 98 °C, 35 sec at 58°C and 3 minutes at 72°C and finished with 10 min at 72°C. The PCR product was cloned into TOPO vector PCR2.1 and restriction analysis with BsiEI (NEB) for 1 hour at 60 °C revealed a G<sub>4</sub>C<sub>2</sub> repeat expansion estimated around 50 repeats. Next, the TRE-90xCGG-GFP vector[230] was restricted with SacII (NEB) and the 90xCGG repeat expansion was replaced with the 50x G<sub>4</sub>C<sub>2</sub> repeat expansion. This vector was sequenced using a primer in the tetracycline response element (TRE) sequence (5'-CGGGTCCAGTAGGCGTGTAC-3') and revealed a repeat expansion of 36x G<sub>4</sub>C<sub>2</sub>. The final vector was cut with Aat II, PvuI and NdeI (NEB) and the

band containing the TRE-36x G<sub>4</sub>C<sub>2</sub>-GFP construct was isolated from gel, dissolved in injection buffer (10 mM Tris-HCl, pH 7.4, 0.25 mM EDTA), and used to generate transgenic mice. Experiments on human material were done under informed consent and approved by the local Medical Ethical Test Committee (METC).

### Animals

Pronuclei from oocytes of C57BL/6JRj wildtype (WT) mice were injected to create a new transgenic line harboring the TRE-36xG<sub>4</sub>C<sub>2</sub>-GFP construct. Genotyping was done 5' of the repeat expansion with the following primers: forward 5'-GGTAC-CCGGGTCGAGGTAGG-3' and reverse 5'-CTACAGGCTGCGGTTGTTTCC-3'. Founder mice, F1 and F2 were screened in an animal welfare assessment by the local animal caretakers and scored normal for litter size and health characteristics. All mice were housed in groups of 2 to 4 and were allowed to have free access to standard laboratory food and water. They were left on a 12h light/dark cycle. TRE-36xG<sub>4</sub>C<sub>2</sub>-GFP mice were crossed with hnRNP-rtTA[231] or Camk2-alpha-rtTA (kind gift of Rob Berman) on a C57BL/6JRj WT background. This gives 25% of double transgenic mice (harboring both the TRE- and one of the rtTA-constructs), 50% of single transgenic littermates (harboring either the TRE- or the rtTA-construct) and 25% of WT littermates (having no transgene). At 6 weeks of age, mice were exposed to doxycycline (dox) (Sigma) (4 grams/L) combined with sucrose (50grams/L) dissolved in drinking water. Both single and double transgenic mice received dox water. To monitor the health and wellbeing mice were weighed every weekday while on dox water. TRE-36xG<sub>4</sub>C<sub>2</sub>-GFP x hnRNP-rtTA mice were sacrificed by cervical dislocation after maximal 4 weeks of dox administration. The TRE-36xG<sub>4</sub>C<sub>2</sub>-GFP x Camk2-alpha-rtTA mice were sacrificed by cervical dislocation after maximal 24 weeks of dox administration. As required by Dutch legislation, all experiments were approved in advance by the institutional Animal Welfare Committee (Erasmus MC, Rotterdam, The Netherlands). Project license: AVD1010020172224, protocol number 17-2224-01.

### Erasmus Ladder & Grip strength

The Erasmus Ladder is a fully automated test for detecting motor performance in mice[232]. It consists of a horizontal ladder between two shelters, which are equipped with a bright white LED spotlight and pressurized air outlets. These are used as cues for departure from the shelter box to the other shelter box. The ladder has 2 x 37 rungs for the left and right side. All rungs have pressure sen-

sors, which are continuously monitoring and registering the walking pattern of the mouse. The mouse was placed in the starting box and after a period varying from 9 to 11 seconds the LED light turned on and the mouse was supposed to leave the box. If the mouse left the box before the light turned on a strong air puff drove the mouse back into the box, and the waiting period restarts. If the mouse does not leave the box within 3 seconds after the light turned on a strong air puff drove the mouse out of the box. When the mouse arrived in the other box the lights and air puff turned off and the waiting period from 9 to 11 seconds starts and the cycle repeats again, making mice run back and forth on the ladder. Mice were trained on the Erasmus Ladder at the age of 5 weeks, every day for 5 days. The mice were trained to walk the ladder for 42 runs each day. At the age of 6 weeks the mice received dox/sucrose water and were tested on Monday, Wednesday and Friday the Erasmusladder. The average percentage of missteps, that were sensed by the descended rungs, was calculated over 42 runs in one test. Grip strength of the mice was measured after 4 weeks of dox treatment with a grip strength meter from Bioseb (Chaville, France). Measurements were performed on all four limbs together.

### **Neuromuscular Junction staining**

Extensor digitorum longus (EDL) muscles were fixed in 1% paraformaldehyde (PFA) in 0.1M phosphate-buffered saline (PBS) overnight (o/n). The muscles were washed in 0.1M PBS and permeabilized in 2.5% Triton-X100 (Sigma) in 0.1M PBS for 30 minutes and incubated in 1 $\mu$ g/ml  $\alpha$ -bungarotoxin-TRITC (Invitrogen) in 1M NaCl for 30 minutes. Subsequently, muscles were incubated for 1 hour in a blocking solution (4% bovine serum albumin, 0.5% Triton-X100 in 0.1M PBS). After blocking the muscles were incubated with a polyclonal chicken anti-neurofilament antibody (2Bscientific) 1:500 in blocking solution o/n at 4°C, followed by incubation for 4 hours with anti-chicken-alexa fluor 488 (Jackson Immuno Labs). Finally, the muscles were mounted on slides with 1.8% low-melting point agarose (ThermoFisher) in 0.1M PBS and images were taken with a Zeiss LSM700 confocal microscope.

### **Fluorescent In Situ Hybridization**

Brain and EDL muscle tissues of mice were fixed in 4% PFA in 0.1M PBS o/n. Tissues were dehydrated and embedded in paraffin and cut into 6 $\mu$ m thick sections using a rotary microtome. Sections were deparaffinized using xylene and rehydrated in a standard alcohol series. Antigen retrieval was established in 0.01M

sodium citrate with pH 6 using microwave treatment of 1x 9min followed by 2x 3min at 800W. The slides were then dehydrated in an alcohol series and shortly dried to air. Next, pre-hybridization was performed in hybridization solution (dextran sulphate 10%w/v, formamide 50%, 2x SSC in diethyl pyrocarbonate (DEPC)-treated water) for 1 hour at 65°C. After pre-hybridization, hexanucleotide sense oligo (5'-Cy5-4xGGGGCC-3') and hexanucleotide antisense oligo (5'-Cy5-4xCCCCGG-3') probes (IDT) were diluted to 40nM in hybridization solution and heated to 95°C for 5 minutes. The slides were hybridized with probe mix o/n at 65°C. After hybridization the slides were washed once with 2xSSC/0.1%Tween-20 in DEPC-treated water and three times with 0.1x SSC in DEPC-treated water at 65°C. Subsequently, slides were stained with Hoechst (Invitrogen), washed with 0.1M PBS and stained with Sudan Black (Sigma). Finally, slides were dehydrated and mounted using Pro-Long Gold mounting solution (Invitrogen) and images were taken with a Zeiss LSM700 confocal microscope.

### **Immunohistochemistry**

Tissues of mice were fixed in 4% PFA in 0.1M PBS o/n, and dehydrated and embedded in paraffin. 6µm thick sections were cut using a rotary microtome. Sections were deparaffinized using xylene and rehydrated in an alcohol series. Antigen retrieval was established in 0.01M sodium citrate with pH 6 using microwave treatment of 1x 9min followed by 2x 3min 800W. Endogenous peroxidase activity was blocked with 3% H<sub>2</sub>O<sub>2</sub> and 1.25% sodiumazide in 0.1M PBS. Immunostaining was performed overnight at 4°C in PBS block buffer (0.1M PBS / 0.5%protifar / 0.15%glycine) and with the primary antibodies (see supplementary table 1 for all antibodies used in this study). The next day, sections were washed with PBS block buffer and antigen-antibody complexes were visualized by incubation with DAB substrate (DAKO) after incubation with Brightvision poly-HRP-linker (Immunologic) or anti-mouse/rabbit HRP (DAKO). Slides were counterstained with Mayer's haematoxylin and mounted with Entellan (Merck Millipore International). The slides were imaged using a Olympus BX40 microscope (Olympus).

## Results

### Generation and expression pattern of the human 36x G<sub>4</sub>C<sub>2</sub> repeat mouse model

We generated our mouse model from DNA isolated from a C9FTD patient's blood and amplified the repeat in three consecutive PCR rounds using primers that flanked the *C9ORF72* repeat expansion (for primer sequences see materials and methods). The PCR product was cloned into a Tet-on vector with a GFP reporter gene[230] (figure 1A). Sequencing of this DNA construct revealed a repeat size of 36x pure G<sub>4</sub>C<sub>2</sub> repeats with 118 bp upstream and 115 bp downstream human flanking region (supplementary figure 1). The transgene (containing the TRE promoter, 36x G<sub>4</sub>C<sub>2</sub> repeats and the GFP gene) was injected into pronu-

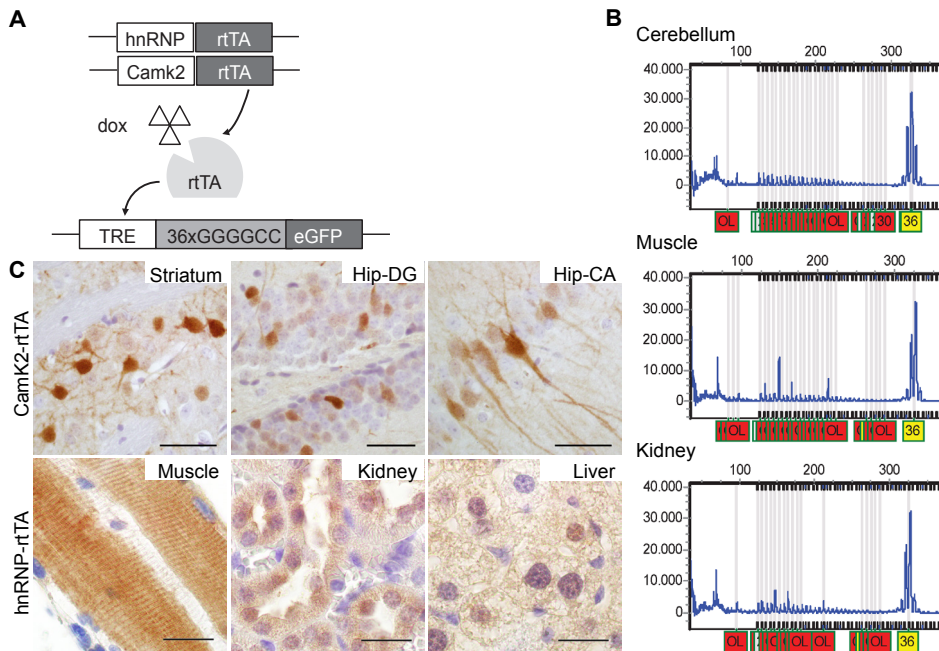


**Figure 1: Generation and expression of the 36x G<sub>4</sub>C<sub>2</sub> repeat mouse model.** A) Schematic of the Tet-on system. Mice either have a *Camk2*- $\alpha$ -rtTA or *hnRNP*-rtTA transgene that expresses rtTA in a brain specific manner or in the whole body, respectively. Upon binding of doxycycline, rtTA can bind the TRE promoter and start transcription of the *C9ORF72* G<sub>4</sub>C<sub>2</sub> repeat expansion and GFP gene, which has its own start site. B) DNA isolated from different tissues from the same mouse was analyzed with the Asuragen *C9ORF72* PCR kit and shows a repeat length of 36 in all tissues. C) Upper panel: GFP expression was detected in striatum and hippocampus cornu ammonis (CA) and hippocampus dentate gyrus (DG) in double transgenic *Camk2*- $\alpha$ -rtTA/TRE-36G<sub>4</sub>C<sub>2</sub>-GFP mice after dox administration. Lower panel; GFP expression in EDL muscle, kidney and liver of double transgenic *hnRNP*-rtTA/TRE-36G<sub>4</sub>C<sub>2</sub>-GFP mice. Scale bars are 20  $\mu$ m.

clei of C57BL/6J mice. Founder mice were screened for the presence and size of the transgene and transmission to their offspring. Genotyping for transgene presence was performed with primers 5' of the repeat. Repeat size estimation was established using the Asuragen C9ORF72 repeat kit that is also used in routine diagnostics. Repeat size remained stable between generations and between multiple organs of the same mouse (figure 1B). Transgenic mice were born at Mendelian frequencies and showed normal viability.

Heterozygous transgenic mice containing the TRE-36xG<sub>4</sub>C<sub>2</sub>-GFP transgene were bred with two different heterozygous rtTA driver lines to evoke specific expression in the brain (CamK2- $\alpha$ -rtTA) or in all tissues (hnRNP-rtTA). Litters of this breeding consist of 4 different genotypes referred to in the rest of the paper as double transgenic (containing both the TRE-36xG<sub>4</sub>C<sub>2</sub>-GFP transgene and one of the rtTA transgenes) or single transgenic (containing only TRE or only an rtTA-driver transgene). WT littermates were not used in this study. Mice were administered doxycycline (dox) in their drinking water at 6 weeks of age to turn on expression, which revealed specific expression of GFP in the double transgenic (DT) mice only and no transgene expression in single transgenic (ST) mice (supplementary figure 2). Using the ubiquitous hnRNP-rtTA driver, we observed expression in almost all tissues, including extensor digitorum longus (EDL) muscle, liver, kidney (figure 1C), heart and lung (supplementary figure 2), but not in brain and spinal cord (supplementary figure 2). Using the Camk2- $\alpha$ -rtTA driver, we observed GFP expression only in striatum and hippocampus dentate gyrus (DG) and cornu ammonis (CA) (figure 1C). GFP expression was detectable after 1 week of dox administration and remained detectable over 6 months (data not shown).

### Human 36x G<sub>4</sub>C<sub>2</sub> repeat mice show DPR expression but no RNA foci

To further characterize the expression of the transgene in our mouse model, we performed fluorescence in situ hybridization (FISH) to test for the presence of sense and antisense RNA foci. We were unable to detect RNA foci in multiple organs at multiple time points in none of the driver lines (supplementary figure 3). Despite the fact that our protocol was optimized to detect RNA foci in post-mortem human C9FTD/ALS frontal cortex paraffin tissue (supplementary figure 3), we could not detect any RNA foci in mouse paraffin tissue. Even though we could not detect any RNA foci, we were able to detect DPRs, illustrating that RNA containing the human 36x G<sub>4</sub>C<sub>2</sub> repeat expansion is expressed in our *in vivo* model. Only sense transcribed DPRs (poly-GA, -GP and -GR) were present in all GFP-posi-

tive tissues of the DT hnRNP-rtTA mice (figure 2). Poly-GA was visible as diffuse nuclear and cytoplasmic labeling, while poly-GP and -GR were only observed in the nucleus (figure 2 and supplementary figure 4). In the DT Camk2-alpha-rtTA mice, we could detect some small perinuclear aggregates in the striatum and hippocampus after 24 weeks of dox administration (figure 2). However, the numbers of aggregates were very rare (about 1 aggregate per sagittal brain section). Longer follow-up of these mice is not possible, as administration of dox for more than 6 months often leads to intestine problems. Also, both Camk2-alpha-rtTA and hnRNP-rtTA driven 36xG<sub>4</sub>C<sub>2</sub> repeat mice show no abundant pathological hallmarks of C9FTD/ALS, including p62 and pTDP-43 aggregates in brain and muscle (supplementary figure 5). Nor did we observe any signs of neurodegeneration (cleaved caspase-3 staining, supplementary figure 5), astrogliosis or microgliosis (supplementary figure 6). As DPR inclusions were very rare in Camk2-alpha-rtTA mice and expression of DPRs was evident in the hnRNP-rtTA mice, we choose to focus on the DT hnRNP-rtTA mice for further assessment of the toxic effect of DPR expression in multiple organs *in vivo*.

### **36x G<sub>4</sub>C<sub>2</sub> repeat mice develop a locomotor phenotype, rapid muscular dystrophy and NMJ abnormalities**

Ubiquitous expression of 36x G<sub>4</sub>C<sub>2</sub> repeats in DT hnRNP-rtTA mice led to profound toxicity. We started with dox treatment in 6 weeks old mice to avoid DPRs affecting normal development, which would complicate behavioral and functional read-out. A large proportion (45%) of DT mice quickly declined in body weight in the first 2-3 weeks after dox administration and had to be sacrificed (figure 3A). Mice that quickly lost weight after 2.5 weeks showed general sickness symptoms (weight loss, bad condition of the fur, reduced activity, shivering) and an enlarged bladder. The majority of mice survived longer and did not lose weight but developed a locomotor phenotype on the Erasmus ladder (figure 3B). This is a locomotor test that counts the number of missteps of mice walking on a horizontal ladder. DT mice began to show more missteps after 2 weeks of dox treatment, while they were first trained and started at the same level as their ST littermates (figure 3B) (Two-way ANOVA analysis p=0.0001 for genotype and p<0.0001 for the interaction between genotype and time). DT mice sacrificed after 4 weeks of dox treatment displayed a white appearance of leg and back muscles macroscopically (figure 3C). At the histological level a massive distortion of muscle fibers could be observed (figure 3D). Histological analysis of other tissues revealed enlarged renal tubules in the kidney and hemorrhages in the bladder of mice that quickly



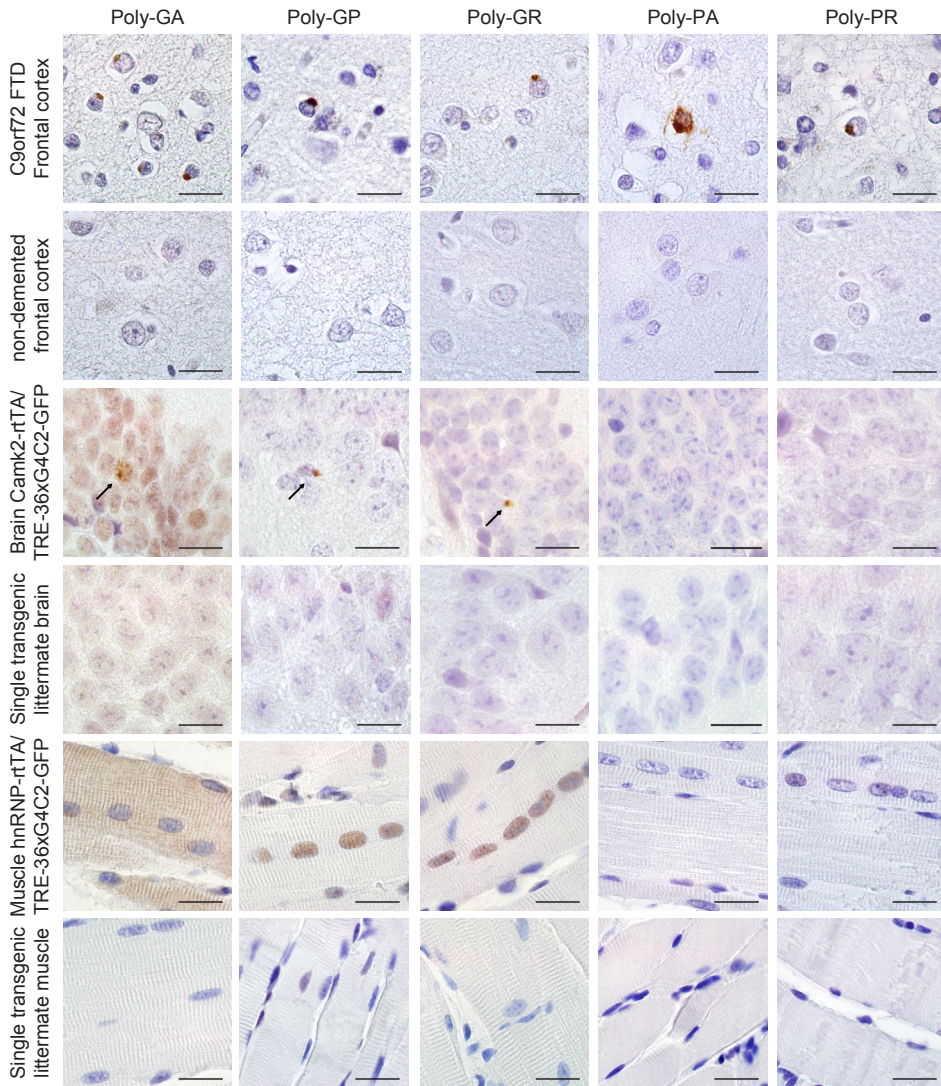


**Figure 2: Expression of 36x G<sub>4</sub>C<sub>2</sub> human repeats is enough to evoke sense DPR formation *in vivo*.** TRE-36xG<sub>4</sub>C<sub>2</sub>-GFP/Camk2-alpha-rtTA double transgenic mice show some sparse perinuclear aggregates of sense DPRs in the hippocampus dentate gyrus (pointed at by arrows). In TRE-36xG<sub>4</sub>C<sub>2</sub>-GFP/hnRNP-rtTA double transgenic mice, poly-GA shows both diffuse cytoplasmic and nuclear localization, while diffuse poly-GP and poly-GR are observed in the nucleus of the EDL muscle. Single transgenic littermates, consisting of either TRE-only or rtTA-only, are all negative for DPRs. Human post-mortem frontal cortex sections from C9FTD patients and non-demented controls was used as positive and negative control for DPR stainings. All scale bars are 20 μm.

3

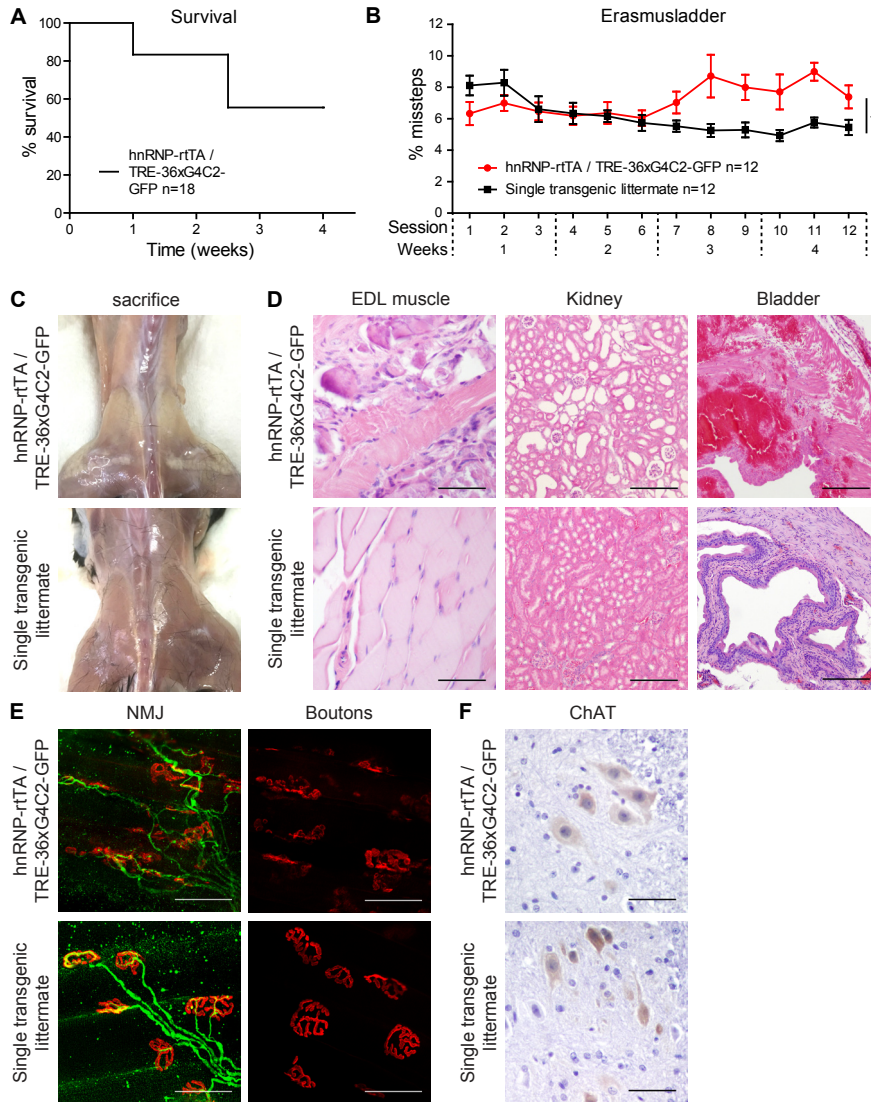


**Figure 3: Expression of 36x G<sub>4</sub>C<sub>2</sub> human repeats in vivo causes a locomotor phenotype and muscular dystrophy within 4 weeks.** A) TRE-36xG<sub>4</sub>C<sub>2</sub>-GFP/hnRNP-rTA double transgenic mice that receive dox show reduced survival after 1-3 weeks. B) Mice that survive develop a locomotor phenotype on the Erasmusladder after 7 sessions (3 sessions/week). Two-way ANOVA  $p=0.0001$  for genotype and  $p<0.0001$  for the interaction between genotype and time. Error bars represent standard error of the mean (SEM) C) Sacrificed DT mice show white appearance of back and upper leg muscles. D) HE staining of the EDL muscle, kidney and bladder of DT mice. Scale bars of EDL and kidney images are 50  $\mu$ m. Scale bar of bladder image is 200  $\mu$ m. E) NMJ staining of the EDL muscle shows dissolving boutons (red,  $\alpha$ -bungarotoxin) and disorganized axonal projections (green, neurofilament antibody). Scale bar 50  $\mu$ m. F) The number of ChAT-positive motor neurons in the spinal cord does not differ between DT and ST mice. Scale bar is 20  $\mu$ m.

lost weight at 2.5 weeks (figure 3D). Analyses of the neuromuscular junctions (NMJ) by whole mount immunostaining of the EDL muscle showed distortion of the muscular boutons and projecting motor neuron axons after 4 weeks of dox treatment (figure 3E). The number of motor neurons assessed by choline acetyltransferase (ChAT) staining of the spinal cord was not different between DT mice and ST control littermates (figure 3F). Together, these data indicate that ubiquitous expression of 36x pure G<sub>4</sub>C<sub>2</sub> repeats in our mouse model causes multi-system dysfunction, including urinary system problems and muscular dystrophy over the time course of one month.

### **No reversibility of DPR expression and muscular dystrophy in mice with 2 weeks expression followed by 2 weeks of wash-out**

In order to investigate whether the phenotype could be reversed, we set-up a pilot experiment in which we administered 6 weeks old DT and ST mice with dox for 2 weeks and then changed them back to normal drinking water for 2 weeks (wash-out). After 4 weeks in total, mice were tested on grip strength and sacrificed to assess pathology. Even though dox administration was stopped after 2 weeks, about half of the DT mice still showed a fast reduction in body weight in the first 2-3 weeks after the start of the experiment and did not survive until the end of the experiment. For the reversibility experiments we applied a simple grip strength test for analyzing the muscular strength. Grip strength only showed a statistical significant difference between DT mice and ST control mice that both were exposed for a total of 4 weeks of dox treatment (figure 4A). Other groups were not significantly different (1-way ANOVA  $p=0.04$  with post Bonferroni test). Haematoxyline-eosine (HE) staining of the EDL muscle from wash-out mice (2 weeks dox treatments followed by 2 weeks normal water) still showed parts that displayed abnormal organization (figure 4B) and the NMJ still showed disrupted boutons and axonal projections (figure 4C). Immunostaining for GFP, poly-GA and -GP in muscles was clearly reduced but was still detectable, especially in nuclei (figure 5). Only poly-GR could not be detected anymore (figure 5). In kidney, GFP and all sense DPRs were cleared efficiently after dox reversal (supplementary figure 7). This indicates that DPR clearance is different per organ or cell type. Together, dox withdrawal for 2 weeks is not sufficient to completely clear DPRs and reverse muscular dystrophy *in vivo*.

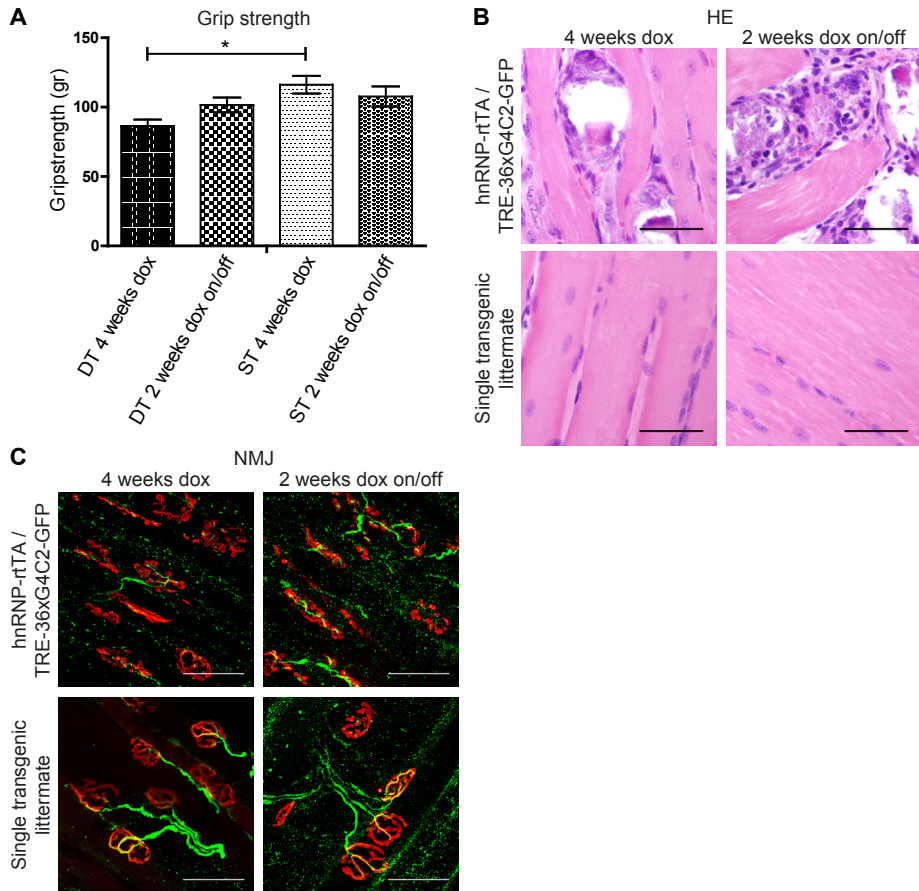


**Figure 4: Two weeks of dox withdrawal is not enough to reverse the muscular dystrophy and NMJ phenotype of TRE-36xG<sub>4</sub>C<sub>2</sub>-GFP/hnRNP-rtTA double transgenic mice.** A) Grip strength test shows a significant difference between TRE-36xG<sub>4</sub>C<sub>2</sub>-GFP/hnRNP-rtTA DT and ST control mice that received 4 weeks of dox. One-way ANOVA analysis  $p=0.04$ . Other groups are not significantly different. Error bars represent standard error of the mean (SEM).  $N=4$  for DT groups and  $n=6$  mice for ST groups. B) HE staining of the EDL muscle shows distortion in TRE-36xG<sub>4</sub>C<sub>2</sub>-GFP/hnRNP-rtTA DT mice that received 4 weeks dox or 2 weeks dox followed by 2 weeks of normal drinking water. Scale bars are 50  $\mu\text{m}$ . C) NMJ of the EDL muscle shows collapsed boutons (red,  $\alpha$ -bungarotoxin) and axonal projections (green, neurofilament antibody) in both groups of double transgenic mice. Scale bars 50  $\mu\text{m}$ .

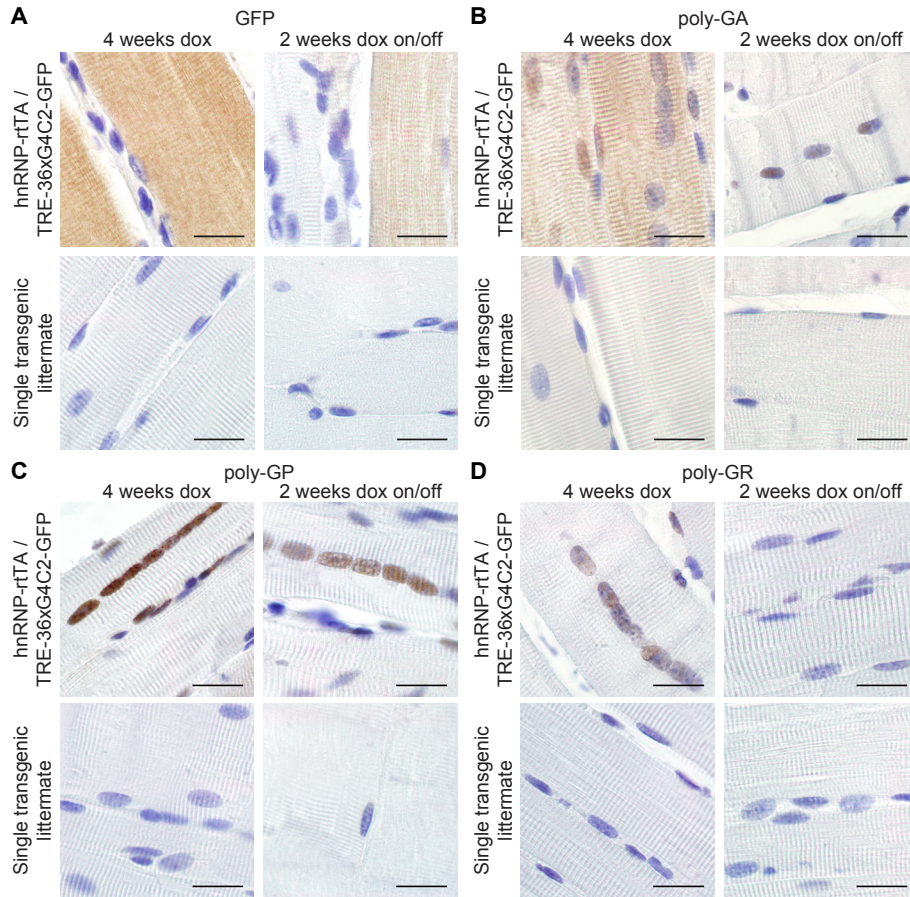


**Figure 5: GFP and sense DPRs are reduced but still visible after 2 weeks of dox withdrawal.**  
 A) GFP staining on EDL muscle of TRE-36xG<sub>4</sub>C<sub>2</sub>-GFP/hnRNP-rtTA double transgenic mice shows reduction in the intensity of staining when mice received 2 weeks of dox water followed by 2 weeks of normal drinking water compared to DT littermates that received 4 weeks of dox. B) Poly-GA staining of EDL muscle shows clearance of cytoplasmic poly-GA but retention of nuclear poly-GA after two weeks of dox withdrawal. C) Poly-GP staining is reduced in the nucleus of EDL muscle and D) Poly-GR staining is cleared from nuclei of EDL muscles after 2 weeks of dox withdrawal. Single transgenic littermates, consisting of either TRE-only or rtTA-only, are all negative for GFP and DPRs. All scale bars are 20 μm.

## Discussion

In this study, we show that ubiquitous expression of 36x pure  $G_4C_2$  repeats *in vivo* is sufficient to cause NMJ abnormalities and muscular dystrophy leading to a specific locomotor phenotype within four weeks. In contrast, expression of 36x pure  $G_4C_2$  repeats for 24 weeks in the murine brain, using a Camk2-alpha-rtTA driver, was not sufficient to result in pathology nor neurodegeneration. We speculate that expression levels of the 36x  $G_4C_2$  repeat RNA and DPRs in our Camk2-alpha-rtTA driven model are not high enough in the brain. Alternatively, the repeat length might not be long enough to evoke these abnormalities. Other gain-of-function mouse models did show sense DPR pathology and a cognitive phenotype upon expression of longer repeats[136, 191, 193, 194], indicating that expression of C9ORF72  $G_4C_2$  repeat RNA is capable of evoking these brain specific changes. Mice expressing 500 repeats show a severe phenotype compared with 29/36 repeat mice[193]. On the other hand, some C9ORF72 mouse models lack locomotor symptoms due to unknown factors [136, 162, 192]. We do detect DPRs and a locomotor phenotype in DT hnRNP-rtTA mice, which might indicate a difference in vulnerability between tissues. Besides our model, neuromuscular junction abnormalities have only been described in one BAC mouse and one AAV-102x interrupted  $G_4C_2$  mouse model [193, 194].

Our mouse model shows similarities to the BAC 29/36 repeat mouse model published by Liu et al.[193], which carries the same repeat length, displays a motor phenotype, NMJ abnormalities and motor neuron loss in the spinal cord. A limitation of our mouse model is the lack of expression of our transgene, RNA foci and DPR pathology in the brain and spinal cord, which indicates that our observed locomotor phenotype might be driven by muscular dysfunction. Also, we use a different background (C57BL/6JRj) than Liu et al., (FVB/NJ)[193]. The phenotype in our mouse model develops faster (within four weeks after dox administration) than reported by Liu et al. (first symptoms started after 16 weeks of age)[193]. Differences in disease onset might be due to expression levels, as no phenotype was observed in a 37 repeat mouse with low expression levels[193]. Our hnRNP-driven model has only 36 repeats but expression levels might be higher than the model of Liu et al, which could explain the early onset of disease symptoms.

Sense DPRs were detected as cytoplasmic or nuclear diffuse and did not form aggregates in our hnRNP-driven mouse model. We did not detect antisense DPRs, maybe because antisense  $C_4G_2$  RNA is not transcribed in our mouse model or antisense DPR levels might be too low to detect. Recent publications on poly-GR and -PR mouse models suggests that soluble

poly-GR and -PR are sufficient to cause neurodegeneration and behavioral deficits[199, 200]. On the other hand, the aggregation of poly-GA seems necessary for its toxicity in another mouse model[213]. DPRs might differ in their abilities to aggregate, their molecular targets and their effects on several cellular compartments and functions. Interestingly, poly-GA can influence the aggregation of poly-GR and -PR[74, 196], and this is confirmed in AAV-66 and AAV-149x mice in which poly-GA and -GR co-aggregate in cells with poly-GA aggregates but poly-GR remains diffuse in cells devoid of poly-GA[195, 199]. Poly-GA expression can even partially suppress poly-GR induced cell loss at the wing in the *Drosophila* model[74]. Co-overexpression of poly-GA also abolished cellular toxicity of low concentrations of poly-PR in NSC34 cells[196]. Other interactions between DPRs are still unknown and need further investigation.

Next to DPRs, we would expect to find RNA foci in our mouse model. Repeat length might influence RNA foci formation. A BAC mouse model of 110 repeats did not contain any RNA foci[136], while BAC mice with longer repeat sizes did present with RNA foci [136, 162, 192, 193]. On the other hand, AAV-mediated overexpression of 10 or 66 repeats did evoke RNA foci[191, 194], indicating that formation of RNA foci could also depend on expression levels. Even though we did not detect any RNA foci in our mouse model, we cannot exclude an effect of repeat RNA on the observed pathogenesis. Repeat-containing RNA molecules might still be able to bind and sequester molecules or proteins and affect the function of cellular processes.

Another point of interest is the lack of apparent pTDP-43 pathology in our mouse model. pTDP-43 pathology is thought to be a late event in the pathogenesis of C9FTD/ALS[77]. TDP-43 cytoplasmic aggregation is also observed during muscle regeneration[233]. Several mouse models already show behavioral phenotypes and some mild neurodegeneration before the onset of pTDP-43 neuropathology[136, 194, 199, 213, 229]. Changes in pTDP-43 solubility or cellular localization could already arise and contribute to cellular distress without the formation of cytoplasmic aggregates per se. Indeed, several reports of C9FTD/ALS showed affected individuals with DPR pathology but mild or absent TDP-43 pathology[27, 59, 66, 234, 235]. Together, our hnRNP-driven mouse model shows that ubiquitous expression of diffuse labeled sense DPRs is sufficient to evoke a locomotor phenotype without the need for RNA foci and pTDP-43 pathology.

The rapid translation of current knowledge into therapeutic intervention studies opens new avenues for drug discovery screens. So far, AON therapy has been tested in a BAC mouse model for C9ORF72 and successfully reduced the

amount of RNA foci and DPRs[136]. However, it remains unknown if this AON can also functionally reduce motor symptoms associated with the *C9ORF72* repeat. New therapies are under development, including small molecules targeting RAN translation[78, 155, 236-239]. These can be easily tested in our mouse model, as it develops a quick and robust phenotype. Our model is suited to study DPR toxicity *in vivo* but has the limitation of lack of expression and absence of neurodegeneration in the brain and spinal cord. We demonstrated that two weeks of expression followed by two weeks of wash-out (expression turned off) is not sufficient to prevent mice from developing muscular dystrophy. This indicates that transgene RNA or DPRs that were already produced during the first two weeks of dox administration continue to exercise their toxic effects. A recent publication estimated the half-time of most DPRs to be >200 hours[226]. Half time was longer for poly-GA puncta than for diffuse poly-GA and increased for poly-GR when localized in the nucleus[226]. Earlier intervention might be able to halt or reverse symptoms, but the preferred time-window for treatment is probably before the onset of symptoms.

Together, we provide evidence that expression of human 36x pure G<sub>4</sub>C<sub>2</sub> repeats is sufficient to evoke RAN translation and a locomotor phenotype *in vivo*. Due to high expression of sense DPRs driven by hnRNP-rtTA, a rapid progression of muscular dystrophy and NMJ disruption phenotype developed. This mouse model allows for determination of time-windows for treatment and for fast *in vivo* screening of new drugs and compounds that act on systemic toxicity of sense DPRs.

### **Acknowledgements**

Authors would like to thank Leonard Petrucelli for providing an aliquot of his anti-PA antibody and Elize Haasdijk for an aliquot of the ChAT antibody. We thank Lies-Anne Severijnen for helping to select the right primary & secondary anti-neurofilament antibodies. This study is supported by the European Joint Programme - Neurodegenerative Disease Research and the Netherlands Organization for Health Research and Development (PreFrontALS: 733051042 to RW) and by Alzheimer Nederland (WE03.2012-XX to RW).

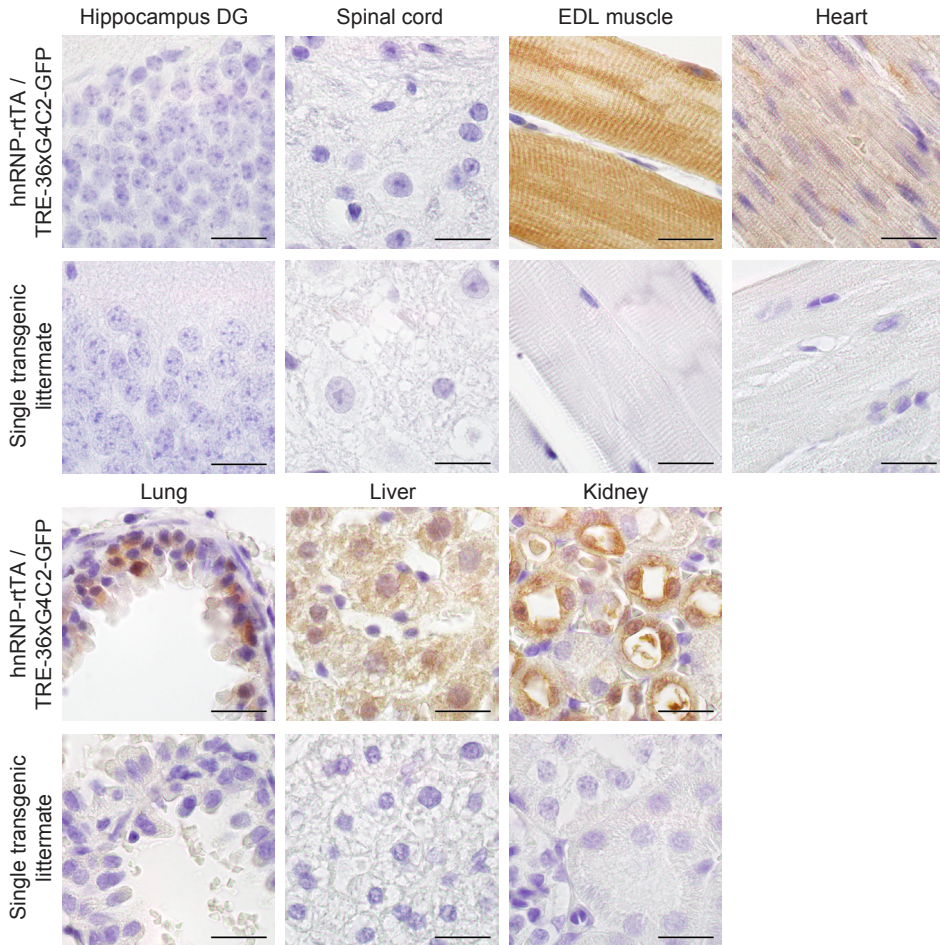


**Supplementary table 1: antibodies**

Ab name	Host	Company	Cat.nr	Dilution
GA	mouse	Millipore, clone 5E9	MABN889	1:500
GP	rabbit	Bio Connect Life Sciences	24494-1-AP	1:250
GR	mouse	LifeTein Services	n.a. (costum-made)	1:4000
PR	mouse	LifeTein Services	n.a. (costum-made)	1:500
PA	mouse	Gift from Petrucelli	n.a.	1:2500
pTDP-43	mouse	Cosmo bio	CAC-TIP-PTD-M01	1:1000
p62	mouse	BD Biosciences	610833	1:100
Neurofilament	chicken	2B Scientific Ltd.	CPCA-NF-H	1:500
GFAP	rabbit	Sigma	G-9269	1:100
Iba1	rabbit	Wako	019-19741	1:200
ChAT	goat	Chemicon	AB144P	1:500
Poly-HRP anti Ms/Rb IgG	goat	Immunologic	DPV055HRP	undiluted
anti-mouse HRP	goat	DAKO	P0260	1:100
anti-rabbit HRP	goat	DAKO	P0217	1:100
anti-mouse Cy2	goat	Jackson	715-255-150	1:100
anti-rabbit Cy3	goat	Jackson	711-165-152	1:100
anti-chicken 488	goat	Jackson	303-545-006	1:100
anti-goat HRP	rabbit	DAKO	P0449	1:100

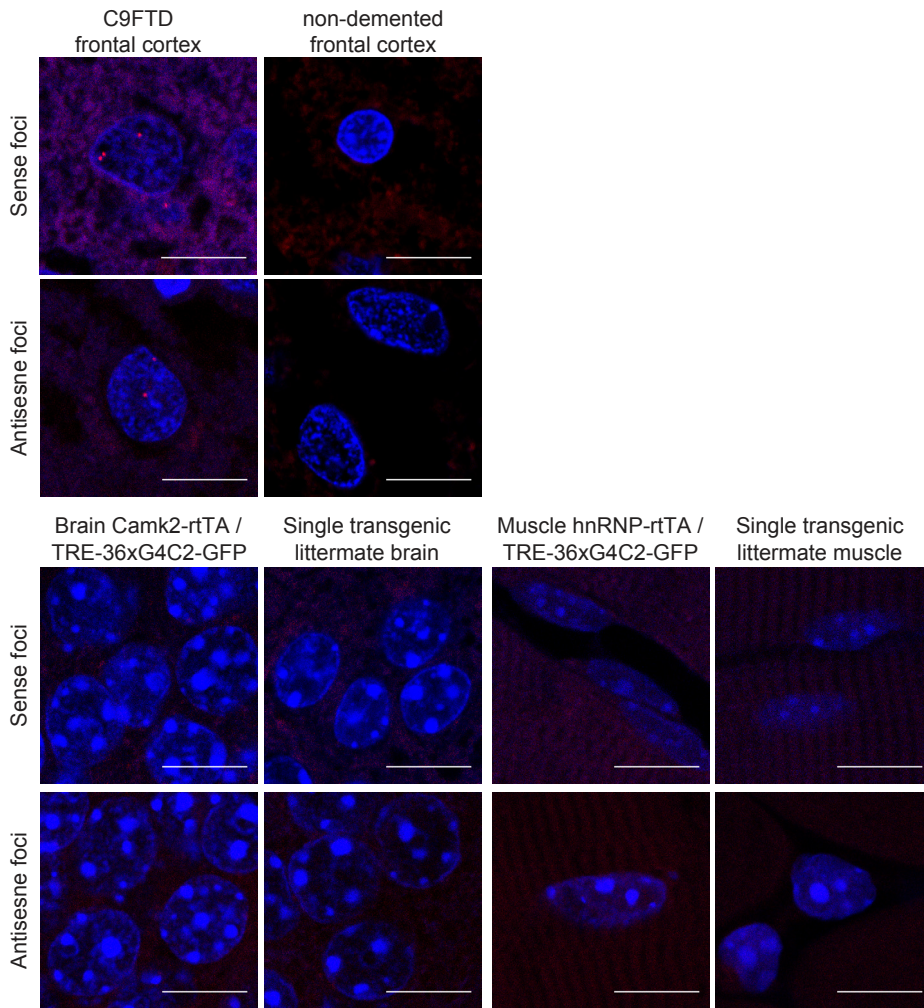


C9ORF72 36x pure G<sub>4</sub>C<sub>2</sub> hexanucleotide repeat mouse model

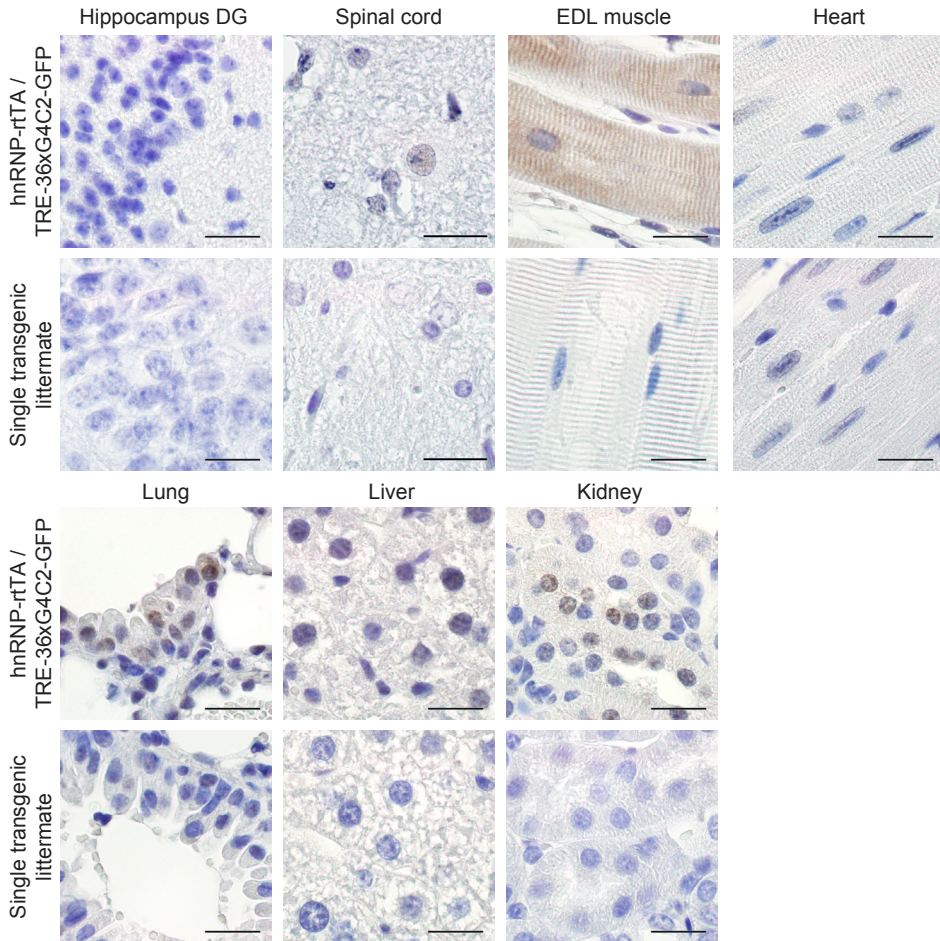


3

**Supplementary figure 2: GFP expression in EDL muscle, heart, lung, liver and kidney of TRE-36xG<sub>4</sub>C<sub>2</sub>-GFP/hnRNP-rtTA double transgenic mice. No GFP staining was observed in the hippocampus dentate gyrus or in the spinal cord of DT mice. Single transgenic littermates, consisting of either TRE-only or rtTA-only, are all negative for GFP staining. Scale bars are 20 μm.**

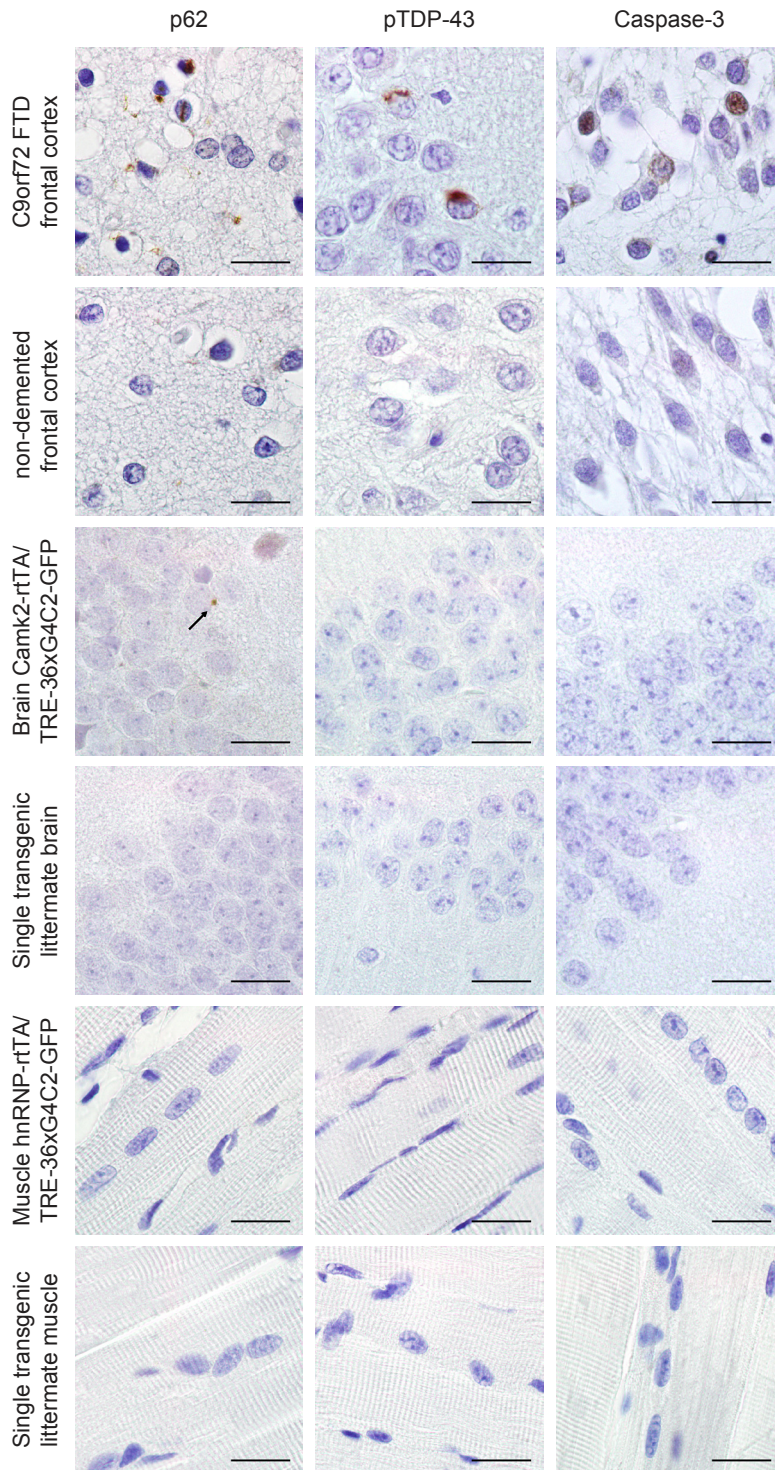


**Supplementary figure 3:** No sense nor antisense RNA foci were found in *TRE-36xG<sub>4</sub>C<sub>2</sub>-GFP/Camk2-rtTA* and *TRE-36xG<sub>4</sub>C<sub>2</sub>-GFP/hnRNP-rtTA* double transgenic mice and control single transgenic littermates. Only frontal cortex samples of C9FTD cases present with some nuclear sense and antisense foci. Scale bars are 10  $\mu$ m.

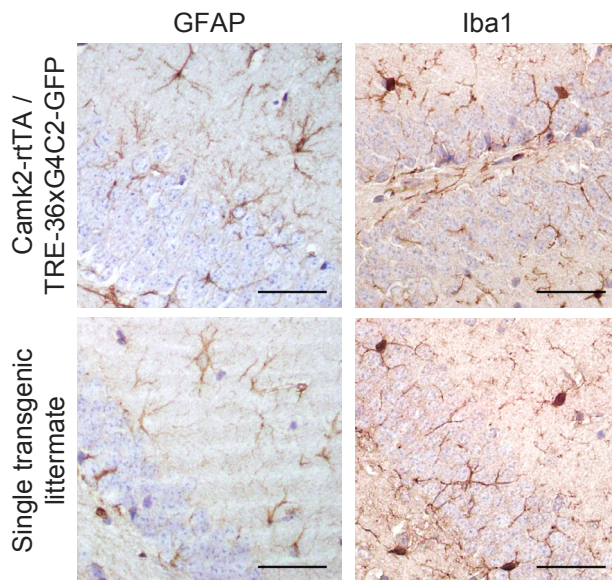


3

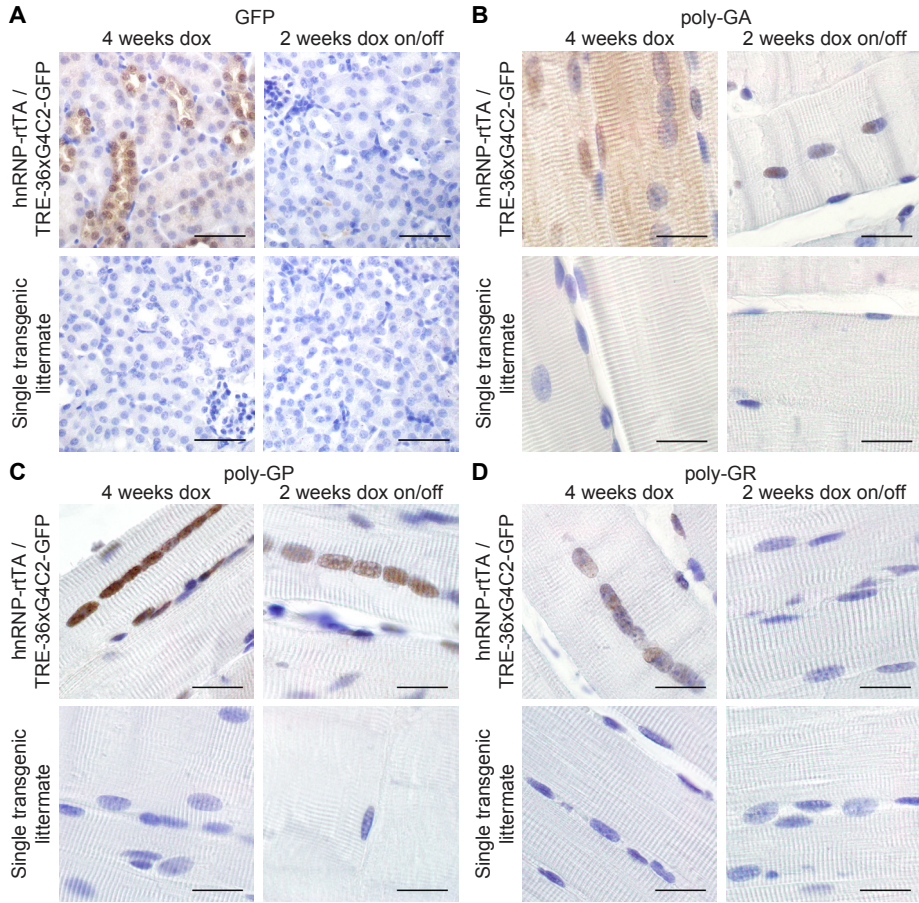
**Supplementary figure 4: Poly-GA expression in EDL muscle, lung, liver and kidney of TRE-36xG<sub>4</sub>C<sub>2</sub>-GFP/hnRNP-rtTA double transgenic mice.** No poly-GA staining was observed in the hippocampus dentate gyrus or in the spinal cord of DT mice. Single transgenic littermates, consisting of either TRE-only or rtTA-only, are all negative for poly-GA staining. Scale bars are 20  $\mu$ m.



**Supplementary figure 5 (left side): Expression of 36x G<sub>4</sub>C<sub>2</sub> human repeats does not cause abundant p62, pTDP-43 and cleaved-caspase 3 pathology.** TRE-36xG<sub>4</sub>C<sub>2</sub>-GFP/Camk2-alpha-rtTA double transgenic mice show some sparse perinuclear aggregates of p62 in the hippocampus dentate gyrus (arrow). TRE-36xG<sub>4</sub>C<sub>2</sub>-GFP/hnRNP-rtTA double transgenic mice do not present with any p62, pTDP-43 or cleaved-caspase-3 pathology in EDL muscle. Single transgenic littermates, consisting of either TRE-only or rtTA-only, are negative for all pathology. All scale bars are 20 μm.



**Supplementary figure 6: TRE-36xG<sub>4</sub>C<sub>2</sub>-GFP/Camk2-alpha-rtTA double transgenic mice do not show astrogliosis or microgliosis.** Astrogliosis was assessed with GFAP labeling and microgliosis was tested with Iba1 staining. No differences in amount or morphology of GFAP-positive and Iba1-positive cells were seen in the hippocampus dentate gyrus of TRE-36xG<sub>4</sub>C<sub>2</sub>-GFP/Camk2-alpha-rtTA double transgenic mice and single transgenic control littermates. Scale bars are 20 μm.



**Supplementary figure 7: GFP and sense DPRs are cleared from the kidney after 2 weeks of dox withdrawal.** A) GFP staining on kidney of TRE-36xG<sub>4</sub>C<sub>2</sub>-GFP/hnRNP-rtTA double transgenic mice shows clearance of GFP staining when mice received 2 weeks of dox water followed by 2 weeks of normal drinking water compared to DT littermates that received 4 weeks of dox. B) Poly-GA staining of kidney shows clearance of poly-GA after two weeks of dox withdrawal. C) Poly-GP staining and D) Poly-GR staining are also cleared from kidneys after 2 weeks of dox withdrawal. Single transgenic littermates received 2 or 4 weeks of dox and are all negative for GFP and DPRs. All scale bars are 50  $\mu$ m.



C9ORF72 36x pure G<sub>4</sub>C<sub>2</sub> hexanucleotide repeat mouse model

3



## Chapter 4

### **HR23B pathology preferentially co-localizes with p62, pTDP-43 and poly-GA in C9ORF72-linked frontotemporal dementia and amyotrophic lateral sclerosis**

F.W. Riemsdagh<sup>1\*</sup>, H. Lans<sup>2</sup>, H. Seelaar<sup>3</sup>, L.W.F.M. Severijnen<sup>1</sup>, S. Melhem<sup>3</sup>, W. Vermeulen<sup>2</sup>, E. Aronica<sup>4</sup>, R.J. Pasterkamp<sup>5</sup>, J.C. van Swieten<sup>3</sup>, R. Willemsen<sup>1</sup>

<sup>1</sup>Department of Clinical Genetics, Erasmus University Medical Center Rotterdam, Rotterdam, The Netherlands.

<sup>2</sup>Department of Molecular Genetics, Oncode Institute, Erasmus University Medical Center Rotterdam, Rotterdam, The Netherlands.

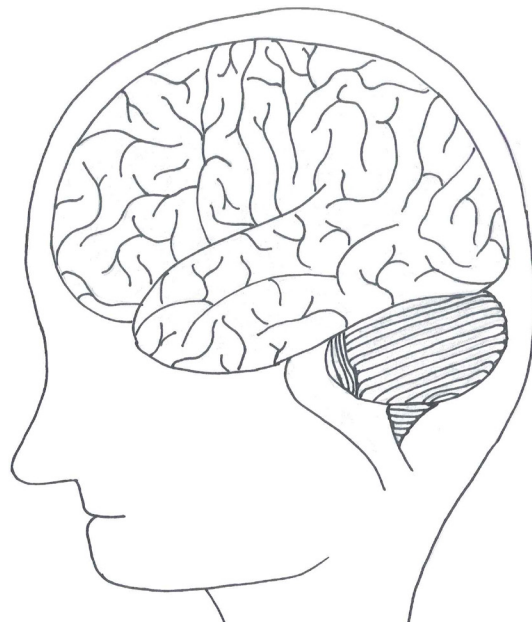
<sup>3</sup>Department of Neurology, Erasmus University Medical Center Rotterdam, Rotterdam, The Netherlands.

<sup>4</sup>Department of (Neuro)Pathology, Amsterdam Neuroscience, Amsterdam UMC, University of Amsterdam, Amsterdam, The Netherlands

<sup>5</sup>Department of Translational Neuroscience, University Medical Center Utrecht Brain Center, Utrecht University, Utrecht, The Netherlands

\*Corresponding author: [f.w.riemsdagh@erasmusmc.nl](mailto:f.w.riemsdagh@erasmusmc.nl)

Acta Neuropathologica Communications 2019 Mar 13;7(1):39.



### **Abstract**

Human homologue of yeast UV excision repair protein Rad23b (HR23B) inclusions are found in a number of neurodegenerative diseases, including frontotemporal dementia (FTD), Huntington's disease (HD), spinocerebellar ataxia type 3 and 7 (SCA3/7), fragile X associated tremor/ataxia syndrome (FXTAS) and Parkinson's disease (PD). Here, we describe HR23B pathology in C9ORF72 linked FTD and amyotrophic lateral sclerosis (ALS) cases. HR23B presented in neuropils, intranuclear inclusions and cytoplasmic and perinuclear inclusions and was predominantly found in cortices (frontal, temporal and motor), spinal cord and hippocampal dentate gyrus. HR23B co-localized with poly-GA-, pTDP-43- and p62-positive inclusions in frontal cortex and in hippocampal dentate gyrus, the latter showing higher co-localization percentages. HR23B binding partners XPC, 20S and ataxin-3, which are involved in nucleotide excision repair (NER) and the ubiquitin-proteasome system (UPS), did not show an aberrant distribution. However, C9ORF72 fibroblasts were more sensitive for UV-C damage than healthy control fibroblasts, even though all factors involved in NER localized normally to DNA damage and the efficiency of DNA repair was not reduced. HR23Bs other binding partner NGly1/PNGase, involved in ER-associated degradation (ERAD) of misfolded proteins, was not expressed in the majority of neurons in C9FTD/ALS brain sections compared to non-demented controls. Our results suggest a difference in HR23B aggregation and co-localization pattern with DPRs, pTDP-43 and p62 between different brain areas from C9FTD/ALS cases. We hypothesize that HR23B may play a role in C9ORF72 pathogenesis, possibly by aberrant ERAD functioning.

### **Keywords**

C9ORF72; ALS; FTD; HR23B; ERAD; NGly1; DPRs; poly-GA

## Introduction

The hexanucleotide (G<sub>4</sub>C<sub>2</sub>) repeat expansion in the chromosome 9 open reading frame 72 (*C9ORF72*) gene is the most common genetic cause of FTD and ALS[22, 23]. FTD is characterized by the degeneration of the frontal and temporal parts of the brain, leading to abnormalities in behavior, language and personality[1]. ALS affects motor neurons in the brain and spinal cord, leading to loss of motor function, muscle weakness, breathing problems and eventually paralysis[7]. Clinical, pathological and genetic factors connect FTD and ALS, and in families often patients present with symptoms of both disorders[14]. The discovery of the *C9ORF72* hexanucleotide repeat expansion confirmed the genetic overlap between FTD and ALS, collectively referred to as C9FTD/ALS. Pathologically, both diseases present with inclusions of autophagy protein p62/sequestosome 1 (p62) and inclusions of phosphorylated 43kDa TAR DNA-binding protein (pTDP-43), of which the latter is predominantly found in areas that are known to display substantial neurodegeneration[51, 85].

The possible pathological mechanisms by which the *C9ORF72* repeat expansion can lead to FTD and ALS are: 1) hypermethylation of the repeat expansion and the CpG promoter region of the *C9ORF72* gene leading to haploinsufficiency [53, 101], 2) retention of repeat containing intron 1 in mRNAs causing RNA foci to appear in both nucleus and cytoplasm that sequester RNA-binding proteins[61, 152] or 3) the production of dipeptide repeats (DPR) by unconventional repeat-associated-non-AUG (RAN) translation of the repeat[57, 66, 67]. These DPRs are produced from both sense and antisense transcripts resulting in 5 possibly toxic peptides (poly-GA, -GP, -GR, -PR and -PA) and are found as inclusions in post-mortem brain material of *C9ORF72* carriers [69, 70].

How these three mechanisms – alone or in combination – cause neurodegeneration is currently under investigation. Several studies have indicated that especially the DPRs are toxic in both cell culture and *in vivo* models, with the arginine-containing poly-GR and -PR DPRs being the most detrimental[77, 168, 171]. And poly-GR has been associated with neurodegeneration in human post-mortem brain sections[72, 73]. DPRs seem to cause various types of stress to the cell, including ER-stress, mitochondrial stress and nucleolar stress[77]. They can disturb the formation of membrane-less organelles, including RNA granules, nucleoli, spliceosomes and the nuclear pore complex (NPC) and facilitate the formation of stress granules[176]. Furthermore, nucleocytoplasmic transport and autophagy defects have been reported[75, 187, 188]. In addition to the list of disturbed pathways found in model systems of C9FTD/ALS, there have

also been a substantial number of proteins found to interact, bind or aggregate with repeat-containing RNA or DPRs[62, 240]. Currently, the primary affected pathways involved in the pathogenesises of C9FTD/ALS are under debate[77, 98, 241]. Constituents of inclusions in human C9FTD/ALS brain material might provide a tool to identify key players in neurodegeneration.

Here, we tested a set of proteins implicated in aberrant pathways in *C9ORF72* disease models for their presence in pathology or abnormal localization in post-mortem human C9FTD/ALS brain sections. We selected Ran-GAP for its implication in nucleocytoplasmic transport defects[155], ADARB2 for its role in RNA binding and editing[107] and HR23B for its dual function in both DNA repair and the UPS[242]. FMRP and Pur-alpha were selected for their binding to *C9ORF72* mRNA, their localization in stress granules and their rescue effect in multiple *C9ORF72* models[149]. Surprisingly, we found only HR23B protein to be a constituent of inclusions observed in C9FTD/ALS cases. In this report, we describe HR23B distribution and its co-localization with known *C9ORF72* pathological hallmarks (DPRs, p62 and pTDP-43). Furthermore, we analyze HR23B function in DNA damage repair, the ubiquitin-proteasome system and ER-associated degradation. Disturbances of these pathways may contribute to the disease onset and/or progression of C9FTD/ALS.

## Methods

Five *C9ORF72* FTD, two *GRN* FTD, two *MAPT* FTD, three sporadic ALS and three non-demented control human brain sections were provided by the Dutch Brain Bank. *C9ORF72* ALS brain material of two patients was collected post-mortem at the department of Neuropathology of Amsterdam UMC, University of Amsterdam, according to local legal and ethical regulations. Patients or relatives gave informed consent for autopsy and use of brain tissue for research purposes. Information about our patient cohort can be found in table 1. Human fibroblasts lines were provided by the cell repository of the department of clinical genetics. All participants gave written informed consent for all obtained materials. The study was approved by the Medical and Ethical Review Committee of the Erasmus Medical Center. All procedures performed in studies involving human participants were in accordance with the ethical standards of the institutional and/or national research committee and with the 1964 Helsinki declaration and its later amendments or comparable ethical standards.

**Table 1: Patient characteristics**

Patient	Clinical diagnosis	Family history	Genetic diagnosis	Age of onset	Disease duration	Male / Female	Brain weight
1	bvFTD	FTD	C9ORF72	51,8	8,7	Male	960 gr
2	bvFTD	FTD	C9ORF72	55,8	9,1	Male	1184 gr
3	bvFTD	FTD and ALS	C9ORF72	66,4	8,1	Female	1060 gr
4	bvFTD	ALS and dementia	C9ORF72	63,2	6,8	Female	958 gr
5	bvFTD	FTD and ALS	C9ORF72	55,2	9,5	Male	1075 gr
6	FTD	N/A	Progranulin (Gln200X)	60,6	5,5	Female	894 gr
7	FTD	FTD	Progranulin (Ser82 ValfsX174)	47,4	4,3	Female	unknown
8	FTD	FTD	MAPT (G272V)	42,6	8,4	Male	962 gr
9	FTD	FTD	MAPT (P301L)	51,1	9,7	Male	887 gr
10	ALS	N/A	unknown	70	1	Male	1428 gr
11	ALS	N/A	unknown	65	2,2	Female	1125 gr
12	ALS	N/A	unknown	75	1,1	Male	1255 gr
13	ALS	N/A	C9ORF72	60	4,4	Female	1390 gr
14	ALS	N/A	C9ORF72	66	3,5	Male	1275 gr
15	ALS	N/A	C9ORF72	71	2,4	Female	1080 gr
16	Non-demented	N/A	unknown	N/A	N/A	Female	1080 gr
17	Non-demented	N/A	unknown	N/A	N/A	Male	1215 gr
18	Non-demented	N/A	unknown	N/A	N/A	Female	1139 gr

**Immunohistochemistry on human brain sections**

Human brain sections (6  $\mu$ m) were deparaffinized in xylene and rehydrated (100%-96%-90%-80%-70%-50% EtOH serie). Antigen retrieval was done in 0.01 M sodium citrate, pH6.0 using pressure cooker treatment. Endogenous peroxidase activity was blocked with 0.6% H<sub>2</sub>O<sub>2</sub> and 1,25% sodium azide in 0.1M PBS. Immunostaining was performed overnight at 4°C in PSB block buffer (0.1M PBS/0.5%protifar/0.15%glycine). Antibodies used in this study are listed

in supplementary table 3, including concentration and brand/catalogue number. Antigen-antibody complexes were visualized by incubation with DAB substrate (DAKO) after incubation with Brightvision poly-HRP-linker (Immunologic) or anti-mouse/rabbit HRP (DAKO). Slides were counterstained with Mayer's haematoxylin and mounted with Entellan (Merck Millipore International). The slides were then left to dry in the fume hood for an hour and thereafter put in an 37°C incubator overnight. Pictures were taken by using an Olympus BX40 microscope (Olympus).

### **Immunofluorescence staining on human brain sections**

Human brain sections were treated as described above. After incubation with the primary antibody, sections were washed with PBS block buffer (1xPBS/0.5%protifar/0.15%glycine) and incubated with secondary anti-mouse/rabbit Cy2/3 linked antibodies (Jackson). To remove background staining, a 10 min incubation with Sudan Black (Sigma, 0.1 gr in 100ml 70% ethanol, filtered) was done. To visualize nuclei, slides were incubated for 10 min with Hoechst 33342(Invitrogen). Slides were mounted with ProLongGold (Invitrogen) and kept at 4°C until imaging at a Zeiss LSM700 Confocal microscope.

### **Assessment of neurodegeneration and protein pathology**

For the neuropathological assessment we used brain sections from 5 *C9ORF72* FTD cases (see table 1). Five different brain regions (frontal cortex, temporal cortex, motor cortex, hippocampus and cerebellum) per patient were semi-quantified on neurodegeneration and pathological score of p62, pTDP-43 and HR23B (supplementary table 1). Counting was not performed in a blinded fashion. Neurodegeneration was assessed on haematoxylin and eosin (HE) sections and graded as absent (0), mild (1), moderate (2) or severe (3) based on the presence of neuronal loss. The neurodegenerative score from the pathological report was also taken into account. Pathological scores were rated as (0) if completely absent, rare (1) if only a few could be found one brain section, occasional (2) if they not present in every microscopic field, moderate (3) if at least a few examples were present in most microscopic fields, and numerous (4) when many were present in every microscopic field[69]. We reported the overall number of immunoreactive inclusions (total score) as well as the number of neuronal cytoplasmic inclusions (NCI), neuronal intranuclear inclusions (NII) and dystrophic neurites (DN) (supplementary table 1). Total scores were assessed independent from NCI, NII and DN scores and represent an impression of the global load of pathology and



the number of inclusions using the same grading system as described above. Quantification of co-localization of HR23B with DPRs, p62 and pTDP-43 was not performed in a blinded fashion.

### Colony forming assays

Human fibroblast lines from 4 *C9ORF72* carriers (13E634, 13E659, 17E0225, 17E0278) and 4 controls (81E253, 86E1375, 06E0717 and 99E0774) were obtained from the cell repository of the department of clinical genetics and the XP25RO fibroblast line was provided by the department of molecular genetics. Fibroblasts were cultured in DMEM medium (Gibco) with 10% fetal calf serum, 1% penicillin/streptavidin and 1% non-essential amino acids. To determine UV-sensitivity, human fibroblasts were seeded in triplicate in 10 cm plates (Greiner Bio-one) in a density of 2000 cells/plate. After 24 hours, cells were treated with increasing doses of UV-C (254 nm UV-C lamp, Philips). After 5-7 days, colonies were fixed with 0.1 % w/v Coomassie Blue (Bio-Rad) in a 50% Methanol, 10% Acetic Acid solution. Colonies were counted with the integrated colony counter GelCount (Oxford Optronix). Counting was performed automatically with the same settings for each fibroblast cell line, but not in a blinded fashion.

4

### Immunofluorescence on human fibroblasts

To determine DNA damage recruitment of NER proteins, human fibroblasts were seeded on coverslips and after 1 week in culture irradiated with 60 J/m<sup>2</sup> (254 nm UVC lamp, Philips) through an 8 µm microporous filter (Millipore) to induce sub-nuclear local DNA damage. Cells were fixed after 30 min with 2% paraformaldehyde and permeabilized with 0.1 % Triton X-100 for 20 min. Next, cells were incubated with fresh 0.07 M NaOH in PBS for 5 min to denature DNA and enable CPD staining. Cells were then washed with PBS containing 0.15% glycine and 0.5% BSA and incubated with primary antibodies (see supplementary table 3) overnight at 4°C. The next day, cells were washed with 0.1% Triton X-100 and incubated with Alexa Fluor conjugated secondary antibodies (488, 555 and 633; Invitrogen) for 1 hour at RT. Coverslips were mounted using ProLongGold with DAPI (Invitrogen) and imaged using a Zeiss LSM700 microscope.

### Unscheduled DNA Synthesis (UDS)

To measure NER capacity, human fibroblasts were grown on coverslips for 1 week in culture and irradiated with 16 J/m<sup>2</sup> UV-C. After irradiation, cells were incubated for 1 h in UDS medium (F10, 1% PS, 10% dialyzed serum) with 2%

HEPES and 1% 5-ethynyl-2'-deoxyuridine (EdU, Invitrogen). After 1 hour, medium was changed to normal DMEM medium (10% FCS, 1% NEAA, 1% PS) for 10 min. Next, cells were fixed in 4% paraformaldehyde and permeabilized with 0.1% Triton X-100. Blocking was done using 1.5% BSA in PBS for 30 min. EdU incorporation was visualized by incubating cells for 1 h at room temperature with Click-it reaction cocktail containing Atto 594 Azide (60  $\mu$ M, Atto Tec.), Tris-HCl (50 mM, pH 7.6),  $\text{CuSO}_4 \cdot 5\text{H}_2\text{O}$  (4 mM, Sigma) and ascorbic acid (10 mM, Sigma). After the Click-it reaction, cells were washed with 0.1% Triton X-100, incubated with Hoechst 33342 (Invitrogen) for 10 min and mounted with ProLongGold (Invitrogen). Images were acquired using a Zeiss LSM700 microscope. UDS levels were quantified by measuring the total nuclear fluorescence intensities (in at least 50 cells per experiment) with FIJI image analysis software. Intensity levels were averaged and normalized to the fluorescence levels in unirradiated cells. Quantification of intensity levels was done automatically with FIJI but was not performed in a blinded fashion.

## Results

### **Characterizing Ran-GAP, ADARB2, HR23B, FMRP and Pur-alpha in a cohort of C9FTD patients and non-demented controls**

We started with assessing the localization of ras-related nuclear protein GTPase activating protein (Ran-GAP) in C9FTD patient brain sections. We studied five FTLD-TDP cases with the *C9ORF72* repeat expansion and three non-demented cases (for information about our cohort, see table 1). We predominantly found a diffuse nuclear staining or nuclear envelop staining of Ran-GAP. Most nuclei were round-shaped but occasionally we observed misfolded nuclei or the invagination of the nuclear membrane (supplementary figure 1). The number of oddly-shaped nuclei did not clearly differ between C9FTD cases and non-demented controls. Next, we investigated Adenosine Deaminase, RNA Specific B2 (ADARB2) localization. ADARB2 immunostaining showed both nuclear and cytoplasmic localization in both C9FTD and non-demented controls. We could detect some intranuclear inclusions in the hippocampus dentate gyrus of C9FTD patients (supplementary figure 2A). However, IF double staining of ADARB2 with p62 showed similar results between hippocampal nuclei of C9FTD patients and non-demented cases (supplementary figure 2B).

Next, we stained for HR23B and found different types of inclusions in cortical areas, hippocampus and cerebellum of C9FTD cases (figure 1 and supplementary figure 5). Most cytoplasmic inclusions showed a round and perinuclear

appearance (figure 1A & 1C), while some inclusions had a negative central core surrounded by a positive halo labeling (figure 1E). Neuropils were mostly found in layer 2 of cortical areas (figure 1A). Intranuclear inclusions were also observed, including cat-eye inclusions (figure 1B). Overall, layer 2/3 and layer 5/6 of frontal and temporal cortices showed the highest HR23B pathological burden in C9FTD cases, followed by motor cortex, hippocampus and cerebellum (figure 1G and supplementary table 1). Hippocampus dentate gyrus (DG) harbored some perinuclear inclusions and hippocampus cornu ammonis (CA) showed some cells with strong nuclear staining (supplementary figure 5). Cerebellum showed low HR23B staining with some nuclear and perinuclear inclusions in the granular layer and nearly absent in the molecular layer (supplementary figure 5). Non-demented controls showed normal nuclear localization of HR23B (supplementary figure 5).

Furthermore, we assessed fragile X mental retardation protein (FMRP) localization in C9FTD cases. Punctuated FMRP staining in the cytoplasm indicative of the formation of stress granules was absent in our C9FTD cases (supple-

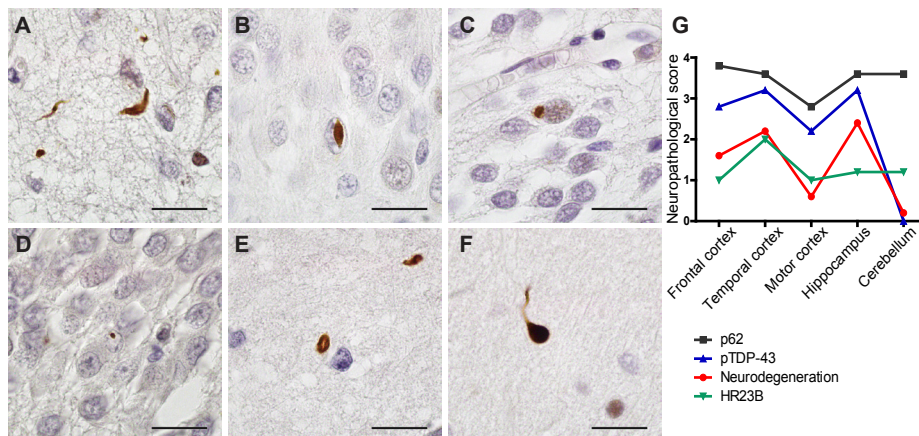


**Figure 1: Type and spreading of HR23B pathology found in C9FTD cases. Different types of HR23B pathology in C9FTD cases:** A) neuropils and puncta in frontal cortex layer 2. B) intranuclear (cat eye) inclusion in hippocampus dentate gyrus. C) perinuclear inclusion in hippocampus dentate gyrus. D) round intranuclear inclusion in hippocampus dentate gyrus. E) round or oval inclusion with a hole in frontal cortex F) dystrophic neuron in cerebellum molecular layer. G) Spreading of HR23B compared to known p62 and pTDP-43 pathology. Depicted are semi-quantitative measures of neurodegeneration and pathological score in C9FTD. Neuronal loss score was based on hematoxylin and eosin (HE) staining and pathological report and scored as absent (0), mild (1), moderate (2) or severe (3). Pathological scores were based on the degree of pathology as absent (0), rare (1), occasional (2), moderate (3), or numerous (4). See also supplementary table 2 for details of pathological quantifications. All scale bars are 20µm.

mentary figure 3). FMRP was evenly distributed in the cytoplasm in both C9FTD cases and controls. Very occasionally, we could detect inclusions in the hippocampus dentate gyrus in both C9FTD cases and controls (supplementary figure 3). Finally, we set out to test Pur-alpha staining, which showed to be located in stress granules in both C9FTD cases and controls (supplementary figure 4). We did not find Pur-alpha intranuclear inclusions in the cerebellum or other brain areas of C9FTD cases nor controls (supplementary figure 4).

### **HR23B pathology is also present in C9ALS and GRN FTD post-mortem brain tissue**

In order to validate the observed HR23B pathology, we used a second independent HR23B antibody (for details see methods) that revealed similar results (supplementary figure 6). Furthermore, we expanded our cohort with three ALS cases with the *C9ORF72* repeat expansion, three sporadic ALS cases with unknown genetic cause, two FTD with *GRN* mutation and two FTD-*MAPT* cases. In non-demented controls, we observed immunoreactivity for HR23B in nuclei (supplementary figure 5 and 6). C9ALS cases showed very strong HR23B staining in nuclei and some cytoplasmic inclusions in motor cortex (figure 2A) and spinal cord sections (figure 2B). Sporadic ALS cases also showed very strong nuclear HR23B staining but no pathology in motor cortex (figure 2C) nor spinal cord (figure 2D). *GRN* FTD cases showed the same extent of HR23B pathology as C9FTD in frontal cortex, consisting of some intranuclear inclusions, cytoplasmic inclusions and neuropils (figure 2E). HR23B pathology was absent in *MAPT* FTD cases (figure 2F).

### **HR23B co-localizes with poly-GA, pTDP-43 and p62 in C9FTD cases**

To evaluate HR23B's aggregation process in C9FTD, we performed double labeling with known pathological hallmarks, including DPRs, pTDP-43 and p62 in five C9FTD frontal cortices (figure 3). HR23B was mostly found to be co-localized with p62 (figure 3), as 66% of all HR23B inclusions were also positive for p62 (supplementary table 2). Next is pTDP-43 with 22.6% of HR23B inclusions being positive for pTDP-43 (figure 3 and supplementary table 2). From all DPRs, HR23B showed partial co-localization with poly-GA (figure 3), for 6.6% (supplementary table 2). The other DPRs only co-stained with 0-3% of all HR23B inclusions. We did not evaluate poly-PA because we found too few inclusions.

Interestingly, hippocampus dentate gyrus showed a much higher co-localization between DPRs and HR23B than frontal cortex (figure 4 and supplement-

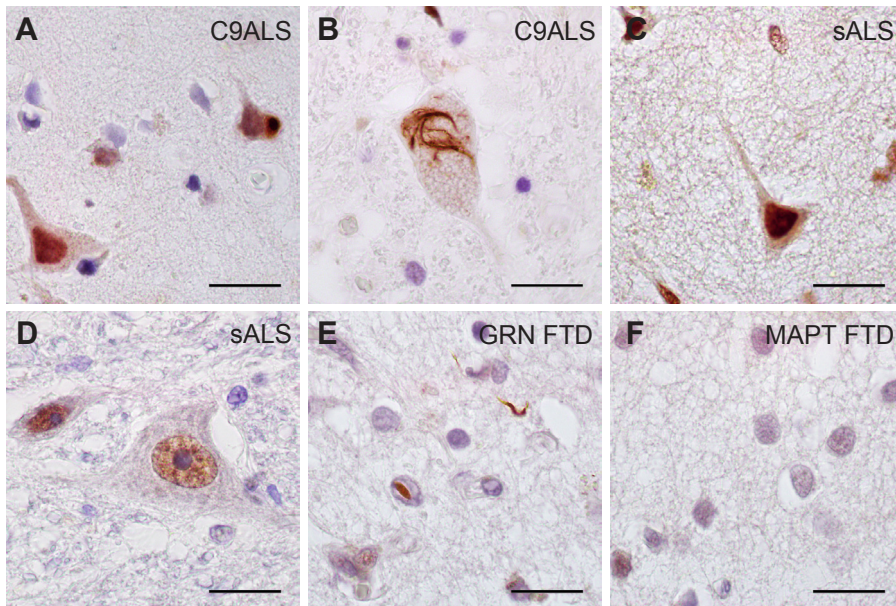


**Figure 2: HR23B pathology is also present in C9ALS and GRN FTD cases.** A) HR23B staining in C9ALS motor cortex shows strong staining in the nucleus and a cytoplasmic inclusion. B) C9ALS spinal cord section with cytoplasmic HR23B pathology. C) Sporadic ALS with very strong nuclear HR23B staining in motor cortex D) and in spinal cord. E) GRN FTD case with an intranuclear inclusion and neurites positive for HR23B in frontal cortex. F) HR23B pathology is absent in frontal cortex of MAPT FTD. All scale bars are 20 $\mu$ m.

tary table 2). We found 60.6% of HR23B inclusions being positive for poly-GA in the dentate gyrus, which is nearly a 10-fold increase compared to the frontal cortex (figure 4 and supplementary table 2). Poly-GP increased from 0.8% in frontal cortex to 4.7% in hippocampus and poly-GR also showed a 10-fold increase from 1% in frontal cortex to 10.5% in hippocampus (figure 4 and supplementary table 2). Only poly-PR stayed fairly undetectable with a slight increase from 0.65% in frontal cortex to almost 1% in hippocampus. HR23B co-localization with p62 in dentate gyrus was also higher in hippocampus than in frontal cortex (87.4% vs 66%) (figure 4 and supplementary table 2). We performed a 2-way ANOVA to compare co-localization percentages of HR23B with pathological hallmarks between different brain areas ( $p < 0.0001$ ). Post Bonferroni test indicated that percentages of poly-GA and p62 were significantly different between hippocampus DG and frontal cortex (figure 4 and supplementary table 2). For the other DPRs and pTDP-43, differences were not significant (figure 4 and supplementary table 2). These data suggest a difference in aggregation formation and co-localization patterns between different brain areas or cell types.

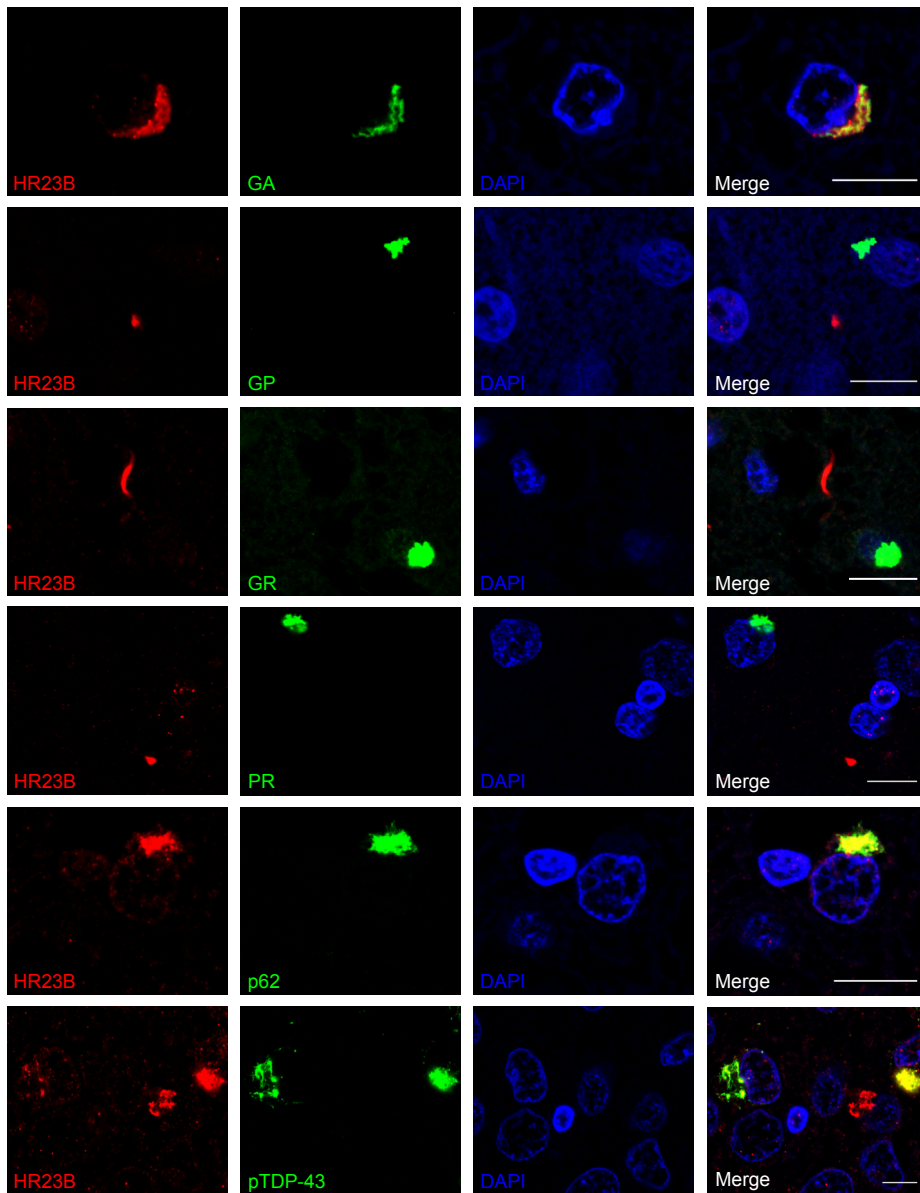


**Figure 3: HR23B co-localizes with p62, TDP-43 and poly-GA in C9FTD cases.** Immunofluorescent staining for HR23B (shown in red) in combination with DPRs (poly-GA, -GP, -GR and -PR) or p62 or pTDP-43 (shown in green). Poly-PA was not evaluated because too few inclusions were found. All pictures are from frontal cortex of C9FTD cases. All scale bars are 10 $\mu$ m.

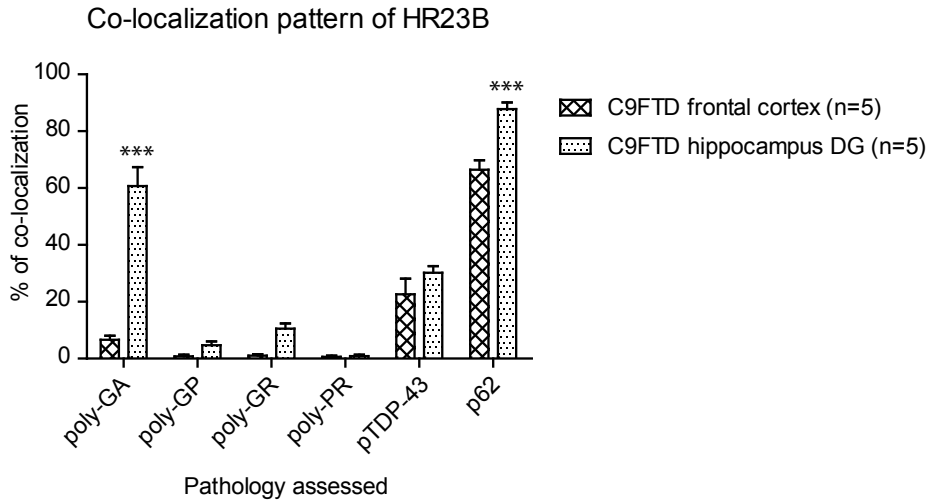


**Figure 4: HR23B co-localization percentages with poly-GA and p62 differ between frontal cortex and hippocampus DG.** Semi-quantification of co-localization of HR23B with pathological hallmarks such as DPRs, p62 and pTDP-43 based on raw data in table S2. Two-way ANOVA is significant ( $p < 0.0001$ ) for pathology, brain area and interaction. Bonferroni test indicates that only poly-GA and p62 are significantly different between frontal cortex and hippocampus DG (both  $p < 0.001$ ).

4

#### Nucleotide excision repair is not affected in C9ORF72 patient fibroblasts

To assess any changes in the normal cellular function of HR23B, we first focused on its role in DNA damage repair. HR23B interacts with and stabilizes Xeroderma pigmentosum, complementation group C (XPC) protein [243], which is involved in the recognition of bulky DNA adducts in global genome nucleotide excision repair (GG-NER). Staining with XPC antibody did not reveal any gross differences between C9FTD and non-demented control post-mortem brain sections (figure 5). To assess nucleotide excision repair capacity in living cells, we performed UV-sensitivity assays with four C9ORF72 patient fibroblast lines and compared these to four healthy control fibroblast lines. Intriguingly, C9ORF72 fibroblasts were more sensitive to UV-C damage than healthy control fibroblasts (supplementary figure 7A), but not as sensitive as a fibroblast line that is fully deficient in NER (XP25RO, homozygous for 619C>T causing an ARG207X change in exon 5 of the XPA gene).

The GG-NER pathway is initiated by recognition of DNA damage by the HR23B/XPC/CETN2 complex, which is then followed by multiple downstream steps to verify and excise the damage [244]. We therefore assessed whether factors involved in each of the steps of the NER pathway were recruited normally to DNA damage in C9ORF72 fibroblasts. To do so, we evoked local DNA damage

by UV-C irradiation through a microporous filter in our fibroblast lines and performed immunofluorescence to visualize DNA damage (by cyclobutane pyrimidine dimers (CPD) antibody) and DNA damage recruitment of NER factors XPC, XPB, XPA, XPF and XPG. All tested NER proteins clearly co-localized with DNA damage in *C9ORF72* patient fibroblasts, indicating that recognition and processing of CPDs is still functional in these cells (supplementary figure 7B). To finally verify that NER is fully operational, we measured incorporation of the thymidine analogue 5-ethynyl-2-deoxyuridine (EdU) after UV-C irradiation to quantify the efficiency of DNA repair in our fibroblast lines. The NER-deficient XP25RO cell line, which we used as negative control, did not show any EdU incorporation. In contrast, we still observed efficient EdU incorporation in our four *C9ORF72* patients cell lines to similar levels as in four healthy control lines (supplementary figure 7C), indicating that NER is not deficient in *C9ORF72* patient fibroblasts.

### **NGly1, ERAD factor and HR23B binding partner, is less abundant in C9FTD brain sections**

Besides its role in DNA damage repair, HR23B is also known for its function in the ubiquitin-proteasome system. Various HR23B binding partners have been identified which are involved in the unfolded protein response (UPR), transcriptional regulation, cell cycle control and ER-associated degradation (ERAD)[242]. To assess if HR23B aggregation also evokes changes in the localization of the proteasome, we stained our sections for proteasome subunit 20S. However, we did not observe any obvious changes in 20S normal localization (figure 5). Another binding partner of HR23B is ataxin-3, a deubiquitinase enzyme in which a poly-glutamine expansion is linked to SCA3[245]. HR23B-positive inclusions have been found in post-mortem brain material of SCA3 patients[246] however we could not detect ataxin-3 pathology in *C9FTD* cases (figure 5). Besides the proteasome, we wondered if we could find any changes in ERAD. HR23B did not sequester NGly1, one of its known binding partners involved in ERAD, into protein inclusions. Strikingly, however, we did observe clearance of NGly1 staining in *C9FTD* frontal cortex (figure 5). Although some neurons showed the same strong peri-nuclear staining as almost all non-demented control cells, in the majority of patient neurons no NGly1 staining was observed, indicating reduced expression of NGly1 in *C9FTD* brains. This may suggest a partial loss of function of ERAD in a subset of neurons in the brain of *C9FTD* patients.



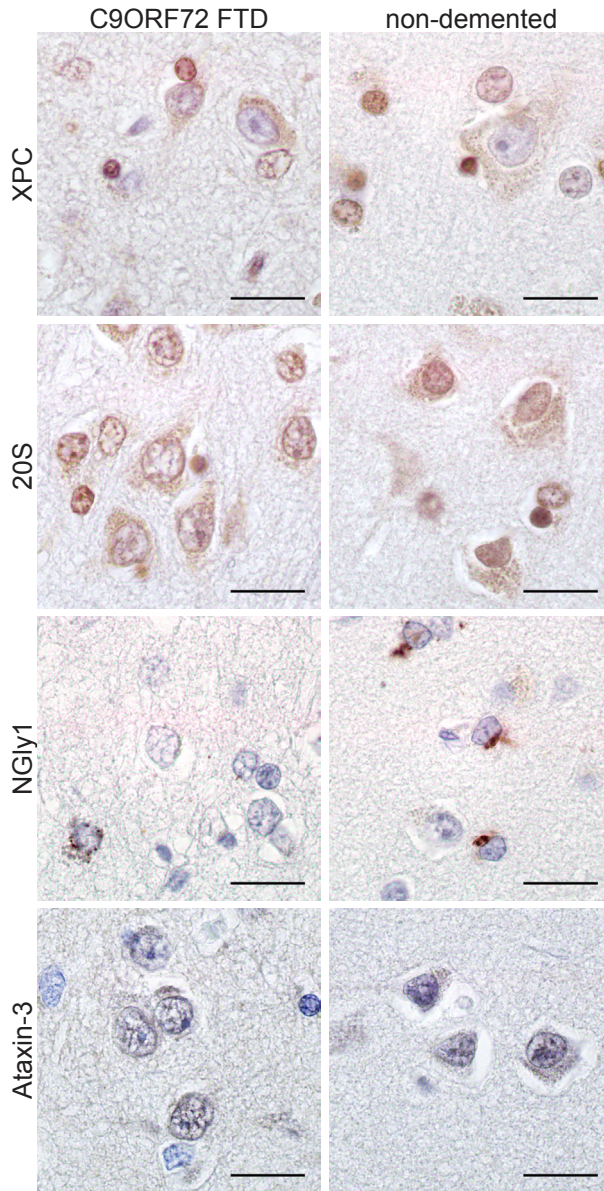


**Figure 5: HR23B does not sequester its bindings partners into inclusions.** XPC, 20S and ataxin-3 staining does not reveal any differences between C9FTD patients and non-demented controls. For NGly1, we observed less nuclei with perinuclear staining in C9ORF72 FTD brains than in non-demented controls. All pictures are from frontal cortex. All scale bars are 20 $\mu$ m.

## Discussion

In the present study, we characterize HR23B pathology distribution and its co-localization pattern with pathological hallmarks. To our knowledge, we are the first to show that HR23B co-localizes with pTDP-43 pathology in brain tissue of C9FTD patients. We could also demonstrate HR23B pathology in C9ALS and sporadic ALS. HR23B pathology has been described before in HD, SCA3, SCA7, FXTAS and PD[246]. HR23B pathology was also present in both C9ORF72 and GRN FTD cases, but not in MAPT FTD cases, in contrast to a previous report of HR23B pathology described for FTDP-17 (FTD with parkinsonism with Pick bodies consisting of tau protein) [246]. Also Alzheimer's disease (AD) brain material did not show HR23B pathology[246]. Why AD and some FTLT-tau patients are an exception and do not present with HR23B pathology is unclear and requires further investigation. It should be noted that our study cohort was rather small (see table 1), which might explain why we could not confirm HR23B pathology in MAPT FTD cases. Next to HR23B, HR23A inclusions have been reported in FXTAS and in C9FTD post-mortem brain tissue[213, 246]. In general, HR23 pathology seems to be widespread among neurodegenerative diseases, which underscores its relevance in a common disease pathogenesis of these disorders.

In our semi-quantitative co-localization studies, we found HR23B to be co-localized predominantly with p62, followed by pTDP-43 and poly-GA. HR23B inclusions were nearly always negative for the other DPRs. Overexpression of poly-GA in mouse models is enough to sequester HR23B[213, 229] and in a co-immunoprecipitation experiment of lysates from cells expressing GFP-tagged poly-GP, -GR and -GA, only poly-GA was found to bind HR23B[213]. This could also be a stochastic event, given the fact that poly-GA inclusions are the most abundant DPR in C9FTD/ALS brains [69]. It could also be caused by the aggregation-prone nature of the poly-GA peptide itself [247], causing HR23B to bind easier or faster to poly-GA peptides than other DPRs. Binding of HR23B to DPRs also differs between brain areas; in the frontal cortex, only 6.6% of HR23B inclusions were poly-GA positive, while this increased to 60.6% in the hippocampus dentate gyrus. The same is true for poly-GP and -GR; co-localization with HR23B increased 5- to 10-fold between frontal cortex and hippocampus, although it remained low (1-10%). Subtypes of neurons may differ in their vulnerability for DPRs or there might be differences in the expression level and availability of HR23B and/or its binding partners between frontal cortex and hippocampus dentate gyrus. Levels of HR23B can influence aggregation of poly-GA and toxicity of mutant TDP-43 and mutant SOD1[213, 248]. Overexpression of

HR23B protected for the formation of poly-GA inclusions in mouse primary neuronal cultures[213]. In contrast, loss of HR23B seems to protect against motor neuron disease by enhancing mutant protein clearance[248]. Levels of HR23B seem to have opposite effects on aggregation, clearance and solubility of several proteins, which could result in differences in aggregation and co-localization patterns observed between different brain areas.

HR23B can directly bind the proteasome and ataxin-3, a deubiquitinase enzyme that binds ubiquitinated proteins and can also bind to the proteasome[245, 249]. Even though HR23B and proteasome subunits are sequestered into intranuclear inclusions of ataxin-3 in SCA3 patients brain tissue[246, 250], ataxin-3 and 20S do not show an aberrant localization in C9FTD patients post-mortem brain tissue. HR23B can also bind PNGase, a deglycosylation hydrolase involved in ERAD of misfolded glycoproteins. The affinity of PNGase for the proteasome is HR23B-dependent, which makes HR23B essential for the shuttling of misfolded proteins to the proteasome[251]. If HR23B is sequestered into inclusions and becomes unavailable for PNGase, this might cause loss of initiation of ERAD. This is in line with our observation that a substantial number of neurons of C9FTD/ALS patients show less abundant NGly1 staining. Many FTD-causing mutations are associated with protein degradation pathways[252]. In addition, mutations in *NGLY1*, the gene encoding PNGase, are linked to motor impairment, intellectual disability, and neuropathy in humans[253].

HR23B is well known for its role in global genome nucleotide excision repair (GG-NER) and genetic polymorphisms in *RAD23B* are modifiers of laryngeal cancer risk in human [254]. The DNA damage response can be induced by the *C9ORF72* repeat expansion[190] and elevated levels of R-loops (DNA-RNA hybrids), double strand breaks and ATM-mediated DNA repair signaling defects have been described before in rat neurons, human cells and C9ALS spinal cord tissue[145, 190]. Furthermore, ALS and *C9ORF72* repeat carriers have an increased risk for melanoma[255, 256], suggesting they may have a reduced response to DNA damage. XPC, the binding partner of HR23B in NER, was found in inclusions in a poly-GA mouse model of C9FTD/ALS[213]. Nonetheless, we could not find XPC pathology in our human brain sections nor deficits in the NER pathway in *C9ORF72* patient fibroblasts, even though *C9ORF72* patient fibroblasts seem to be more sensitive for UV-C damage than healthy control fibroblasts. Why we do not find a clear impairment of NER in our study is unknown. Species-specific factors, overexpression of poly-GA in the mouse model or difference between fibroblasts and neurons might explain a part of the absence

of an effect. In addition, it could be possible that HR23A takes over the DNA repair function of HR23B when the latter is sequestered or dysfunctional. This has been demonstrated in mHr23b knockout (KO) mice that show no impairment in NER[242]. Still, mHr23b KO mice display impaired embryonic development, retarded growth and facial dysmorphologies that are not observed in mouse models deficient in other NER genes[242], which suggests a second function of HR23B. Although HR23A and HR23B have similar functions in DNA repair, they form distinct interactions with various cellular factors, including proteasomes, multi-ubiquitinated proteins and stress-related factors[257].

Here, we set out to validate the aggregation of several proteins that have been described to mis-localize or bind RNA foci in C9FTD/ALS. Strikingly, we could not reproduce earlier published pathology for Ran-GAP, ADARB2, Pur-alpha and FMRP. The differences observed between our study and previous publications can be explained by multiple factors. First of all, we used post-mortem brain material that only presents the end-stage of the disease, so changes in localization of proteins in early stages of the disease can be missed. Also, the number of cells presenting with stress granules varies a lot between subjects and might be attributed to autolytic processes during human brain preservation, which can make it hard to detect subtle differences. Secondly, this study focused on FTD rather than ALS. This could especially be important for ADARB2, as one of the targets of ADAR proteins is the Q/R site of the GluR2 AMPA receptor [156]. Changes in ADARB2 localization could therefore mostly affect ALS cases and may be missed in our FTD cohort. Thirdly, pathology observed in cell culture and in vivo models could be due to overexpression of C9ORF72 RNA or DPRs in these models. Changes in patient neurons with endogenous expression can be more subtle but still act disturbing over time. Most model systems used so far do not include haploinsufficiency, which can be a modifying factor for cellular toxicity as well[126]. Finally, effects might be missed due to our small cohort. For example, differences in oddly-shaped nuclei in the Ran-GAP staining might only become evident when quantifying large number of cells. However, Saberi et al. also were unable to confirm Ran-GAP pathology[72], which strengthens our findings and illustrates the need for validation studies in biomedical research. Even though we did not observe any pathology of Ran-GAP, ADARB2, FMRP and Pur-alpha, their levels could still have a modifying effect on disease progression of FTD, as has been shown in iPSC-derived neurons and Drosophila models[107, 153, 155, 258].

## Conclusion

In this study, we confirm HR23B aggregation and its implication in C9FTD/ALS. HR23B has an important function in both the DNA damage response and the degradation of proteins via the UPS, UPR and ERAD. Our results in human postmortem brain tissue suggests that especially the degradation of proteins via ERAD may be involved in the pathogenesis of ALS and FTD. The exact role and timing of HR23B in disease onset and progression needs further investigation, including its interaction with and possible degradation of proteins implicated in neurodegenerative disorders.

## List of abbreviations

ALS: amyotrophic lateral sclerosis; FTD: frontotemporal dementia; HD: Huntington's Disease; SCA3/7: spinocerebellar ataxia type 3 and 7; FXTAS: fragile X associated tremor/ataxia syndrome; PD: Parkinson's disease; AD: Alzheimer's disease; C9ORF72: chromosome 9 open reading frame 72; HR23B: human homologue of yeast UV excision repair protein Rad23b; NER: nucleotide excision repair; GG-NER: global genome nucleotide excision repair; UPS: ubiquitin-proteasome system; UPR: unfolded-protein response; ERAD: endoplasmic reticulum associated degradation; p62: sequestosome 1; pTDP-43: phosphorylated 43kDa TAR DNA-binding protein; DPRs: dipeptide repeat proteins; poly-GA: poly-glycine-alanine; poly-GP: poly-glycine-proline; poly-GR: poly-glycine-arginine; poly-PA: poly-proline-alanine; poly-PR: poly-proline-arginine; RAN: repeat-associated-non-AUG; Ran-GAP: ras-related nuclear protein GTPase activating protein; ADARB2: Adenosine Deaminase, RNA Specific B2; FMRP: fragile X mental retardation protein; XPC: Xeroderma pigmentosum complementation group C; CPD: cyclobutane pyrimidine dimers; UDS: Unscheduled DNA Synthesis; EdU: 5-ethynyl-2-deoxyuridine; NPC: nuclear pore complex; NCT: nucleocytoplasmic transport; IHC: Immunohistochemistry; IF: immunofluorescence; HE: haematoxylin and eosin; NCI: neuronal cytoplasmic inclusions; NII: neuronal intranuclear inclusions; DN: dystrophic neurites

## Declarations

### Ethics approval and consent to participate

All procedures performed in studies involving human participants were in accordance with the ethical standards of the institutional and/or national research committee and with the 1964 Helsinki declaration and its later amendments or comparable ethical standards. All participants gave written informed consent for

all obtained materials. The study was approved by the Medical and Ethical Review Committee of the Erasmus Medical Center.

**Consent for publication** - Not applicable

**Availability of data and materials**

The data supporting the conclusions of this article is included within the article (and its additional file). Raw datasets (including UV-C treatment of human fibroblasts) analyzed during the study are available from the corresponding author on reasonable request.

**Competing interest**

The authors declare that they have no conflict of interest.

**Funding**

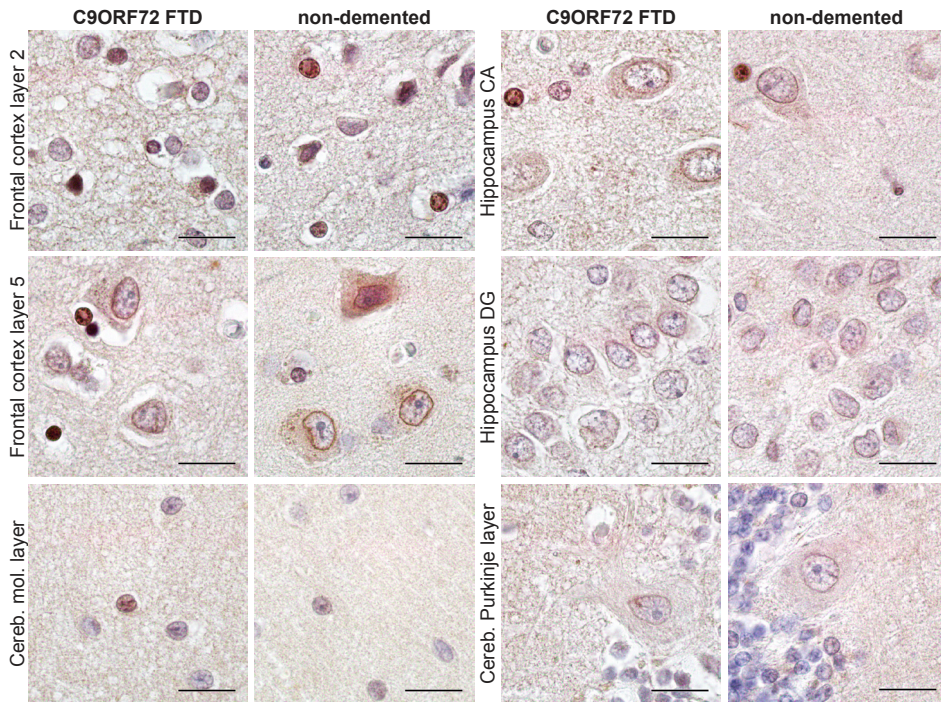
This study was supported by the European Joint Programme - Neurodegenerative Disease Research and the Netherlands Organization for Health Research and Development (PreFrontALS: 733051042; RW and JS). European Research Council Advanced Grant to WV (grant 340988-ERC-ID) and ALS Stichting (2014-28, TOTALS) to RJP.

**Authors' contributions**

FWR has designed, performed and analyzed experiments and drafted the manuscript. HL has designed, performed and analyzed experiments. HS has designed, performed and analyzed experiments. L.S and S.M have helped performing experiments. WV, EA, JP and JCS provided human fibroblasts and post-mortem brain samples and helped interpreted data. JCS and RW guided study design, have interpreted data, and substantively revised the work. All authors read and approved the final manuscript.

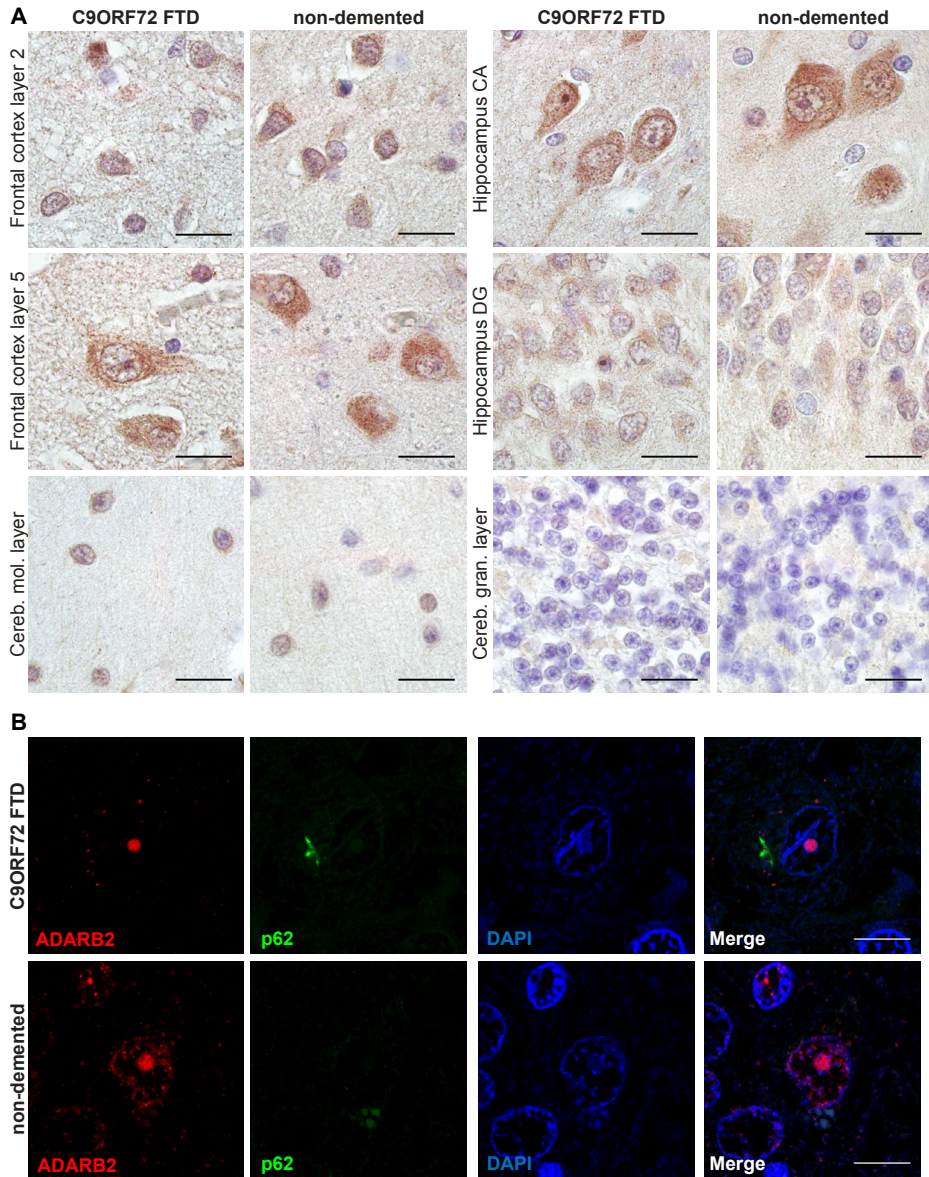
**Acknowledgements**

Authors would like to thank Arjan F. Theil for his practical advice on colony forming assay experiments and Michiel Kooreman from the Dutch Brain Bank for his assistance in selecting and sending C9ORF72 FTD patient and sporadic ALS patient brain sections. We also would like to thank Ronald Buijsen for providing the ataxin-3 antibody. We acknowledge the Netherlands ALS foundation ("The Dutch ALS Tissue Bank"; EA). We thank the team who helped in the collection of ALS tissue samples (Prof. dr. D. Troost, Prof. dr. M. de Visser, Dr. A.J. van der Kooi and Dr. J. Raaphorst).



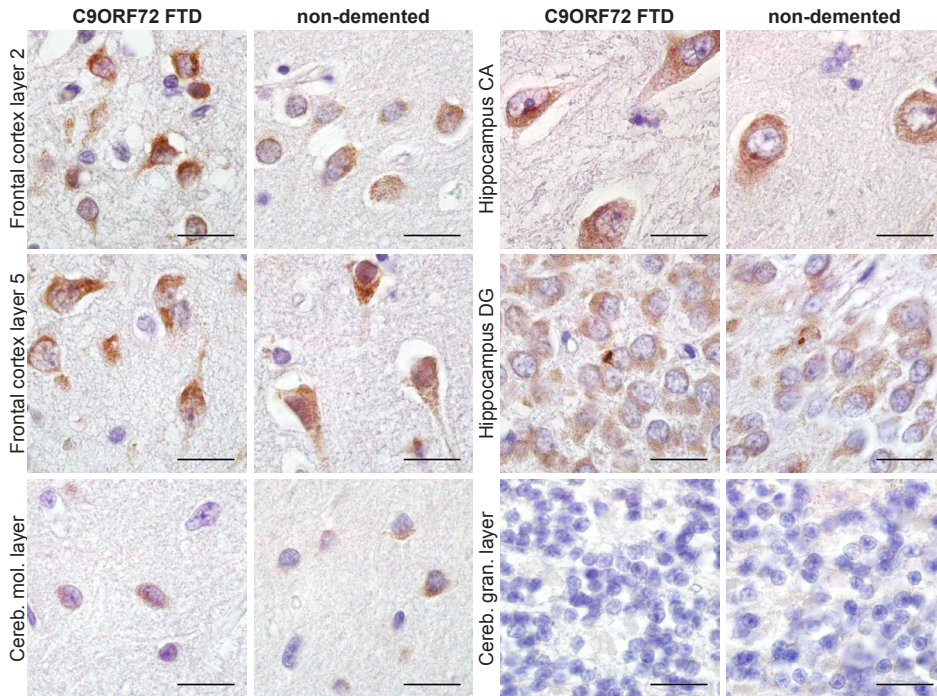
**Supplementary figure 1: Ran-GAP staining in C9FTD cases and non-demented controls.** Ran-GAP is predominantly localized to the nucleus and nuclear membrane. Unevenly shaped nuclear membranes occur in both C9ORF72 FTD cases (n=5) and non-demented controls (n=3). All scale bars are 20 $\mu$ m.

4



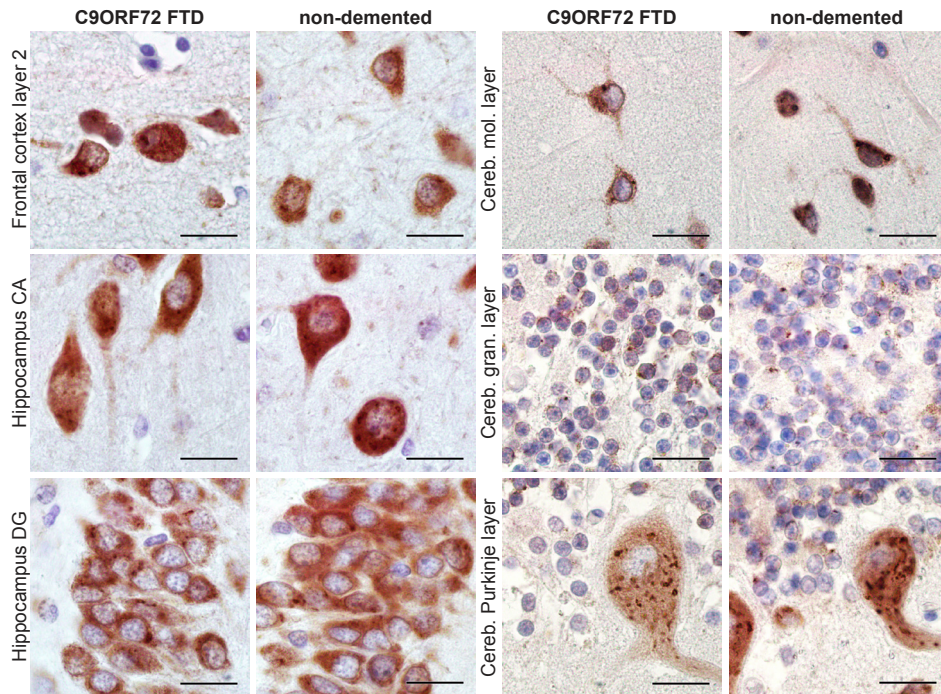
**Supplementary figure 2: ADARB2 staining in C9FTD cases and non-demented controls.** A) Staining of ADARB2 in C9ORF72 FTD cases (n=5) and non-demented control (n=3) post-mortem brain sections shows some intranuclear inclusions in hippocampus CA and DG. All scale bars are 20µm B) Immunofluorescence staining of ADARB2 (red) and p62 (green) in hippocampal dentate gyrus reveals ADARB2 punctuated staining and some intranuclear inclusions in both C9ORF72 FTD cases (n=5) and non-demented controls (n=3). Scale bars in fluorescent pictures are 10µm.



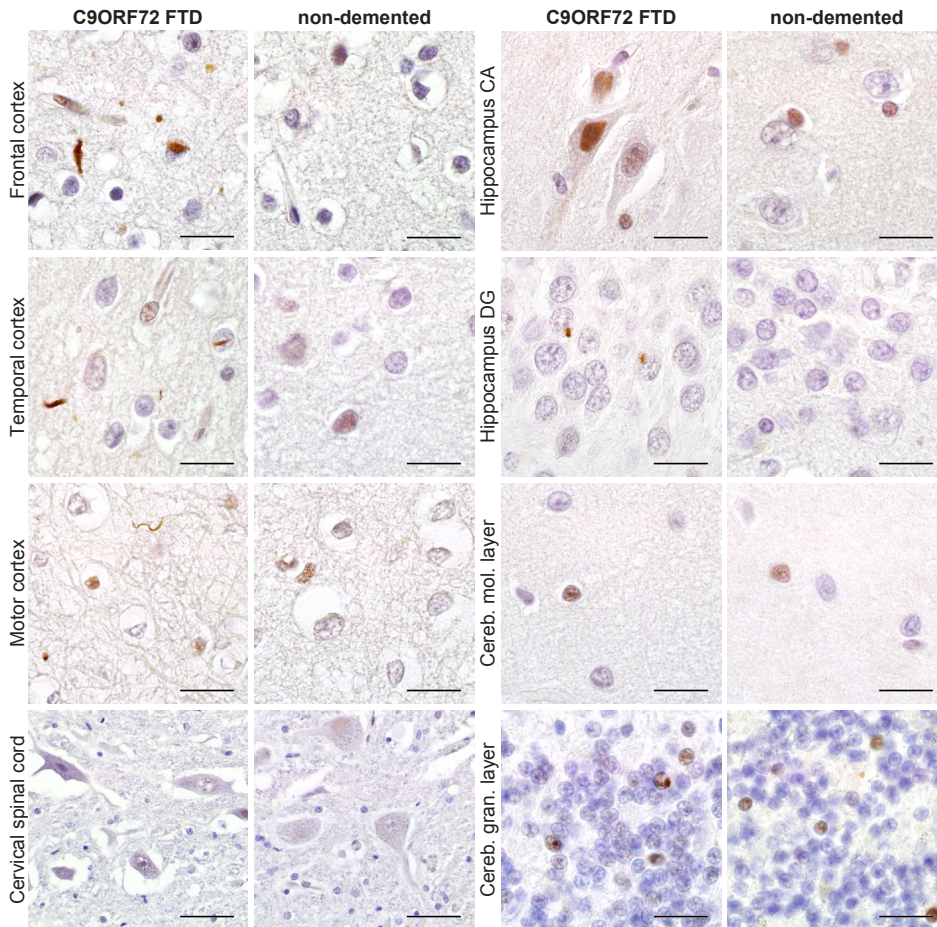


**Supplementary figure 3: FMRP staining in C9FTD cases and non-demented controls.** FMRP staining does not reveal any differences between C9ORF72 FTD cases (n=5) and non-demented control (n=3) post-mortem brain sections. Occasional inclusions are found in the hippocampus dentate gyrus in both C9FTD cases and controls. All scale bars are 20 $\mu$ m.

4

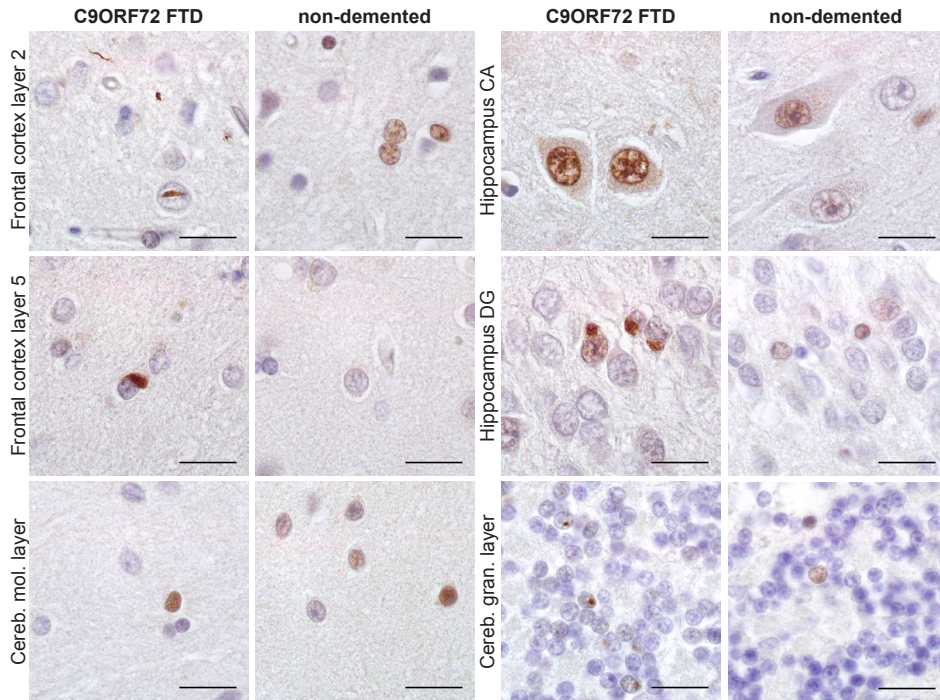


**Supplementary figure 4: Pur-alpha staining in C9FTD cases and non-demented controls.** Pur-alpha staining reveals abundant stress granules in both C9ORF72 FTD cases ( $n=5$ ) and non-demented controls ( $n=3$ ) post-mortem brain sections. All scale bars are  $20\mu\text{m}$ .

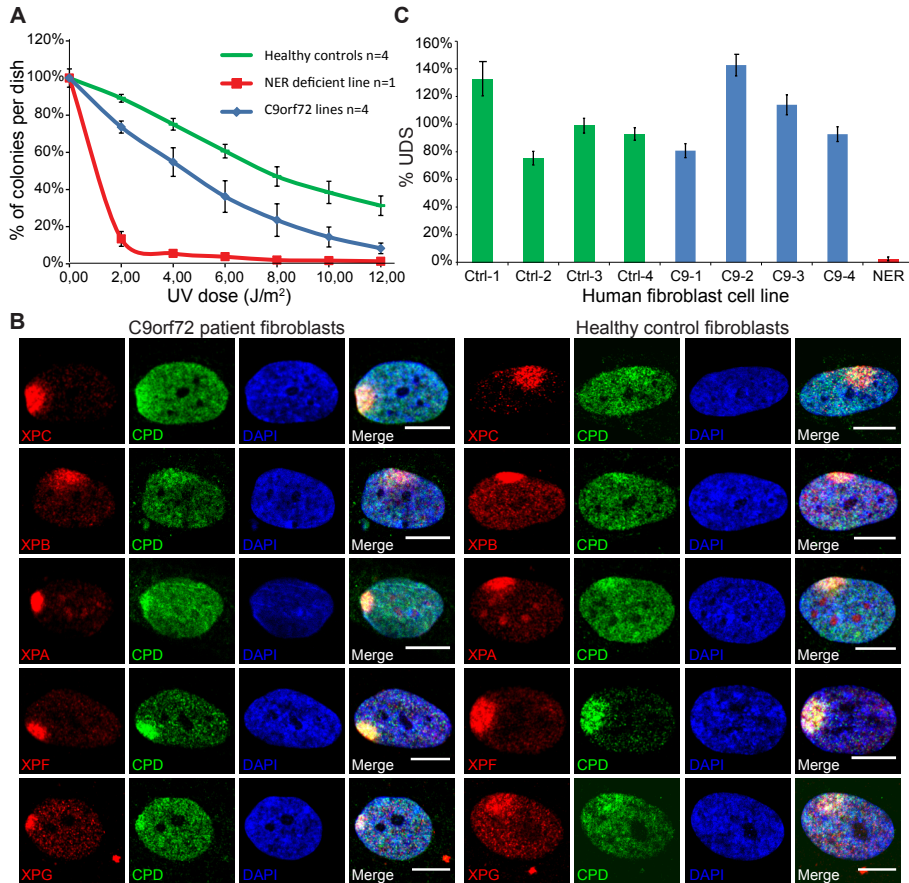


**Supplementary figure 5: HR23B pathology in different brain areas of C9FTD cases.** Staining of HR23B in several brain areas of C9FTD cases and non-demented controls. Pathology burden was highest in cortices (frontal, temporal and motor) and was mostly cytoplasmic (inclusions and neuro-pilils) and intranuclear (cateye). Hippocampus dentate gyrus (DG) harbors perinuclear inclusions, and hippocampus cornu ammonis (CA) had some cells with strong nuclear staining. Pathology was low in cerebellum granular layer with only some nuclear and perinuclear inclusions and almost absent in cerebellum molecular layer. Our C9FTD cases did not show HR23B pathology in spinal cord neurons. All scale bars are 20µm

4



**Supplementary figure 6: Validation of HR23B pathology by a second independent antibody.** HR23B staining using Abcam antibody in C9ORF72 FTD cases (n=5) and non-demented control (n=3) post-mortem brain sections. Staining pattern is consistent with HR23B GeneTex antibody (see figure 1 and 2). All scale bars are 20 $\mu$ m



**Supplementary figure 7: Nucleotide excision repair is not affected in C9ORF72 human fibroblasts.** A) Dose-response curve for 4 healthy control human fibroblast lines and 4 C9ORF72 human fibroblast lines and the NER deficient XP25RO human fibroblast line treated with increasing dose of UV-C light (0-12 J/m<sup>2</sup>). B) Immunofluorescence staining showing the recruitment of NER factors XPC, XPB, XPA, XPF and XPG to local DNA damage (visualized by CPD antibody), induced by 60 J/m<sup>2</sup> UV-C irradiation through a microporous filter. C) Human fibroblasts lines were treated with 16 J/m<sup>2</sup> UV-C light and incubated with EdU for 1 h to measure unscheduled DNA synthesis (UDS) as measure of DNA repair. The NER-deficient XPC25RO cell line is shown as negative control.

4

Patient ID	1					2					3					4					5				
	C9ORF72 FTD					C9ORF72 FTD					C9ORF72 FTD					C9ORF72 FTD					C9ORF72 FTD				
Brain area	F	T	M	H	C	F	T	M	H	C	F	T	M	H	C	F	T	M	H	C	F	T	M	H	C
Neuronal loss score	2	2	1	2	0	1	3	0	2	0	2	2	1	3	0	1	2	0	2	0	2	2	1	3	1
P62 score	Total	4	4	4	4	4	4	2	4	3	4	3	3	4	3	4	3	3	3	4	4	4	2	3	4
	NCI	4	4	4	4	4	4	2	4	3	3	2	2	4	3	4	3	3	3	4	4	4	2	3	4
pTDP-43 score	Total	3	3	3	3	3	3	1	4	0	2	3	3	4	0	3	3	3	2	0	3	4	1	3	0
	NCI	3	3	3	3	3	3	2	4	0	1	3	3	4	0	3	3	3	2	0	3	4	1	3	0
HR23B score	Total	1	1	1	0	0	1	1	0	0	0	0	0	0	0	1	1	1	0	0	1	1	1	0	0
	NCI	1	1	1	1	1	1	1	2	1	1	2	1	1	1	1	1	1	1	1	1	1	1	1	2
Dysphagia score	Total	0	1	1	0	1	0	0	0	1	1	1	0	0	0	1	1	1	1	1	1	1	0	0	1
	DNs	1	3	1	0	0	1	2	1	0	0	2	3	1	0	0	1	3	1	0	0	2	2	1	0

**Supplementary table 1: Neuropathological scores of C9ORF72 FTD patients.** Neuronal loss score was based on hematoxylin and eosin (HE) staining and pathological report and scored as absent (0), mild (1), moderate (2) or severe (3). Pathological scores were based on the degree of pathology as absent (0), rare (1), occasional (2), moderate (3), or numerous (4). Brain areas: F= frontal cortex, T= temporal cortex, M = motor cortex, H = hippocampus dentate gyrus, C = cerebellum. NCI = neuronal cytoplasmic inclusion, NII = neuronal intranuclear inclusion, DNs = dystrophic neurites.

Gene & diagnosis	ID	Brain area	HR23B +						pTDP-43	p62
			Poly-GA	Poly-GP*1	Poly-GR	Poly-PR	Poly-PA *2			
C9ORF72 FTD	1	F	11/153 = 7%	0/103 = 0%	1/109 = 1%	0/150 = 0%	N/A	19/121 = 16 %	72/105 = 68%	
		H	77/90 = 85%	3/91 = 3,3%	20/191 = 10%	2/285 = 0,7%	N/A	32/104 = 31%	118/150 = 78%	
	2	F	7/62 = 11%	3/102 = 3%	3/102 = 3%	1/80 = 1,25%	N/A	42/101 = 42 %	72/107 = 67%	
		H	62/135 = 46%	3/173 = 1,7%	9/212 = 4,3%	3/469 = 0,6%	N/A	39/111 = 35%	140/156 = 90%	
	3	F	11/180 = 6%	0/107 = 0%	1/237 = 0,4%	0/120 = 0%	N/A	35/140 = 25%	79/106 = 75%	
		H	52/97 = 54%	5/115 = 4,3%	13/99 = 13%	1/176 = 0,5%	N/A	31/106 = 30%	65/74 = 88%	
	4	F	6/103 = 6%	1/105 = 1%	0/115 = 0%	2/100 = 2%	N/A	26/117 = 22%	63/116 = 54%	
		H	42/72 = 58%	5/102 = 4,9%	16/105 = 15%	4/154 = 2,6%	N/A	39/115 = 34 %	92/102 = 90%	
	5	F	5/175 = 3%	0/100 = 0%	1/131 = 0,8%	0/160 = 0%	N/A	9/105 = 9%	92/136 = 68%	
		H	54/90 = 60%	10/107 = 9,3%	10/105 = 9,5%	0/68 = 0%	N/A	22/100 = 22%	61/66 = 92%	
GRN FTD	6	F	0%	0%	0%	0%	N/A	59/178 = 33%	118/157 = 75%	
		H	0%	0%	0%	0%	N/A	5/33 = 15%	5/5 = 100%	
	7	F	0%	0%	0%	0%	N/A	61/125 = 49%	100/154 = 65%	
		H	0%	0%	0%	0%	N/A	1/13 = 8%	3/3 = 100%	
Non-demented cases *3	16	F	0%	0%	0%	0%	N/A	0%	1/2 = 50%	
		H	0%	0%	0%	0%	N/A	0%	0%	
	17	F	0%	0%	0%	0%	N/A	0%	1/3 = 33%	
		H	0%	0%	0%	0%	N/A	0%	1/1=100%	
	18	F	0%	0%	0%	0%	N/A	0%	2/2 = 100%	
H		0%	0%	0%	0%	N/A	0%	1/1=100%		

**Supplementary table 2: Co-localization of HR23B with DPRs/pTDP-43/p62 differs between brain areas. Legend see next page**

**Supplementary table 2 (continued):** *The percentage is the amount of HR23B inclusions also positive for other pathological hallmarks (not the other way around). For example 11/153 for poly-GA in C9FTD patient 1 means that out of 153 HR23B inclusions, 11 were also positive for poly-GA, which is 7%. F = frontal cortex. H = hippocampus dentate gyrus. \*1 = All co-localizations are fibrils of poly-GP and HR23B in frontal cortex. Perinuclear inclusions of poly-GP did not stain positive for HR23B. \*2 = In total 2 poly-PA inclusions have been found in frontal cortex of 5 C9FTD patients, too less to quantify. We therefore state N/A = non-applicable in this table. \*3 = Non-demented cases had some p62 and some HR23B inclusions per person per section, which sometimes overlapped. No pTDP-43 inclusions were found so no co-localization of pTDP-43 with HR23B in non-demented cases.*



**Supplementary table 3: Antibodies**

Ab name	Host	Company	Cat.nr	Dilution
Rad23B	mouse	GeneTex	GTX16485	1:50
Rad23B	rabbit	Abcam	ab86781	1:250
XPC	rabbit	Bethyl	A301-122A	1:100
20S	rabbit	ENZO life sciences	BML-PW8155-0025	1:100
NGly	rabbit	Novus	NBP1-83793	1:100
Ataxin-3	mouse	Millipore	MAP5360	1:1000
ADARB2	rabbit	Atlas Antibodies	HPA031333	1:100
Pur-alpha	rabbit	LS Bio	LS-B6784	1:200
FMRP	mouse	N/A	N/A	1:100
Ran-GAP	rabbit	Abcam	Ab4784	1:1000
Poly-GR	mouse	LifeTein Services	N/A	1:4000
Poly-PR	mouse	LifeTein Services	N/A	1:500
Poly-GP	rabbit	Bio Connect Life Sciences	24494-1-AP	1:250
Poly-GA	mouse	Millipore, clone 5E9	MABN889	1:500
Poly-PA	mouse	Gift from Petrucelli	n.a.	1:2500
pTDP-43	mouse	Cosmo bio	CAC-TIP-PTD-M01	1:1000
p62	mouse	BD Biosciences	610833	1:100
XPA	rabbit	Santa Cruz	sc-853	1:50
XPB	rabbit	Santa Cruz	sc-293	1:1000
XPC	rabbit	Bethyl	A301-121A	1:1000
XPF	mouse	Santa Cruz	sc-136153	1:1000
XPG	rabbit	Bethyl	A301-484A	1:100
CPD	mouse	CosmoBio	TDM-2	1:1000
poly-HRP anti Ms/ Rb IgG	goat	Immunologic	DPV055HRP	undiluted
anti-mouse HRP	goat	DAKO	P0260	1:100
anti-rabbit HRP	goat	DAKO	P0217	1:100
anti-mouse Cy2	goat	Jackson	715-255-150	1:100
anti-rabbit Cy3	goat	Jackson	711-165-152	1:100



# Chapter 5

## **Poly-GR is not detected in CSF and PBMCs of C9ORF72-linked frontotemporal dementia and amyotrophic lateral sclerosis cases and carriers**

F.W. Riemsdagh<sup>1</sup>\*, R.F.M. Verhagen<sup>1</sup>, H. de Boer<sup>1</sup>, E.L. van der Ende<sup>2</sup>, H.H. Meeter<sup>2</sup>, S. Melhem<sup>2</sup>, M. Schreurs<sup>3</sup>, J. H. Veldink<sup>4</sup>, R.J. Pasterkamp<sup>5</sup>, J.C. van Swieten<sup>2</sup> and R. Willemsen<sup>1</sup>.

<sup>1</sup>Department of Clinical Genetics, Erasmus University Medical Center Rotterdam, Rotterdam, The Netherlands

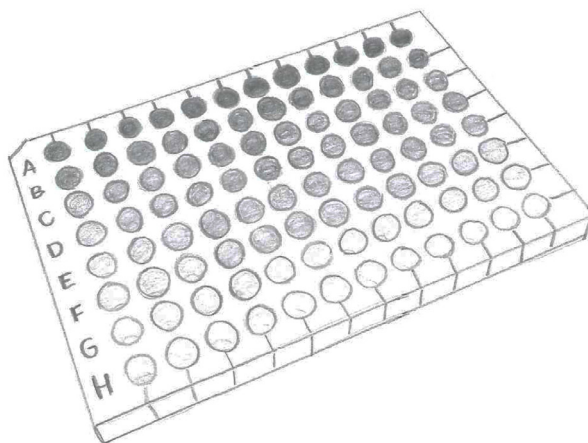
<sup>2</sup>Department of Neurology, Erasmus University Medical Center Rotterdam, Rotterdam, The Netherlands

<sup>3</sup>Department of Immunology, Erasmus University Medical Center Rotterdam, Rotterdam, The Netherlands

<sup>4</sup>Department of Neurology, University Medical Center Utrecht Brain Center, Utrecht University, Utrecht, The Netherlands

<sup>5</sup>Department of Translational Neuroscience, University Medical Center Utrecht Brain Center, Utrecht University, Utrecht, The Netherlands

\*Corresponding author: [f.w.riemsdagh@erasmusmc.nl](mailto:f.w.riemsdagh@erasmusmc.nl)



### **Abstract**

The *C9ORF72* hexanucleotide G<sub>4</sub>C<sub>2</sub> repeat expansion explains the majority of genetic frontotemporal dementia (FTD) and amyotrophic lateral sclerosis (ALS) cases. The expanded G<sub>4</sub>C<sub>2</sub> repeat is translated into dipeptide repeat proteins (DPRs) that can form cellular aggregates in the central nervous system (CNS) of C9FTD/ALS patients. Especially arginine-containing DPRs are very toxic in cell culture and animal models. Poly-glycine-arginine (poly-GR) has been associated with neurodegeneration in human post-mortem brain. To date, rapid progression has been made in the development of therapies for C9FTD/ALS in the preclinical phase. However, biomarkers that assess efficacy of treatment response in human clinical studies are much needed. Here we show that poly-GR can be specifically detected in brain sections and protein homogenates from frontal cortex of C9FTD/ALS cases using a new monoclonal antibody against poly-GR. The average amount of poly-GR measured in frontal cortex of seven C9FTD patients was 22.7 ng/ml. Next, we investigated if poly-GR is present in cerebrospinal fluid (CSF) and could be used as a potential fluid biomarker in C9FTD/ALS. Unfortunately, we were unable to detect poly-GR levels in CSF of both pre- and symptomatic *C9ORF72* repeat carriers using an Enzyme-Linked Immuno Sorbent Assay (ELISA). This indicates that poly-GR may not be present in CSF or the levels are below our detection limit of 200pg/ml. In addition, poly-GR levels in peripheral blood mononuclear cells (PBMCs) of both pre- and symptomatic *C9ORF72* repeat carriers were also below the detection level of our assay. More sensitive methods, like single molecule array (SI-MOA), might be able to detect poly-GR in CSF and PBMCs in the near future using this new antibody.

### **Keywords**

*C9ORF72*, biomarker, poly-GR, FTD, ALS, ELISA, CSF

## Introduction

FTD is a neurological disease that is caused by degeneration of neurons in the frontal and temporal lobes of the brain, leading to changes in language, behavior and personality[1, 4]. ALS is a motor neuron disorder in which the upper motor neurons in the motor cortex and the lower motor neurons in the anterior horn of the spinal cord are affected[8, 9]. The hexanucleotide G<sub>4</sub>C<sub>2</sub> repeat expansion in the *C9ORF72* gene has been identified in 2011 as the most common genetic cause for both ALS and FTD[22, 23]. Individuals carrying this mutation can develop symptoms related to both disorders[13, 33, 227] and are collectively referred to as C9FTD/ALS patients. The *C9ORF72* repeat expansion can cause neurodegeneration via three potential mechanisms: 1) partial loss of function of the normal *C9ORF72* protein, 2) gain of function of RNA foci that could sequester RNA binding proteins and 3) gain of function of possible toxic DPRs[77]. DPRs are produced from the expanded G<sub>4</sub>C<sub>2</sub> repeat expansion via repeat-associated-non-AUG (RAN) translation. This occurs in both sense and antisense direction resulting in six different dipeptides; poly-glycine-alanine (GA), -glycine-proline (GP), -glycine-arginine (GR), poly-proline-alanine (PA), -proline-arginine (PR) and -proline-glycine (PG)[52, 57, 67]. Note that poly-GP and PG are similar products from the sense and antisense strand but can differ in their N- and C-terminus. DPRs accumulate during life in the CNS of C9FTD/ALS patients, with the sense products being most prominently found[51, 59, 69]. However, only poly-GR has been associated with neurodegeneration[72, 73]. Furthermore, the arginine containing DPRs, poly-GR and poly-PR, seem to be the most toxic in multiple *in vitro* and *in vivo* models of *C9ORF72*[168, 172-174, 176, 199, 220].

Currently, antisense oligonucleotide (AON) therapy has provided promising results in preclinical studies for the treatment of C9FTD/ALS[136, 259]. For the successful implementation into clinical trials, biomarkers that measure target engagement, disease onset and progression are highly needed. Neurofilament light chain is a marker for axonal injury that correlates with prognosis and disease severity in genetic FTD, but is not suited for pharmacodynamic studies[260, 261]. DPRs might be used as fluid biomarkers because of their high specificity for C9FTD/ALS. Assessment of DPR levels in for example brain samples from *C9ORF72* mouse models has proven to be useful in target engagement studies that estimate the efficiency of drugs or compounds that directly target the repeat or RAN translation and ameliorate *C9ORF72* repeat toxicity[78, 136, 197, 236]. Quantification of DPR levels could be used for the same reason in clinical trials. In 2014, Su et al. showed for the first time that poly-GP could be detected in CSF

of C9ALS patients[78]. Quantification of poly-GP in CSF in 3 cohorts containing C9ALS, C9FTD and C9FTD/ALS patients revealed stable levels over time that enables its potential use as pharmacodynamic marker in clinical trials[197, 262, 263]. However, poly-GP levels did not correlate with age of onset or survival, cognitive or behavioral impairment nor gray matter deficits in any of these cohorts[197, 262, 263]. Also in cellular and *in vivo* models of *C9ORF72*, poly-GP has been proven as non-toxic, in contrast to other DPRs like poly-GR (reviewed in [77, 264]). From all DPRs, poly-GR most often co-localizes with pTDP-43 and it is the only DPR that has been correlated with neurodegeneration in C9FTD/ALS cases[72, 73]. We therefore assessed if poly-GR could be used as fluid biomarker in C9FTD/ALS cases. Here, we characterize a new monoclonal antibody against poly-GR and developed an ELISA that specifically detects poly-GR in the frontal cortex of C9FTD patients. Next, we tested for presence of poly-GR in CSF and PBMCs in a cohort of *C9ORF72* carriers (pre-symptomatic and symptomatic FTD and ALS) and healthy controls.

## Methods

C9FTD/ALS and non-demented control human brain sections were provided by the Dutch Brain Bank. CSF samples were obtained from 6 patients with C9FTD, 3 patients with C9ALS and 16 healthy first-degree family members. The unaffected family members consisted of 11 pre-symptomatic *C9ORF72* repeat carriers and 5 healthy control non-carriers. PBMC samples consisted of 3 C9FTD, 9 pre-symptomatic *C9ORF72* repeat carriers and 8 non-*C9ORF72* healthy controls. The presence of a *C9ORF72* repeat expansion >30 was ascertained at the local clinical genetics diagnostics laboratory. C9ALS CSF samples were provided by the population based ALS study in the Netherlands (PAN)[265]. CSF of C9FTD, pre-symptomatic *C9ORF72* carriers and healthy control samples were provided by the Frontotemporal Dementia Risk Cohort (FTD-RisC) study, in which C9FTD patients and healthy at-risk first-degree relatives are longitudinally followed. Participants are followed yearly or two-yearly by a semi-structured health questionnaire, neurological and neuropsychological examination, blood sample collection, MRI imaging and CSF sampling. This study was approved by the local ethics committee (MEC-2009-409) and all participants (or a legal representative) provided written informed consent. Patient information regarding age-of-onset and disease duration can be found in supplementary table 1.

### **COS7 and primary hippocampal mouse neuronal culture**

COS7 cells were cultured in Dulbecco's modified Eagle's medium (DMEM, Gibco) supplemented with 10% fetal calf serum (FCS), 1% Penicillin/Streptomycin (P/S) and 1% non-essential amino acids (NEAA; Lonza) at 37°C in a 5% CO<sub>2</sub> humidified incubator. Primary hippocampal neurons of C57Bl/6J mice were prepared and cultured as described in de Vrij et al. (2008)[266]. In short, a pregnant female mouse from the C57Bl/6J background was sacrificed when embryos were at day E17. Neurons were pooled from all embryos per litter, plated 100.000 cells dropwise in a 6-wells plate and cultured with Neurobasal medium (Gibco) supplemented with 1% P/S, 1% glutamax (Gibco) and 2% B27 (Gibco). Mice were housed at the Erasmus MC animal facility (Rotterdam, the Netherlands), under standard housing and husbandry conditions, approved by the local animal welfare committee. Project license: AVD1010020172224, protocol number 17-2224-04.

### **Transfection and immunocytochemistry**

COS7 cells were plated at 150.000 cells/well in a 6-wells plate and transfected with 3 µl GeneJuice (Novagen) for 1µg DNA. Neurons were cultured for 14 days and transfected with 7µl Lipofectamin 2000 (Invitrogen) per 1 µg DNA. Two days after transfection, the cells were fixed with 4% paraformaldehyde (PFA) in 0.1M PBS and permeabilized with 0.5% Triton X-100 in 0.1M PBS. Immunostaining was performed overnight at 4°C in PBS block buffer (0.1M PBS/ 0.5% protifar/ 0.15% glycine) with the monoclonal poly-GR antibody diluted 1:4000. The next day, cells were washed with block buffer and incubated with secondary antibody anti-mouse Cy3 (Jackson) 1:200 in block buffer at room temperature for 1 hour. After washing with 0.1M PBS, cells were shortly incubated with Hoechst 33342 (Invitrogen) and mounted with ProLong Gold (Invitrogen).

### **Immunohistochemistry on paraffin brain sections**

Human brain sections (6µm) were deparaffinized with xylene and rehydrated (100%-96%-90%-80%-70%-50% EtOH serie). Antigen retrieval was done in 0.01M sodium citrate, pH6.0 using pressure cooker treatment. Endogenous peroxidase activity was blocked with 0,6% H<sub>2</sub>O<sub>2</sub> and 1,25% sodiumazide in 0.1M PBS. Immunostaining was performed overnight at 4°C in PBS block buffer (0.1M PBS/ 0.5% protifar/ 0.15% glycine) with the poly-GR antibody diluted 1:4000. Antigen-antibody complexes were visualized by incubation with DAB substrate (DAKO) after incubation with Brightvision poly-HRP-linker (Immunologic). Slides

were counterstained with Mayer's haematoxylin and mounted with Entellan (Merck Millipore International). Pictures were taken using an Olympus BX40 microscope (Olympus).

### **Protein isolation from frozen frontal cortex and PBMCs**

Prior to lysing, frontal cortex samples were thawed on ice and supplied with RIPA buffer containing 0.05% protease inhibitors (Roche) and 0.3% 1M DTT (Invitrogen). Samples were mechanically lysed, followed by 30 min incubation on ice. After 30 min incubation, mechanical lysing was repeated and samples were centrifuged for 20 min at 4°C, followed by 3x 1 min sonication. After sonication, samples were centrifuged for 20 min at 4°C and the supernatant was used for ELISA. Whole protein content was determined using BCA assay (Thermo Fisher Scientific). The pellet was incubated at 95°C for 2.5 hours in 150µl 20% SDS with every 30 min 5 sec vortexing at max intensity. After incubation, samples were added up to 500µl with 2% SDS and tested on ELISA.

PBMCs were isolated from peripheral blood ACD tubes following standard operating procedures. For lysing, samples were thawed on ice and supplied with ice cold Co-IP buffer (50mM Tris-HCl, pH 7.4; 300mM NaCl, 5mM EDTA, 1% Triton-X 100, 2% SDS) containing 0.01% protease and phosphatase inhibitors (Roche) and 0.3% 1M DTT (Invitrogen). Samples were lysed by agitation for 30 min at 4°C. After 30 min agitation, samples were centrifuged for 20 min at 4°C, followed by 3x 1 min sonication. After sonication, samples were centrifuged for 20 min at 4°C. Whole protein content of the supernatant was determined using BCA assay (Thermo Fisher Scientific).

### **Enzyme-Linked Immuno Sorbent Assay (ELISA)**

MaxiSorp 96 well F-bottom plates (Thermo Fisher) were coated for 2h with 5.0 µg/ml monoclonal GR antibody followed by overnight blocking with 1% BSA in PBS-Tween (0.05% Tween-20, Sigma Aldrich) at 4°C. After washing, 300µg total protein lysate was added per sample. As positive control, a 15x GR synthetic peptide (LifeTein) was used. This peptide was serial diluted to create a standard curve (in duplo). All samples were measured both undiluted and diluted 2x and 4x with 0.1M PBS. Samples and GR peptide were incubated on the plate for 1h at room temperature. After washing, all wells were incubated for 1h with biotinylated monoclonal anti-GR antibody at a final concentration of 0.25 µg/ml in PBS-Tween/1% BSA. After washing again, samples were incubated for 20 min with Poly-HRP conjugate (Thermo Scientific) diluted 1:15.000 in PBS-Tween/1%



BSA. Following extensive washing, samples were incubated with substrate reaction mix (R&D Sciences) for 15 min and stopped using 2N H<sub>2</sub>SO<sub>4</sub>. Read-out was carried out using a plate reader (Varioskan) at 450nm and 570nm. 1-way ANOVA with Bartlett's test for equal variances showed a significant difference in the variance per group, so we performed a Kruskal-Wallis test that does not assume equal variances and post Dunn's multiple comparison test to compare groups.

## Results

In this study we use a newly generated mouse monoclonal antibody against a synthetic 15xGR peptide (LifeTein). To validate this antibody we first co-transfected COS7 and wildtype primary mouse hippocampal neurons with GFP and a construct encoding 100xGR (ATG-mediated, kind gift of Isaacs lab) and performed immunocytochemistry (ICC). Only cells positive for GFP (transfection ratio GFP 3:1 GR) were stained with our anti-GR antibody clone 1G3 (supplementary figure 1). We selected and purified this clone for further use (for information about the production process of this antibody and selection of clone 1G3, see supplementary figure 2). As a second validation, we performed immunohistochemistry

5

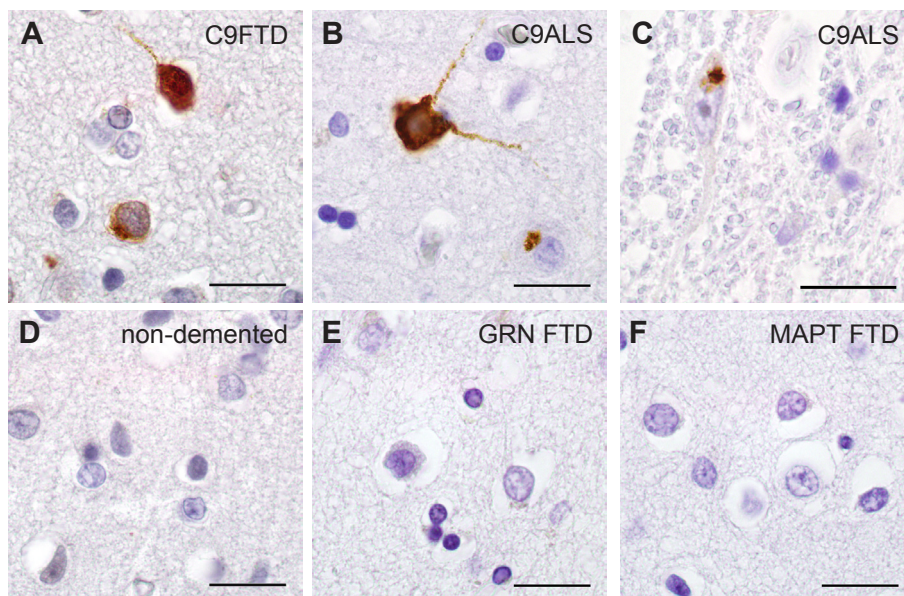


**Figure 1: Poly-GR pathology is selectively detected in C9FTD and C9ALS cases.** A) Frontal cortex of C9FTD and B) motor cortex of C9ALS shows poly-GR staining in brown. Poly-GR can be found as neuronal cytoplasmic inclusions or shows a complete staining of a neuron and its neurites. C) Poly-GR inclusions are occasionally found in the spinal cord of C9ALS. D) Non-demented control frontal cortex, E) GRN FTD frontal cortex and F) MAPT FTD frontal cortex are negative for poly-GR staining.

(IHC) labeling of post-mortem brain sections of C9FTD and C9ALS patients and non-demented controls. This revealed specific staining of poly-GR in perinuclear inclusions in frontal and temporal cortex, hippocampus and cerebellum of C9FTD patients but not of non-demented controls (figure 1 and supplementary figure 3). C9ALS patients showed poly-GR neuronal cytoplasmic inclusions (NCIs) in motor cortex and occasionally in spinal cord (figure 1B-C). Poly-GR staining was mostly perinuclear in neurons, but sometimes also diffusely stained the cytoplasm (figure 1A-B). We also observed some neuropils in the temporal cortex of C9FTD cases (supplementary figure 3). Neuronal intranuclear inclusions (NIIs) were occasionally observed. We further tested the specificity of our antibody by including some post-mortem brain sections of *GRN* FTD and *MAPT* FTD cases, that did not reveal any positive poly-GR staining in the frontal cortex (figure 1E-F).

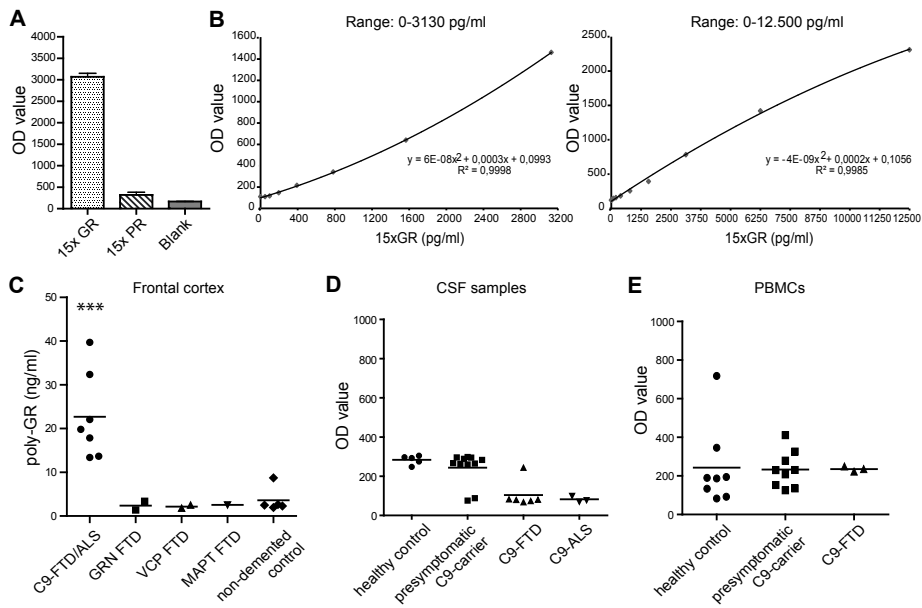


**Figure 2: ELISA analysis shows poly-GR in human frontal cortex of C9FTD cases but not in CSF and PBMC samples.** A) Our ELISA shows a positive selective signal for a synthetic 15xGR peptide over a synthetic 15xPR peptide. B) Dose-response curves for the synthetic 15xGR peptide in the low (0-3130pg) and high (1-12.500pg) range. The limit of detection in the low range is 200pg. C) ELISA on frontal cortex samples of C9FTD/ALS patients (n=7), FTD cases with other genetic mutations in *GRN* (n=2), *VCP* (n=2) and *MAPT* (n=1) and in non-demented controls (n=5). Poly-GR was significantly higher in C9FTD patients with an average of 22.7 ng/ml. Kruskal-Wallis test with post Dunn's multiple comparison test  $p = 0.0017$  D) ELISA on CSF samples from C9FTD (n=6), C9ALS (n=3), C9ORF72-carrier pre-symptomatic (n=11) and non-C9ORF72 healthy control (n=5). No difference could be detected between OD values of the different CSF samples. E) ELISA on PBMCs of C9FTD (n=3), pre-symptomatic C9ORF72 repeat carriers (n=9) and non-C9ORF72 healthy controls (n=8). No difference could be detected between OD values of all PBMC samples.

After using our poly-GR antibody for immunohistochemistry in human C9FTD and C9ALS cases, we developed an ELISA using a synthetic 15xGR peptide (LifeTein) (figure 2). Our ELISA shows high specificity for GR, as it did not show any signal for a 15xPR synthetic peptide (LifeTein) (figure 2A). Next, we diluted the 15xGR peptide to make a dose-response curve in the high and low range, which revealed a sensitivity of 200 pg/ml (figure 2B). To further validate our ELISA we isolated proteins from the frontal cortex of seven C9FTD/ALS cases, five FTD cases due to other genetic causes (*GRN*, *VCP* or *MAPT*) and five non-demented controls (figure 2C). Poly-GR was significantly higher in frontal cortex samples of C9FTD/ALS cases (Kruskal-Wallis test with post Dunn's multiple comparison test  $p = 0.0017$ ), again illustrating the specificity of our assay. The calculated amount of poly-GR was on average 22.7 ng/ml in frontal cortices of C9FTD/ALS patients. Additional protein isolation using 20% SDS and 95°C incubation (see methods) to extract more poly-GR from the insoluble fraction only yielded 1.28 ng/ml extra poly-GR (data not shown). Next, we tested for the presence of the poly-GR peptide in CSF from a cohort of pre-symptomatic *C9ORF72* expanded repeat carriers, symptomatic *C9ORF72* expanded repeat FTD and ALS cases and related healthy controls. Unfortunately, we could not detect poly-GR in the CSF of any of the *C9ORF72* expanded repeat carriers nor controls (figure 2D). Finally, we tested protein lysates from PBMCs isolated from peripheral blood of expanded repeat carriers (pre-symptomatic and symptomatic) but could not detect poly-GR, in none of the *C9ORF72* repeat carriers nor controls (figure 2E).

### Discussion

In this study we show that poly-GR can be specifically detected in brain sections and protein isolates from frontal cortex of C9FTD/ALS cases using a new monoclonal antibody against poly-GR. We could not detect poly-GR in CSF from *C9ORF72* repeat carriers, which suggests that poly-GR levels might be below our detection limit of 200 pg/ml or poly-GR is simply absent from CSF. More sensitive techniques such as SIMOA might be able to detect lower poly-GR levels. It could also be that poly-GR is mainly present as insoluble inclusions which complicates assessment by ELISA. Our antibody is able to recognize both the cytoplasmic form of poly-GR in transfected cells and poly-GR inclusions in post-mortem brain tissue. Stringent protein isolation protocols of C9FTD frontal cortex samples did not yield a higher ELISA signal, indicating that almost all poly-GR was already detected in our standard ELISA procedure. Still, some insoluble poly-GR molecules

might be missed in CSF samples in our ELISA set-up.

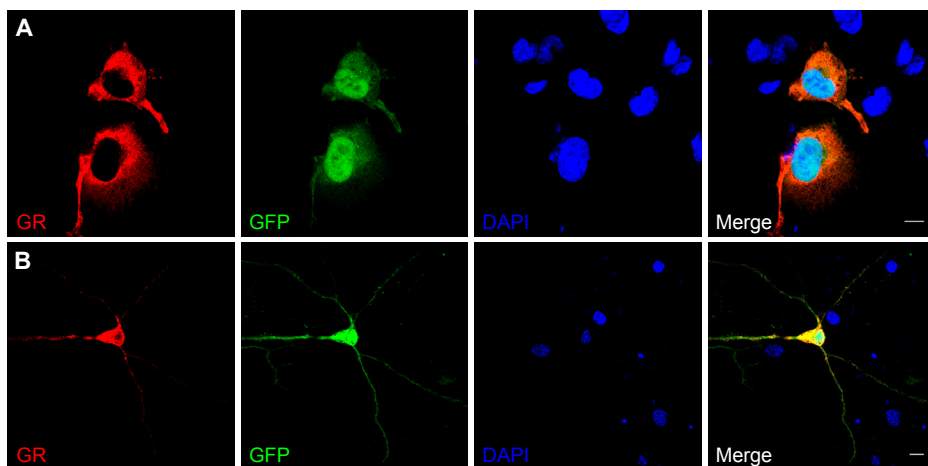
Previous assessment of poly-GP levels in CSF by Gendron et al. revealed an average of 0.5ng/ml for asymptomatic *C9ORF72* repeat carriers and 0.8ng/ml for symptomatic C9ALS/FTD patients[197]. Our ELISA should be sensitive enough to detect poly-GR levels in the same range. However, poly-GR pathology is less abundant than poly-GP in *C9ORF72* human post-mortem brain sections[69] and might therefore also be lower in CSF than poly-GP. In addition, it could be possible that only poly-GP is present in CSF because of its high solubility compared to the other DPRs that are more polar and aggregation prone[264]. Since DPRs were detected in ependymal and sub-ependymal cells of the ventricle wall[70], it is conceivable that DPRs might be secreted in CSF by these cells. Notably, DPRs are almost always observed as neuronal cytoplasmic inclusions throughout the CNS[51] and thus might be released in the extracellular space after neuronal death as well. DPRs are rare in spinal cord and lower motor neurons of C9ALS cases[71], making a release of DPRs in CSF from axonal injury unlikely to contribute to DPR levels in CSF. In addition, DPRs can also be transmitted from cell-to-cell *in vitro*[267] and arginine-containing DPRs can penetrate the membrane[268]. Interestingly, antibody therapy inhibits cell-to-cell transmission, seeding and aggregation of poly-GA[269], indicating an important role for detection of extracellular DPRs for drug discovery and treatment.

*C9ORF72* is highly expressed in myeloid cells, particularly CD14+ cells[97] and poly-GP levels in PBMCs were previously reported[197]. We were unable to detect poly-GR in PBMCs of *C9ORF72* repeat carriers, maybe because the levels are too low to detect with our ELISA. In contrast, Poly-GP might have higher levels in PBMCs because it is produced from both sense and antisense *C9ORF72* transcripts. Therefore, Poly-GP does show great promise as a pharmacodynamic biomarker for assessing new therapeutic approaches that target *C9ORF72* repeat RNA, RAN translation or DPRs directly[197]. A combination with neurofilament light chain levels, that reflect neurodegeneration, will probably best predict disease progression and survival of C9FTD/ALS patients[260, 262]. As the field is now moving towards the development of therapies for C9FTD/ALS from the preclinical to the clinical phase, such fluid biomarkers are essential for successful assessment of clinical trials[270, 271].

### Acknowledgements

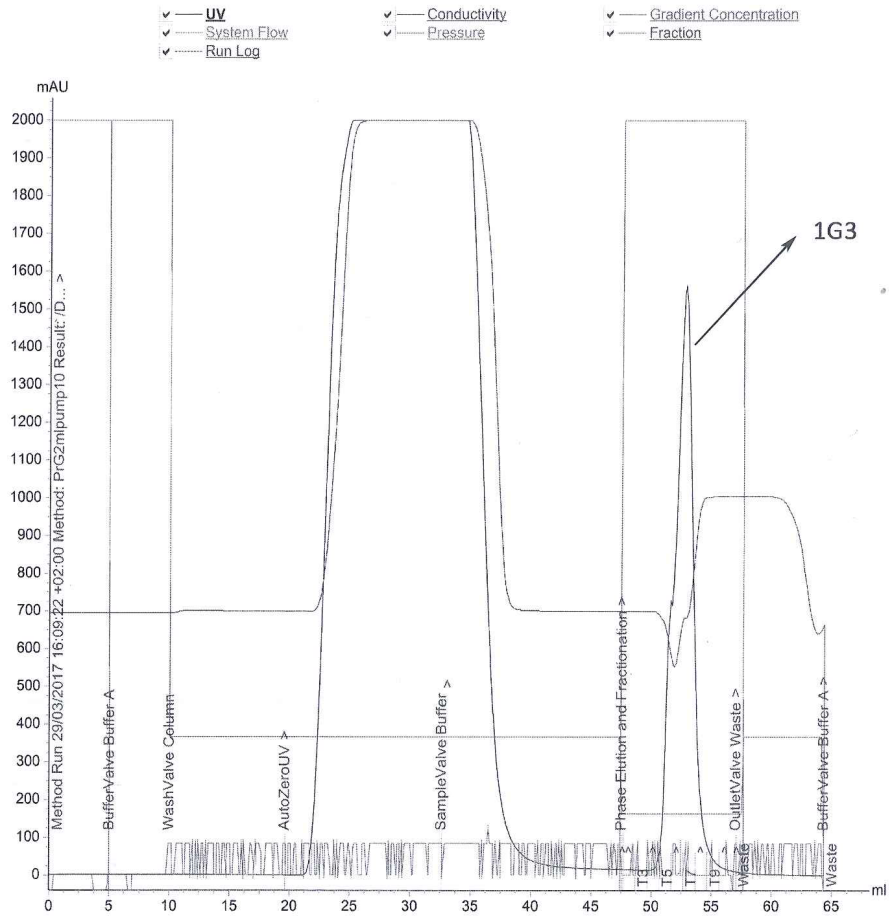
Authors would like to thank Adrian Isaacs for his kind gift of the pcDNA3.1+ CMV-100xGR plasmid and Michiel Kooreman from the Dutch brain bank for his help in selecting post-mortem brain sections and frozen material for our study. This study was supported by the European Joint Programme - Neurodegenerative Disease Research and the Netherlands Organization for Health Research and Development (PreFrontALS: 733051042 to RW and JCS).

5



**Supplementary figure 1: GR antibody specifically stains transfected cells.** A) COS7 cells were transfected with a CMV-GFP plasmid and a 100xGR plasmid (both ATG-mediated, pcDNA3.1+ vector) in ratio GFP 3:1 GR. Two days after transfection, cells were fixed and stained for poly-GR and revealed co-localization between GFP expressing cells and poly-GR staining. B) The same procedure was performed using primary hippocampal neurons from wildtype C57BL/6J mice. Untransfected cells never showed positive poly-GR staining.

1G3 purification, protein G column:




1G3 biotinylation:

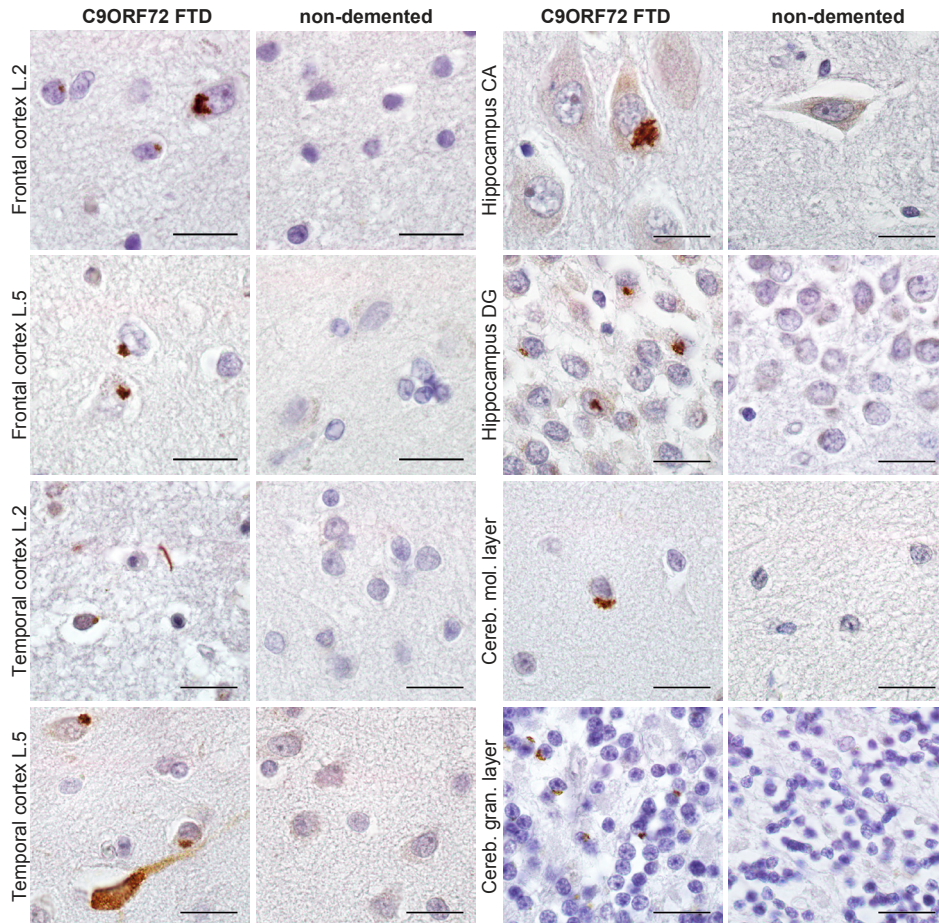
Biotin ratio: 4.23 of biotin/mole of IgG

Concentration of biotin in sample: 0.000141 mmol/ml

**Result:** direct ELISA:

	Supernatant:	Negatif	
Antigen:	polyRG peptide	0.006	0.559

**Supplementary figure 2: Information about poly-GR mouse monoclonal antibody production process provided by IGBMC.**



**Supplementary figure 3: Poly-GR pathology in several brain areas of C9FTD cases.** Poly-GR neuropathology was most often observed as neuronal cytoplasmic inclusions (NCIs) in layer 2 and 5 of the frontal and temporal cortex. In addition, temporal cortex harbored some neuropils. Hippocampus dentate gyrus and cornu ammonis and cerebellum granular and molecular layers also show the presence of NCIs. Non-demented controls did not show any positive poly-GR staining using our new mouse monoclonal antibody.

**Supplementary table 1: Patient characteristics**

Patient ID	Clinical diagnosis	Genetic diagnosis	Age of onset	Disease duration in years *	Male / Female	Used for
1	bvFTD	C9ORF72	51,8	8,7	Male	IHC
2	bvFTD	C9ORF72	55,8	9,1	Male	IHC
3	bvFTD	C9ORF72	66,4	8,1	Female	IHC
4	bvFTD	C9ORF72	63,2	6,8	Female	IHC
5	bvFTD	C9ORF72	55,2	9,5	Male	IHC
6	FTD	GRN (Gln200X)	60,6	5,5	Female	IHC
7	FTD	GRN (Ser82 ValfsX174)	47,4	4,3	Female	IHC
8	FTD	MAPT (G272V)	42,6	8,4	Male	IHC
9	FTD	MAPT (P301L)	51,1	9,7	Male	IHC
10	ALS	unknown	70	1	Male	IHC
11	ALS	unknown	65	2,2	Female	IHC
12	ALS	unknown	75	1,1	Male	IHC
13	ALS	C9ORF72	60	4,4	Female	IHC
14	ALS	C9ORF72	66	3,5	Male	IHC
15	ALS	C9ORF72	71	2,4	Female	IHC
16	FTD	C9ORF72	48	10	Male	Protein isolation of frontal cortex (PFC)
17	FTD/ALS	C9ORF72	60	8	Female	proteins PFC
18	FTD	C9ORF72	61	7	Female	proteins PFC
19	FTD	C9ORF72	71	7	Male	proteins PFC
20	FTD	C9ORF72	69	6	Male	proteins PFC
21	FTD/ALS	C9ORF72	39	3	Female	proteins PFC
22	FTD/ALS	C9ORF72	61	2,8	Female	proteins PFC
23	FTD	GRN (Gln24X)	54	5	Male	proteins PFC
24	FTD	GRN (Gly387fs)	57	3	Male	proteins PFC
25	FTD	VCP (p.R159S)	56	5	Female	proteins PFC
26	FTD	VCP (p.T262S)	60	7	Female	proteins PFC
27	FTD	MAPT (P301L)	58	8	Female	proteins PFC
28	Non-demented	N/A	N/A	N/A	Male	proteins PFC
29	Non-demented	N/A	N/A	N/A	Female	proteins PFC
30	Non-demented	N/A	N/A	N/A	Male	proteins PFC
31	Non-demented	N/A	N/A	N/A	Female	proteins PFC
32	Non-demented	N/A	N/A	N/A	Female	proteins PFC
33	bvFTD	C9ORF72	38	8,3	Female	CSF& PBMcs



34	bvFTD	C9ORF72	51	3,2	Male	CSF& PBMCs
35	AD-like FTD	C9ORF72	71	4	Male	CSF
36	bvFTD	C9ORF72	79	2	Male	CSF
37	ALS	C9ORF72	57	0,3	Female	CSF
38	bvFTD	C9ORF72	52	7,2	Male	CSF
39	bvFTD	C9ORF72	61	11,3	Male	CSF
40	ALS	C9ORF72	53	4	Male	CSF
41	ALS	C9ORF72	56	2	Male	CSF
42	presymptomatic	C9ORF72	N/A	N/A	Female	CSF& PBMCs
43	presymptomatic	C9ORF72	N/A	N/A	Female	CSF
44	presymptomatic	C9ORF72	N/A	N/A	Female	CSF
45	presymptomatic	C9ORF72	N/A	N/A	Female	CSF
46	presymptomatic	C9ORF72	N/A	N/A	Female	CSF& PBMCs
47	presymptomatic	C9ORF72	N/A	N/A	Female	CSF& PBMCs
48	presymptomatic	C9ORF72	N/A	N/A	Female	CSF& PBMCs
49	presymptomatic	C9ORF72	N/A	N/A	Male	CSF
50	presymptomatic	C9ORF72	N/A	N/A	Male	CSF& PBMCs
51	presymptomatic	C9ORF72	N/A	N/A	Male	CSF& PBMCs
52	presymptomatic	C9ORF72	N/A	N/A	Male	CSF& PBMCs
53	presymptomatic	C9ORF72	N/A	N/A	Female	PBMCs
54	presymptomatic	C9ORF72	N/A	N/A	Female	PBMCs
55	Healthy control	N/A	N/A	N/A	Male	CSF
56	Healthy control	N/A	N/A	N/A	Male	CSF& PBMCs
57	Healthy control	N/A	N/A	N/A	Female	CSF& PBMCs
58	Healthy control	N/A	N/A	N/A	Male	CSF
59	Healthy control	N/A	N/A	N/A	Male	CSF& PBMCs
60	Healthy control	N/A	N/A	N/A	Female	PBMCs
61	Healthy control	N/A	N/A	N/A	Male	PBMCs
62	Healthy control	N/A	N/A	N/A	Female	PBMCs
63	Healthy control	N/A	N/A	N/A	Male	PBMCs
64	Healthy control	N/A	N/A	N/A	Female	PBMCs

\* Disease duration has been estimated from the onset of first symptoms (retrospectively determined, not date of diagnosis) until death or until CSF sample collection.



# Chapter 6

## General discussion



**Abstract**

In this thesis, we have shown that both poly-GR and –PR clearly evoke cellular toxicity in our zebrafish model. In our inducible transgenic mouse model, overexpression of 36x pure G<sub>4</sub>C<sub>2</sub> repeats produces sense DPRs and elicits a motor phenotype. Our data therefore support a gain-of-function mechanism as major cause of the neurodegeneration observed in C9FTD/ALS cases. However, we do not assess the effect of loss-of-function, which could be a disease modifying factor. Also, expression of all DPRs, RNA foci and haploinsufficiency together might differently affect molecular targets and cellular functioning. In this discussion, we will evaluate our own data and recent literature to identify key pathological and molecular events that drive neurodegeneration in C9FTD/ALS patients. In the last part, we will address the development of reliable biomarkers that can help to find the best time to start treatment and can provide information on treatment response, which is essential for the right implementation of new therapies.

## 1. What is the toxic culprit?

### 1.1 RNA vs DPR toxicity

In our zebrafish study, we observed a combined effect of RNA and DPR cellular toxicity. We used ATG-mediated constructs encoding poly-GR and –PR without  $G_4C_2$  sequence (using alternative codons) to investigate protein-only toxicity. Mutating the ATG start site generated constructs to investigate RNA-only toxicity. Injections with these RNA-only constructs evoked cellular toxicity in zebrafish embryos. However, this does not provide any information about RNA toxicity of the pure  $G_4C_2$  repeat structure. We can therefore only use our model to obtain information about relative toxicity of protein-only constructs, which was clearly higher than the sole effect of RNA-only injections.

Several studies have made a direct comparison between  $G_4C_2$  RNA and DPR toxicity. In *Drosophila*, overexpression of 36x and 100+ expanded  $G_4C_2$  repeats in eyes or neurons caused profound neurodegeneration[168]. This effect disappeared when repeats were interrupted with stop-codons (RNA-only construct)[168], indicating that DPRs were responsible for the observed toxicity. Indeed, overexpression of ATG-mediated DPR constructs were far more toxic than the RNA-only construct[168]. However, the introduction of stop-codons could affect secondary structures of the  $G_4C_2$  repeat and thereby alter its biological effect. To circumvent this problem, two other *Drosophila* studies investigated pure  $G_4C_2$  repeats. Overexpression of 160x pure  $G_4C_2$  repeats in an intronic context caused formation of RNA foci in both glia and neurons, but did not cause neurodegeneration[212]. Also long (100-1000x) sense and antisense repeat constructs either inside an intron of GFP or part of a poly-adenylated transcript generated many nuclear and cytoplasmic RNA foci, but neither construct led to cellular toxicity[272]. These three drosophila models indicate that DPRs are more toxic than the expression of  $G_4C_2$  repeats in an (intronic) RNA context.

Other studies interpret their results as caused by RNA toxicity only, because DPRs were undetectable. Swinnen et al. injected zebrafish embryos with pure 70x  $G_4C_2$  repeat RNA, which led to cellular toxicity[154]. In *Drosophila*, overexpressing 30x  $G_4C_2$  interrupted repeats caused toxicity in eyes and motor neurons[153, 155]. Also in primary rat cortical and motor neuron cultures, overexpression of expanded  $G_4C_2$  repeats caused reduced survival[171]. As DPRs were not detectable in these studies, the toxic effect could be attributed to an RNA-only gain-of-function mechanism[153-155, 171]. However, in our experience very low poly-GR and –PR levels already can have an effect on cell death in zebrafish, while DPR levels are too low to detect with dot blot or Western blot and could only

be detected with ELISA. We should therefore be cautious with interpreting these studies as RNA-only models. Combined with the studies discussed above, DPRs seem to have a more profound effect on cellular toxicity than  $G_4C_2$  RNA toxicity alone. However, we have to keep in mind that these are all overexpression studies, which makes it hard to translate these models to the human situation.

### 1.2 Functional effects of RNA foci

The  $G_4C_2$  repeat RNA can capture several RNA-binding proteins, such as hnRNP-A3, hnRNP-H, eIF2 $\alpha$ , FUS, SC35, ALYREF, Ran-GAP and Pur-alpha (see also table 1 of the general introduction). But this does not always seem to have functional consequences, as only a small percentage of a certain protein is sequestered or other proteins can compensate for its loss. In *Drosophila*, RNA foci were able to sequester Glorund, the *Drosophila* ortholog of hnRNP-H, but this did not lead to cellular toxicity[272]. Also, the number of neurons in which RNA foci co-localized with hnRNP-H in cerebellum of C9ALS cases was extremely low (less than 3%)[149]. Other sequestered proteins like eIF2 $\alpha$ , FUS and SC35 also rarely (<5%) co-localized with  $G_4C_2$  RNA foci in cerebellum of C9FTD/ALS patients[149, 152]. This suggests that the formation of RNA foci does not affect the overall distribution of these sequestered proteins and that sufficient free proteins remains available to fulfill their normal cellular function. Alternatively, other proteins may take over their function; when ALYREF was depleted from HeLa cells, this only caused a partial block of nuclear export, suggesting the existence of other proteins with redundant function[148]. Binding of some proteins to RNA foci might even be protective, as has been suggested for hnRNP-A3[273]. Knock-down of hnRNP-A3 causes more RNA foci and DPR formation in primary rat hippocampal neurons and fibroblasts from C9ALS patients[273]. These studies illustrate that the sequestration of proteins by RNA foci does not necessary result in their reduced normal functioning.

In contrast, several rescue experiments indicate that RNA foci do have an effect on the availability and function of the sequestered proteins. Overexpression of Pur-alpha in *Drosophila* rescued the phenotype observed in eye development[153]. Overexpression of Ran-GAP also rescued 30x $G_4C_2$  repeat induced-toxicity in *Drosophila* eyes and motor neurons[155]. Furthermore, Conlon et al. showed that splicing targets of hnRNP-H were changed in cerebellum tissue of seven C9ALS cases compared to non-demented controls[274]. Sequencing of RNA isolated from brain tissue of C9ALS patients revealed global changes in alternative splicing, particularly skipping of exons that are predicted targets of

hnRNP-H[158]. These results illustrate that the  $G_4C_2$  repeat is able to sequester these proteins, causing the loss of their normal cellular function and thereby have an impact on for example splicing. In general, the effect of sequestration by RNA foci might be different for each protein. Reduction of Ran-GAP and Pur-alpha levels clearly impacts cellular viability. On the other hand, RNA foci might not sequester enough eIF2 $\alpha$ , FUS and SC35 proteins to affect their normal functioning.

### 1.3 Correlation of RNA foci and DPRs with clinical features

Two studies investigated the relationship between RNA foci and clinical features. The first study showed that more sense RNA foci in the frontal cortex correlated with an *earlier* age of onset[56]. The second, a larger study, showed that more antisense RNA foci in the middle frontal gyrus were correlated with a *later* age at onset[58]. Thus, these two studies reported contradictory findings for sense versus antisense foci and to date we cannot conclude that numbers of RNA foci show an association with any feature of *C9ORF72* carriers[58]. For DPRs, the correlation with neurodegeneration has often been assessed but never found when all DPRs or only poly-GA was taken into account (reviewed in [51]). When focusing on poly-GR alone, an association was found in two recent studies[72, 73]. Poly-GR was significantly more abundant in clinically-related areas compared to unrelated areas of C9ALS cases[72] and correlated with neurodegeneration in a cohort of 40 C9FTD, C9ALS and C9FTD/ALS cases[73]. Together, this highlights a role for poly-GR in the pathophysiology of C9FTD/ALS, and less for RNA foci and other DPRs.

### 1.4 Contribution of loss-of-function

Loss-of-function is not sufficient to cause FTD and/or ALS symptoms in knock-out mouse models of *C9ORF72* (reviewed in [228]). But haploinsufficiency can influence gain-of-function mechanisms. This was nicely shown in C9FTD/ALS iPSC-derived motor neurons, which are susceptible to glutamate toxicity[126]. Overexpression of poly-GR or -PR in C9FTD/ALS or *C9ORF72* crispr-cas9 knock-out (C9KO) iPSC-derived neurons resulted in enhanced cellular toxicity[126]. C9FTD/ALS or C9KO iPSC-derived motor neurons contain less lysosomes and more glutamate receptors at spines. They also show a slower degradation of poly-PR[126]. All these effects could be rescued by overexpression of both the short and long isoform of the *C9ORF72* protein or by enhancing endosome and lysosome function with small molecules[126].

The *in vivo* synergistic effect of both loss- and gain-of-function mech-

anisms in the pathogenesis of C9FTD/ALS was confirmed by Qiang Zhu et al.[275]. Previously published BAC mice expressing 450x G<sub>4</sub>C<sub>2</sub> repeats (C9BAC) were crossed with previously published C9KO mice[136]. These combination C9KO/C9BAC mice showed enhanced cognitive deficits, hippocampal neuron loss and glial activation. C9BAC repeat mice also showed an elevation of LC3B levels indicative for enhanced autophagy, which was reduced by depletion of the C9orf72 protein, suggesting that loss of C9orf72 protein reduces autophagy in the C9BAC mouse. Interestingly, combination C9KO/C9BAC mice showed accelerated accumulation of poly-GA and higher soluble levels of poly-GP in the cortex using ELISA. Strikingly, injections of AAV-66xG<sub>4</sub>C<sub>2</sub> repeats in ventricles of heterozygous C9KO mice caused premature death. Normally, both the AAV-66x G<sub>4</sub>C<sub>2</sub> repeat mouse model and the heterozygous C9KO mouse model have a normal life span, but the combination of the two apparently causes a higher toxic effect than their sole effect. These results provide direct support that reduced C9orf72 protein enhances the repeat-dependent gain-of-function mechanisms in C9FTD/ALS.

C9ORF72 haploinsufficiency could also influence the aggregation or accumulation of other proteins than DPRs. Neurons with reduced levels of the short isoform of C9ORF72 protein (C9-S) more often contained cytoplasmic pTDP-43 inclusions[276]. C9-S shuttles between the nucleus and the cytoplasm and loss of C9-S might induce pTDP-43 mis-localization[276]. A combination between alfa-1 KO (homologue of C9ORF72) in *C. elegans* and dominant active TDP-43<sup>A315T</sup> mutant worms also led to an additive effect on aberrant motor dysfunction[128]. Finally, C9orf72 protein knock-down using shRNA increased the aggregation and cellular toxicity of Ataxin 2 Q30x in primary mouse cortical neurons[118]. Altogether, this provides evidence that C9ORF72 loss-of-function is a disease modifying factor.

## 2. Pathological hallmarks in C9FTD/ALS

RNA foci and neuronal cytoplasmic inclusions of DPRs are known to be the first pathological hallmarks that arise in C9FTD/ALS patients' brain, even before the onset of symptoms, as shown in C9ORF72 repeat carriers that died due to other causes[59]. But accumulation of DPRs might not be necessary for their toxicity, and could even alter their cellular target(s). Sequestered proteins or their interaction with RNA foci and/or DPRs might be the target of new drugs in the future. Validation of newly identified protein pathology in post-mortem brain tissue is therefore essential to gain information about the pathogenesis of C9FTD/ALS.



### 2.1 Is the aggregation of DPRs necessary for their toxicity?

In chapter 2 of this thesis, we overexpressed ATG-mediated poly-GR or -PR in zebrafish embryo's and show their immediate effect on cell death. Detection of DPRs by immunohistochemistry and ELISA indicated that poly-GR seems to be present in both a diffuse form and as puncta in the nucleus, while poly-PR was mostly present as nuclear puncta. This indicates that the observed cellular toxicity is predominantly caused by soluble and aggregated poly-GR and nuclear accumulation of poly-PR. However, more research is needed to confirm these observations. In our mouse model, we mainly observed soluble forms of sense DPRs; poly-GA, -GP and -GR. Poly-GA was present in a diffuse form in the nucleus and cytoplasm, while poly-GP and -GR were mainly diffusely localized in the nucleus. It is unclear if one single DPR or the simultaneous expression of all soluble sense DPRs is responsible for the muscular toxicity observed in this model. Mouse models investigating the sole expression of poly-GA, -GR or -PR may provide more information about this phenomenon and are discussed below[199, 200, 213].

In a mouse model for poly-GA, Zhang and colleagues nicely demonstrated that aggregation of poly-GA was essential for its cellular toxicity[213]. They generated mice expressing GFP-tagged 50x poly-GA<sub>mutated</sub> in which the GA sequence was interrupted by proline residues that disrupted fibril formation. Poly-GA<sub>mutated</sub> remained soluble both in HEK293T cells and mouse cortical tissue and did not cause caspase-3 activation nor any cell loss or behavioral changes in mice. In contrast, mice expressing 'normal' GFP-tagged 50x poly-GA did show inclusions that were ubiquitin-positive, exhibited neurodegeneration in several brain areas and developed motor deficits, hyperactivity, anxiety and cognitive deficits[213].

In contrast to poly-GA, expression of soluble poly-GR or poly-PR was enough to evoke a phenotype in two AAV-mediated mouse models[199, 200]. GFP-tagged poly-GR<sub>100</sub> was mostly cytoplasmic and diffusely localized in neurons in the cortex and led to cortical thinning, hippocampal and cerebellar Purkinje cell loss. After 6 months, mice showed (loco)motor impairment in open field and rotarod tests in combination with decreased cued freezing in a fear-conditioning test[199]. Overexpressed GFP-tagged poly-PR<sub>50</sub> showed a diffuse nuclear distribution and led to 60% mortality of mice at 4 weeks of age[200]. Surviving mice showed a reduction in the number of PR-positive cells, displayed cortical thinning and reduced hippocampal volume at 3 months of age, combined with worse performance on the rotarod and cued freezing in fear-conditioning[200].

This suggests that aggregation of poly-GR and -PR is not necessary to evoke toxic effects.

Poly-GR might even have different effects depending on its conformational state. In AAV-66x  $G_4C_2$  and AAV-149x  $G_4C_2$  mice, cytoplasmic inclusions of poly-GR were observed. These mouse models exhibit both RNA foci and all other DPRs, suggesting that these or other factors are needed to evoke aggregation of poly-GR[195, 199]. In the AAV-66x and 149x  $G_4C_2$  mouse models, cytoplasmic inclusions of poly-GR co-localized with pTDP-43 and TIA1, a constituent of stress granules[195]. This phenomenon was not observed in the – soluble – poly-GR only mouse model[199], implying that the aggregation of poly-GR is needed to sequester pTDP-43 and to influence stress granule dynamics. This indicates that poly-GR has different cellular targets depending on its conformational state but can be toxic in both soluble and aggregated form.

Interestingly, poly-GA can sequester both poly-GR and –PR in inclusions and partially reduce their cellular toxicity[74, 196]. In AAV-66x and AAV-149x  $G_4C_2$  repeat mouse models for *C9ORF72*, poly-GR co-aggregated with poly-GA in cells expressing poly-GA, but remained diffuse in cells devoid of poly-GA expression[199]. Co-overexpression of poly-GA and –GR altered the localization of poly-GR from diffuse to inclusions in the cytoplasm of *Drosophila* salivary gland cells[74]. Furthermore, poly-GA overexpression partially suppressed the poly-GR induced cell loss in the wings of *Drosophila*[74]. The same holds true for the combination of poly-GA and -PR. Co-overexpression of poly-GA abolished cellular toxicity of low concentrations of poly-PR and changed its localization from diffuse nuclear to cytoplasmic inclusions in NSC34 cells[196]. This suggests that soluble poly-GR and –PR are more toxic than their aggregated form, but this effect has only been observed for low concentrations. Together, these data suggest that the combined overexpression of all DPRs produces different cellular outcomes and structural conformations compared with the effects of overexpression of single DPRs.

## 2.2 Validation of sequestered proteins in human post-mortem brain tissue

Identification of new protein pathology in post-mortem brain material could provide clues about the pathophysiology of C9FTD/ALS. In chapter 4 of this thesis, we show that HR23B is mis-localized in the CNS of C9FTD/ALS cases. HR23B is a multifunctional protein that plays a role in DNA repair and in the degradation of proteins via endoplasmic reticulum-associated degradation (ERAD) and via the proteasome[242]. We showed that HR23B mostly co-localized with poly-GA

and less with other DPRs. Other proteins that show mis-localization in C9FTD/ALS patient post-mortem brain material are Drosha[277], KPNA2/4[278], hnRNP-A3[150] and Unc119[175]. Drosha is an endonuclease and is involved in miRNA biogenesis[277]. Almost all Drosha neuronal cytoplasmic inclusions were also positive for poly-GA[277]. KPNA2 and KPNA4 are involved in the classical nuclear import pathway[278]. They show nuclear clearing and cytoplasmic inclusions in C9FTD cases and sometimes co-localize with DPRs and pTDP-43[278]. HnRNP-A3 is involved in both pre-mRNA splicing and export of mRNA into the cytoplasm. Reduction of hnRNP-A3 from hippocampal nuclei in brain tissue of 34 C9FTD/ALS patients correlated with increased poly-GA aggregation[273]. Unc119 is a trafficking factor for myristoylated proteins and *Unc119* knockout *C. elegans* caused paralysis and disturbed axonal development[279]. All together, these studies indicate that the aggregation or nuclear clearing of these specific proteins might impact normal nucleocytoplasmic transport (NCT) and RNA processing, as many of the described proteins function in these cellular processes. Interestingly, most of these proteins co-localize with poly-GA and might provide information on how poly-GA affects normal cellular functioning. For example, overexpression of Unc119 and HR23B rescued poly-GA toxicity in primary murine neuronal cultures[175, 213].

Mis-localization of some proteins identified in cell and animal models could not be confirmed in post-mortem brain tissue of C9FTD/ALS patients. Ran-GAP was found to be sequestered in a poly-GA mouse model[213] and significantly more cells showed nuclear invagination of Ran-GAP in an AAV-149xG<sub>4</sub>C<sub>2</sub> mouse model[195]. However, we (chapter 4) and others[51, 72] were unable to confirm Ran-GAP neuropathology in C9FTD/ALS patients. A possible explanation for this discrepancy may be that post-mortem brain material only represent the end-stage of FTD/ALS and early changes might be missed. Also, differences in oddly-shaped nuclei in the Ran-GAP staining might only become evident if large number of cells are quantified. We were also unable to confirm FMRP, Pur-alpha and ADARB2 pathology in post-mortem brain sections of C9FTD patients (chapter 4). This illustrates the importance of validation of results obtained from cell and mouse models to human post-mortem brain material.

Finally, Poly-GR has been shown to co-localize with several ribosomal proteins (S6, S25, L19, L21, L36A), RNA binding protein STAU2 and translation initiation factor eIF3n in the frontal cortex of C9FTD/ALS cases[199, 280]. These last findings indicate that poly-GR aggregation might evoke reduced translation by the sequestration of ribosomes and translation initiation factors.

### 2.3 Co-localization patterns between pathological hallmarks of C9FTD/ALS

Co-localization patterns between pathological hallmarks can also provide essential information about the order and impact of (neuro)pathological processes. Interestingly, the presence of antisense foci in motor neurons was associated with nuclear loss of TDP-43, as 77% of all antisense RNA foci positive cells showed loss of nuclear TDP-43[60]. Especially antisense foci that surround the nucleolus have been associated with cytoplasmic TDP-43 pathology in the anterior horn of the spinal cord of C9ALS cases[164]. Antisense RNA foci that sequester NCT factors or antisense DPR products like poly-PR can affect NCT[155, 177, 178, 187] which could cause nuclear clearing of TDP-43, but to date no empirical data is available to support the last part of this hypothesis. No correlation exists between the presence of RNA foci and the amount of DPRs or p62 inclusions in a cell[56, 61].

Saberi et al. showed that poly-GR is the only DPR that showed co-localization with pTDP-43[72]. From all poly-GR dendritic inclusions in the motor cortex, 80% was pTDP-43 positive, while none of the other DPR-positive dendritic inclusions were pTDP-43 positive[72]. Twenty percent of perinuclear poly-GR inclusions in the motor cortex co-localized with pTDP-43, compared to 1-10% of the other DPRs[72]. Occasionally, poly-PA inclusions in the spinal cord were also positive for pTDP-43[71]. And sometimes, pTDP-43 has been detected around perinuclear poly-GA inclusions[66]. In SH-SY5Y cells, poly-GA preceded TDP-43 aggregation[281]. But co-localization studies between poly-GA and pTDP-43 in human post-mortem brain sections of C9FTD/ALS patients are missing. So far, the most prominent DPR that co-localizes with pTDP-43 is poly-GR. Importantly, only pTDP-43 and poly-GR are associated with neurodegeneration[72, 73], while RNA foci, the other DPRs and ubiquitin/p62 are not[51].

Co-localization patterns can differ between brain regions, which we show for HR23B and poly-GA in chapter 4. In the frontal cortex, only 7% of HR23B inclusions were poly-GA positive, while this increased to 60% in the hippocampal dentate gyrus. The same phenomenon has been reported for Mif2, a chaperone-associated protein. Co-localization of Mif2 with poly-GA increased from 1% in frontal cortex to 3% in the hippocampus dentate gyrus[229]. Also hnRNP-A3 inclusions were more often observed in hippocampal dentate gyrus than in cerebellum[282]. An explanation for this phenomenon could be that subtypes of neurons may influence aggregation patterns by differences in expression levels and availability of HR23B, Mif2, hnRNP-A3 and/or their binding partners. Interestingly, overexpression of HR23B protected for the formation of poly-GA inclusions in

mouse primary neuronal cultures[213]. Also, reduced nuclear hnRNPA3 in the hippocampus of 34 C9FTD/ALS patients correlated with increased poly-GA aggregation[273]. Further in depth studies about expression levels and aggregation patterns are warranted to gain knowledge on the different vulnerability of specific subtypes of neurons. This could provide crucial information why the *C9ORF72* repeat mutation causes abundant neurodegeneration in certain brain areas while other brain areas are relatively spared.

#### 2.4 The role of pTDP-43 aggregation in neurodegeneration

In chapter 2 and 3 (zebrafish and mouse models) we show that overexpression of  $G_4C_2$  repeat RNA and/or DPRs is sufficient to evoke cellular toxicity and a behavioral phenotype without aggregation or mis-localization of pTDP-43 from the nucleus to the cytoplasm. This raises the question whether pTDP-43 pathology is essential to cause neurodegeneration or if it is simply a “by-product” of neuropathological processes. The presence of pTDP-43 neuropathology is thought to be a late event[59, 77]. Many mouse models already show behavior phenotypes and some mild neurodegeneration before the onset of pTDP-43 neuropathology[136, 194, 199, 213, 229]. Also in humans several examples have been reported of affected C9FTD/ALS individuals with DPR pathology but moderate or lack of TDP-43 neuropathology[27, 59, 66, 234, 235]. Together, this implies that pTDP-43 aggregation is not essential to evoke initial neurodegeneration. However, changes in subcellular localization or solubility of TDP-43 could already arise earlier and add to cellular distress before the onset of pathology. This is also confirmed by mouse models for *TARDBP*, in which cytoplasmic aggregation of pTDP-43 is not essential for its cellular toxicity[283]. TDP-43 functionality is very important for many cellular processes and for cellular survival[96] and any changes in its availability might shift the balance to cellular dysfunction[284]. Together, this argues for an important role for pTDP-43 in C9FTD/ALS pathogenesis without the need for cytoplasmic aggregation per se.

### **3. Aberrant downstream molecular pathways in C9FTD/ALS pathogenesis**

The *C9ORF72* research field has produced a multitude of abrogated molecular pathways (also see general introduction). RNA foci, poly-GR, -GA and -PR are able to bind many different proteins inside the cell and probably affect many pathways simultaneously. It may therefore be important to identify pathways that are primary affected or that are dysregulated via multiple directions.

### 3.1 Central role of the integrated stress response

In this thesis, we have shown that poly-PR mediated cell death could be prevented by ISRIB, indicating that activation of the integrated stress response (ISR) underlies poly-PR mediated toxicity (chapter 2). Endoplasmic reticulum (ER) stress is one of the factors that can activate the ISR (see figure 1 about the ISR [207]). Downstream effects of ISR activation are translation inhibition and increase in ATF4 and CHOP levels, which are known to induce apoptosis[207]. The formation of stress granules and NCT defects can be indirect downstream effects[183, 188]. Interestingly, in C9ALS iPSC-derived motor neurons, poly-PR cellular toxicity can be modified by the ER membrane protein complex and ER-resident proteins such as TMX2 and CANX[210], which strengthens the involvement of ER-stress and the ISR in PR-mediated cellular toxicity. Recent reports indicate that both poly-GR and -PR interact with many ribosomal proteins and inhibit

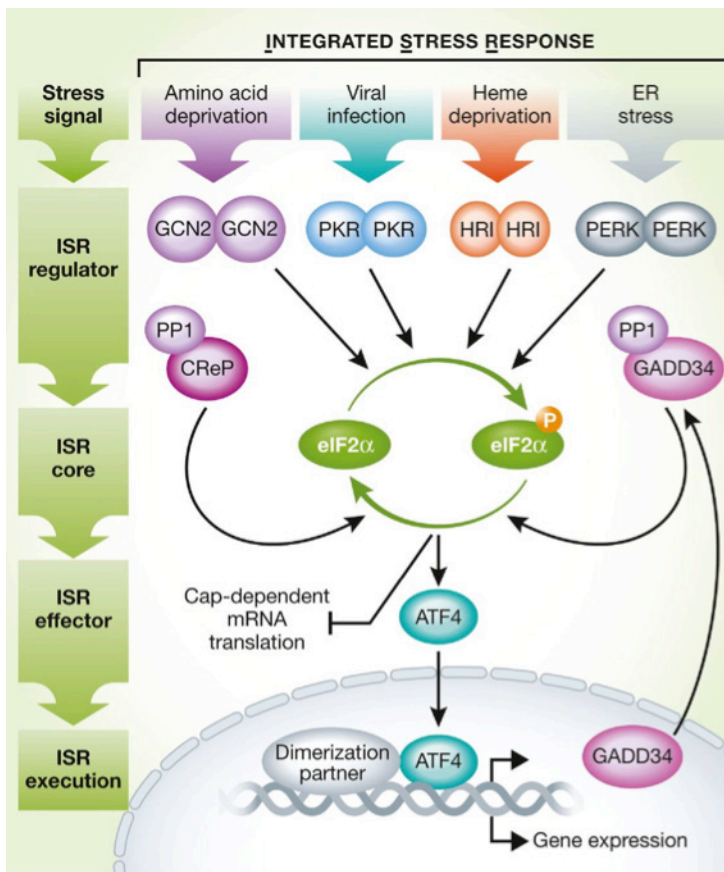


**Figure 1: schematic representation of the integrated stress response.** Image reused with permission from Pakos-Zebrucka et al. [207]. Copyright © EMBO reports.

translation when expressed in healthy iPSC-derived neurons, in *Drosophila* and in a poly-GR mouse model[199, 220, 280]. Cytoplasmic poly-GR co-localized with ribosomal subunits and translation initiation factor eIF3n in poly-GR<sub>100</sub> mice and C9FTD/ALS patients brain[199]. Poly-GR and –PR could therefore inhibit translation in multiple ways; directly by binding ribosomal proteins and translation initiation factors or indirectly by ISR pathway activation.

Next to poly-PR, we found that poly-GR mainly mediates its cellular toxicity in zebrafish embryo's via oxidative stress of mitochondria (chapter 2). Other papers indicate that poly-GR mainly affects the ER and translation[174, 199, 220]. These findings might seem contradictory, but many connections exist between ER and mitochondrial stress. For example, the membrane of the ER and mitochondria are interconnected, thus dysregulation of one cell organelle can lead to disruptions of the other cell organelle[225]. Oxidative stress can worsen ER stress by reducing the efficiency of the protein folding pathways and thereby increasing the amount of misfolded proteins[208]. The accumulation of misfolded proteins in the ER causes ER stress and consequently activation of the ISR and the unfolded protein response (UPR)[207]. A nice example of combined ER and mitochondrial dysfunction has been found in C9FTD/ALS iPSC-derived motor neurons; decreased cell survival correlated with dysfunction in Ca<sup>2+</sup> homeostasis, increased ER stress, and reduced mitochondrial membrane potential[201]. This indicates that poly-GR might exert its toxic effect via both mitochondrial and ER stress.

Finally, poly-GR cytoplasmic inclusions co-localized with various stress markers in a mouse model expressing AAV-149x G<sub>4</sub>C<sub>2</sub>[195]. As formation of stress granules is a downstream effect of activation of the ISR, poly-GR may cause translational inhibition and chronic stress granule formation via activation of this pathway. Thus, both poly-GR and –PR might activate the ISR via multiple ways, which suggests an important role of this pathway in the pathogenesis of C9FTD/ALS.

### 3.2 Overlap between RNA and DPR gain-of-function mechanisms

Synergy and overlap between RNA and DPR gain-of-function mechanisms has been observed and can help to identify important affected molecular pathways. For example, the overexpression of poly-PR in combination with expanded G<sub>4</sub>C<sub>2</sub> repeat RNA in primary rat cortical neurons synergized cellular toxicity, suggesting a convergence of mechanisms[171]. Also, injections of a pure 70x G<sub>4</sub>C<sub>2</sub> repeat construct, producing RNA and DPRs, was more toxic than RNA-only injections in

zebrafish, indicating a synergistic effect on cellular toxicity[154]. Both expanded  $G_4C_2$  repeat RNA and poly-GR and –PR can bind many RNA-binding proteins, nucleolar proteins, hnRNPs and spliceosome components and thereby disrupt normal splicing[169, 174]. Furthermore, translation initiation factors such as hnRNP-A1 and Pur-alpha co-localized with RNA foci[61, 151] and poly-GR co-localized with hnRNP-A1 in post-mortem brain sections of C9ALS patients[174]. These results indicate that both expanded  $G_4C_2$  repeat RNA and poly-GR and –PR can synergize their cellular toxicity, and probably convergence on aberrant splicing and translation, as many interacting proteins function in these pathways.

NCT defects could also be mediated by expanded  $G_4C_2$  repeat RNA and DPRs simultaneously. Both  $G_4C_2$  repeat RNA and DPRs seem to affect Ran-GAP, an important nucleocytoplasmic transport factor.  $G_4C_2$  repeat RNA binds Ran-GAP[107] and RNA foci co-localized with Ran-GAP in C9ALS iPSC-derived neurons[155]. Furthermore, Ran-GAP was sequestered by poly-GA in a AAV-50x poly-GA mouse model[213]. Splicing of Ran-GAP was found to be altered in cultured human astrocyte cells that were exposed to a synthetic  $PR_{20}$  peptide[169] and NCT factors are modifiers of poly-PR toxicity in *Drosophila*[178]. Next to Ran-GAP, other NCT factors such as importins, NUPs and the laminin B receptor could bind to poly-GR and –PR[176, 186, 187]. Poly-PR can also directly bind to the nuclear pore and reduce trafficking through the pore[187].

In animal models for *C9ORF72* gain-of-function, profound NCT defects have been found. Overexpression of pure  $G_4C_2$  repeats (thus investigating both RNA and DPR toxicity) in *Drosophila* models caused NCT defects[155, 177]. And in an AAV-149x pure  $G_4C_2$  mouse model, aberrant invaginations of the nuclear membrane of neurons has been reported using immunostaining with Ran-GAP[195]. Together, this implies that both RNA and DPR gain-of-function mechanisms can evoke NCT defects and highlight NCT as central pathological mechanism in *C9ORF72* pathogenesis.

### 3.3 Hypothetical model of *C9ORF72* pathogenesis

Here we propose a hypothetical model of the underlying pathogenesis of *C9ORF72*-linked neurodegeneration (see figure 2) in which we include insights from our own studies combined with literature.

The starting point in *C9ORF72* pathogenesis is the expression of RNA containing an expanded  $G_4C_2$  repeat, causing the formation of RNA foci and production of DPRs. Expression of  $G_4C_2$  RNA-only is not always sufficient to cause cellular toxicity but can synergize with DPR toxicity (as discussed above) and



might be disease modifying[154, 171, 195]. RNA toxicity probably disturbs the normal function of splicing factors, NCT transport factors and translation initiation factors, as these factors can be bound by RNA molecules containing an expanded  $G_4C_2$  repeat[61, 149, 152, 155]. Reduced expression of C9ORF72 protein in neurons disturbed normal autophagy and may cause additional accumulation of DPRs[126, 275], classifying loss-of-function as disease modifier.

Soluble arginine-containing DPRs, poly-GR and poly-PR, probably cause the first and immediate effect on cellular processes. They are able to bind heterochromatin, mitochondrial proteins, ribosomal proteins, nucleolar proteins, RNA-binding proteins and proteins containing low-complexity domains (LCDs) [169, 174, 176, 181, 186, 200]. LCD proteins can form membrane-less organelles such as nucleoli, the nuclear pore and stress granules. Poly-GR and -PR have been shown to alter phase transition and the dynamics and assembly of these organelles, leading to heterochromatin changes, nucleolar stress and ER stress[176, 181, 200]. In our zebrafish model, we showed that poly-GR increased ROS levels and poly-PR exerted its toxicity via the ISR. Probably, this causes a feedback loop in the pathological process. Activation of the ISR has been shown to increase RAN translation and DPR formation[82, 83, 226, 285]. More DPRs are produced in the cell and start to further disturb the processes described above.

Poly-GA has been shown to sequester proteasome subunits[75, 175] and HR23B into cytoplasmic inclusions[213, 229], which could lead to reduced functionality of the UPS, UPR and ERAD, the latter shown in our chapter 4. Disturbance of these processes may cause the next feedback loop in the pathological process: insufficient clearing of DPRs leads to even faster accumulation of DPRs and other protein inclusions in the cell. Poly-GA inclusions sequester poly-GR and -PR, which subsequently start to sequester ribosomal proteins and stress granule factors[74, 195, 196, 199].

The aggregation of poly-GR and -PR completes their 3-fold effect on translation: first, they disrupt splicing and nucleolar functioning, which causes reduced ribosomal RNA maturation and reduces the pool of ribosomes[169, 174]. Secondly, they activate the ISR and impair the disassembly of stress granules, which inhibits normal translation (this thesis and [210, 226]). Thirdly, they bind and sequester ribosomal proteins[199, 220]. These combined actions make the block on translation complete. Together with the effects of poly-GA on the UPS, UPR and ERAD[75, 175, 213], normal cellular functioning is probably at serious risk.

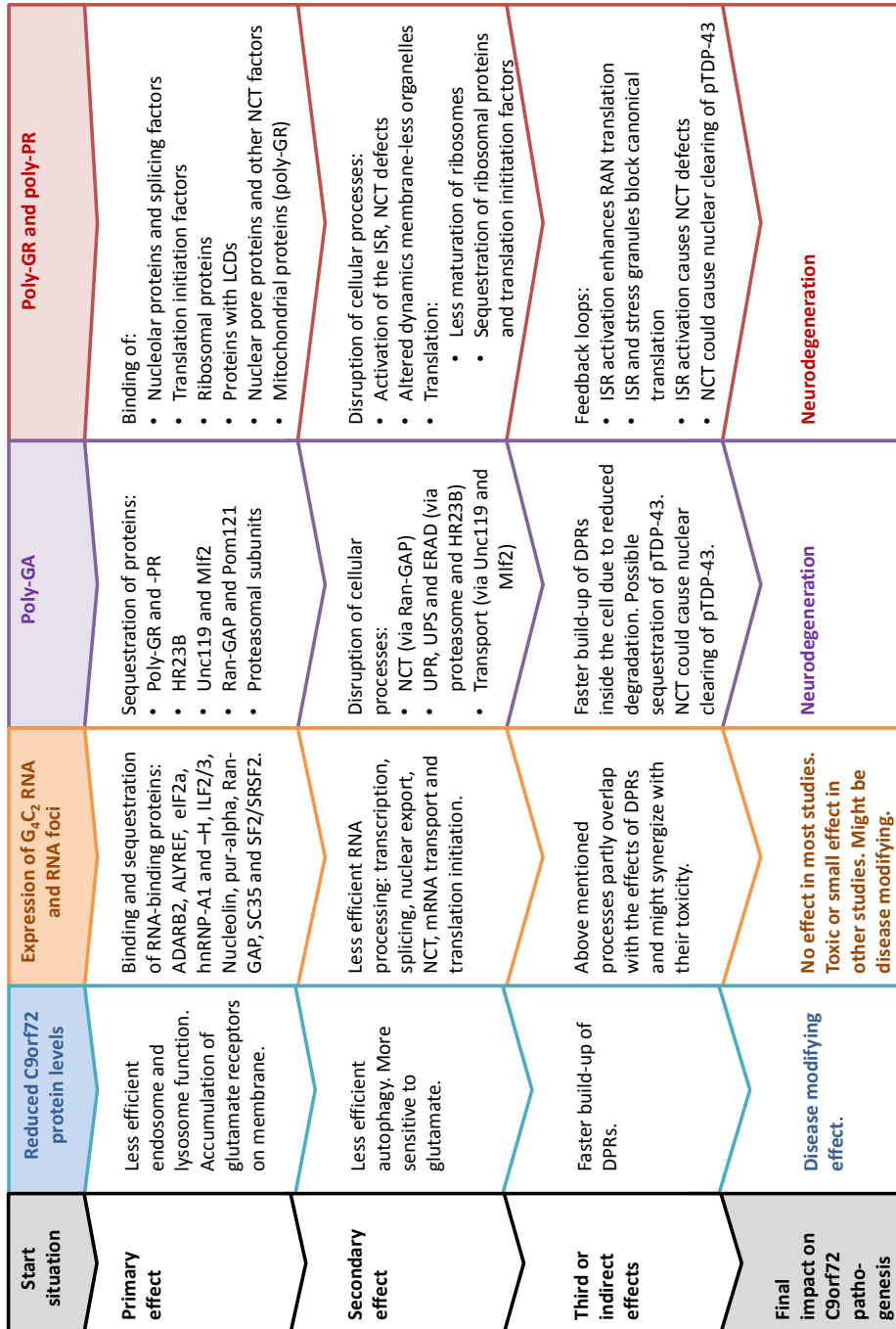


**Figure 2: Overview of impact and important steps in the pathogenesis of C9FTD/ALS.** Indicated for loss-of-function, RNA gain-of-function and poly-GA, -GR and -PR DPR gain-of-function mechanisms. NCT = nucleocytoplasmic transport, ISR = integrated stress response.

Furthermore NCT defects arise, due to direct binding of poly-PR to the nuclear pore[187], binding of NUPs and importins by poly-GR and -PR[176, 187] and sequestration of NCT factors by poly-GA[213]. Overexpression of poly-PR in a recent mouse model also evoked nuclear lamina invaginations[200]. Prolonged ISR activation and stress granule formation can also cause NCT defects[188]. Altogether, this could lead to the final step in *C9ORF72* pathogenesis process: NCT defects can evoke the mis-localization of pTDP-43 from the nucleus to the cytoplasm. In addition, poly-GR might be able to sequester pTDP-43 in inclusions, as co-localization has been demonstrated in an AAV-149xG<sub>4</sub>C<sub>2</sub> mouse model[195] and in human post-mortem brain tissue from C9ALS patients[72]. Cytoplasmic aggregation of pTDP-43 is a known late event[51, 59, 77] and nuclear clearing of pTDP-43 has a major impact on normal cellular functioning[283, 286]. This might be the last straw that breaks the camel's back.

## 4. Therapies

### 4.1 Determining treatment windows

In chapter 3 of this thesis, we started to investigate potential treatment windows of C9FTD/ALS in our transgenic mouse model. Since this is an inducible mouse model, we can turn expression of 36xG<sub>4</sub>C<sub>2</sub> repeat RNA on and off, at different time intervals. We showed that two weeks of expression followed by two weeks of wash-out (expression turned off) is not sufficient to prevent mice from developing muscle degeneration. RNA or DPR cellular toxicity that is initiated in the first two weeks apparently lasts long enough to evoke a phenotype at 4 weeks of age. Indeed, we found poly-GA and -GP still present in muscles after 2 weeks of wash out, indicating that DPRs are long-lasting. Recently, Westergard et al showed that the half-lives of most DPRs is estimated to be >200 hours[226]. These data suggest that long treatment is essential to reduce DPR levels.

In order to further estimate the correct time for targeted treatment, information about DPR levels and neurodegeneration in C9FTD/ALS patients is highly needed, especially at the pre-clinical stage. Most treatments that are currently being developed (and discussed below) focus on G<sub>4</sub>C<sub>2</sub> RNA and DPR expression and are not targeting downstream effects. These therapies will therefore be most useful in preventing pre-symptomatic *C9ORF72* repeat carriers from developing FTD and ALS symptoms. It is unknown if future therapies will also be able to stop disease progression in the symptomatic phase. The development of reliable biomarkers assessing pre-clinical changes in behavior, (motor-) neurodegeneration or rise of DPR levels will therefore be essential. In chapter

5 of this thesis, we show that poly-GR levels in CSF and PBMCs of C9FTD/ALS cases and pre-symptomatic carriers is extremely low, if not absent. So far, only poly-GP could be detected in CSF and PBMCs of C9FTD/ALS cases and pre-symptomatic carriers[197]. Poly-GP levels remain constant over time but do not correlate with disease progression or diagnosis[197]. Poly-GP levels in CSF can be used for determining pharmacodynamics of treatments that target the expression of DPRs[197]. Interestingly, neurofilament light levels in CSF did associate with gray matter atrophy, disease severity and shorter survival of C9FTD/ALS patients[262]. A combination of these two fluid biomarkers could be used in clinical trials. Tracing DPR accumulation in the brains of C9FTD/ALS patients using tracers and PET scanning might also be an interesting approach if liquid biomarkers are unable to provide information about increasing DPR levels. This technology has been used for Alzheimer's Disease; Pittsburgh compound B sensitively detects amyloid-B deposits *in vivo*[287]. Other imaging techniques assessing gray matter atrophy and hypometabolism are validated biomarkers that show (pre-clinical) changes at a group level, but longitudinal research is needed before they can be used at the individual level[271]. Thus, more research is needed to develop sensitive and specific biomarkers that detect pre-clinical changes in C9FTD/ALS patients and to correctly implement potential therapies.

#### 4.2 AON therapy

Antisense oligonucleotides (AONs) are small oligonucleotides that can bind RNA and recruit RNase-H to degrade the target mRNA. AONs can also block (RAN) translation without degradation of the target RNA. AON therapy is currently developed for ALS, Duchenne muscular dystrophy, spinal muscular atrophy, myotonic dystrophy, Alzheimer's disease and Huntington's disease[259]. In C9BAC mice expressing 450x G<sub>4</sub>C<sub>2</sub> repeats, a single injection of an AON that specifically targets the G<sub>4</sub>C<sub>2</sub> repeat RNA reduced the amount of RNA foci, DPRs and ameliorated behavioral deficits[136]. This AON was intraventricular injected at 9 months of age, a time point that C9BAC mice already show abundant RNA foci and DPRs in cortex and hippocampus but before the onset of behavioral symptoms[136]. This indicates that early AON treatment can prevent the development of behavioral deficits, despite the presence of RNA foci and DPRs. Furthermore, deficits in nuclear import and Ran-GAP mis-localization were rescued by AON treatment of *Drosophila* expressing 30x G<sub>4</sub>C<sub>2</sub> RNA and iPSC-derived neurons of C9ALS patients[155]. Of note, AONs should be specifically targeted at the transcripts containing an G<sub>4</sub>C<sub>2</sub> repeat without affecting normal C9ORF72 protein levels, as

reduction in those levels may cause immunologic problems[77, 136]. To date, clinical trials using AON therapy targeting the *C9ORF72* repeat expansion are ongoing, also in the Netherlands (<https://www.umcutrecht.nl/nl/Nieuws/Start-experimentele-behandeling-tegen-ziekte-ALS?feed=news>).

#### 4.3 Small molecules targeting repeat RNA and/or RAN translation

Several compounds have been developed that specifically bind the expanded  $G_4C_2$  repeat and block RAN translation. In iPSC-derived neurons from C9FTD/ALS patients, compound 1a interferes with the hairpin structure of the expanded  $G_4C_2$  repeat and significantly reduced RNA foci and expression of DPR proteins[78]. Other compounds can specifically bind the G-quadruplex structure in mRNA containing an expanded  $G_4C_2$  repeat followed by degradation[236, 237]. The compound TMPyP4 can bind the G-quadruplex formed by  $8xG_4C_2$  repeat RNA, and this blocks the interaction of either hnRNPA1 or ASF/SF2 with this normal sized  $G_4C_2$  repeat[237]. Administration of another compound, DB1273, to C9ALS iPSC-derived neurons and *Drosophila* expressing  $36x G_4C_2$  repeat RNA, reduced RNA foci, poly-GP and -GR levels and increased the life-span of the flies[236]. These results seem promising, but it remains unclear whether the compounds actually prevent degradation of RNA foci or just impair the binding of probes that visualize RNA foci and block their detection.

New studies on RAN translation indicate that a number of stressors, including neuronal excitation, can activate RAN translation[226]. All identified stressors convene at the ISR pathway[82, 83, 226]. Activation of the ISR blocks canonical translation while enhancing RAN translation[82, 83, 226]. Compounds that inhibit phosphorylation of eIF2 $\alpha$ , the core initiator of the ISR, are shown to suppress RAN translation[82, 83, 226]. These studies were performed in HeLa cells [83], HEK293T cells[82], NSC34 cells, primary rat cortical neurons and iPSC-derived motor neurons from C9ALS patients[226, 285]. As DPRs induce activation of the ISR (this thesis and [210, 285]), this creates a feed-forward loop in which enhanced RAN translation produces more DPRs that further activate the ISR. Inhibition of the ISR might therefore be a double hit therapy; inhibiting both the downstream effects of DPRs while at the same time the prevention of formation of more DPRs.

#### 4.4 Therapies blocking spreading of DPRs

Interestingly, in C9ALS patients DPR pathology has been described as a distinct clustered pattern[55] and it has been shown that DPRs are able to spread via

cell-to-cell transmission *in vitro*[267]. This can occur via the take-up of exosomes from culture media of cells expressing DPRs, or via direct cell-to-cell contact between neurons[267]. Especially arginine-rich DPRs can penetrate the membrane of HEK293T and NSC34 cells[268]. Also extracellular (GFP-tagged) poly-GA inclusions can be taken up by HEK239T cells and primary neurons and act as seeds to enhance cellular aggregation of (Flag-tagged) poly-GA[247, 269]. Exposure to recombinant poly-GA or cerebellar extracts of C9FTD patients increased  $G_4C_2$  repeat RNA levels and seeded aggregation of all DPRs in HEK293T cells expressing 80x $G_4C_2$ [269]. Treatment with anti-poly-GA antibodies inhibited the seeding effect of C9FTD brain extracts and reduced poly-GA aggregation[269]. These results highlight the possibility of antibody therapy to reduce spreading and seeding of DPRs in C9FTD/ALS.

### Conclusion

In conclusion, research described in this thesis shows that ubiquitous overexpression of 36x $G_4C_2$  repeat RNA results in production of sense DPRs and evokes a locomotor phenotype in an inducible transgenic mouse model. Furthermore, overexpression of poly-GR and -PR in zebrafish embryo's is sufficient to cause cellular toxicity and cell death. Our data therefore supports a gain-of-function hypothesis as the underlying molecular mechanism for C9FTD/ALS. C9ORF72 protein haploinsufficiency has been categorized as disease modifier in recent publications. Synergy between loss- and gain-of-function mechanism can easily be studied by crossing our mouse or zebrafish model with C9KO mouse or zebrafish. The functional consequences of RNA molecules containing expanded  $G_4C_2$  repeats and RNA foci, that bind and sequester several RNA-binding proteins, is unclear and needs further investigation. Important downstream pathways underlying cellular toxicity probably converge at the ISR and NCT defects. Reduced function and saturation of the UPR, UPS, ERAD and autophagy systems probably adds to the accumulation of toxic proteins in the cell. Furthermore, activation of the ISR stimulates RAN translation, causing a possible feedback loop. Potential therapeutic interventions for C9FTD/ALS include AONs or small compounds that degrade or block translation of mRNA containing an expanded  $G_4C_2$  repeat. Pre-clinically, AON therapy shows promising results and is currently being assessed in clinical trials. However, for the correct implementation of efficient therapeutic interventions, more information is needed about the best treatment window. First insights from mouse models suggests that early and long treatment is essential to prevent RNA and DPR cellular toxicity and the development of be-

havioral symptoms. Finally, the development of reliable biomarkers assessing the precise time to start treatment and treatment response is essential for the successful implementation of new therapies. We hope that in the future, *C9ORF72* repeat expansion carriers can be (pre-clinically) treated to prevent the onset of disease or halt disease progression of FTD and ALS.





# Appendix

References

List of abbreviations

Summary & Samenvatting

CV, List of publications & PhD Portfolio

Dankwoord



## References

1. Woollacott, I.O. and J.D. Rohrer, The clinical spectrum of sporadic and familial forms of frontotemporal dementia. *J Neurochem*, 2016. 138 Suppl 1: p. 6-31.
2. Hernandez, I., et al., Frontotemporal Lobar Degeneration (FTLD): Review and Update for Clinical Neurologists. *Curr Alzheimer Res*, 2018. 15(6): p. 511-530.
3. Gorno-Tempini, M.L., et al., Classification of primary progressive aphasia and its variants. *Neurology*, 2011. 76(11): p. 1006-14.
4. Rascovsky, K., et al., Sensitivity of revised diagnostic criteria for the behavioural variant of frontotemporal dementia. *Brain*, 2011. 134(Pt 9): p. 2456-77.
5. Harvey, R.J., M. Skelton-Robinson, and M.N. Rossor, The prevalence and causes of dementia in people under the age of 65 years. *J Neurol Neurosurg Psychiatry*, 2003. 74(9): p. 1206-9.
6. Onyike, C.U. and J. Diehl-Schmid, The epidemiology of frontotemporal dementia. *Int Rev Psychiatry*, 2013. 25(2): p. 130-7.
7. Zarei, S., et al., A comprehensive review of amyotrophic lateral sclerosis. *Surg Neurol Int*, 2015. 6: p. 171.
8. Grad, L.I., et al., Clinical Spectrum of Amyotrophic Lateral Sclerosis (ALS). *Cold Spring Harb Perspect Med*, 2017. 7(8).
9. Oskarsson, B., T.F. Gendron, and N.P. Staff, Amyotrophic Lateral Sclerosis: An Update for 2018. *Mayo Clin Proc*, 2018. 93(11): p. 1617-1628.
10. Miller, R.G., J.D. Mitchell, and D.H. Moore, Riluzole for amyotrophic lateral sclerosis (ALS)/motor neuron disease (MND). *Cochrane Database Syst Rev*, 2012. 3: p. CD001447.
11. Ikeda, K. and Y. Iwasaki, Edaravone, a Free Radical Scavenger, Delayed Symptomatic and Pathological Progression of Motor Neuron Disease in the Wobbler Mouse. *PLoS One*, 2015. 10(10): p. e0140316.
12. Burrell, J.R., et al., The frontotemporal dementia-motor neuron disease continuum. *Lancet*, 2016. 388(10047): p. 919-31.
13. Strong, M.J., et al., Amyotrophic lateral sclerosis - frontotemporal spectrum disorder (ALS-FTSD): Revised diagnostic criteria. *Amyotroph Lateral Scler Frontotemporal Degener*, 2017. 18(3-4): p. 153-174.
14. Beeldman, E., et al., The cognitive profile of behavioural variant FTD and its similarities with ALS: a systematic review and meta-analysis. *J Neurol Neurosurg Psychiatry*, 2018. 89(9): p. 995-1002.
15. Cruts, M., et al., Current insights into the C9orf72 repeat expansion diseases of the FTLD/ALS spectrum. *Trends Neurosci*, 2013. 36(8): p. 450-9.
16. Van Langenhove, T., J. van der Zee, and C. Van Broeckhoven, The molecular basis of the frontotemporal lobar degeneration-amyotrophic lateral sclerosis spectrum. *Ann Med*, 2012. 44(8): p. 817-28.
17. Bennion Callister, J. and S.M. Pickering-Brown, Pathogenesis/genetics of frontotemporal dementia and how it relates to ALS. *Exp Neurol*, 2014. 262 Pt B: p. 84-90.
18. Guerreiro, R., J. Bras, and J. Hardy, Snapshot: Genetics of ALS and FTD. *Cell*, 2015. 160(4): p. 798 e1.
19. Gros-Louis, F., C. Gaspar, and G.A. Rouleau, Genetics of familial and sporadic amyotrophic lateral sclerosis. *Biochim Biophys Acta*, 2006. 1762(11-12): p. 956-72.
20. Ng, A.S., R. Rademakers, and B.L. Miller, Frontotemporal dementia: a bridge between dementia and neuromuscular disease. *Ann N Y Acad Sci*, 2015. 1338: p. 71-93.
21. van Blitterswijk, M., et al., TMEM106B protects C9ORF72 expansion carriers against frontotemporal dementia. *Acta Neuropathol*, 2014. 127(3): p. 397-406.
22. DeJesus-Hernandez, M., et al., Expanded GGGGCC hexanucleotide repeat in noncoding region of C9ORF72 causes chromosome 9p-linked FTD and ALS. *Neuron*, 2011. 72(2): p. 245-56.
23. Renton, A.E., et al., A hexanucleotide repeat expansion in C9ORF72 is the cause of chromosome 9p21-linked ALS-FTD. *Neuron*, 2011. 72(2): p. 257-68.
24. van Blitterswijk, M., M. DeJesus-Hernandez, and R. Rademakers, How do C9ORF72 repeat expansions cause amyotrophic lateral sclerosis and frontotemporal dementia: can we learn from other noncoding repeat expansion disorders? *Curr Opin Neurol*, 2012. 25(6): p. 689-700.
25. Majounie, E., et al., Frequency of the C9orf72 hexanucleotide repeat expansion in patients with amyotrophic lateral sclerosis and frontotemporal dementia: a cross-sectional study. *Lancet Neurol*, 2012. 11(4): p. 323-30.
26. Rutherford, N.J., et al., Length of normal alleles of C9ORF72 GGGGCC repeat do not influence disease phenotype. *Neurobiol Aging*, 2012. 33(12): p. 2950 e5-7.

27. Gijssels, I., et al., A C9orf72 promoter repeat expansion in a Flanders-Belgian cohort with disorders of the frontotemporal lobar degeneration-amyotrophic lateral sclerosis spectrum: a gene identification study. *Lancet Neurol*, 2012. 11(1): p. 54-65.
28. van der Zee, J., et al., A pan-European study of the C9orf72 repeat associated with FTL: geographic prevalence, genomic instability, and intermediate repeats. *Hum Mutat*, 2013. 34(2): p. 363-73.
29. Smith, B.N., et al., The C9ORF72 expansion mutation is a common cause of ALS+/-FTD in Europe and has a single founder. *Eur J Hum Genet*, 2013. 21(1): p. 102-8.
30. Ratti, A., et al., C9ORF72 repeat expansion in a large Italian ALS cohort: evidence of a founder effect. *Neurobiol Aging*, 2012. 33(10): p. 2528 e7-14.
31. Chiang, H.H., et al., No common founder for C9orf72 expansion mutation in Sweden. *J Hum Genet*, 2017. 62(2): p. 321-324.
32. Goldstein, O., et al., High frequency of C9orf72 hexanucleotide repeat expansion in amyotrophic lateral sclerosis patients from two founder populations sharing the same risk haplotype. *Neurobiol Aging*, 2018. 64: p. 160 e1-160 e7.
33. Cooper-Knock, J., P.J. Shaw, and J. Kirby, The widening spectrum of C9ORF72-related disease; genotype/phenotype correlations and potential modifiers of clinical phenotype. *Acta Neuropathol*, 2014. 127(3): p. 333-45.
34. Rohrer, J.D., et al., C9orf72 expansions in frontotemporal dementia and amyotrophic lateral sclerosis. *Lancet Neurol*, 2015. 14(3): p. 291-301.
35. Boeve, B.F. and N.R. Graff-Radford, Cognitive and behavioral features of c9FTD/ALS. *Alzheimers Res Ther*, 2012. 4(4): p. 29.
36. Simon-Sanchez, J., et al., The clinical and pathological phenotype of C9ORF72 hexanucleotide repeat expansions. *Brain*, 2012. 135(Pt 3): p. 723-35.
37. Stewart, H., et al., Clinical and pathological features of amyotrophic lateral sclerosis caused by mutation in the C9ORF72 gene on chromosome 9p. *Acta Neuropathol*, 2012. 123(3): p. 409-17.
38. Lall, D. and R.H. Baloh, Microglia and C9orf72 in neuroinflammation and ALS and frontotemporal dementia. *J Clin Invest*, 2017. 127(9): p. 3250-3258.
39. Van Mossevelde, S., et al., Relationship between C9orf72 repeat size and clinical phenotype. *Curr Opin Genet Dev*, 2017. 44: p. 117-124.
40. Beck, J., et al., Large C9orf72 hexanucleotide repeat expansions are seen in multiple neurodegenerative syndromes and are more frequent than expected in the UK population. *Am J Hum Genet*, 2013. 92(3): p. 345-53.
41. Murphy, N.A., et al., Age-related penetrance of the C9orf72 repeat expansion. *Sci Rep*, 2017. 7(1): p. 2116.
42. Fournier, C., et al., Relations between C9orf72 expansion size in blood, age at onset, age at collection and transmission across generations in patients and presymptomatic carriers. *Neurobiol Aging*, 2018.
43. van Blitterswijk, M., et al., Association between repeat sizes and clinical and pathological characteristics in carriers of C9ORF72 repeat expansions (Xpansize-72): a cross-sectional cohort study. *Lancet Neurol*, 2013. 12(10): p. 978-88.
44. Gijssels, I., et al., The C9orf72 repeat size correlates with onset age of disease, DNA methylation and transcriptional downregulation of the promoter. *Mol Psychiatry*, 2015.
45. Dols-Icardo, O., et al., Characterization of the repeat expansion size in C9orf72 in amyotrophic lateral sclerosis and frontotemporal dementia. *Hum Mol Genet*, 2014. 23(3): p. 749-54.
46. Nordin, A., et al., Extensive size variability of the GGGGCC expansion in C9orf72 in both neuronal and non-neuronal tissues in 18 patients with ALS or FTD. *Hum Mol Genet*, 2015. 24(11): p. 3133-42.
47. Gomez-Tortosa, E., et al., C9ORF72 hexanucleotide expansions of 20-22 repeats are associated with frontotemporal deterioration. *Neurology*, 2013. 80(4): p. 366-70.
48. Millecamps, S., et al., Phenotype difference between ALS patients with expanded repeats in C9ORF72 and patients with mutations in other ALS-related genes. *J Med Genet*, 2012. 49(4): p. 258-63.
49. Ng, A.S.L. and E.K. Tan, Intermediate C9orf72 alleles in neurological disorders: does size really matter? *J Med Genet*, 2017. 54(9): p. 591-597.
50. Van Mossevelde, S., et al., Clinical Evidence of Disease Anticipation in Families Segregating a C9orf72 Repeat Expansion. *JAMA Neurol*, 2017. 74(4): p. 445-452.
51. Vatsavayai, S.C., et al., C9orf72-FTD/ALS pathogenesis: evidence from human neuropathological studies.



## Appendix

Acta Neuropathol, 2018.

52. Mori, K., et al., Bidirectional transcripts of the expanded C9orf72 hexanucleotide repeat are translated into aggregating dipeptide repeat proteins. *Acta Neuropathol*, 2013. 126(6): p. 881-93.
53. van Blitterswijk, M., et al., Novel clinical associations with specific C9ORF72 transcripts in patients with repeat expansions in C9ORF72. *Acta Neuropathol*, 2015. 130(6): p. 863-76.
54. Niblock, M., et al., Retention of hexanucleotide repeat-containing intron in C9orf72 mRNA: implications for the pathogenesis of ALS/FTD. *Acta Neuropathol Commun*, 2016. 4(1): p. 18.
55. Zu, T., et al., RAN proteins and RNA foci from antisense transcripts in C9ORF72 ALS and frontotemporal dementia. *Proc Natl Acad Sci U S A*, 2013. 110(51): p. E4968-77.
56. Mizielinska, S., et al., C9orf72 frontotemporal lobar degeneration is characterised by frequent neuronal sense and antisense RNA foci. *Acta Neuropathol*, 2013. 126(6): p. 845-57.
57. Gendron, T.F., et al., Antisense transcripts of the expanded C9ORF72 hexanucleotide repeat form nuclear RNA foci and undergo repeat-associated non-ATG translation in c9FTD/ALS. *Acta Neuropathol*, 2013. 126(6): p. 829-44.
58. DeJesus-Hernandez, M., et al., In-depth clinico-pathological examination of RNA foci in a large cohort of C9ORF72 expansion carriers. *Acta Neuropathol*, 2017. 134(2): p. 255-269.
59. Vatsavayai, S.C., et al., Timing and significance of pathological features in C9orf72 expansion-associated frontotemporal dementia. *Brain*, 2016. 139(Pt 12): p. 3202-3216.
60. Cooper-Knock, J., et al., Antisense RNA foci in the motor neurons of C9ORF72-ALS patients are associated with TDP-43 proteinopathy. *Acta Neuropathol*, 2015. 130(1): p. 63-75.
61. Cooper-Knock, J., et al., Sequestration of multiple RNA recognition motif-containing proteins by C9orf72 repeat expansions. *Brain*, 2014. 137(Pt 7): p. 2040-51.
62. Haeusler, A.R., C.J. Donnelly, and J.D. Rothstein, The expanding biology of the C9orf72 nucleotide repeat expansion in neurodegenerative disease. *Nat Rev Neurosci*, 2016. 17(6): p. 383-95.
63. Lagier-Tourenne, C., et al., Targeted degradation of sense and antisense C9orf72 RNA foci as therapy for ALS and frontotemporal degeneration. *Proc Natl Acad Sci U S A*, 2013. 110(47): p. E4530-9.
64. Zu, T., et al., Non-ATG-initiated translation directed by microsatellite expansions. *Proc Natl Acad Sci U S A*, 2011. 108(1): p. 260-5.
65. Cleary, J.D., A. Pattamatta, and L.P.W. Ranum, Repeat-associated non-ATG (RAN) translation. *J Biol Chem*, 2018. 293(42): p. 16127-16141.
66. Mori, K., et al., The C9orf72 GGGGCC repeat is translated into aggregating dipeptide-repeat proteins in FTL/D/ALS. *Science*, 2013. 339(6125): p. 1335-8.
67. Ash, P.E., et al., Unconventional translation of C9ORF72 GGGGCC expansion generates insoluble polypeptides specific to c9FTD/ALS. *Neuron*, 2013. 77(4): p. 639-46.
68. Sellier, C., et al., Translation of Expanded CGG Repeats into FMRpolyG Is Pathogenic and May Contribute to Fragile X Tremor Ataxia Syndrome. *Neuron*, 2017. 93(2): p. 331-347.
69. Mackenzie, I.R., et al., Quantitative analysis and clinico-pathological correlations of different dipeptide repeat protein pathologies in C9ORF72 mutation carriers. *Acta Neuropathol*, 2015. 130(6): p. 845-61.
70. Schludi, M.H., et al., Distribution of dipeptide repeat proteins in cellular models and C9orf72 mutation cases suggests link to transcriptional silencing. *Acta Neuropathol*, 2015. 130(4): p. 537-55.
71. Gomez-Deza, J., et al., Dipeptide repeat protein inclusions are rare in the spinal cord and almost absent from motor neurons in C9ORF72 mutant amyotrophic lateral sclerosis and are unlikely to cause their degeneration. *Acta Neuropathol Commun*, 2015. 3(1): p. 38.
72. Saberi, S., et al., Sense-encoded poly-GR dipeptide repeat proteins correlate to neurodegeneration and uniquely co-localize with TDP-43 in dendrites of repeat-expanded C9orf72 amyotrophic lateral sclerosis. *Acta Neuropathol*, 2018. 135(3): p. 459-474.
73. Sakae, N., et al., Poly-GR dipeptide repeat polymers correlate with neurodegeneration and Clinicopathological subtypes in C9ORF72-related brain disease. *Acta Neuropathol Commun*, 2018. 6(1): p. 63.
74. Yang, D., et al., FTD/ALS-associated poly(GR) protein impairs the Notch pathway and is recruited by poly(GA) into cytoplasmic inclusions. *Acta Neuropathol*, 2015. 130(4): p. 525-35.
75. Zhang, Y.J., et al., Aggregation-prone c9FTD/ALS poly(GA) RAN-translated proteins cause neurotoxicity by inducing ER stress. *Acta Neuropathol*, 2014. 128(4): p. 505-24.
76. Gendron, T.F., et al., Cerebellar c9RAN proteins associate with clinical and neuropathological characteristics

- of C9ORF72 repeat expansion carriers. *Acta Neuropathol*, 2015. 130(4): p. 559-73.
77. Balendra, R. and A.M. Isaacs, C9orf72-mediated ALS and FTD: multiple pathways to disease. *Nat Rev Neurol*, 2018. 14(9): p. 544-558.
  78. Su, Z., et al., Discovery of a biomarker and lead small molecules to target r(GGGGCC)-associated defects in c9FTD/ALS. *Neuron*, 2014. 83(5): p. 1043-50.
  79. Green, K.M., A.E. Linsalata, and P.K. Todd, RAN translation-What makes it run? *Brain Res*, 2016. 1647: p. 30-42.
  80. Gao, F.B., J.D. Richter, and D.W. Cleveland, Rethinking Unconventional Translation in Neurodegeneration. *Cell*, 2017. 171(5): p. 994-1000.
  81. Tabet, R., et al., CUG initiation and frameshifting enable production of dipeptide repeat proteins from ALS/FTD C9ORF72 transcripts. *Nat Commun*, 2018. 9(1): p. 152.
  82. Green, K.M., et al., RAN translation at C9orf72-associated repeat expansions is selectively enhanced by the integrated stress response. *Nat Commun*, 2017. 8(1): p. 2005.
  83. Cheng, W., et al., C9ORF72 GGGGCC repeat-associated non-AUG translation is upregulated by stress through eIF2alpha phosphorylation. *Nat Commun*, 2018. 9(1): p. 51.
  84. Bigio, E.H., et al., Frontotemporal lobar degeneration with TDP-43 proteinopathy and chromosome 9p repeat expansion in C9ORF72: clinicopathologic correlation. *Neuropathology*, 2013. 33(2): p. 122-33.
  85. Lashley, T., et al., Review: An update on clinical, genetic and pathological aspects of frontotemporal lobar degenerations. *Neuropathol Appl Neurobiol*, 2015. 41(7): p. 858-81.
  86. Saberi, S., et al., Neuropathology of Amyotrophic Lateral Sclerosis and Its Variants. *Neurol Clin*, 2015. 33(4): p. 855-76.
  87. Davidson, Y., et al., Neurodegeneration in Frontotemporal Lobar Degeneration and Motor Neurone Disease associated with expansions in C9orf72 is linked to TDP-43 pathology and not associated with aggregated forms of dipeptide repeat proteins. *Neuropathol Appl Neurobiol*, 2015.
  88. Neumann, M., et al., TDP-43-positive white matter pathology in frontotemporal lobar degeneration with ubiquitin-positive inclusions. *J Neuropathol Exp Neurol*, 2007. 66(3): p. 177-83.
  89. Davidson, Y., et al., Ubiquitinated pathological lesions in frontotemporal lobar degeneration contain the TAR DNA-binding protein, TDP-43. *Acta Neuropathol*, 2007. 113(5): p. 521-33.
  90. Sieben, A., et al., The genetics and neuropathology of frontotemporal lobar degeneration. *Acta Neuropathol*, 2012. 124(3): p. 353-72.
  91. Murray, M.E., et al., Clinical and neuropathologic heterogeneity of c9FTD/ALS associated with hexanucleotide repeat expansion in C9ORF72. *Acta Neuropathol*, 2011. 122(6): p. 673-90.
  92. Brettschneider, J., et al., Stages of pTDP-43 pathology in amyotrophic lateral sclerosis. *Ann Neurol*, 2013. 74(1): p. 20-38.
  93. Kraemer, B.C., et al., Loss of murine TDP-43 disrupts motor function and plays an essential role in embryogenesis. *Acta Neuropathol*, 2010. 119(4): p. 409-19.
  94. Yang, C., et al., Partial loss of TDP-43 function causes phenotypes of amyotrophic lateral sclerosis. *Proc Natl Acad Sci U S A*, 2014. 111(12): p. E1121-9.
  95. Seibenhener, M.L., T. Geetha, and M.W. Wooten, Sequestosome 1/p62--more than just a scaffold. *FEBS Lett*, 2007. 581(2): p. 175-9.
  96. Heyburn, L. and C.E. Moussa, TDP-43 in the spectrum of MND-FTLD pathologies. *Mol Cell Neurosci*, 2017. 83: p. 46-54.
  97. Rizzu, P., et al., C9orf72 is differentially expressed in the central nervous system and myeloid cells and consistently reduced in C9orf72, MAPT and GRN mutation carriers. *Acta Neuropathol Commun*, 2016. 4(1): p. 37.
  98. Gendron, T.F. and L. Petrucelli, Disease Mechanisms of C9ORF72 Repeat Expansions. *Cold Spring Harb Perspect Med*, 2018. 8(4).
  99. Xi, Z., et al., Hypermethylation of the CpG island near the G4C2 repeat in ALS with a C9orf72 expansion. *Am J Hum Genet*, 2013. 92(6): p. 981-9.
  100. Xi, Z., et al., The C9orf72 repeat expansion itself is methylated in ALS and FTLD patients. *Acta Neuropathol*, 2015. 129(5): p. 715-27.
  101. Belzil, V.V., et al., Reduced C9orf72 gene expression in c9FTD/ALS is caused by histone trimethylation, an epigenetic event detectable in blood. *Acta Neuropathol*, 2013. 126(6): p. 895-905.



## Appendix

102. Zeier, Z., et al., Bromodomain inhibitors regulate the C9ORF72 locus in ALS. *Exp Neurol*, 2015. 271: p. 241-50.
103. Chen, X., et al., Evidence for peripheral immune activation in amyotrophic lateral sclerosis. *J Neurol Sci*, 2014. 347(1-2): p. 90-5.
104. Liu, E.Y., et al., C9orf72 hypermethylation protects against repeat expansion-associated pathology in ALS/FTD. *Acta Neuropathol*, 2014. 128(4): p. 525-41.
105. McMillan, C.T., et al., C9orf72 promoter hypermethylation is neuroprotective: Neuroimaging and neuropathologic evidence. *Neurology*, 2015. 84(16): p. 1622-30.
106. Russ, J., et al., Hypermethylation of repeat expanded C9orf72 is a clinical and molecular disease modifier. *Acta Neuropathol*, 2015. 129(1): p. 39-52.
107. Donnelly, C.J., et al., RNA toxicity from the ALS/FTD C9ORF72 expansion is mitigated by antisense intervention. *Neuron*, 2013. 80(2): p. 415-28.
108. Frick, P., et al., Novel antibodies reveal presynaptic localization of C9orf72 protein and reduced protein levels in C9orf72 mutation carriers. *Acta Neuropathol Commun*, 2018. 6(1): p. 72.
109. Waite, A.J., et al., Reduced C9orf72 protein levels in frontal cortex of amyotrophic lateral sclerosis and frontotemporal degeneration brain with the C9ORF72 hexanucleotide repeat expansion. *Neurobiol Aging*, 2014. 35(7): p. 1779 e5-1779 e13.
110. Xiao, S., et al., Isoform-specific antibodies reveal distinct subcellular localizations of C9orf72 in amyotrophic lateral sclerosis. *Ann Neurol*, 2015. 78(4): p. 568-83.
111. Suzuki, N., et al., The mouse C9ORF72 ortholog is enriched in neurons known to degenerate in ALS and FTD. *Nat Neurosci*, 2013. 16(12): p. 1725-7.
112. Levine, T.P., et al., The product of C9orf72, a gene strongly implicated in neurodegeneration, is structurally related to DENN Rab-GEFs. *Bioinformatics*, 2013. 29(4): p. 499-503.
113. Zhang, D., et al., Discovery of Novel DENN Proteins: Implications for the Evolution of Eukaryotic Intracellular Membrane Structures and Human Disease. *Front Genet*, 2012. 3: p. 283.
114. Marat, A.L., H. Dokainish, and P.S. McPherson, DENN domain proteins: regulators of Rab GTPases. *J Biol Chem*, 2011. 286(16): p. 13791-800.
115. Hadano, S., et al., Loss of ALS2/Alsin exacerbates motor dysfunction in a SOD1-expressing mouse ALS model by disturbing endolysosomal trafficking. *PLoS One*, 2010. 5(3): p. e9805.
116. Del Villar, K. and C.A. Miller, Down-regulation of DENN/MADD, a TNF receptor binding protein, correlates with neuronal cell death in Alzheimer's disease brain and hippocampal neurons. *Proc Natl Acad Sci U S A*, 2004. 101(12): p. 4210-5.
117. Webster, C.P., et al., The C9orf72 protein interacts with Rab1a and the ULK1 complex to regulate initiation of autophagy. *EMBO J*, 2016. 35(15): p. 1656-76.
118. Sellier, C., et al., Loss of C9ORF72 impairs autophagy and synergizes with polyQ Ataxin-2 to induce motor neuron dysfunction and cell death. *EMBO J*, 2016. 35(12): p. 1276-97.
119. Sullivan, P.M., et al., The ALS/FTLD associated protein C9orf72 associates with SMCR8 and WDR41 to regulate the autophagy-lysosome pathway. *Acta Neuropathol Commun*, 2016. 4(1): p. 51.
120. Yang, M., et al., A C9ORF72/SMCR8-containing complex regulates ULK1 and plays a dual role in autophagy. *Sci Adv*, 2016. 2(9): p. e1601167.
121. Farg, M.A., et al., C9ORF72, implicated in amyotrophic lateral sclerosis and frontotemporal dementia, regulates endosomal trafficking. *Hum Mol Genet*, 2014. 23(13): p. 3579-95.
122. Freischmidt, A., et al., Haploinsufficiency of TBK1 causes familial ALS and fronto-temporal dementia. *Nat Neurosci*, 2015. 18(5): p. 631-6.
123. Almeida, S., et al., Modeling key pathological features of frontotemporal dementia with C9ORF72 repeat expansion in iPSC-derived human neurons. *Acta Neuropathol*, 2013. 126(3): p. 385-99.
124. Aoki, Y., et al., C9orf72 and RAB7L1 regulate vesicle trafficking in amyotrophic lateral sclerosis and frontotemporal dementia. *Brain*, 2017. 140(4): p. 887-897.
125. Imamura, K., et al., The Src/c-Abl pathway is a potential therapeutic target in amyotrophic lateral sclerosis. *Sci Transl Med*, 2017. 9(391).
126. Shi, Y., et al., Haploinsufficiency leads to neurodegeneration in C9ORF72 ALS/FTD human induced motor neurons. *Nat Med*, 2018. 24(3): p. 313-325.
127. Selvaraj, B.T., et al., C9ORF72 repeat expansion causes vulnerability of motor neurons to Ca(2+)-permeable

- AMPA receptor-mediated excitotoxicity. *Nat Commun*, 2018. 9(1): p. 347.
128. Therrien, M., et al., Deletion of C9ORF72 results in motor neuron degeneration and stress sensitivity in *C. elegans*. *PLoS One*, 2013. 8(12): p. e83450.
  129. Vaccaro, A., et al., Mutant TDP-43 and FUS cause age-dependent paralysis and neurodegeneration in *C. elegans*. *PLoS One*, 2012. 7(2): p. e31321.
  130. Ciura, S., et al., Loss of function of C9orf72 causes motor deficits in a zebrafish model of amyotrophic lateral sclerosis. *Ann Neurol*, 2013. 74(2): p. 180-7.
  131. Kabashi, E., et al., Zebrafish models for the functional genomics of neurogenetic disorders. *Biochim Biophys Acta*, 2011. 1812(3): p. 335-45.
  132. Van Hoecke, A., et al., EPHA4 is a disease modifier of amyotrophic lateral sclerosis in animal models and in humans. *Nat Med*, 2012. 18(9): p. 1418-22.
  133. O'Rourke, J.G., et al., C9orf72 is required for proper macrophage and microglial function in mice. *Science*, 2016. 351(6279): p. 1324-9.
  134. Miller, Z.A., et al., Increased prevalence of autoimmune disease within C9 and FTD/MND cohorts: Completing the picture. *Neurol Neuroimmunol Neuroinflamm*, 2017. 4(1): p. e301.
  135. Turner, M.R., et al., Autoimmune disease preceding amyotrophic lateral sclerosis: an epidemiologic study. *Neurology*, 2013. 81(14): p. 1222-5.
  136. Jiang, J., et al., Gain of Toxicity from ALS/FTD-Linked Repeat Expansions in C9ORF72 Is Alleviated by Antisense Oligonucleotides Targeting GGGGCC-Containing RNAs. *Neuron*, 2016. 90(3): p. 535-50.
  137. Atanasio, A., et al., C9orf72 ablation causes immune dysregulation characterized by leukocyte expansion, autoantibody production, and glomerulonephropathy in mice. *Sci Rep*, 2016. 6: p. 23204.
  138. Klein, A.F., et al., Therapeutic Approaches for Dominant Muscle Diseases: Highlight on Myotonic Dystrophy. *Curr Gene Ther*, 2015. 15(4): p. 329-37.
  139. Haeusler, A.R., et al., C9orf72 nucleotide repeat structures initiate molecular cascades of disease. *Nature*, 2014. 507(7491): p. 195-200.
  140. Fratta, P., et al., C9orf72 hexanucleotide repeat associated with amyotrophic lateral sclerosis and frontotemporal dementia forms RNA G-quadruplexes. *Sci Rep*, 2012. 2: p. 1016.
  141. Zhou, B., et al., Characterizations of distinct parallel and antiparallel G-quadruplexes formed by two-repeat ALS and FTD related GGGGCC sequence. *Sci Rep*, 2018. 8(1): p. 2366.
  142. Vatovec, S., A. Kovanda, and B. Rogelj, Unconventional features of C9ORF72 expanded repeat in amyotrophic lateral sclerosis and frontotemporal lobar degeneration. *Neurobiol Aging*, 2014. 35(10): p. 2421 e1-2421 e12.
  143. Reddy, K., et al., The disease-associated r(GGGGCC)<sub>n</sub> repeat from the C9orf72 gene forms tract length-dependent uni- and multimolecular RNA G-quadruplex structures. *J Biol Chem*, 2013. 288(14): p. 9860-6.
  144. Subramanian, M., et al., G-quadruplex RNA structure as a signal for neurite mRNA targeting. *EMBO Rep*, 2011. 12(7): p. 697-704.
  145. Walker, C., et al., C9orf72 expansion disrupts ATM-mediated chromosomal break repair. *Nat Neurosci*, 2017. 20(9): p. 1225-1235.
  146. Kovanda, A., et al., Anti-sense DNA d(GGCCCC)<sub>n</sub> expansions in C9ORF72 form i-motifs and protonated hairpins. *Sci Rep*, 2015. 5: p. 17944.
  147. Zamiri, B., et al., Stress-induced acidification may contribute to formation of unusual structures in C9orf72-repeats. *Biochim Biophys Acta*, 2018.
  148. Hautbergue, G.M., et al., SRSF1-dependent nuclear export inhibition of C9ORF72 repeat transcripts prevents neurodegeneration and associated motor deficits. *Nat Commun*, 2017. 8: p. 16063.
  149. Rossi, S., et al., Nuclear accumulation of mRNAs underlies G4C2-repeat-induced translational repression in a cellular model of C9orf72 ALS. *J Cell Sci*, 2015. 128(9): p. 1787-99.
  150. Mori, K., et al., hnRNP A3 binds to GGGGCC repeats and is a constituent of p62-positive/TDP43-negative inclusions in the hippocampus of patients with C9orf72 mutations. *Acta Neuropathol*, 2013. 125(3): p. 413-23.
  151. Sareen, D., et al., Targeting RNA foci in iPSC-derived motor neurons from ALS patients with a C9ORF72 repeat expansion. *Sci Transl Med*, 2013. 5(208): p. 208ra149.
  152. Lee, Y.B., et al., Hexanucleotide repeats in ALS/FTD form length-dependent RNA foci, sequester RNA binding proteins, and are neurotoxic. *Cell Rep*, 2013. 5(5): p. 1178-86.
  153. Xu, Z., et al., Expanded GGGGCC repeat RNA associated with amyotrophic lateral sclerosis and frontotemporal dementia causes neurodegeneration. *Proc Natl Acad Sci U S A*, 2013. 110(19): p. 7778-83.



## Appendix

154. Swinnen, B., et al., A zebrafish model for C9orf72 ALS reveals RNA toxicity as a pathogenic mechanism. *Acta Neuropathol*, 2018. 135(3): p. 427-443.
155. Zhang, K., et al., The C9orf72 repeat expansion disrupts nucleocytoplasmic transport. *Nature*, 2015. 525(7567): p. 56-61.
156. Hideyama, T., et al., Profound downregulation of the RNA editing enzyme ADAR2 in ALS spinal motor neurons. *Neurobiol Dis*, 2012. 45(3): p. 1121-8.
157. Shi, M., et al., ALYREF mainly binds to the 5' and the 3' regions of the mRNA in vivo. *Nucleic Acids Res*, 2017. 45(16): p. 9640-9653.
158. Prudencio, M., et al., Distinct brain transcriptome profiles in C9orf72-associated and sporadic ALS. *Nat Neurosci*, 2015. 18(8): p. 1175-82.
159. Romano, M., et al., Evolutionarily conserved heterogeneous nuclear ribonucleoprotein (hnRNP) A/B proteins functionally interact with human and Drosophila TAR DNA-binding protein 43 (TDP-43). *J Biol Chem*, 2014. 289(10): p. 7121-30.
160. Kim, H.J., et al., Mutations in prion-like domains in hnRNPA2B1 and hnRNPA1 cause multisystem proteinopathy and ALS. *Nature*, 2013. 495(7442): p. 467-73.
161. White, M.K., E.M. Johnson, and K. Khalili, Multiple roles for Puralpha in cellular and viral regulation. *Cell Cycle*, 2009. 8(3): p. 1-7.
162. O'Rourke, J.G., et al., C9orf72 BAC Transgenic Mice Display Typical Pathologic Features of ALS/FTD. *Neuron*, 2015. 88(5): p. 892-901.
163. Mizielinska, S., et al., Bidirectional nucleolar dysfunction in C9orf72 frontotemporal lobar degeneration. *Acta Neuropathol Commun*, 2017. 5(1): p. 29.
164. Aladesuyi Arogundade, O., et al., Antisense RNA foci are associated with nucleoli and TDP-43 mislocalization in C9orf72-ALS/FTD: a quantitative study. *Acta Neuropathol*, 2019.
165. Cesnik, A.B., et al., Nuclear RNA foci from C9ORF72 expansion mutation form paraspeckle-like bodies. *J Cell Sci*, 2019.
166. Nishimoto, Y., et al., The long non-coding RNA nuclear-enriched abundant transcript 1\_2 induces paraspeckle formation in the motor neuron during the early phase of amyotrophic lateral sclerosis. *Mol Brain*, 2013. 6: p. 31.
167. Cooper-Knock, J., et al., C9ORF72 GGGGCC Expanded Repeats Produce Splicing Dysregulation which Correlates with Disease Severity in Amyotrophic Lateral Sclerosis. *PLoS One*, 2015. 10(5): p. e0127376.
168. Mizielinska, S., et al., C9orf72 repeat expansions cause neurodegeneration in Drosophila through arginine-rich proteins. *Science*, 2014. 345(6201): p. 1192-4.
169. Kwon, I., et al., Poly-dipeptides encoded by the C9orf72 repeats bind nucleoli, impede RNA biogenesis, and kill cells. *Science*, 2014. 345(6201): p. 1139-45.
170. Flores, B.N., et al., Distinct C9orf72-Associated Dipeptide Repeat Structures Correlate with Neuronal Toxicity. *PLoS One*, 2016. 11(10): p. e0165084.
171. Wen, X., et al., Antisense proline-arginine RAN dipeptides linked to C9ORF72-ALS/FTD form toxic nuclear aggregates that initiate in vitro and in vivo neuronal death. *Neuron*, 2014. 84(6): p. 1213-25.
172. Yamakawa, M., et al., Characterization of the dipeptide repeat protein in the molecular pathogenesis of c9FTD/ALS. *Hum Mol Genet*, 2015. 24(6): p. 1630-45.
173. Tao, Z., et al., Nucleolar stress and impaired stress granule formation contribute to C9orf72 RAN translation-induced cytotoxicity. *Hum Mol Genet*, 2015. 24(9): p. 2426-41.
174. Kanekura, K., et al., Poly-dipeptides encoded by the C9ORF72 repeats block global protein translation. *Hum Mol Genet*, 2016. 25(9): p. 1803-13.
175. May, S., et al., C9orf72 FTL/ALS-associated Gly-Ala dipeptide repeat proteins cause neuronal toxicity and Unc119 sequestration. *Acta Neuropathol*, 2014. 128(4): p. 485-503.
176. Lee, K.H., et al., C9orf72 Dipeptide Repeats Impair the Assembly, Dynamics, and Function of Membrane-Less Organelles. *Cell*, 2016. 167(3): p. 774-788 e17.
177. Freibaum, B.D., et al., GGGGCC repeat expansion in C9orf72 compromises nucleocytoplasmic transport. *Nature*, 2015. 525(7567): p. 129-33.
178. Boeynaems, S., et al., Drosophila screen connects nuclear transport genes to DPR pathology in c9ALS/FTD. *Sci Rep*, 2016. 6: p. 20877.
179. Swaminathan, A., et al., Expression of C9orf72-related dipeptides impairs motor function in a vertebrate model. *Hum Mol Genet*, 2018.



180. Ohki, Y., et al., Glycine-alanine dipeptide repeat protein contributes to toxicity in a zebrafish model of C9orf72 associated neurodegeneration. *Mol Neurodegener*, 2017. 12(1): p. 6.
181. Lin, Y., et al., Toxic PR Poly-Dipeptides Encoded by the C9orf72 Repeat Expansion Target LC Domain Polymers. *Cell*, 2016. 167(3): p. 789-802 e12.
182. Lagier-Tourenne, C., M. Polymenidou, and D.W. Cleveland, TDP-43 and FUS/TLS: emerging roles in RNA processing and neurodegeneration. *Hum Mol Genet*, 2010. 19(R1): p. R46-64.
183. Boeynaems, S., et al., Phase Separation of C9orf72 Dipeptide Repeats Perturbs Stress Granule Dynamics. *Mol Cell*, 2017. 65(6): p. 1044-1055 e5.
184. Yin, S., et al., Evidence that C9ORF72 Dipeptide Repeat Proteins Associate with U2 snRNP to Cause Missplicing in ALS/FTD Patients. *Cell Rep*, 2017. 19(11): p. 2244-2256.
185. Bennion Callister, J., et al., Modelling C9orf72 dipeptide repeat proteins of a physiologically relevant size. *Hum Mol Genet*, 2016. 25(23): p. 5069-5082.
186. Lopez-Gonzalez, R., et al., Poly(GR) in C9ORF72-Related ALS/FTD Compromises Mitochondrial Function and Increases Oxidative Stress and DNA Damage in iPSC-Derived Motor Neurons. *Neuron*, 2016. 92(2): p. 383-391.
187. Shi, K.Y., et al., Toxic PRn poly-dipeptides encoded by the C9orf72 repeat expansion block nuclear import and export. *Proc Natl Acad Sci U S A*, 2017. 114(7): p. E1111-E1117.
188. Zhang, K., et al., Stress Granule Assembly Disrupts Nucleocytoplasmic Transport. *Cell*, 2018. 173(4): p. 958-971 e17.
189. Jovicic, A., et al., Modifiers of C9orf72 dipeptide repeat toxicity connect nucleocytoplasmic transport defects to FTD/ALS. *Nat Neurosci*, 2015. 18(9): p. 1226-9.
190. Farg, M.A., et al., The DNA damage response (DDR) is induced by the C9orf72 repeat expansion in amyotrophic lateral sclerosis. *Hum Mol Genet*, 2017. 26(15): p. 2882-2896.
191. Chew, J., et al., Neurodegeneration. C9ORF72 repeat expansions in mice cause TDP-43 pathology, neuronal loss, and behavioral deficits. *Science*, 2015. 348(6239): p. 1151-4.
192. Peters, O.M., et al., Human C9ORF72 Hexanucleotide Expansion Reproduces RNA Foci and Dipeptide Repeat Proteins but Not Neurodegeneration in BAC Transgenic Mice. *Neuron*, 2015. 88(5): p. 902-9.
193. Liu, Y., et al., C9orf72 BAC Mouse Model with Motor Deficits and Neurodegenerative Features of ALS/FTD. *Neuron*, 2016. 90(3): p. 521-34.
194. Herranz-Martin, S., et al., Viral delivery of C9orf72 hexanucleotide repeat expansions in mice leads to repeat-length-dependent neuropathology and behavioural deficits. *Dis Model Mech*, 2017. 10(7): p. 859-868.
195. Chew, J., et al., Aberrant deposition of stress granule-resident proteins linked to C9orf72-associated TDP-43 proteinopathy. *Mol Neurodegener*, 2019. 14(1): p. 9.
196. Darling, A.L., et al., Repeated repeat problems: Combinatorial effect of C9orf72-derived dipeptide repeat proteins. *Int J Biol Macromol*, 2019.
197. Gendron, T.F., et al., Poly(GP) proteins are a useful pharmacodynamic marker for C9ORF72-associated amyotrophic lateral sclerosis. *Sci Transl Med*, 2017. 9(383).
198. Mackenzie, I.R., et al., Dipeptide repeat protein pathology in C9ORF72 mutation cases: clinico-pathological correlations. *Acta Neuropathol*, 2013. 126(6): p. 859-79.
199. Zhang, Y.J., et al., Poly(GR) impairs protein translation and stress granule dynamics in C9orf72-associated frontotemporal dementia and amyotrophic lateral sclerosis. *Nat Med*, 2018.
200. Zhang, Y.J., et al., Heterochromatin anomalies and double-stranded RNA accumulation underlie C9orf72 poly(PR) toxicity. *Science*, 2019. 363(6428).
201. Dafinca, R., et al., C9orf72 Hexanucleotide Expansions Are Associated with Altered Endoplasmic Reticulum Calcium Homeostasis and Stress Granule Formation in Induced Pluripotent Stem Cell-Derived Neurons from Patients with Amyotrophic Lateral Sclerosis and Frontotemporal Dementia. *Stem Cells*, 2016. 34(8): p. 2063-78.
202. Van Houcke, J., et al., The zebrafish as a gerontology model in nervous system aging, disease, and repair. *Ageing Res Rev*, 2015. 24(Pt B): p. 358-68.
203. Wiley, D.S., S.E. Redfield, and L.I. Zon, Chemical screening in zebrafish for novel biological and therapeutic discovery. *Methods Cell Biol*, 2017. 138: p. 651-679.
204. van Ham, T.J., et al., Live imaging of apoptotic cells in zebrafish. *Faseb J*, 2010. 24(11): p. 4336-42.
205. Santoriello, C. and L.I. Zon, Hooked! Modeling human disease in zebrafish. *J Clin Invest*, 2012. 122(7): p.



## Appendix

- 2337-43.
206. Bhat, A.H., et al., Oxidative stress, mitochondrial dysfunction and neurodegenerative diseases; a mechanistic insight. *Biomed Pharmacother*, 2015. 74: p. 101-10.
  207. Pakos-Zebrucka, K., et al., The integrated stress response. *EMBO Rep*, 2016. 17(10): p. 1374-1395.
  208. Chong, W.C., M.D. Shastri, and R. Eri, Endoplasmic Reticulum Stress and Oxidative Stress: A Vicious Nexus Implicated in Bowel Disease Pathophysiology. *Int J Mol Sci*, 2017. 18(4).
  209. Zeeshan, H.M., et al., Endoplasmic Reticulum Stress and Associated ROS. *Int J Mol Sci*, 2016. 17(3): p. 327.
  210. Kramer, N.J., et al., CRISPR-Cas9 screens in human cells and primary neurons identify modifiers of C9ORF72 dipeptide-repeat-protein toxicity. *Nat Genet*, 2018. 50(4): p. 603-612.
  211. Tabas, I. and D. Ron, Integrating the mechanisms of apoptosis induced by endoplasmic reticulum stress. *Nat Cell Biol*, 2011. 13(3): p. 184-90.
  212. Tran, H., et al., Differential Toxicity of Nuclear RNA Foci versus Dipeptide Repeat Proteins in a Drosophila Model of C9ORF72 FTD/ALS. *Neuron*, 2015. 87(6): p. 1207-14.
  213. Zhang, Y.J., et al., C9ORF72 poly(GA) aggregates sequester and impair HR23 and nucleocytoplasmic transport proteins. *Nat Neurosci*, 2016. 19(5): p. 668-77.
  214. Yuan, J. and B.A. Yankner, Apoptosis in the nervous system. *Nature*, 2000. 407(6805): p. 802-9.
  215. Yoshiyama, Y., et al., Apoptosis related antigen, Le(Y) and nick-end labeling are positive in spinal motor neurons in amyotrophic lateral sclerosis. *Acta Neuropathol*, 1994. 88(3): p. 207-11.
  216. Pedersen, W.A., et al., The prostate apoptosis response-4 protein participates in motor neuron degeneration in amyotrophic lateral sclerosis. *Faseb J*, 2000. 14(7): p. 913-24.
  217. Su, J.H., et al., DNA damage and activated caspase-3 expression in neurons and astrocytes: evidence for apoptosis in frontotemporal dementia. *Exp Neurol*, 2000. 163(1): p. 9-19.
  218. Laird, A.S., et al., Progranulin is neurotrophic in vivo and protects against a mutant TDP-43 induced axonopathy. *PLoS One*, 2010. 5(10): p. e13368.
  219. Sakowski, S.A., et al., Neuromuscular effects of G93A-SOD1 expression in zebrafish. *Mol Neurodegener*, 2012. 7: p. 44.
  220. Moens, T.G., et al., C9orf72 arginine-rich dipeptide proteins interact with ribosomal proteins in vivo to induce a toxic translational arrest that is rescued by eIF1A. *Acta Neuropathol*, 2019.
  221. Atkin, J.D., et al., Endoplasmic reticulum stress and induction of the unfolded protein response in human sporadic amyotrophic lateral sclerosis. *Neurobiol Dis*, 2008. 30(3): p. 400-7.
  222. Ilieva, E.V., et al., Oxidative and endoplasmic reticulum stress interplay in sporadic amyotrophic lateral sclerosis. *Brain*, 2007. 130(Pt 12): p. 3111-23.
  223. Ito, Y., et al., Involvement of CHOP, an ER-stress apoptotic mediator, in both human sporadic ALS and ALS model mice. *Neurobiol Dis*, 2009. 36(3): p. 470-6.
  224. Matus, S., et al., ER Dysfunction and Protein Folding Stress in ALS. *Int J Cell Biol*, 2013. 2013: p. 674751.
  225. Lau, D.H.W., et al., Disruption of ER-mitochondria signalling in fronto-temporal dementia and related amyotrophic lateral sclerosis. *Cell Death Dis*, 2018. 9(3): p. 327.
  226. Westergard, T., et al., Repeat-associated non-AUG translation in C9orf72-ALS/FTD is driven by neuronal excitation and stress. *EMBO Mol Med*, 2019.
  227. Couratier, P., et al., ALS and frontotemporal dementia belong to a common disease spectrum. *Rev Neurol (Paris)*, 2017. 173(5): p. 273-279.
  228. Batra, R. and C.W. Lee, Mouse Models of C9orf72 Hexanucleotide Repeat Expansion in Amyotrophic Lateral Sclerosis/ Frontotemporal Dementia. *Front Cell Neurosci*, 2017. 11: p. 196.
  229. Schludi, M.H., et al., Spinal poly-GA inclusions in a C9orf72 mouse model trigger motor deficits and inflammation without neuron loss. *Acta Neuropathol*, 2017. 134(2): p. 241-254.
  230. Hukema, R.K., et al., Induced expression of expanded CGG RNA causes mitochondrial dysfunction in vivo. *Cell Cycle*, 2014. 13(16): p. 2600-8.
  231. Katsantoni, E.Z., et al., Ubiquitous expression of the rTA2S-M2 inducible system in transgenic mice driven by the human hnRNPA2B1/CBX3 CpG island. *BMC Dev Biol*, 2007. 7: p. 108.
  232. Vinueza Veloz, M.F., et al., The effect of an mGluR5 inhibitor on procedural memory and avoidance discrimination impairments in Fmr1 KO mice. *Genes Brain Behav*, 2012. 11(3): p. 325-31.
  233. Vogler, T.O., et al., TDP-43 and RNA form amyloid-like myo-granules in regenerating muscle. *Nature*, 2018. 563(7732): p. 508-513.

234. Baborie, A., et al., Accumulation of dipeptide repeat proteins predates that of TDP-43 in frontotemporal lobar degeneration associated with hexanucleotide repeat expansions in C9ORF72 gene. *Neuropathol Appl Neurobiol*, 2015. 41(5): p. 601-12.
235. Proudfoot, M., et al., Early dipeptide repeat pathology in a frontotemporal dementia kindred with C9ORF72 mutation and intellectual disability. *Acta Neuropathol*, 2014. 127(3): p. 451-8.
236. Simone, R., et al., G-quadruplex-binding small molecules ameliorate C9orf72 FTD/ALS pathology in vitro and in vivo. *EMBO Mol Med*, 2018. 10(1): p. 22-31.
237. Zamiri, B., et al., TMPyP4 porphyrin distorts RNA G-quadruplex structures of the disease-associated r(GGGGCC)<sub>n</sub> repeat of the C9orf72 gene and blocks interaction of RNA-binding proteins. *J Biol Chem*, 2014. 289(8): p. 4653-9.
238. Kramer, N.J., et al., Spt4 selectively regulates the expression of C9orf72 sense and antisense mutant transcripts. *Science*, 2016. 353(6300): p. 708-12.
239. Hu, J., et al., Recognition of c9orf72 Mutant RNA by Single-Stranded Silencing RNAs. *Nucleic Acid Ther*, 2017. 27(2): p. 87-94.
240. Wen, X., et al., Pathogenic determinants and mechanisms of ALS/FTD linked to hexanucleotide repeat expansions in the C9orf72 gene. *Neurosci Lett*, 2017. 636: p. 16-26.
241. Gao, F.B., S. Almeida, and R. Lopez-Gonzalez, Dysregulated molecular pathways in amyotrophic lateral sclerosis-frontotemporal dementia spectrum disorder. *EMBO J*, 2017. 36(20): p. 2931-2950.
242. Yokoi, M. and F. Hanaoka, Two mammalian homologs of yeast Rad23, HR23A and HR23B, as multifunctional proteins. *Gene*, 2017. 597: p. 1-9.
243. Ng, J.M., et al., A novel regulation mechanism of DNA repair by damage-induced and RAD23-dependent stabilization of xeroderma pigmentosum group C protein. *Genes Dev*, 2003. 17(13): p. 1630-45.
244. Marteijn, J.A., et al., Understanding nucleotide excision repair and its roles in cancer and ageing. *Nat Rev Mol Cell Biol*, 2014. 15(7): p. 465-81.
245. Wang, G., et al., Ataxin-3, the MJD1 gene product, interacts with the two human homologs of yeast DNA repair protein RAD23, HHR23A and HHR23B. *Hum Mol Genet*, 2000. 9(12): p. 1795-803.
246. Bergink, S., et al., The DNA repair-ubiquitin-associated HR23 proteins are constituents of neuronal inclusions in specific neurodegenerative disorders without hampering DNA repair. *Neurobiol Dis*, 2006. 23(3): p. 708-16.
247. Chang, Y.J., et al., The Glycine-Alanine Dipeptide Repeat from C9orf72 Hexanucleotide Expansions Forms Toxic Amyloids Possessing Cell-to-Cell Transmission Properties. *J Biol Chem*, 2016. 291(10): p. 4903-11.
248. Jablonski, A.M., et al., Loss of RAD-23 Protects Against Models of Motor Neuron Disease by Enhancing Mutant Protein Clearance. *J Neurosci*, 2015. 35(42): p. 14286-306.
249. Doss-Pepe, E.W., et al., Ataxin-3 interactions with rad23 and valosin-containing protein and its associations with ubiquitin chains and the proteasome are consistent with a role in ubiquitin-mediated proteolysis. *Mol Cell Biol*, 2003. 23(18): p. 6469-83.
250. Schmidt, T., et al., Protein surveillance machinery in brains with spinocerebellar ataxia type 3: redistribution and differential recruitment of 26S proteasome subunits and chaperones to neuronal intranuclear inclusions. *Ann Neurol*, 2002. 51(3): p. 302-10.
251. Lee, J.H., et al., Structure of a peptide:N-glycanase-Rad23 complex: insight into the deglycosylation for denatured glycoproteins. *Proc Natl Acad Sci U S A*, 2005. 102(26): p. 9144-9.
252. Gotzl, J.K., et al., Impaired protein degradation in FTLD and related disorders. *Ageing Res Rev*, 2016. 32: p. 122-139.
253. Caglayan, A.O., et al., NGLY1 mutation causes neuromotor impairment, intellectual disability, and neuropathy. *Eur J Med Genet*, 2015. 58(1): p. 39-43.
254. Abbasi, R., et al., Laryngeal cancer risk associated with smoking and alcohol consumption is modified by genetic polymorphisms in ERCC5, ERCC6 and RAD23B but not by polymorphisms in five other nucleotide excision repair genes. *Int J Cancer*, 2009. 125(6): p. 1431-9.
255. Tabuas-Pereira, M., et al., Increased risk of melanoma in C9ORF72 repeat expansion carriers: A case-control study. *Muscle Nerve*, 2018.
256. Freedman, D.M., et al., The association between cancer and amyotrophic lateral sclerosis. *Cancer Causes Control*, 2013. 24(1): p. 55-60.
257. Chen, L. and K. Madura, Evidence for distinct functions for human DNA repair factors hHR23A and hHR23B. *FEBS Lett*, 2006. 580(14): p. 3401-8.



## Appendix

258. Burguete, A.S., et al., GGGGCC microsatellite RNA is neuritically localized, induces branching defects, and perturbs transport granule function. *Elife*, 2015. 4: p. e08881.
259. Wurster, C.D. and A.C. Ludolph, Antisense oligonucleotides in neurological disorders. *Ther Adv Neurol Disord*, 2018. 11: p. 1756286418776932.
260. Meeter, L.H., et al., Neurofilament light chain: a biomarker for genetic frontotemporal dementia. *Ann Clin Transl Neurol*, 2016. 3(8): p. 623-36.
261. Scherling, C.S., et al., Cerebrospinal fluid neurofilament concentration reflects disease severity in frontotemporal degeneration. *Ann Neurol*, 2014. 75(1): p. 116-26.
262. Meeter, L.H.H., et al., Poly(GP), neurofilament and grey matter deficits in C9orf72 expansion carriers. *Ann Clin Transl Neurol*, 2018. 5(5): p. 583-597.
263. Lehmer, C., et al., Poly-GP in cerebrospinal fluid links C9orf72-associated dipeptide repeat expression to the asymptomatic phase of ALS/FTD. *EMBO Mol Med*, 2017. 9(7): p. 859-868.
264. Freibaum, B.D. and J.P. Taylor, The Role of Dipeptide Repeats in C9ORF72-Related ALS-FTD. *Front Mol Neurosci*, 2017. 10: p. 35.
265. Huisman, M.H., et al., Population based epidemiology of amyotrophic lateral sclerosis using capture-recapture methodology. *J Neurol Neurosurg Psychiatry*, 2011. 82(10): p. 1165-70.
266. de Vrij, F.M., et al., Rescue of behavioral phenotype and neuronal protrusion morphology in Fmr1 KO mice. *Neurobiol Dis*, 2008. 31(1): p. 127-32.
267. Westergard, T., et al., Cell-to-Cell Transmission of Dipeptide Repeat Proteins Linked to C9orf72-ALS/FTD. *Cell Rep*, 2016. 17(3): p. 645-652.
268. Kanekura, K., et al., Characterization of membrane penetration and cytotoxicity of C9orf72-encoding arginine-rich dipeptides. *Sci Rep*, 2018. 8(1): p. 12740.
269. Zhou, Q., et al., Antibodies inhibit transmission and aggregation of C9orf72 poly-GA dipeptide repeat proteins. *EMBO Mol Med*, 2017. 9(5): p. 687-702.
270. Balendra, R., T.G. Moens, and A.M. Isaacs, Specific biomarkers for C9orf72 FTD/ALS could expedite the journey towards effective therapies. *EMBO Mol Med*, 2017. 9(7): p. 853-855.
271. Meeter, L.H., et al., Imaging and fluid biomarkers in frontotemporal dementia. *Nat Rev Neurol*, 2017. 13(7): p. 406-419.
272. Moens, T.G., et al., Sense and antisense RNA are not toxic in Drosophila models of C9orf72-associated ALS/FTD. *Acta Neuropathol*, 2018. 135(3): p. 445-457.
273. Mori, K., et al., Reduced hnRNPA3 increases C9orf72 repeat RNA levels and dipeptide-repeat protein deposition. *EMBO Rep*, 2016. 17(9): p. 1314-25.
274. Conlon, E.G., et al., The C9ORF72 GGGGCC expansion forms RNA G-quadruplex inclusions and sequesters hnRNP H to disrupt splicing in ALS brains. *Elife*, 2016. 5.
275. Zhu Q., J.J., Gendron T., McAlonis M., King P., Maldonado M., Taylor A.E., Garcia S., Rodriguez M., Myers B., Dastidar S., Kim J., Heyser C., Spada A., Petrucelli L., Cruz S., Ravits J., Lagier-Tourenne C., Cleveland D., Reduced C9ORF72 function exacerbates gain-of-toxicity from ALS/FTD-causing repeat expansion in C9ORF72, in Neuroscience meeting San Diego. 2018.
276. Xiao, S., et al., C9orf72 isoforms in Amyotrophic Lateral Sclerosis and Frontotemporal Lobar Degeneration. *Brain Res*, 2016. 1647: p. 43-49.
277. Porta, S., et al., Droscha inclusions are new components of dipeptide-repeat protein aggregates in FTLTDP and ALS C9orf72 expansion cases. *J Neuropathol Exp Neurol*, 2015. 74(4): p. 380-7.
278. Solomon, D.A., et al., A feedback loop between dipeptide-repeat protein, TDP-43 and karyopherin-alpha mediates C9orf72-related neurodegeneration. *Brain*, 2018. 141(10): p. 2908-2924.
279. Knobel, K.M., et al., UNC-119 suppresses axon branching in *C. elegans*. *Development*, 2001. 128(20): p. 4079-92.
280. Hartmann, H., et al., Proteomics and C9orf72 neuropathology identify ribosomes as poly-GR/PR interactors driving toxicity. *Life Sci Alliance*, 2018. 1(2): p. e201800070.
281. Nonaka, T., et al., C9ORF72 dipeptide repeat poly-GA inclusions promote: intracellular aggregation of phosphorylated TDP-43. *Hum Mol Genet*, 2018.
282. Davidson, Y.S., et al., Heterogeneous ribonuclear protein A3 (hnRNP A3) is present in dipeptide repeat protein containing inclusions in Frontotemporal Lobar Degeneration and Motor Neurone disease associated with expansions in C9orf72 gene. *Acta Neuropathol Commun*, 2017. 5(1): p. 31.

283. Tsao, W., et al., Rodent models of TDP-43: recent advances. *Brain Res*, 2012. 1462: p. 26-39.
284. Schmid, B., et al., Loss of ALS-associated TDP-43 in zebrafish causes muscle degeneration, vascular dysfunction, and reduced motor neuron axon outgrowth. *Proc Natl Acad Sci U S A*, 2013. 110(13): p. 4986-91.
285. Sonobe, Y., et al., Translation of dipeptide repeat proteins from the C9ORF72 expanded repeat is associated with cellular stress. *Neurobiol Dis*, 2018. 116: p. 155-165.
286. Nana, A.L., et al., Neurons selectively targeted in frontotemporal dementia reveal early stage TDP-43 pathobiology. *Acta Neuropathol*, 2018.
287. Ishii, K., PET approaches for diagnosis of dementia. *AJNR Am J Neuroradiol*, 2014. 35(11): p. 2030-8.



**List of abbreviations**

5-AZA	5-aza-2-deoxycytidine
A-I	Adenosine to inosine
AChRs	Acetylcholine receptors
AD	Alzheimer's Disease
ADARB2	Adenosine Deaminase, RNA Specific B2
ALS	Amyotrophic Lateral Sclerosis
AON	Antisense oligonucleotide
BAC	Bacterial artificial chromosome
bvFTD	Behavioral variant FTD
C9-L	C9ORF72 long protein isoform A
C9-S	C9ORF72 short protein isoform B
C9ALS	C9ORF72-linked ALS
C9BAC	C9ORF72 bacterial artificial chromosome
C9FTD	C9ORF72-linked FTD
C9FTD/ALS	C9ORF72-linked FTD and/or ALS
C9KO	C9ORF72 knock-out
C9ORF72	Chromosome 9 open reading frame 72
CA	Cornu ammonis
CamK2	Ca <sup>2+</sup> /calmodulin-dependent protein kinase II
ChAT	Choline acetyltransferase
CHCHD10	Coiled-coil-helix-coiled-coil-helix domain containing 10
CHMP2B	Multivesicular body protein 2B gene
CNS	Central nervous system
CPD	Cyclobutane pyrimidine dimers
CpG	Cytosine-phosphate-guanine
CSF	Cerebrospinal fluid
DENN	Differentially expressed in normal and neoplastic cells
DG	Dentate gyrus
DM1/2	Myotonic Dystrophy type 1 or 2
DNs	Dystrophic neurites
Dox	Doxycycline
DPRs	Dipeptide repeats
DT	Double transgenic
EDL	Extensor digitorum longus
EdU	5-ethynyl-2-deoxyuridine

ERAD	Endoplasmic reticulum associated degradation
FISH	Fluorescent in situ hybridization
FMRP	Fragile X mental retardation protein
FTD	Frontotemporal Dementia
FUS	Fused in sarcoma
FXTAS	Fragile X-associated tremor/ataxia syndrome
GEFs	Rab-GDP/GTP exchange factors
GG-NER	Global genome nucleotide excision repair
GRN	Progranulin
HD	Huntington's disease
HE	Haematoxyline-eosine
HNRNP	Heterogeneous nuclear ribonucleoprotein
HR23B	Human homologue of yeast UV excision repair protein Rad23b
ICC	Immunocytochemistry
ICV	Intracerebroventricular
IHC	Immunohistochemistry
iPSCs	Induced pluripotent stem cells
LCDs	low-complexity domains
LMN	Lower Motor Neuron
lvPPA	Logopenic variant PPA
MAPT	Microtubule-associated protein tau
MBNL1	Muscleblind-like 1
METC	Medical Ethical Test Committee
MND	Motor Neuron Disease
Morphants	Morpholino-injected zebrafish
NCI	Neuronal cytoplasmic inclusions
NCT	Nucleocytoplasmic transport
NER	Nucleotide excision repair
nvPPA	Nonfluent variant PPA
NII	Neuronal intranuclear inclusions
NMJ	Neuromuscular junction
NPC	Nuclear pore complex
o/n	Overnight
OPTN	Optineurin
P0	Postnatal day 0
P62	Autophagy protein p62/sequestosome 1
PBMCs	Peripheral blood mononuclear cells



Appendix

PBP	Progressive Bulbar Palsy
PBS	Phosphate-buffered saline
PD	Parkinson's Disease
PFA	Paraformaldehyde
PFC	Prefrontal cortex
PiD	Pick's Disease
PLS	Primary Lateral Sclerosis
PMA	Progressive Muscular Atrophy
Poly-GA	Poly-glycine-alanine
Poly-GP	Poly-glycine-proline
Poly-GR	Poly-glycine-arginine
Poly-PA	Poly-proline-alanine
Poly-PG	Poly-proline-glycine
Poly-PR	Poly-proline-arginine
PPA	Primary Progressive Aphasia
pTDP-43	Phosphorylated 43kDa TAR DNA-binding protein
RAN	Repeat-associated non-AUG translation
Ran-GAP	Ras-related nuclear protein GTPase activating protein
RBPs	RNA-binding proteins
rtTA	Reverse tetracycline-controlled trans-activator
SCA8/31/37	Spinocerebellar Ataxia type 8 , 31 or 37
SEM	Standard error of the mean
SIMOA	Single molecule array
snRNP	Small nuclear ribonucleoprotein
SOD1	Superoxide dismutase 1
SQSTM1	Sequestosome-1
ST	Single transgenic
svPPA	Somatic variant PPA
TA	Tibialis anterior muscle
TARDBP	Trans-activation response element DNA-binding protein 43 encoding gene
TBK1	TANK-binding kinase 1
TMEM106B	Transmembrane protein 106B
TRE	Tetracycline response element
UBQLN2	Ubiquilin 2
UDS	Unscheduled DNA Synthesis
UMN	Upper Motor Neuron



UPR	Unfolded-protein response
UPS	Ubiquitin-proteasome system
VCP	Valosin-containing protein
XPC	Xeroderma pigmentosum complementation group C
zC9ORF72	Zebrafish orthologue of C9ORF72



## Summary

Frontotemporal dementia (FTD) and amyotrophic lateral sclerosis (ALS) are two neurological disorders that are part of a disease continuum. FTD is characterized by the degeneration of frontal and temporal lobes of the brain. Patients develop behavioral and personality changes, often including less empathy and foresight. Language speaking, writing and comprehension can sometimes also be affected. The prevalence of FTD is about 15 in 100.000 people and it is the most common type of dementia after Alzheimer's disease under the age of 65. FTD is often diagnosed between 50 and 60 years of age and disease duration can be 20 years.

ALS is a motor neuron disorder in which the nerve cells that innervate the muscles are affected. This causes muscle weakening starting in extremities and spreading over the body eventually leading to walking, eating, speaking and breathing problems. ALS is the most common motor neuron disease with a prevalence of 5 in 100.000 people. ALS is often diagnosed between 40 and 60 years of age and disease duration is only a few (1-5) years.

Patients diagnosed with FTD can sometimes develop ALS symptoms and about half of all ALS patients develop cognitive problems. Several genes have been identified that can cause both FTD and ALS, including the chromosome 9 open reading frame 72 (*C9ORF72*) gene. A hexanucleotide ( $G_4C_2$ ) repeat expansion in this gene is the most common genetic cause of FTD and ALS. Healthy individuals often carry 2-8 repeats while repeat lengths of 30-4400 are linked to FTD and ALS. Patients harboring the mutation in this gene can develop symptoms of both FTD and ALS and are collectively referred to as C9FTD/ALS patients.

The pathological mechanism of the repeat expansion is not completely understood but could work in three different ways. First of all, the repeat expansion can methylate the *C9ORF72* gene causing (partial) loss-of-function of the normal *C9ORF72* protein. Knock-out mouse models of *C9orf72* display immune system problems but no FTD or ALS symptoms, suggesting that reduced levels of *C9ORF72* protein are not sufficient to cause neurodegeneration.

Secondly, RNA molecules containing the  $G_4C_2$  repeat can form RNA foci and bind several RNA-binding proteins in the cell. These proteins can be sequestered by  $G_4C_2$  repeat RNA and might become unable to fulfill their normal function in the cell.

Thirdly, the  $G_4C_2$  repeat is translated into dipeptides via a newly identified mechanism called repeat-associated non-AUG (RAN) translation. RAN transla-

tion happens in both sense and antisense direction and produces the following dipeptide repeat (DPR) proteins: poly-glycine-alanine (GA), poly-glycine-proline (GP), poly-glycine-arginine (GR), poly-proline-alanine (PA) and poly-proline-arginine (PR). These DPRs can form protein aggregates and are found in post-mortem brain sections of C9FTD/ALS patients.

Both loss-of-function, RNA gain-of-function and DPR protein gain-of-function could contribute to the neurodegeneration observed in C9FTD/ALS. The aim of this thesis is to study the molecular mechanisms underlying the pathogenesis of C9FTD/ALS in order to gain more information for the development of new drugs and to facilitate clinical research.

First of all, we overexpress poly-GR and poly-PR individually in zebrafish embryos to investigate their cellular toxicity and mode of action (chapter 2). Both arginine-containing poly-GR and poly-PR DPRs evoke abundant apoptosis in the brain and abnormal motor neuron morphology in the tail of embryos at 1-4 days post fertilization (dpf). Both poly-GR and -PR can bind to several molecules and proteins in the cell, which could disrupt basic cellular processes and eventually causes cell death. In order to separate primary from secondary effects, we use a pharmacological approach. To our surprise, we identify both Trolox (reactive oxygen species inhibitor) and ISRIB (integrated stress response inhibitor) to give a full rescue of poly-GR and -PR induced cell death, respectively. This highlights the role of mitochondrial and oxidative stress and the activation of the integrated stress response pathway in the pathogenesis of C9FTD/ALS.

Besides studying poly-GR and -PR DPRs in a zebrafish model, we investigated the combination of RNA and DPR toxicity in a mouse model for C9FTD/ALS. This inducible transgenic mouse model contains 36x pure  $G_4C_2$  repeats with 100bp upstream and downstream human flanking regions (chapter 3). Brain specific expression causes the formation of sporadic sense DPRs aggregates after six months of induction, but no apparent neurodegeneration. Ubiquitous expression evokes abundant sense DPRs in multiple organs, leading to weight loss, neuromuscular junction disruption, myopathy and a locomotor phenotype within the time frame of four weeks. The inducible system in the mouse model allows us to study time-windows for treatment. In a pilot study, we show that expression of two weeks followed by two weeks wash-out (expression turned off) was not enough to reduce muscle dystrophy. Sense DPRs were reduced but not completely cleared from muscle tissues. This indicates that toxic entities produced in the first two weeks of expression continue to excise their effects in the following 2 weeks.



In chapter 4, we shift our focus to human post-mortem brain material of C9FTD/ALS cases to further characterize human homologue of yeast UV excision repair protein Rad23b (HR23B) neuropathology. HR23B presented in neuropils, intranuclear inclusions and cytoplasmic and perinuclear inclusions and was predominantly found in cortices (frontal, temporal and motor), spinal cord and hippocampal dentate gyrus. HR23B preferentially co-localized with poly-GA-, pTDP-43- and p62-positive inclusions in frontal cortex and in hippocampal dentate gyrus, the latter showing higher co-localization percentages. HR23B binding partners XPC, 20S and ataxin-3, which are involved in nucleotide excision repair (NER) and the ubiquitin-proteasome system (UPS), did not show an aberrant distribution. Another binding partner of HR23B is NGly1/PNGase, involved in ER-associated degradation (ERAD) of misfolded proteins. NGly1/PNGase was not expressed in the majority of neurons in C9FTD/ALS brain sections compared to non-demented controls. Our results suggest a difference in HR23B aggregation and co-localization pattern with DPRs, pTDP-43 and p62 between different brain areas from C9FTD/ALS cases. Also, we hypothesize that HR23B may play a role in *C9ORF72* pathogenesis, possibly by aberrant ERAD functioning.

To date, rapid progression has been made in the development of therapeutic interventions for C9FTD/ALS in the preclinical phase. However, biomarkers that assess efficacy of treatment response in human clinical studies are much needed. We therefore investigated if poly-GR can be used as a reliable fluid biomarker for C9FTD/ALS. We show that poly-GR can be specifically detected in brain sections and protein isolates from frontal cortex of C9FTD/ALS cases using a new monoclonal antibody against poly-GR. Unfortunately, we are unable to detect poly-GR in cerebrospinal fluid (CSF) and peripheral blood mononuclear cells (PBMCs) of C9FTD/ALS patients and pre-symptomatic C9 mutation carriers. Levels of poly-GR could be below our detection limit of 200pg in our ELISA set-up or simply be absent from CSF. More sensitive techniques might be able to detect poly-GR or other dipeptides that could be used as biomarkers.

The final chapter (6) gives a general discussion of our results in the context of the research field. We discuss the contribution of each of the pathological mechanism (loss- and gain-of-function) and their downstream effects on normal cellular functioning. C9ORF72 protein loss-of-function has been categorized as disease modifier in recent publications. At the same time, the effect of RNA containing the G<sub>4</sub>C<sub>2</sub> repeat and RNA foci is variable and needs further investigation. Especially arginine-containing DPRs seem to be very toxic in multiple models of C9FTD/ALS, which is supported by our data. Important molecular mechanisms

underlying DPR toxicity seem to converge at the integrated stress response, inhibition of translation and nucleocytoplasmic transport defects. DPRs might also affect multiple protein degradation systems.

Together, the research in this thesis indicates an important role of DPRs and supports a gain-of-function in the pathogenesis of C9ORF72. Future research is needed to further disentangle pathological mechanisms in C9FTD/ALS. So far, antisense oligonucleotide therapy that targets repeat-containing RNA and reduces DPRs has been successful in a mouse model for C9FTD/ALS and is currently being set-up in clinical trials. To enable correct implementation of this therapy, biomarkers are needed to provide information about disease progression and treatment response. Many new drugs are under development and we hope that C9FTD/ALS patients can be successfully treated in the near future.



## Samenvatting

Frontotemporale dementie (FTD) en amyotrofische laterale sclerosis (ALS) zijn twee neurologische ziektes die soms samen voorkomen. FTD wordt veroorzaakt door het verlies van hersencellen in de frontale en de temporale kwab van het brein. FTD patiënten ontwikkelen gedrags- en persoonlijkheidsveranderingen, zo laten ze minder empathie zien en hebben ze minder inzicht in de consequenties van eigen handelen. Ook hebben ze moeite met spreken, schrijven en begrijpen van taal. FTD komt gemiddeld bij 15 op de 100.000 personen voor. Onder de leeftijd van 65 jaar is FTD de meest voorkomende vorm van dementie na de ziekte van Alzheimer. FTD wordt vaak gediagnosticeerd bij personen tussen 50 en 60 jaar en het ziekteproces kan 20 jaar duren.

ALS is een neuromusculaire ziekte waarbij de zenuwcellen die de spieren aansturen afsterven. Dit veroorzaakt spierzwakte, welke vaak begint in de ledematen en zich daarna verspreidt over het lichaam. Uiteindelijk krijgen ALS patiënten problemen met lopen, eten, praten en ademen. ALS is de meest voorkomende vorm van neuromusculaire ziekte en komt voor bij 5 op de 100.000 personen. ALS wordt vaak gediagnosticeerd bij personen tussen de 40 en 60 jaar en de ziekte voltrekt zich erg snel, meestal tussen de 1 en 5 jaar.

Sommige patiënten met FTD krijgen later in het ziekteproces symptomen van ALS. Andersom krijgt ongeveer de helft van de ALS patiënten te maken met cognitieve achteruitgang. Er zijn meerdere genen bekend die FTD en ALS veroorzaken, zoals het chromosoom 9 open reading frame 72 (*C9ORF72*) gen. Gezonde personen hebben in dit *C9ORF72* gen 2 a 8 keer de lettervolgorde GG-GGCC. Bij patiënten met FTD en/of ALS worden wel 30 tot 4000 keer deze letters herhaald (GGGGCCGGGGCC etc.). Dit is de meest voorkomende genetische oorzaak van FTD en ALS. Personen met deze genetische mutatie kunnen zowel symptomen krijgen van FTD als ALS en hebben een erg divers ziekteverloop. Deze patiënten worden in het kort C9FTD/ALS patiënten genoemd.

Hoe de verlengde GGGGCC herhaling in het *C9ORF72* gen kan leiden tot de hersenceldood die we in ALS en FTD zien is onbekend. Er zijn drie verschillende theorieën hierover. Volgens de eerste theorie kan de verlengde GGGGCC herhaling het *C9ORF72* gen uitschakelen met als gevolg (gedeeltelijk) verlies van het *C9ORF72* eiwit. Echter bij muis modellen waarin het *C9orf72* gen is uitgeschakeld komen wel vaak immunologische problemen voor, maar geen FTD of ALS. Hieruit kunnen we opmaken dat verminderde *C9ORF72* eiwit niveaus op zichzelf waarschijnlijk niet genoeg zijn voor het veroorzaken van hersenceldood.

Volgens de tweede theorie kan de verlengde GGGGCC herhaling ook problemen veroorzaken op RNA niveau (RNA dient als communicatie tussen DNA en eiwit). RNA dat de verlengde GGGGCC herhaling bevat kan ophopen waardoor zogenaemde RNA foci worden gevormd. Ook kan de GGGGCC herhaling in het RNA binden aan allerlei eiwitten die daardoor hun normale rol in de cel niet meer kunnen uitoefenen.

Als derde wordt de verlengde GGGGCC herhaling in het RNA vertaald in korte eiwitten genaamd dipeptiden (DPRs). Dit gebeurt via een nieuw ontdekt mechanisme: repeat-geassocieerde non-AUG (RAN) vertaling. RAN vertaling gebeurt zowel in sense als antisense richting (van links naar rechts in het RNA en andersom) en produceert de volgende dipeptiden: poly-glycine-alanine (GA), poly-glycine-proline (GP), poly-glycine-arginine (GR), poly-proline-alanine (PA) en poly-proline-arginine (PR). Deze dipeptiden zijn teruggevonden als eiwitophopingen in het brein van overleden patiënten met C9FTD/ALS. Het is echter nog onduidelijk of deze dipeptiden en de ophopingen hiervan schadelijk zijn voor de hersencellen. Zowel verlies van het C9ORF72 eiwit (theorie 1), RNA giftigheid (theorie 2) en dipeptide giftigheid (theorie 3) kunnen leiden tot de hersenceldood welke optreedt bij C9FTD/ALS patiënten.

Het doel van het onderzoek in deze thesis is te na te gaan hoe de hersenceldood ontstaat om zo nieuwe aangrijppunten te ontdekken voor medicijn ontwikkeling en om verder klinisch onderzoek te faciliteren.

In het eerste deel van het onderzoek (hoofdstuk 2) hebben we ons gericht op het poly-GR en poly-PR dipeptide (onderdeel van theorie 3). Deze dipeptiden hebben we los van elkaar geïnjecteerd in zebrawis embryo's om zo het effect van deze dipeptiden te onderzoeken. Beide dipeptiden veroorzaakten grote hoeveelheden celdood in het brein van de zebrawis embryo's. In de staart van 1-4 dagen oude zebrawis embryo's zagen we ook een abnormale structuur van de motor neuronen. Zowel poly-GR als -PR binden verschillende moleculen en eiwitten in de cel en verstoren daarmee verschillende cellulaire processen. Onduidelijk is welke van deze verstoorde cellulaire processen de hoofdoorzaak van de celdood is. Om hier meer informatie over te verkrijgen hebben we de embryo's behandeld met diverse bekende medicijnen die verschillende processen herstellen. Twee medicijnen, Trolox (zuurstofradicalen remmer) en ISRIB (integratieve stress reactie remmer), brachten de hoeveelheid celdood terug naar het niveau van controle zebrawis embryo's. Dit geeft aan dat stress door zuurstofradicalen en de activatie van de integratieve stress reactie een belangrijke rol spelen in de hersenceldood die optreedt bij C9FTD/ALS patiënten.



Verder hebben we ook de combinatie van RNA en dipeptide giftigheid (theorie 2 en 3) onderzocht in een muismodel (hoofdstuk 3). Dit muismodel bevat 36 keer de verlengde GGGGCC herhaling met 100 letters menselijk DNA aan beide kanten van de GGGGCC herhaling. Deze 36 keer verlengde GGGGCC herhaling kan aan en uit worden gezet door het zogenaamde Tet-on systeem. Dit Tet-on systeem stelt ons in staat de locatie (waar in het lichaam van de muis) en de tijdsduur (wanneer in het leven van de muis) van de 36 keer GGGGCC herhaling te bepalen. Activatie in alleen het brein van de muis veroorzaakte na 6 maanden sporadische eiwit ophopingen van sense dipeptiden, maar veroorzaakte geen duidelijke hersenceldood. Activatie in het hele lichaam van de muis veroorzaakte aanwezigheid van sense dipeptiden in meerdere organen. Binnen 4 weken na activatie zagen we bij deze muizen gewichtsverlies, verstoring van de aanhechting van de zenuw op de spier, spierschade en problemen met lopen. Om te kijken of het ziekteproces geremd kon worden hebben we een experiment gedaan waarin we de 36 keer GGGGCC herhaling eerst 2 weken aan hebben gezet en daarna 2 weken uit hebben gezet. Gevolg: sense dipeptiden waren verminderd maar nog steeds aanwezig in de spieren. Ook was er nog steeds schade aan de spieren en schade aan de aanhechting van de zenuw aan de spier. Dit geeft aan dat de giftige producten die in de eerste twee weken zijn aangemaakt lang aanwezig blijven en dat hun effect in de twee weken daarna nog aantoonbaar is.

We leren niet alleen veel over het ziekteproces door het gebruik van diermodellen maar ook door het bestuderen van brein materiaal van overleden C9FTD/ALS patiënten. In hoofdstuk 4 brengen we afwijkingen in kaart van het eiwit HR23B in brein materiaal van overleden C9FTD/ALS patiënten. HR23B kan gaan ophopen en deze eiwit ophopingen bevinden zich vooral in de frontale, temporale en motor kwab van het brein van C9FTD/ALS patiënten. HR23B ophopingen bevatten ook vaak andere ziektekenmerken van C9FTD/ALS patiënten zoals het ophopen van de eiwitten p62, pTDP-43 en poly-GA. Overlap tussen HR23B en deze andere kenmerken kwam voor in de frontale kwab maar vaker nog in de hippocampus. Waarom dit patroon verschilt tussen hersengebieden is onbekend maar kan wellicht informatie verschaffen over verschillen in ziektemechanismen tussen hersengebieden.

Het HR23B eiwit heeft twee positieve functies: hij repareert DNA schade (via nucleotide excisie herstel; NER) en breekt eiwitten af (via het ubiquitine-proteasoom systeem; UPS). HR23B kan aan verschillende andere eiwitten binden zoals XPC, 20S en ataxin-3 (bindingspartners). Uit ons onderzoek blijkt dat deze



eiwitten XPC, 20S en ataxin-3 op hun normale locatie in de cel blijven en niet ophopen zoals HR23B zelf. Een vierde bindingspartner van HR23B is NGly1/PNGase, welke ervoor zorgt dat verkeerd gevouwen eiwitten worden afgebroken (via ER-geassocieerde afbraak; ERAD). In hersencellen van C9FTD/ALS patiënten kwam minder vaak NGly1/PNGase voor dan in hersencellen van controle personen. Dit zou kunnen betekenen dat het ophopen van het HR23B eiwit kan leiden tot verminderde functie van het ERAD proces in het brein van C9FTD/ALS patiënten.

Op dit moment worden er nieuwe therapieën ontwikkeld voor C9FTD/ALS patiënten. De doelgerichtheid en efficiëntie van deze nieuwe behandelingen zijn niet altijd goed te meten. Hiervoor hebben we nieuwe biomarkers (indicatoren over het ziekteproces) nodig. We hebben onderzocht of het poly-GR dipeptide te gebruiken is als biomarker voor C9ALS/FTD patiënten (hoofdstuk 5). We hebben de aanwezigheid van het poly-GR dipeptide aangetoond en de hoeveelheid gemeten in de frontale kwab van het brein van overleden C9FTD/ALS patiënten. In hersenvocht en bloedcellen van levende C9FTD/ALS patiënten kunnen wij op dit moment het poly-GR dipeptide niet detecteren. Het is mogelijk dat het poly-GR dipeptide hierin niet aanwezig is, of dat onze (ELISA) techniek om het poly-GR dipeptide op te sporen niet gevoelig genoeg is. We hopen dat gevoeliger technieken in de toekomst poly-GR wel kunnen detecteren, zodat dit extra informatie kan verschaffen over het verloop van het ziekteproces en de effectiviteit van behandelingen voor C9FTD/ALS patiënten.

Samengevat bevat het onderzoek in deze thesis nieuwe informatie over pathologische mechanismen die C9FTD/ALS kunnen veroorzaken. Onze resultaten ondersteunen vooral de giftigheid van de dipeptiden (theorie 3). Meer onderzoek is nodig om de gezamenlijke effecten van verlies van het C9ORF72 eiwit (theorie 1) en RNA en dipeptide giftigheid (theorie 2 en 3) te bepalen. Meerdere nieuwe therapieën zijn momenteel in ontwikkeling en we hopen dat in de toekomst patiënten met FTD en/of ALS succesvol behandeld kunnen worden.



## Curriculum vitae



Frédérique (Fenne) Wivinneke Riemslagh was born on the 9<sup>th</sup> of July 1989 in Amsterdam, The Netherlands. In September 2007 she started her university education at the VU University in Amsterdam. For her first internship, she joined the lab of Prof. Dr. Peter Heutink at the VU University to analyze the effect of different variations in the promotor region on the expression of the alpha-synuclein gene, linked to Parkinson's Disease. In 2011 she obtained her Bachelor of Science degree with honours program in Biomedical sciences and continued with the Master of Neuroscience at the VU University. Fenne followed the specialization molecular neurosciences and conducted two internships during her masters. The first master internship was at the Erasmus Medical Center in Rotterdam, in the department of Neuroscience, under the supervision of Prof. Dr. Ype Elgersma. Fenne studied the loss of Rheb in excitatory neurons in a mouse model for Tuberous Sclerosis Complex. For her second master internship, Fenne went to the Icahn School of Medicine at Mount Sinai in New York City, to study the role of cadherin-8 in corticostriatal circuit development under the supervision of Prof. Dr. Deanna Benson and Prof. Dr. George Huntley. For both master internships, her contribution to the research resulted in scientific publications. In 2013, Fenne graduated *cum laude* for her Master of Neuroscience and started to work as PhD candidate at the Erasmus Medical Center in Rotterdam, The Netherlands. During her PhD, she studied the molecular mechanisms of C9ORF72-linked frontotemporal dementia (FTD) and amyotrophic lateral sclerosis (ALS). For this research, she used *in vitro* models (primary mouse hippocampal neurons and patients fibroblasts), *in vivo* models (zebrafish and mouse) and post-mortem brain tissue of FTD and ALS patients. The results of these studies are presented in this thesis.

**List of publications**

**Riemsлагh FW**, Lans H, Seelaar H, Severijnen LWFM, Melhem S, Vermeulen W, Aronica E, Pasterkamp RJ, van Swieten JC, Willemsen R. HR23B pathology preferentially co-localizes with p62, pTDP-43 and poly-GA in C9ORF72-linked frontotemporal dementia and amyotrophic lateral sclerosis. *Acta Neuropathol Commun.* 2019 Mar 13;7(1):39.

Hukema RK, **Riemsлагh FW**, Melhem S, van der Linde HC, Severijnen LW, Edbauer D, Maas A, Charlet-Berguerand N, Willemsen R, van Swieten JC. Retraction Note to: A new inducible transgenic mouse model for C9orf72-associated GGGG-CC repeat expansion supports a gain-of-function mechanism in C9orf72-associated ALS and FTD. *Acta Neuropathol Commun.* 2016 Dec 9;4(1):129.

Friedman LG, **Riemsлагh FW**, Sullivan JM, Mesias R, Williams FM, Huntley GW, Benson DL. Cadherin-8 expression, synaptic localization, and molecular control of neuronal form in prefrontal corticostriatal circuits. *J Comp Neurol.* 2015 Jan 1;523(1):75-92.

Goorden SM, Abs E, Bruinsma CF, **Riemsлагh FW**, van Woerden GM, Elgersma Y. Intact neuronal function in Rheb1 mutant mice: implications for TORC1-based treatments. *Hum Mol Genet.* 2015 Jun 15;24(12):3390-8.



**PhD Portfolio**

Courses	Year	ECTS
Art. 9 Laboratory Animal Science	2013	3
Safely working in the laboratory	2013	0.3
Research integrity course	2014	0.3
Cell and developmental Biology	2014	3
Genetics	2014	3
Biomedical research techniques	2014	1.5
Biochemistry and Biophysics	2014	3
Biomedical English Writing and Communication	2015	3
Microscopic Image Analysis	2017	0.8
Genetic engineering in model organisms	2017	1.8
Animated Science	2017	1
Deel Basiskwalificatie Onderwijs	2018	2
Adobe Photoshop and Illustrator + follow-up course	2018	0.6
Adobe InDesign	2018	0.3

Seminars and workshops	Year	ECTS
MGC PhD workshop Munster	2014	1
MGC PhD workshop Maastricht	2015	1
MGC PhD workshop Dortmund	2016	1
MGC PhD workshop Leuven	2017	1
Clinical Genetics meetings	2013-2018	1
Sophia Research Days	2013-2018	1
Journal clubs PhD students	2013-2018	1

(Inter)national conferences	Year	ECTS
Consortium meeting Tubingen	2014	1
Poster at the 9th International Conference on Frontotemporal Dementias, Vancouver	2014	1
Poster at the 10th Brain Research Conference, Chicago	2015	1
Oral presentation at the TN2 conference, Amsterdam	2015	2
Poster at the 10th International Conference on Frontotemporal Dementias, Munich	2016	1
Poster at the Zebrafish Disease Models, Leiden	2018	1
Poster at the 5th RNA Metabolism in Neurological Disease Conference, San Diego	2018	1
Poster at the Society for Neuroscience, San Diego	2018	1

Teaching	Year	ECTS
Workshop bachelor students: 'Overerving in de praktijk'	2014-2017	3
5 HBO Bachelor students	2013-2018	5
Junior Med School	2014-2017	1.5
Master student Neurobiology, University of Amsterdam	2016	2
Master student Biotechnology, University of Milan	2017	2
Master student Molecular Medicine, Erasmus University of Rotterdam	2018	2

<b>Total</b>		<b>55.1</b>
--------------	--	-------------



## Dankwoord

Jaaaaaaaaaaaa! Het gaat eindelijk gebeuren! Ik ga nu echt promoveren! Dat had natuurlijk nooit gekund zonder de hulp van een aantal mensen die ik hierbij graag wil bedanken.

Als eerste mijn promotoren en co-promotor. Beste Rob, bedankt voor het vertrouwen dat je in mij hebt gehad. Toen ik halverwege mijn PhD op het punt stond om op te geven heb je van alles geregeld zodat ik toch kon en wilde blijven. Daaruit sprak veel vertrouwen en dat heb ik erg gewaardeerd. Het leukste moment van de afgelopen jaren was wat mij betreft het conferentie diner in het aquarium in Vancouver. Tijdens het diner heb ik de bewaker overgehaald om ons naar de beluga's te laten kijken. Je laat je eigenlijk nooit gek maken door mijn ideeën of ongeduld, maar die keer stond je toch wel perplex dat ik dat voor elkaar had gekregen. Ook aan de leuke etentjes bij jullie huisje op de Veluwe heb ik goede herinneringen. Beste John, bedankt voor je advies bij alle humane studies en het beschikbaar stellen van de biobank. Ik kan me meerdere leuke etentjes op congressen en een kerstborrel bij je thuis herinneren. Aan het einde van elk jaar kreeg ik ook een mooi flesje wijn, bedankt! Renate, het was niet altijd makkelijk om met je samen te werken, maar ik heb er veel van geleerd. Bedankt voor de vele leuke discussies over o.a. RAN translatie, het begeleiden van studenten en meer vrouwen in de wetenschap!

Ik wil ook graag de rest van de commissie bedanken. Peter Heutink, mijn allereerste stage liep ik op jouw lab. Je hebt me geadviseerd om functioneel werk te gaan doen en dat is me zeer goed bevallen! Bedankt ook dat ik halverwege mijn PhD bij je terecht kon voor advies. Rick Wansink, bedankt voor de leuke RNA meetings en discussies die we hebben gevoerd over repeats en AONs. Max Kros, bedankt voor je tips voor mijn wetenschappelijke carrière, ik hoop dat mij ook een mooi avontuur in het buitenland te wachten staat! Robert Hofstra, bedankt voor je interesse in mijn onderzoek en je steun tijdens mijn PhD.

De meeste hulp de afgelopen jaren kreeg ik van mijn twee paranimfen. Rob en Esmay, zonder jullie harde werk had dit boekje er niet zo mooi uitgezien. Rob bedankt voor je tomeloze inzet en enthousiasme. Je was altijd nog gemotiveerder dan ikzelf als we iets nieuws wilden proberen en je kunt eindeloos doorgaan met perfectioneren. Esmay, bedankt voor al je hulp met de muizenstudie. De cover is mede voor en van jou, de mooiste kleuring van de afgelopen jaren :). Ook buiten het lab zijn jullie mijn vrienden geworden. Het is altijd lachen met jullie en ik zal onze vakantie naar Bergamo nooit vergeten!

Naast mijn twee paranimfen wil ik natuurlijk ook de rest van de FXS-FTD-FXTAS groep bedanken. Ronald, ik heb super veel van je geleerd in de eerste paar jaar van mijn PhD. Bedankt dat je me overal bij hebt betrokken, ook bij alle sociale activiteiten. Ik zal je grappen en grollen op het lab nooit vergeten, evenals de inmiddels legendarische quote: “Ik kan niet veel, maar DNA isoleren dát kan ik”. Lieve Shimriet en Helen, het duurde niet lang voordat ik ook buiten het lab met jullie begon af te spreken. Na meerdere avonden gevuld met etentjes kan ik jullie niet meer wegdenken uit mijn vriendengroep. Shimriet, het was mooi om jouw paranimf te mogen zijn. Twee dagen na mijn eigen bruiloft, het was met recht een echte feestweek! Helen, laten we snel weer eens samen een dagje sauna doen! Lies-Anne en Shami, ook jullie zijn onmisbaar. Lies-Anne, je bent werkelijk het geheugen van het lab en ik kon altijd bij je terecht met al mijn vragen over kleuringen en antilichamen. Shami je was mijn eerste student en bent sindsdien op het lab gebleven als analist. Je doet het super goed en ik ben nog steeds trots op je! Je legt snel contact met mensen en bent mijn informatiebron over alles van de neurologie afdeling. Saif, ook met jou was het meteen gezellig op het lab, tijdens de MGC workshops en op WIDM avondjes. Ik hoop dat je vanaf nu in rustiger vaarwater komt en je kan genieten van je laatste paar jaar op het lab, net zoals ik heb gedaan.

De afgelopen jaren heb ik maar liefst 10 studenten gehad. Mijn eerste twee studenten waren Shami en Santoesha, die nu allebei op de afdeling werken als analist. Shami, ik ga je lach missen. Santoesha, naast je werk heb je ook altijd veel inzet getoond voor je familie. Ik hoop dat je nu meer tijd hebt voor jezelf en volop kan genieten van de komende periode. Daarna Charlene en Chantal, ook al kon Rob jullie niet uit elkaar halen, voor mij zijn jullie allebei bijzonder. Charlene bedankt voor alle kleuringen die je hebt gedaan. Op donderdag had je altijd al alle taken af voor de hele week. Chantal, bedankt voor de vele FISH op vis experimenten. Niels en Feiko, het was erg gezellig met jullie op het lab tijdens de Junior Med School. De vortex en magnetische roerbonen waren jullie favoriet, net zoals het maken van cappuccino van PBS+. Mijn masterstudenten Wim en Daphne, het zebravis hoofdstuk is voor het grootste gedeelte gebaseerd op jullie werk. Bedankt voor jullie hulp en ik ben ook super trots dat jullie nu allebei als PhD op de afdeling zijn begonnen. Martina, thank you for your happiness and joy in the lab. We had some cultural miscommunications at the beginning of your internship but in the end we celebrated your graduation together in Bergamo. You are a very social person and I wish you all the best with your new job! Als laatste Samantha, bedankt voor al je hulp met de celkweek. Je bent een stoere en super lieve meid.



Ook buiten onze eigen groep heb ik een zeer leuke tijd gehad met vele mensen van de afdeling Klinische Genetica. Als eerste mijn kamergenoten Atze, Rajendra, Danny, Roy, Judith, Stefan en Gerben, het was vaak erg gezellig en we konden naast werkaangelegenheden ook praten over voetbal, vakanties, politiek en nog veel meer. Nynke, Laura K, Katherine, Laura V, Martyna, Demy, Ana, Eva en Elena, bedankt voor de leuke uitjes zoals schaatsen, girls-nights en escape rooms. Ik kan nog steeds in een deuk liggen als ik het filmpje van Roy terugkijk! Alle PhD studenten bedankt voor de gezellige MGC workshops. Atze, Silvia en Madeleine, ik vond het super leuk om een MGC workshop met jullie te organiseren! Michelle, Bianca, Rachel en Marianne, bedankt voor alle leuke lunches en etentjes. Koffie om 3 uur zit nog steeds in mijn systeem. Tjakko en Herma, bedankt voor jullie (gevraagde en ongevraagde) adviezen en de leuke wetenschappelijke discussies. Alle andere collega's van de afdeling bedankt voor de leuke tijd op het lab, tijdens de borrels en laser-game activiteiten: Erik, Kyra, Natasha, Wojtek, Stijn, Tom, Guido, Esmee, Adriana, Quishi, Soheil, Erwin, William, Nathalie, Isa, Maria, Wim M, Monica, Douglas, Pablo, Rodrigo, Mike, Alessandro, Fabio, Pim, Joon, Merel, Anita, Vincenzo, Chantal, Jonathan, Mark, Leontien, Yuying and Almira. Beste Jeannette, Bep, Rachel, Marike en Marjoleine bedankt voor al jullie administratieve hulp; voor het Simonsfonds, het verzenden van vele pakketjes en het regelen van allerlei contracten voor mij en mijn studenten. Voor iedereen: ik heb me altijd welkom gevoeld op de afdeling, bedankt voor de leuke tijd!

Daarnaast heb ik ook veel contact gehad met mensen buiten onze eigen afdeling, als eerste natuurlijk de Neurologie afdeling. Lieke, Emma, Harro, Leonie, Janne, Jessica, Tsz, Jeroen, Laura, Diana, Rebecca, Sophie, Elise en Lize. Bedankt voor de gezelligheid tijdens de FTD meetings in Vancouver en München. Het was fijn dat ik altijd bij jullie kon komen buurten als ik weer eens coupes nodig had. Lieke en Emma bedankt voor jullie hulp bij het uitzoeken van alle patiënten gegevens van NHB nummers en CSF samples. En Harro super bedankt voor je hulp bij het scoren van de HR23B pathologie!

Ook wil ik graag meerdere mensen bedanken voor de goede samenwerking. Als eerste Hannes Lans. Toen ik opeens voor je neus stond omdat ik een artikel van je had gelezen en met je wilde samenwerken werd ik met open armen ontvangen. Bedankt voor je enthousiasme, ik heb veel van je geleerd over DNA repair. Wim Vermeulen en Arjen Theil, jullie ook bedankt voor het warme welkom en de hulp op het lab. Laurens Bosman, bedankt voor je hulp bij het opzetten van de gedragsstudies voor ons muismodel. Jeroen Pasterkamp, Jan Veltink en



Eleonora Aronica, bedankt voor het delen van de C9ORF72 ALS coupes en CSF. Charlotte Teunissen, Anne Koelewijn en Inge Verberk, bedankt dat jullie meteen open stonden voor het idee om de SIMOA techniek te gebruiken voor de poly-GR biomarker studie. Het was leuk om een dagje samen te werken op jullie lab op het VUmc. Ik heb ondertussen jullie vriezer vol gestopt met samples en ben erg benieuwd naar de resultaten. Ik wil ook graag alle dierverzorgers bedanken voor hun goede zorgen voor de muizen en de vissen. Alex Maas bedankt voor het beantwoorden van allerlei vragen over het muizenwerk en de hulp bij bestellingen en injecties. Gert-Jan, Gert en Alex van het OIC, bedankt voor de hulp met de microscopen. Zonder jullie uitleg had ik nooit zulke mooie plaatjes kunnen schieten.

Lieve vrienden, jullie ook bedankt voor de steun en interesse die jullie altijd hebben getoond in mijn werk. Arwen, met jou kan ik altijd over alle leuke en lastige dingen van een PhD praten. Ik vond het super leuk om je paranimf te zijn en wens je alle succes met je post-doc in Cambridge. Ayla, jouw PhD ging ook niet vanzelf. We kunnen daar goed over praten en ik heb het idee dat we elkaar daardoor nog beter begrijpen. Ik heb genoten van onze weekendjes weg. Petra, Emma, Marit en Renske, bedankt voor alle leuke etentjes, borrels, weekendjes Groningen en sauna-uitjes waarbij ik helemaal mezelf kon zijn. Voor alle andere vrienden, bedankt voor jullie interesse en gezelligheid afgelopen jaren. Het leven draait om zo veel meer dan werk en door jullie kon en kan ik daar nog meer van genieten.

Lieve Joke en Dis, bedankt voor jullie onvoorwaardelijke liefde en steun. Jullie hebben mijn liefde voor wetenschap altijd gevoed met vele uitjes naar musea, het knutselen van mummies en het spelen van 'Hoe werkt het' en 'Meesters van Macht'. Als iemand vroeg wat ik later wilde worden was het 'Ontdekker'. Ik heb een fantastische jeugd gehad en ik kan altijd bij jullie terecht als ik me onzeker voel over hoe ik dingen moet aanpakken. Bedankt voor jullie steun en vertrouwen.

Lieve Willem, het waren voor ons beiden jaren met ups en downs, met lastige momenten in ons werk en het verlies van Vincent. Maar we hebben ook veel prachtige momenten beleefd, zoals de mooie reizen die we hebben gemaakt en natuurlijk onze bruiloft. We worden samen steeds sterker en hechter. Met jou is het leven zo veel leuker en ik kan niet wachten op onze volgende avonturen. Ik hou van jou.



